Dissertation zur Erlangung des Doktorgrades
der Fakultät für Chemie und Pharmazie
der Ludwig-Maximilians-Universität München

Receptor-specific delivery of Cas9 ribonucleoprotein for cancer therapy

Yi Lin

aus

Wenzhou, Zhejiang, China

2022

Erklärung

Diese Dissertation wurde im Sinne von § 7 der Promotionsordnung vom 28. November 2011 von Herrn Prof. Dr. Ernst Wagner betreut.

Eidesstattliche Versicherung

Diese Dissertation wurde eigenständig und ohne unerlaubte Hilfe erarbeitet.

München, 28.06.2022

.....

Yi Lin

Dissertation eingereicht am 29.06.2022

1. Gutachter: Prof. Dr. Ernst Wagner

2. Gutachter: Ass.-Prof. Dr. Ulrich Lächelt

Mündliche Prüfung am 27.07.2022

To my family

致家人

Table of Contents

1 Introduction

This chapter was adapted from: Yi Lin, Ernst Wagner and Ulrich Lächelt. Non-viral delivery of the CRISPR/Cas system: DNA versus RNA versus RNP. Biomaterials Science., 2022, 10, 1166-1192.

1.1 The CRISPR/Cas9 system as a genome editing tool

The CRISPR/Cas9 system, which was initially discovered as a type of adaptive immune system in bacteria,[1] revolutionized biomedical research due to the applicability as a programmable endonuclease.[2] The genome editing tool is composed of the endonuclease Cas9 and a guide RNA (gRNA) which guides the protein to the target DNA sequence followed by a proto-spacer adjacent motif (PAM). The double-stranded DNA is unwound and a double-strand break (DSB) introduced 3–4 base-pairs upstream of the PAM sequence. The cellular machinery repairs DSBs in genomic DNA primarily via two distinct pathways (Figure 1), non-homologous end joining (NHEJ) and homology directed repair (HDR).[3,4] NHEJ represents the direct re-ligation of the cleaved DNA strands without involvement of a homologous DNA template. This error prone mechanism can lead to random insertions and deletions of nucleotides (indels) at the cleavage site which in part result in frameshift mutations and target gene knockout. In presence of a DNA template with homologous flanks, HDR mediates an accurate repair and the insertion of a defined DNA sequence, embedded between the homology arms at the cleavage site, can be realized. These strategies of using the cellular DSB repair machinery for introducing gene knock-outs or knock-ins are generally independent of the utilized endonuclease. However, the flexible control over the sequence recognition by simple variation of the gRNA component explains the uniqueness of CRISPR/Cas9 compared to other genome editors, such as transcription activator-like effector nucleases (TALENs) or zinc finger nucleases (ZFNs), which require individual protein design for each alteration of the target site.[5] The functional unit of the CRISPR/Cas system is represented by the Cas9/gRNA ribonucleoprotein (RNP) complex which has to reach the nucleus of eukaryotic cells (eventually together with template DNA) for mediating the intended

genomic modifications. To achieve this, different biomolecular formats can be selected and utilized for cellular delivery: plasmid DNA (pDNA) encoding for the Cas9 protein and the specific guide RNA (gRNA); a mixture of Cas9 mRNA and gRNA; or the pre-assembled RNP complex. Each strategy has its own features, prerequisites, advantages or drawbacks. This review presents approaches for the cellular delivery of the different biomolecular CRISPR/Cas9 formats and highlights their differences and characteristics.

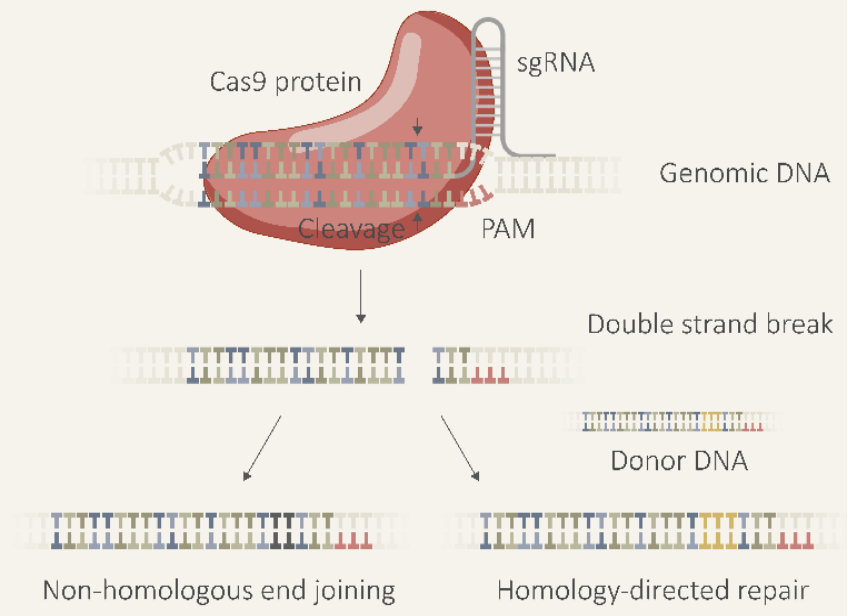

Figure 1. Mechanisms of CRISPR-Cas9 genome editing.

1.2 Physicochemical and physiological characteristics of different CRISPR/Cas9 formats

1.2.1 Cas9 plasmid DNA

Typical and well-established SpCas9 plasmids for transfection of mammalian cells are pX260 and pX330 from the Zhang laboratory. pX260 is an older CRISPR/Cas plasmid system, which contains three expression cassettes; one is used to drive SpCas9 nuclease expression and the other two are used to express the CRISPR RNA array and tracrRNA.[6] At present, the most commonly used SpCas9 plasmid is pX330 that contains only two expression cassettes, a human codon-optimized SpCas9 and a chimeric single guide RNA. It has 8484 bp with 1.68×10^4 negative charges and a molecular weight of around 5.24×10^3 kDa. Generally, the pX330 vector can be digested by the restriction enzyme BbsI to insert a pair of annealed oligonucleotides that are designed based on the specific target site (20 bp) upstream of the NGG PAM sequence. Larger plasmid constructs containing an additional reporter gene (e.g. pX458 encoding GFP) to identify and enrich transfected cells, or a selection marker (e.g. pX459 encoding resistance to puromycin) to generate stable cell lines are also available.[6]

1.2.2 Cas9 mRNA and sgRNA

Different from the two-in-one Cas9 plasmids, co-delivery of two individual components, Cas9 mRNA and sgRNA, is required in case of RNA-based strategies of the CRISPR/Cas system. Cas9 mRNA with the length of approximately 4500 nt is a linearized single-stranded RNA which is produced via in vitro transcription (IVT) followed by 5’ capping and 3’ poly-A modification.[7,8] The 5’ capping of IVT mRNA mimics the natural eukaryotic mRNA which has a 7-methylguanosine (m7G) cap at the 5' end.[9] It can protect the mRNA against exonuclease degradation and assists in eukaryotic initiation factor (eIF) 4E recognition and binding during translation.[10] The poly-A tail is a long chain of adenine nucleotides. It is added to the 3’ end of the mRNA transcript to increase its enzymatic stability, and it can act synergistically with the 5’ m7G cap to regulate translation efficiency as well as enhance protein

expression.[11,12] With regard to mRNA stabilization, introduction of phosphorothioates especially into the 5' untranslated mRNA sequence has been shown to increase protein translation and to result in up to 22-fold enhanced protein expression.[13] Generally, endocytosed IVT mRNA can be recognized by several endosomal innate immune receptors (TLR3, TLR7 and TLR8) and cytoplasmic proteins such as melanoma differentiation-associated protein 5 (MDA5) and retinoic acid inducible gene I protein (RIG-I), which may induce immune responses and inhibit the function of mRNA.[14,15] The intrinsic immune activation activity of IVT mRNA is usually considered beneficial for immunotherapeutic vaccination, but a major disadvantage for non-immunotherapy-related applications since the induced immune responses can slow down the translation of mRNA and promote RNA degradation.[14,15] Incorporation of chemically modified nucleotides, such as 2-thiouridine (s2U), 5-methyluridine (m5U), pseudouridine (Ψ), N1-methylpseudouridine (m1Ψ), 5-methylcytidine (m5C), 5-hydroxymethylcytosine (5hmC), into mRNA sequences are the mostly used strategies to overcome the high immunogenicity of IVT mRNA.[16-18] Besides, some studies showed that lower immunogenicity can be achieved by sequential engineering and the use of high-performance liquid chromatography (HPLC)-purified mRNA.[19,20]

Another key component of the RNA-based strategy is the sgRNA which has a smaller size of approximately 100 nt. sgRNA can either be generated by IVT or, due to the much shorter length, by solid-phase synthesis.[21,22] IVT is a widely used approach for sgRNA production, since it is cost-effective, high-yielding and easy to implement. On the other hand, IVT sgRNA can be expected to face similar problems as other IVT generated RNA products, such as IVT mRNA, which could limit its applicability in vivo. Firstly, IVT RNA contains diverse variants with different lengths and structures which may cause variable and inconsistent editing efficiencies.[14,23] Secondly, the stability of unmodified IVT RNA generally is not favourable for in vivo usage.[24] Even if modified nucleotides are used for the IVT reaction, random incorporations of the nucleotides into the RNA sequence can still be a non-negligible issue.[25] With regards to the CRISPR/Cas system, it has been reported that IVT sgRNA can induce immune responses and even cause cell apoptosis.[26-28] In contrast to IVT sgRNA, chemically synthesized sgRNA is structurally well-defined and homogenous. Synthetic sgRNA which lacks a 5'-triphosphate group is less immunogenic and does not induce

detectable immune response in many cell types.[27-29] Moreover, the chemical oligonucleotide assembly enables site-specific incorporation of modified nucleotides during solid-phase synthesis. Various chemically modified nucleotides, including 2'-methyl (M), 2'-O-methyl-PS (MS), 2'-O-methyl-3'-thiophosphonoacetate (MSP), phosphorothioates, 2'-fluoro (F), 2'-O-methyl-3'-phosphonoacetate (MP), locked nucleic acids (LNA) and bridged nucleic acids (BNA), are developed to enhance the enzymatic stability, editing efficiency, specificity as well as to reduce the immunogenicity and off-target effects of sgRNA.[30-37]

1.2.3 Cas9/gRNA ribonucleoprotein (RNP)

Similar to the RNA strategy, protein-based delivery of the CRISPR/Cas system also requires two critical components in the formulation: the Cas9 nuclease and a guide RNA (gRNA). But in contrast to the mRNA-based strategy, which requires co-delivery of the discrete mRNA and sgRNA species, the Cas9 protein is first pre-complexed with gRNA to form the negatively charged Cas9/gRNA ribonucleoprotein (Cas9 RNP) complex, which can then be delivered as one single cargo entity. The typical SpCas9 protein comprises 1368 amino acids with a molecular weight of 158.4 kDa and a net positive charge of +22.[38] The structure of the SpCas9 protein exhibits two lobes: an α-helix recognition lobe (REC) and a nuclease lobe (NUC).[39] These two lobes are linked by the arginine-rich bridge helix (Arg) and the disordered linker (DL).[39] The NUC lobe contains a RuvC domain and a HNH nuclease domain for cleavage of the target DNA, as well as a C-terminal domain (CTD) for recognizing the PAM sequence.[39] The REC lobe consists of three α-helical domains and plays a vital role in recognition of DNA, regulation of conformational transition of the HNH nuclease domain and directing HNH to the cleavage site.[39,40]

As gRNA component for Cas9 RNP assembly, two different variants can be utilized: (1) a crRNA : tracrRNA duplex, or (2) a single guide RNA (sgRNA). The two-component guide RNA represents the naturally occurring form of the bacterial CRISPR/Cas9 system and comprises a CRISPR RNA (crRNA) with a custom 20 nt targeting sequence and a trans-activating crRNA (tracrRNA), which is crucial for Cas9 recruitment.[41] sgRNA is created by fusing the crRNA and tracrRNA sequences via a scaffold loop into a single RNA chimera, which became the most popular format

for RNP-based CRISPR delivery. In the absence of gRNA, the Cas9 protein remains in an inactive conformation.[42] When it is bound to gRNA, the REC lobe undergoes a conformational change which converts the inactive protein into the active RNP form.[39,42] Since the binding of gRNA is highly associated with the functional domains of the Cas9 protein, the types and positions of modified nucleotides need to be carefully selected to avoid a potential interference with RNP formation. A very special feature of Cas9 RNPs, with high relevance for delivery, is the charge-conversion of the positively charged Cas9 protein upon binding of the negatively charged sgRNA component. The work by Zuris et al. on genetically engineered supercharged proteins demonstrated, that the sgRNA component in Cas9 RNPs already provides sufficient negative charge for the delivery with cationic lipids.[43] Kuhn et al. reported the cellular delivery of Cas9 RNPs with oligoaminoamides, containing lipid-modifications and stabilizing tyrosine trimers,[44] and determined by fluorescence correlation spectroscopy that the cationic oligomers only interact with fluorescently labelled Cas9, if the negatively charged sgRNA has been loaded.[45] These results illustrate a significant characteristic of Cas9 RNPs which provides the basis for cellular delivery by cationic transfecting agents without requirement of protein derivatization or individual nanocarrier design.

1.2.4 Comparison of different formats of CRISPR/Cas9

Since each format has its intrinsically unique physicochemical and physiologic features, it is crucial to understand how these features affect the Cas9 action process and then select the best format for practical applications. The most direct distinction is the stability. Cas9 plasmid DNA (Cas9 pDNA) possesses the highest stability among the three formats. Chemically, DNA contains deoxyribose while RNA contains ribose. The absence of the single hydroxyl group in 2’ position of the pentose ring makes DNA more stable and less reactive than RNA.[46] Moreover, Cas9 pDNA is a circular double-stranded DNA which is not vulnerable to exonucleases.[47,48] Although Cas9 mRNA is more fragile than Cas9 pDNA, chemical modifications on the nucleotides can be applied to improve the stability as mentioned above.[49]

Compared to pDNA and mRNA, which contain only a single type of biomolecules, Cas9 RNPs consist of protein and sgRNA and are susceptible to degradation by both

proteases and RNases, hypothetically making it the least stable format. Besides, the Cas9 protein may not be resistant to organic solvents and is easily denatured. For example, denaturation of Cas9 RNP is observed in acidic citrate buffer at pH 4.0, which represent standard conditions for the formulations of nucleic acid loaded LNPs.[50]

Another obvious difference is the place of action. As discussed in the previous section, nuclear entry is an essential prerequisite for the transfer of pDNA. In contrast, Cas9 mRNA only requires delivery to the cytoplasm where the translation process may start immediately. However, in both cases, the RNP complex has to be assembled with gRNA after the Cas9 protein has been produced, which inevitably results in a certain latency between the intracellular availabilities of the protein and RNA components. In this regards, delivery of a priori formed functional RNPs is the most direct way for cellular genome editing, which generally is also considered the most efficient strategy.[51] As a last step, the Cas9 RNP has to enter the nucleus to reach its target site and for this reasons nuclear localization signal (NLS)-fused Cas9 is commonly used.[52] As discussed above, the duration of intracellular persistence depends on the stability of the genetic 'blue prints' and degradation of encoded protein. For genome editing applications, the CRISPR/Cas components are only transiently required until the intended genome modification has occurred; an additional presence in the cell generally is not favored, since the risk of off-target events can increase with the duration of presence in the cell. Therefore, a high control over the availability of the functional CRISPR/Cas system and a degradation or inactivation after the intended task has been fulfilled, are desirable. Due to the more rapid degradation within the target cells, Cas9 RNP and mRNA provide a shorter exposure time of the cellular genome to active Cas9 proteins and decrease the potential risk of off-target effects.[53,54] In contrast, Cas9 pDNA can mediate longer gene expression that may increase off-target editing events.[55]

Independent of the biomolecular format, additional strategies to minimize mutations at unintended sites include shortening Cas9 half-life by tagging with degradation signals,[56,57] reducing Cas9 activity by coupling to inhibitory domains,[58] or selective activation of Cas9 variants by external triggers such as chemical reagents[59,60] or light.[61] In addition, other Cas9 variants have been designed to optimize the on-/off-target ratio, such as catalytically inactive Cas9 fused to the catalytic domain of the

endonuclease FokI (dCas9-FokI),[62] mutated variants with attenuated activity at mismatch targets, such as high-fidelity Cas9 (SpCas9-HF1),[63] enhanced specificity Cas9 (eSpCas9),[64] hyper-accurate Cas9 (HypaCas9),[65] evoCas9,[66] Sniper-Cas9[67] and expanded PAM SpCas9 (xCas9).[68] Nickases, generated by deactivation of the nucleolytic RuvC (Cas9-D10A) or HNH (Cas9-H840A) domain, induce single-strand nicks instead of double-strand breaks and therefore require a pair of gRNAs for gene disruption, which strongly increases the specificity.[69]

Apart from their stability and action features, safety is a major concern, especially considering potential in vivo applications. As stated above, random integration of Cas9 pDNA into the host genome may cause potentially harmful insertional mutagenesis as well as persistent Cas9 expression that can lead to off-target effects and MHC class I immune responses.[70] In this regard, Cas9 RNP and mRNA appear as the safer choices for genome editing. Besides, the main type of immune response induced by these three formats is also different. Cas9 pDNA and mRNA mainly trigger innate immune responses by activating Toll-like receptors (TLRs), while Cas9 RNP can induce adaptive immune reactions.[70-74] Recent studies have demonstrated that anti-Cas9 antibodies and T cells are pre-existing due to preceding bacterial infections.[70,73,74] IgG antibodies against SpCas9 and anti-SpCas9 T cells were detected in 58 % and 67 % of human adults, respectively.[70]

Although Cas9 mRNA and RNP have certain advantages in terms of editing efficiency and safety, the costs are generally higher than for pDNA, since pDNA design, production and scale up are more feasible. In contrast, obtaining pure active Cas9 proteins is a time-consuming and complex process, which includes a series of critical steps, such as protein isolation from bacterial cultures, purification, suitable storage of the sensitive protein product etc.[75] Notably, endotoxin contamination could occur during both pDNA and Cas9 protein preparation, while the cell-free mRNA production exhibits a much lower risk. Finally, the clinical translation of nucleic acid-based therapeutics is more mature than intracellular delivery of proteins, which is impressively demonstrated by the recent success of siRNA-based drugs and mRNA vaccines.[76,77] To sum up this section, the individual CRISPR/Cas9 formats differ in their physicochemical properties, stability, action features, safety and production. Figure 2 presents a summary of the distinction and individual characteristics. The direct delivery of Cas9 RNP has several advantages over the other two formats and

has drawn much attention. Therefore, the delivery strategies utilized for RNP-based CRISPR/Cas9 systems are reviewed in the following section.

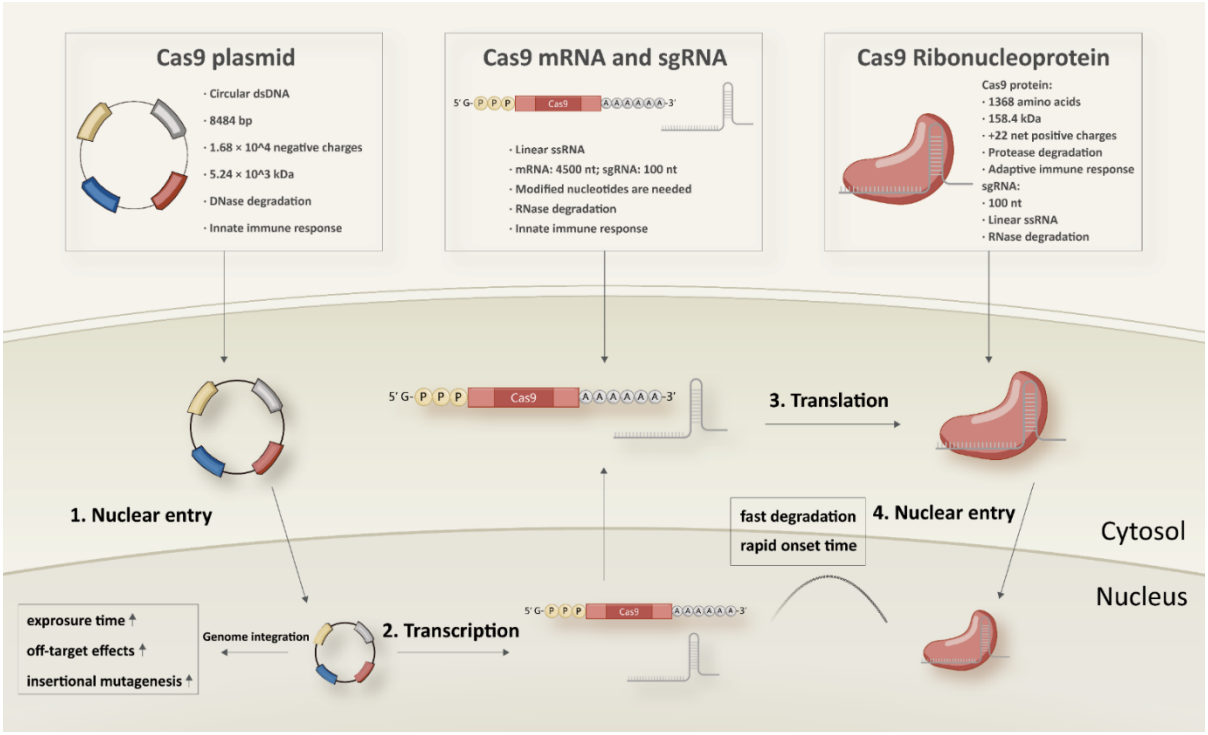

Figure 2. Comparison of different biomolecular CRISPR/Cas9 formats: Cas9 plasmid, Cas9 mRNA and sgRNA, and Cas9/sgRNA ribonucleoprotein.

1.3 Non-viral delivery of Cas9 RNPs

1.3.1 Polymeric delivery systems

PEI as a cationic unit with favourable properties for cellular transport of biomolecules is widely used for Cas9 RNP delivery. For example, core-shell liposome-templated hydrogel nanoparticles (LHNPs) were developed by crosslinking cyclodextrin (CD)-engrafted PEI (25K) (PEI-CD) with adamantine (AD)-engrafted PEI (25K) (PEI-AD) through CD-AD host–guest interactions and subsequent DOTAP liposome coating.[78] The study indicated that LHNPs carrying Cas9/sgPlk1 effectively inhibited tumor growth and prolonged the survival time of tumor-bearing mice. The concept of constructing supramolecular nanoparticles via CD-AD mediated host-guest

interaction was also validated in other systems for Cas9 RNP delivery.[79-81] Wan et al. complexed disulfide-bridged guanidyl AD (AD-SS-GD) with β-CD-conjugated low-molecular-weight PEI (CP) to generate CP/AD-SS-GD for loading Cas9 RNPs.[79] CP/AD-SS-GD/RNP exhibited efficient cellular uptake and could readily release Cas9 RNPs in the reductive intracellular environment. They further found that hyaluronic acid coated CP/AD-SS-GD/RNP targeting mutant KRAS could effectively suppress tumor growth and metastasis in vivo. In another work, the CP/AD-SS-GD/RNP targeting NLRP3 were packaged together with dexamethasone-loaded polymeric nanoparticles into a dissolvable microneedle (MN) patch. The transdermal co-delivery achieved synergistic therapeutic effects against inflammatory skin disorders in mouse models.[80] Ban et al. prepared Cas9 RNP-loaded supramolecular nanoparticles (RNP-SMNPs) via mixing AD-PAMAM, AD-PEG, AD-PEG-TAT, CD-PEI and Cas9 RNPs. The optimized RNP-SMNPs enabled specific deletion of the dystrophin exons 45–55 as a potential approach for the treatment of Duchenne muscular dystrophy.[81]

In addition to PEI, cationic polypeptides such as polylysine and poly(aspartic acid) with cationic side-chain modifications were developed which generally feature higher biocompatibility and lower toxicity.[82,83] Liu et al. reported a nano-Cas9 RNP system (nanoRNP) based on 2,5-dihydro-2,5-dioxofuran-3-acetic acid (CA)-bridged polylysine-g-poly(ethylene glycol) (PLys100-CA-mPEG77).[82] The nanoRNP detached its mPEG shell in the acidic tumor microenvironment, facilitated cellular uptake of Cas9 and a combination of sgRNAs targeting STAT3 and RUNX1, which resulted in effective tumor growth inhibition in a heterogenous tumor model. Deng et al. utilized two copolymers to construct a tumor-targeted gene editing system for synergistic gene and photodynamic antitumoral effects.[83] Firstly, nitrilotriacetic acid-disulfanediyldipropionate-polyethyleneglycol-b-polycaprolactone (NTA-SS-PEG-PCL) was assembled with the hydrophobic photosensitizer chlorin e6 (Ce6) into a micellar core. Then the chelate complexes of NTA with nickel ions on the surface of the micelles bound oligohistidine-tag containing Cas9 RNPs via coordinative interactions. Finally, iRGD-PEG-b-polyasparte-g-1,4-butanediamine [RGD-PEG-pAsp(DAB)] was added to neutralize the negative charge of the NPs and to provide tumor-targeting ability. The obtained T-CC-NPs escaped from lysosomes via NIR-induced production of reactive oxygen species (ROS) by Ce6 and released their Cas9/sgNrf2 cargo due to the reduction of disulfide bonds. The study indicated that Nrf2 deletion enhanced

tumor cell sensitivity to ROS, leading to synergistic effects of PDT and Nrf2 gene knockout in vivo.

PBAEs have been utilized as vectors for CRISPR-Cas9 plasmid delivery. In the context of protein delivery, classical PBAEs with highly positive charge may not be appropriate to encapsulate Cas9 proteins due to incompatibility with the surface charge density. Therefore, Green et al. synthesized a new class of PBAEs which contain both cationic and anionic functions via polymer end-capping with carboxylate ligands.[84] The carboxylated PBAEs could self-assemble into nanoparticles with various types of proteins including Cas9 RNPs. The study demonstrated that a single intracranial injection of the nanoparticles carrying 3.5 pmol Cas9 RNP induced robust gene editing in an orthotopic murine glioma model. Likewise, Chen et al. synthesized a glutathione (GSH)-cleavable cross-linked polymer containing both cationic and anionic residues for better encapsulation of inhomogenously charged Cas9 RNPs.[85] After local administration in vivo, the optimized nanoparticles enabled robust gene editing in retinal pigment epithelium (RPE) tissues and skeletal muscles. Recently, Liu et al. reported a phenylboronic acid-modified dendrimer that could also bind both negatively and positively charged proteins.[86] The dendrimer effectively delivered various native proteins with different isoelectric points and sizes into cells. Particularly, it enabled efficient delivery of Cas9 RNPs into multiple cell lines and achieved excellent editing efficiency. Although numerous types of polymers were successfully synthesized and optimized for Cas9 RNP delivery, the question on structure-activity relationships is still hard to answer. For this purpose, Kumar et al. validated that combinatorial synthesis and high-throughput characterization methodologies coupled with machine learning enables the rapid discovery of potential polymers for Cas9 RNP delivery, which may accelerate the clinical translation of polymeric vectors in the future.[87]

1.3.2 Lipidic delivery systems

In 2015, Zuris et al. first validated that a commercially available cationic lipid reagent (Lipofectamine RNAiMAX) could efficiently deliver engineered highly anionic proteins as well as pre-assembled Cas9/sgRNA RNPs into cells.[43] Particularly for Cas9 RNPs, cationic lipid-mediated delivery achieved up to 80 % genome modification *in*

vitro and 20 % in the mouse inner ear *in vivo*. After the success of common transfection reagents, LNPs which are mostly used for Cas9 mRNA delivery were also optimized for Cas9 RNPs. For example, bioreducible LNPs were loaded with the chemokine CXCL12α and Cas9 RNPs targeting the interleukin-1 receptor accessory protein (IL1RAP). After the fabrication, the LNPs were loaded onto mesenchymal stem cell membrane-coated nanofibril (MSCM-NF) scaffolds to enhance targeting of leukemia stem cells for the therapy of acute myeloid leukemia (AML).[88] It is worth noting that the common LNP formulation process for nucleic acids is performed in acidic buffer which is not suitable for Cas9 RNPs, due to potential denaturation of the protein and decrease of the final editing efficiency. To circumvent this problem, Wei et al. developed a generalizable approach that allows Cas9 RNP encapsulation in neutral buffers by adding a permanently cationic lipid to the conventional LNP formulations.[50] By optimizing the lipid components and ratios, the generated LNPs enabled tissue-specific gene editing and multiple genome modifications in mice. Recently, stimuli-triggered liposomes were designed for temporal and spatial control of Cas9 RNP-mediated gene editing.[89,90] Aksoy et al. developed light-triggered liposomes by integrating a photosensitive compound, verteporfin (VP), into the lipid bilayer.[89] Upon 690 nm light illumination, singlet oxygen generated by VP destabilized the liposomal structure and facilitated Cas9 RNP release. The temporal and spatial control of gene editing was achieved both *in vitro* and in a zebrafish model. In another study, Ryu et al. designed an ultrasound (US)-activated microbubble conjugated nanoliposome (MB-NL) to utilize Cas9 RNPs for the therapy of androgenic alopecia.[90] Under high acoustical wave ultrasound frequency, MB-NL enabled improved Cas9 RNP delivery to dermal papilla cells (DPC), resulting in efficient steroid type II 5-alpha-reductase (SRD5A2) gene knockout and subsequent hair growth recovery.

1.3.3 Inorganic and inorganic/organic hybrid delivery systems

Recently, Lee et al. developed DNA-thiol modified gold nanoparticles (GNPs) that could firstly hybridize with donor DNA and then absorb Cas9 RNPs onto the surface of GNPs.[91] The Cas9 RNP-loaded GNPs were further coated with a layer of silica for increasing the negative charge density and finally complexed with the cationic polymer PAsp(DET). The obtained CRISPR-gold induced 5.4 % correction of the

dystrophin gene in *mdx* mice and improved animal strength under clinically relevant conditions. Other gold nanoparticles modified with PEI were reported that could not only deliver Cas9 but also the alternative RNA-guided endonuclease Cpf1 (Cas12a) together with the required crRNA and ssDNA template into haematopoietic stem and progenitor cells (HSPCs).[92] Zhang et al. constructed a multi-targeting Cas9 RNP delivery systems from gold nanoclusters by conjugation of the cell penetrating HIV-1-transactivator-of-transcription (TAT) peptide and lipid-coating with galactopyranoside (Gal)-modified DOTAP.[93] Encapsulated Cas9 RNPs targeting the PCSK9 gene enabled about 60 % PCSK9 knockout *in vitro* and around 30 % plasma LDL cholesterol reduction *in vivo*. Interestingly, the recent studies found that the Cas9 RNP corona, which is formed on the surface of AuNPs, could already mediate efficient cellular uptake without requirement of further complexation by polymers or lipids.[94] Utilizing the interactions between carboxylates and guanidinium groups, Rotello and colleagues assembled arginine AuNPs (ArgNPs) with oligo(glutamic acid)-tagged Cas9 protein to generate a series of Cas9En-ArgNP nanoassemblies for direct cytosolic delivery of Cas9 RNPs.[95] The study demonstrated that the delivery efficiency of Cas9En increased with increasing E-tag length from E0 to E20, and up to 90 % of the cells were reached when Cas9E20 was used. After systemic injection of Cas9E20-ArgNPs, the efficient gene editing of the PTEN gene was observed, especially in macrophages in the liver and spleens.[96] Apart from spherical gold nanoparticles, nanoparticles with other shapes, such as nanorods (AuNRs) and nanowires (AuNWs), were also utilized.[97,98] For instance, Li et al. developed azobenzene-4,4'-dicarboxylic acid (p-AZO) modified AuNRs to achieve hypoxia-responsive on-demand release of Cas9 RNPs for mild-photothermal therapy.[97] Hansen-Bruhn et al. constructed an ultrasound-propelled nanomotor based on AuNWs for active and direct intracellular delivery of Cas9 RNPs.[98] The nanomotors achieved efficient knockout with only 0.6 nM of Cas9 protein.

In 2017, zeolitic imidazolate framework-8 (ZIF-8), a subclass of metal-organic frameworks (MOFs), was reported as the first example of MOF-based Cas9 RNP delivery by Khashab and colleagues.[99] The CRISPR/Cas9 ZIF-8 (CC-ZIF) achieved 17 % loading efficiency of Cas9 RNPs and 37 % EGFP knockout in vitro. Moreover, they coated CC-ZIF with cancer cell membranes (C3-ZIF$_{\text{cell membrane type}}$) to enable cell-type-specific delivery of Cas9 RNPs.[100] *In vitro* studies demonstrated higher

repression of EGFP reporter expression when MCF-7 cells where treated with C3-ZIF_{MCF-7} compared to C3-ZIF_{HeLa}, and in HeLa cells *vice versa*. *In vivo* fluorescence imaging confirmed that C3-ZIF_{MCF-7} could specifically accumulate in MCF-7 tumor sites. Recently, Yang et al. assembled imidazole-2-carboxaldehyde (2-ICA) and Zn^{2+} with Cas9 RNPs to generate an ATP-responsive delivery system (ZIF-90).[101] The intracellular high concentration (10 mM) of ATP disassembled ZIF-90 due to the competitive coordination between Zn^{2+} and ATP, released Cas9 RNPs and induced up to 35 % GFP knockout in HeLa cells. Liu et al. reported a novel approach for controlling hierarchical self-assembly of metal–organic cages (MOC) into supramolecular nanoparticles (SNPs) for Cas9 RNP delivery.[102] The adamantane-functionalized Pd12L24 MOC (Ada-MOC) and β-cyclodextrin-conjugated PEI (PEI-βCD) assembled via host-guest interaction and encapsulated Cas9 RNPs. The obtained Cas9 SNPs achieved 40 % knockout of GFP expression compared to non-treated cells.

Mesoporous silica nanoparticles (MSNs) are widely used for delivery purposes, including the CRISPR/Cas9 system in nucleic acid or RNP form. However, the common technique of protein loading into MSNs is based on nonspecific physical absorption, which generally results in rather weak binding. To enhance the encapsulation efficiency of the protein in MSNs, Liu et al. developed a novel approach by modifying the surface of Cas9 protein with boronic acid and MSN scaffolds with amine groups.[103] The dative bond formation between boronic acids and amines as well as electrostatic interactions increased the loading and intracellular delivery of Cas9 RNPs. Recently, Pan et al. constructed NIR-responsive upconversion nanoparticles (UCNPs) for Plk1 gene disruption in tumors.[104] In this system, Cas9 RNPs were covalently anchored on the surface of UCNPs via a photocleavable 4-(hydroxymethyl)-3-nitrobenzoic acid (ONA) linker, and the formed UCNPs-Cas9 complexes were coated with PEI to facilitate endosomal escape after cellular internalization. Upon irradiation, UCNPs-Cas9@PEI converted 980 nm NIR light into local ultraviolet light which resulted in photo-responsive release of Cas9 RNPs and significant inhibition of tumor cell growth both *in vitro* and *in vivo*. In another study, Chen et al. used semiconducting copper sulfide (CuS) NPs as NIR-absorbing nanomaterials along with Cas9 RNPs, doxorubicin (DOX) and PEI to establish multifunctional NIR-triggered nanocomplexes for cancer combination

therapy based on photothermal and chemotherapy.[105] Besides, several 2D-nanomaterials were reported for Cas9 RNP delivery.[106,107] Yue et al. developed a PEG and PEI dual-functionalized graphene oxide (GO) platform which enabled Cas9 RNP loading and CRISPR-mediated gene editing.[106] Zhou et al. engineered a Cas9 protein with three NLS tags (Cas9N3) at the C terminus for a better loading onto black phosphorus nanosheets (BPs) via electrostatic interactions.[107] The constructed Cas9N3-BPs entered the cells via both direct membrane penetration and endocytosis pathways, and the Cas9N3 with improved nuclear entry led to robust gene editing *in vitro* and *in vivo*.

1.3.4 Peptidic delivery systems

In general, peptide-mediated RNP delivery can be divided into two strategies: (1) covalent linkage of cell-penetrating peptides (CPPs) to the Cas9 protein; and (2) non-covalent assembly of peptides with Cas9 RNPs into nanocomplexes. The first strategy can be further sub-classified into chemical conjugation of CPPs or genetic engineering. Kim and colleagues reported the first example of chemical Cas9 protein delivery based on CPPs in 2014.[108] They conjugated arginine-rich CPPs to Cas9 protein via thiol-maleimide reaction and treated cells along with CPP-complexed sgRNA. The results showed that CPP-mediated Cas9 delivery exhibited efficient gene editing in multiple cell lines with reduced off-target effects compared to plasmid transfections. Gao and colleagues genetically fused a supercharged polypeptide (SCP) to proteins to facilitate direct intracellular transduction without requirement of additional delivery agents.[109] They found that K4-tagged proteins achieved highest cellular uptake and distribution into the nucleus. For genome editing, Cas9-K4/sgRNA induced 15.2 % indels in the CCR5 gene in HeLa cells. However, the activity of Cas9 was affected by the modification and the cleavage efficiency of SCP-fused Cas9 decreased, eventually due to steric hindrance. To solve this drawback, they introduced a cleavable dithiocyclopeptide linker between Cas9 and SCP which contains a matrix metalloproteinase 2 (MMP-2) recognition site and an intramolecular disulfide bond (denoted Cas9-linker-SCP).[110] Free Cas9 proteins were sufficiently released from Cas9-linker-SCP via extracellular MMP-2 cleavage and subsequent intracellular GSH-induced disulfide break, which resulted in enhanced genome editing efficiency. In another study, Kim et al. developed a carrier-free Cas9 RNP

delivery strategy by engineering Cas9 protein containing a NLS and a low-molecular-weight protamine (LMWP).[111] The generated Cas9-LMWP self-assembled with crRNA:tracrRNA to form ternary Cas9 RNPs, which were efficiently taken up by cells and enabled KRAS gene disruption *in vitro* and *in vivo*. In addition to covalent conjugates, various types of peptides were synthesized to form nanocomplexes with Cas9 RNPs via electrostatic interactions. Park et al. reported that amphiphilic R7L10 peptides could form stable complexes with Cas9 RNPs.[112] The obtained complexes were able to knockout Bace1 gene in the mouse brain, resulting in the suppression of amyloid beta (Aβ)-associated pathologies and cognitive deficits in two mouse models of Alzheimer's disease. Krishnamurthy et al. rationally designed three shuttle peptides derived from the endosomolytic peptide CM19 and the CPP PTD4 for protein delivery.[113] These shuttle peptides could bind Cas proteins (SpCas9 or AsCas12a) via noncovalent interactions and mediated entry into mouse airway epithelial cells, which enabled gene editing of loxP sites in airway epithelia of ROSAmT/mG mice. Lipid-modified peptides (lipopeptides) were widely used for Cas9 RNP delivery as amphiphilic molecules with tunable properties which can assemble into nanomicelles and have favourable interaction potential with cellular membranes. For example, Thach et al. synthesized lipopeptides derived from a blood–brain barrier permeable peptide dNP2 which was modified with different saturated fatty acids (C8:0, C10:0, C14:0) for the delivery of ‘hyperaccurate’ Cas9 RNPs (HypaRNP).[114] The dNP2 lipopeptides allowed efficient intracellular delivery of HypaRNPs, resulting in up to 26. 7% and 19.7 % genome modifications in human embryonic kidney and glioblastoma cells, respectively. Likewise, Jain et al. designed a tandem peptide that consists of a targeting peptide, a CPP and a lipid tail.[115] By structural optimization, the created tandem peptides successfully delivered Cas9 RNPs in multiple cell lines and achieved robust gene editing. Kuhn et al. developed a library of sequence-defined oligo(ethylenamino) amides, a type of artificial peptides, which are based on the oligoamino acid succinoyl-tetraethylene-pentamine (Stp). The oligomers with T-shape architecture contain a cationizable hydrophilic backbone, flanking tyrosine trimers and fatty acid modifications (lipo-OAA).[45] These lipo-OAAs were demonstrated to form nanoparticles with Cas9/sgRNA without disturbing the integrity of the RNP complex. The systematic variation of fatty acid residues (stearic acid, oleic acid, linoleic acid, nonanamidooctanoic acid, hydroxystearic acid) (Figure 3) revealed a particular importance of this structural element for the editing efficiency.

The lipo-OAA which contains hydroxy-stearic acid outperformed all analogues, inducing up to 40 % EGFP knockout in Neuro2a cells and up to 89 % knockout in HeLa cells. Montenegro and collaborators reported cellular delivery of Cas9 by amphiphilic peptides which were synthesized via hydrazone bond formation between a cationic peptide (Ac-RRLKRLLRRLKRL-NH2) and hydrophobic aldehyde tails.[116] It was found that oleic aldehyde bound peptides (PT24) achieved the best EGFP disruption efficiency.

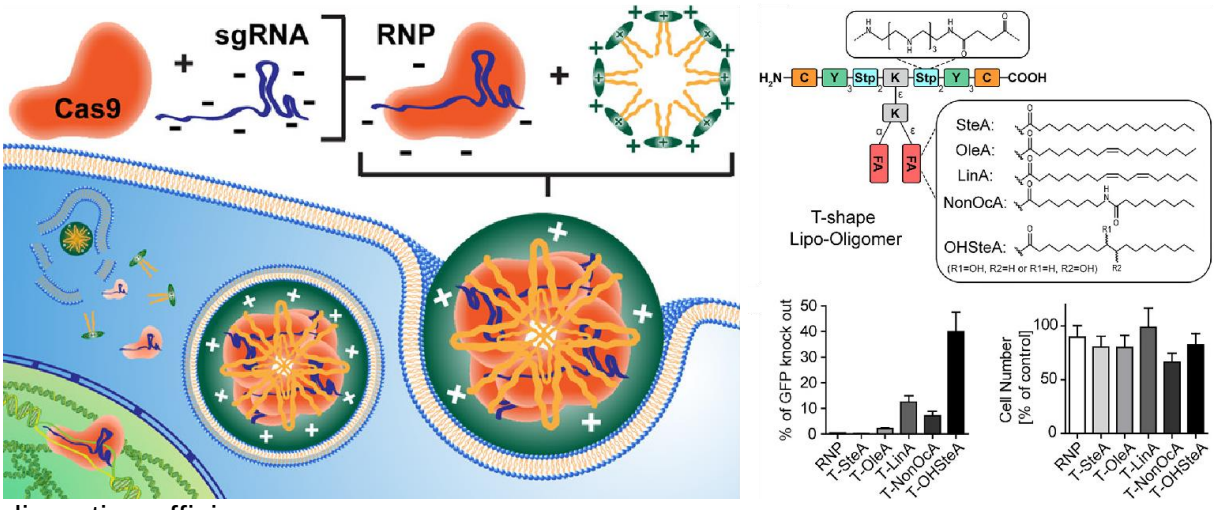

Figure 3. Cas9/sgRNA ribonucleoprotein delivery by lipo-oligoamino amides. Reproduced with permission from ref 45, https://pubs.acs.org/doi/10.1021/acs.bioconjchem.9b00853. Copyright 2020 American Chemical Society. Permission requests related to the material should be directed to the ACS.

1.3.5 Bio-derived vesicles

In recent years, great interest has aroused to construct bio-derived vesicles for Cas9 RNP delivery. Montagna et al. developed vesicular stomatitis virus fusogenic glycoprotein decorated vesicles (VEsiCas), which demonstrated high transfection efficiency and low toxicity in target cells.[117] The study indicated that VEsiCas enabled genome editing in the cardiac muscles of mice and was able to target multiple genome loci. In another study, Campbell et al. produced gesicles by expression of vesicular stomatitis virus glycoprotein with packaged Cas9 RNPs as the cargo.[118] Gesicles with Cas9/sgRNA RNPs targeting the HIV long terminal repeat (LTR) could efficiently edit the LTR region of HIV-NanoLuc CHME-5 cells, which resulted in

reduced proviral activity. Using two different homing mechanisms, Gee et al. developed an all-in-one Cas9 RNP delivery system named NanoMEDIC with significantly enhanced RNP packaging capacity.[119] Specifically, Cas9 protein was loaded into extracellular nanovesicles through chemical induced dimerization and sgRNA was released into vesicles via a viral RNA packaging signal and two self-cleaving riboswitches. It was demonstrated that NanoMEDIC induced over 90 % DMD exon skipping by disruption of splicing regulatory sites in skeletal muscle cells *in vitro* and permanent genomic exon skipping in *mdx* mice *in vivo*. Other RNP loading strategies which were reported make use of the specific interaction of RNA aptamers and aptamer-binding proteins (ABP) or the high binding affinity between GFP and GFP nanobodies.[120,121] Recently, Zhuang et al. developed EVs that were modified with DNA aptamer-conjugated tetrahedral DNA nanostructures (TDNs) via cholesterol anchoring for cell-selective delivery of Cas9 RNPs.[122] The targeting efficiency of different ratios of aptamer/cholesterol were evaluated and it was found that TDNs with 1 : 3 ratio of aptamer/cholesterol increased the accumulation of EVs in HepG2 cells, human primary liver cancer-derived organoids and xenograft tumor models which could be utilized for WNT10B gene disruption with significant tumor growth suppression.

Apart from extracellular vesicles, virus-like particles were reported for Cas9 RNP delivery as another class of bio-derived vehicles. Mangeot et al. fabricated murine leukemia virus (MLV)-like particles to encapsulate Cas9 RNPs.[123] The obtained nanoblades induced efficient genome editing in multiple primary cell lines and enabled genome editing in mouse embryos and livers. Doudna and colleagues demonstrated that HIV envelope glycoprotein-pseudotyped Cas9-VLPs could selectively edit genomes in CD4+ T cells.[124]

1.3.6 DNA-based delivery systems

Based on the principle of complementary base pairing, various types of DNA-based delivery systems were created for the delivery of Cas9 RNPs. Sun et al. reported the first example of DNA nanoclews (DNA NCs) which were synthesized via a rolling circle amplification (RCA).[125] The designed DNA NCs bound to the guide segment of Cas9/sgRNA due to their partially complementary sequences. The obtained

Cas9/sgRNA/NC was further coated with PEI (Cas9/sgRNA/NC/PEI) for enhancement of the endosomal escape. After intratumoral injection, Cas9/sgRNA/NC/PEI induced ~25 % EGFP disruption at the tumor site. Instead of using PEI, Ding et al. generated a non-cationic cross-linked DNA nanogel for Cas9 RNP encapsulation and delivery. Specifically, DNA which is complementary to the tail of sgRNA was firstly grafted on PCL to obtain DNA-*g*-PCL. After binding of the DNA to Cas9/sgRNA, the residual DNA sequences were cross-linked with DNA via hybridization to obtain nanogel-Cas9/sgRNA.[126] *In vitro* transfection showed that the nanogel-Cas9/sgRNA achieved 21.1 % reduction of EGFP fluorescence intensity. Recently, Liu et al. designed a branched DNA-based multifunctional system for co-delivery of Cas9 RNPs and antisense oligonucleotides.[127] By simultaneous targeting DNA in the nucleus and mRNA in the cytoplasm, the resultant DNA nanocomplexes induced efficient down regulation of Plk1 gene and thus resulted in remarkable synergistic antitumoral effects. Besides, stimuli-responsive DNA nanoflowers (DNF) were developed by Shi and co-workers for cell-type-specific genome editing.[128] The designed DNA sequences included DNA aptamers with specificity for tumor cells and miR-21 responsive elements for miRNA-triggered Cas9 RNP release. Compared to non-responsive nanoparticles, the established DNF exhibited enhanced knockout efficiency, resulting in significant suppression of EGFP expression in tumor-bearing mice after intratumoral injection.

1.3.7 Other delivery systems

The asialoglycoprotein receptor (ASGPR), which is predominantly expressed by hepatocytes, is a well-established target receptor for specific delivery to the liver. Rouet et al. designed direct Cas9 conjugates with trimeric ligands of the ASGPR to realize cell-specific delivery of RNPs and genome editing without requirement for an additional delivery system.[129] Cas9-ASGPrL showed increased uptake into HepG2 cells due to receptor-mediated endocytosis and genome modification was observed in the presence of endosomolytic peptides. He et al. reported a multi-armed amphiphilic cyclodextrin (CDEH)-based delivery system for protein delivery. They demonstrated that CDEH could self-assemble with proteins in aqueous environment to form nanoparticles.[130] After further modification with folate ligands via host–guest interactions, the folate-targeted CDEH achieved 47.1 % Plk1 gene deletion and 64.1

% Plk1 protein reduction, which led to efficient inhibition of HeLa tumor growth in vivo. Recently, protein-based delivery systems for Cas9 RNPs were reported. Qiao et al. fabricated a chitosan-coated red fluorescent protein (RFP@CS) core for binding E-tagged Cas9 RNPs and a ssDNA template.[131] The RFP@CS nanoparticles could not only serve as a fluorescent probe but also enabled HDR-editing in vitro. Besides, Zhu et al. reported the first example of a DNAzyme-controlled editing system based on a Y-shaped DNA, biotin–streptavidin interaction and a DNAzyme which releases Cas9 RNPs upon exposure to Mn^{2+}.[132] Pan et al. developed a tetralysine-conjugated H-chain apoferritin (TL-HFn) system for packaging and delivery of Cas9 RNPs. The TL-HFn systems delivered Cas9 RNP into the target cells through TfR1-mediated endocytosis and induced EGFP disruption both *in vitro* and *in vivo*.[133]

1.4 Current clinical trials of CRISPR/Cas

Although numerous delivery technologies and Cas9 variants were developed and scientists from industry as well as academia have put much efforts into the translation of these technologies, the clinical application of the CRISPR/Cas systems is still at an early stage. Generally, *ex vivo* and *in vivo* therapies can be discriminated, depending on the genome editing procedure occurring externally or internally of the human body. T cells, CAR-T cells, lymphocytes, hematopoietic stem and progenitor cells (HSPCs), induced pluripotent stem cells (iPSCs) and induced hepatic stem cells (iHSCs) are cell types of particular interest in current *ex vivo* applications.[134] The native cells are isolated from patients, engineered by genomic modifications and then re-infused into the patients. In 2016, the first CRISPR clinical trial of PD-1 edited T cells in patients with advanced non-small-cell lung cancer (NCT02793856) started at the West China Hospital, Sichuan University. The researchers reported that T cells edited by nucleofection with Cas9 plasmids were generally safe for patients and off-target effects were observed at a low level.[135] However, the desired responses were not observed in the patients, which may be due to insufficient T cell expansion, lack of antigen specificity or low editing efficiency. To improve this, several CRISPR-based ex vivo clinical trials using Cas9 mRNA or Cas9 RNPs as well as combinations with chimeric antigen receptor T cell (CAR-T) therapies are under investigation (NCT03166878, NCT03398967, NCT03545815, NCT03747965 and NCT04037566).

Besides engineered T cells and CAR-T cells, modification of CCR5, BCL11A or mutant HBB in hematopoietic stem and progenitor cells (HSPCs) for treating hematologic diseases using CRISPR/Cas9 systems are in development.[136] In contrast to *ex vivo* applications, where physical methods such as electroporation or nucleofection are feasible approaches to deliver the CRISPR/Cas9 systems, for *in vivo* applications, viral or non-viral vectors are generally required. The first *in vivo* administration of the CRISPR/Cas9 system to humans was conducted with EDIT-101, an AAV5 vector encoding for SaCas9 and two sgRNAs to mediate deletion of a mutated intronic sequence of the CPE290 gene (IVS26) after subretinal injections in patients suffering from Leber's Congenital Amaurosis Type 10.[137] In the ongoing single ascending dose study, 18 participants with LCA10-IVS26 are treated with EDIT-101 (NCT03872479). As discussed above, lipid nanoparticles are used in the first systemically administered CRISPR therapy NTLA-2001 in patients with hereditary transthyretin amyloidosis with polyneuropathy (NCT04601051). An interim report of the ongoing phase 1 clinical study showed an impressive mean reduction of serum TTR protein by 87 % in patients who received a single treatment of NTLA-2001 at a dose of 0.3 mg kg^{-1}, which can be considered a first clinical demonstration of safe and efficient direct *in vivo* genome editing in humans.[138]

1.5 Aim of the thesis

The discovery of the CRISPR/Cas9 system has revolutionized the biomedical research due to its versatility and ease of use. It offers extraordinary potential for developing novel therapeutic approaches for a variety of diseases including cancer. Immune checkpoint blockade (ICB) has recently become one of the most promising strategies in cancer immunotherapies by blocking inhibiting factors of immunity and reverting tumor-induced immune suppression. However, only a portion of patients can respond to this treatment. Permanent disruption of multiple immune checkpoints by CRISPR/Cas9 mayb provide a novel strategy to address this issue.

To achieve it, different CRISPR/Cas9 formats including Cas9 plasmid DNA, Cas9 mRNA/sgRNA and Cas9/sgRNA ribonucleoprotein (RNP) can be selected and introduced into target cells. Direct delivery of pre-assembled Cas9 RNP is generally

considered as a most efficient way since it bypasses transcription and translation processes and can be immediately funcionaly when Cas9 RNP is translocated in the cytosol. Besides, it has less risk of insertional mutagenesis and lower off-target effects. However, efficient intracellular delivery of Cas9 RNP is a major challenge due to its large size and negative charge.

The first aim of the thesis was to develop a receptor-specific Cas9 ribonucleoprotein nanocarrier for ICB-based cancer immunotherapy. The nanocarrier is based on a hydroxystearic acid-containing lipopeptide and further conjugated with a receptor-specific ligand. Cas9 RNPs targeting immune checkpoint genes needed to be loaded in the nanocarriers for immune checkpoint disruption in cancer cells. *In vitro* knockout efficiency of receptor-specific Cas9 RNP nanocarriers needed optimization. The cellular uptake and endosomal escape process of the nanocarriers needed to be investigated. Immune checkpoint knockout efficiency and therapeutic efficacy of the nanocarriers needed to be validated both *in vitro* and *in vivo*.

The second aim of the thesis was to develop a series of hydrophobically balanced lipopeptides for improved intracellular Cas9 RNP delivery and evaluate the correlation between hydrophobicity and gene editing efficiency in Cas9 RNP lipopeptide carriers. The systematic structure variations needed to be introduced into lipopeptide sequences. New hydrophobic artificial amino acids needed to be synthesized. Screening in eGFP knockout and eGFP/BFP HDR assays (required establishment of the assay) needed to be conducted. The impact of individual delivery stages (cellular uptake, endosomal escape, etc.) needed to be demonstrated.

2 Chapter I:

Dual PD-L1/PVR immune checkpoint disruption by receptor-specific Cas9 RNP nanocarriers

Yi Lin[1], Ulrich Wilk[1], Jana Pöhmerer[1], Elisa Hörterer[1], Miriam Höhn[1], Hongcheng Mai[2,3], Ernst Wagner[1], and Ulrich Lächelt[1,4]

[1]Department of Pharmacy and Center for NanoScience (CeNS), LMU Munich, 81377 Munich, Germany
[2]Institute for Tissue Engineering and Regenerative Medicine (iTERM), Helmholtz Zentrum München, 85764 Neuherberg, Germany
[3]Institute for Stroke and Dementia Research (ISD), University Hospital, LMU Munich, 81377 Munich, Germany
[4]Department of Pharmaceutical Sciences, University of Vienna, 1090 Vienna, Austria

The following sections are adapted from the submitted manuscript.

Sections may have been moved for consistency.

2.1 Abstract

Immune checkpoint blockade (ICB) therapy based on monoclonal antibodies has shown remarkable benefits for the treatment of multiple types of cancer. However, not all patients respond to this treatment and immune-related adverse events are often observed during systemic immunotherapies. The CRISPR-Cas system offers new opportunities for cancer therapy by specific targeting and permanent modification of cancer associated genes but is frequently limited by a lack of efficient and tumor-selective delivery systems. Here, we describe a Cas9 ribonucleoprotein (RNP) nanocarrier based on hydroxystearyl oligoamino amides and folic acid (FolA)-PEG as targeting ligand to realize folate receptor (FRα)-specific delivery and gene editing in cancer cells. In vitro studies show that the FolA-modified nanocarriers mediate receptor-dependent cellular delivery of Cas9 RNPs and significantly enhance the knockout of the immune checkpoint genes PD-L1 and PVR in FRα-positive CT26 colon cancer cells. Moreover, the FolA-modified nanocarriers achieve ~25 % dual PD-L1/PVR gene disruption, totally ~40 % gene editing in CT26 tumors *in*

vivo and induce CD8+ T cell recruitment in the tumor tissue. We suggest that the reported receptor-specific Cas9 RNP delivery system represents a versatile platform for therapeutic gene editing and provides a promising strategy to improve cancer immunotherapy by permanent and combined immune checkpoint disruption.

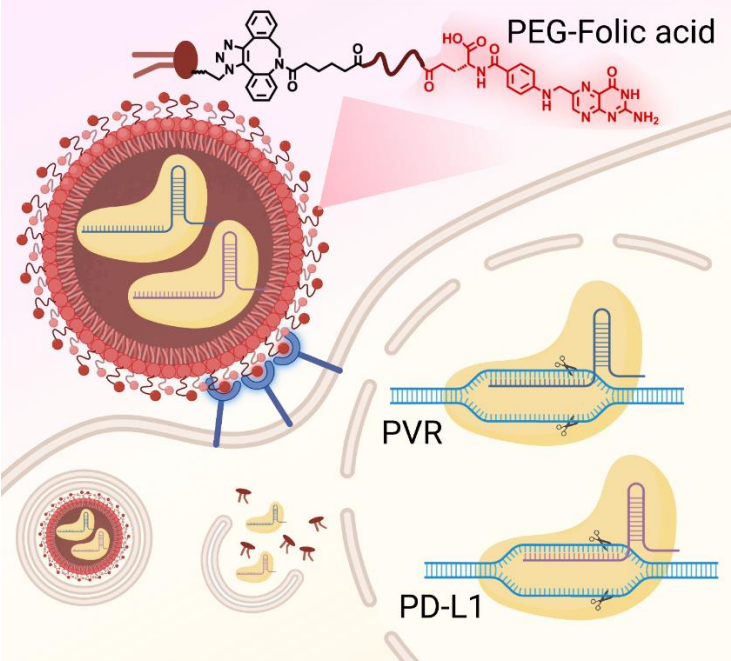

2.2 Introduction

Immune checkpoint blockade (ICB) has emerged as a promising strategy in cancer immunotherapy by blocking inhibition of immunity and reverting tumor-induced immune suppression.[139] Monoclonal antibodies (mAbs) targeting immune checkpoint molecules or their ligands are the most well-established ICB agents.[140] Several ICB therapeutics, such as anti-cytotoxic T lymphocyte-associated antigen 4 (CTLA-4),[141] anti-programmed cell death-1 (PD-1),[142] and anti-programmed cell death ligand-1 (PD-L1) inhibitors,[143] have been approved by the regulatory authorities and demonstrated effectiveness in difficult-to-treat types of cancer. Despite impressive clinical outcome, immune-related adverse events (irAEs), presumably caused by off-target effects after systemic administration of mAbs, were frequently observed.[144] The development of targeted delivery of ICB agents to maximize the therapeutic outcome while minimizing the side effects is highly desirable.[145]

The clustered regularly interspaced short palindromic repeats (CRISPR)/CRISPR-associated protein 9 (Cas9) technology, originally discovered as a type of bacterial adaptive immune system, is a groundbreaking genetic engineering tool which enables editing of genes by introducing double-strand breaks (DSB) at target genomic loci.[2,3,6] Compared to traditional mAbs-based and RNA interference (RNAi)-based checkpoint blockade approaches, the CRISPR/Cas9 system offers the opportunity to permanently disrupt inhibitory genes, which holds great potential for inducing more durable therapeutic immune responses.[146] The first CRISPR clinical trial of PD-1 disrupted T cells generated by *ex vivo* electroporation with Cas9 plasmids was recently reported to be safe and feasible but unfortunately lack sufficient therapeutic efficacy.[135] Instead of disrupting PD-1, knockout of its ligand PD-L1 in tumor cells is an alternative to achieve blockade of the PD-1/PD-L1 axis and has been demonstrated to be effective in evoking the immune system against tumors.[147] However, distinct response towards anti-PD-1/PD-L1 monotherapy was only seen in a minority of treated patients.[148] Thus, discovery of new immune checkpoint pathways and investigation of novel ICB combination therapies are of great interest.[149]

T cell immunoreceptor with immunoglobulin (Ig) and ITIM domain (TIGIT)/poliovirus receptor (PVR) is a newly identified checkpoint axis that recently emerged as a promising immunological target.[150] Blockade of the TIGIT/PVR axis has been found to reverse T cell exhaustion and enhance antitumor efficacy in diverse types of cancer, including breast cancer,[151] hepatocellular carcinoma,[152] head and neck squamous cell carcinoma,[153] colorectal carcinoma[154] and melanoma[155]. Moreover, PVR has been identified as an oncogene with high expression levels in numerous cancers.[156] The increased PVR expression promotes invasion, migration, proliferation and angiogenesis of tumor cells.[157] Studies have shown that knockdown of PVR inhibited tumor growth and reduced metastatic burden in several mouse tumor models.[157,158] Notably, anti-TIGIT/PVR therapy has been found to be more effective in combination with anti-PD-1/PD-L1 therapy.[159] In a recent phase II study, the immunotherapy combination of tiragolumab, an anti-TIGIT antibody, plus atezolizumab, the first anti-PD-L1 antibody, showed clinically relevant improvements for patients with PD-L1-positive metastatic non-small cell lung cancer (NSCLC).[160] Taken together, we speculated that targeted delivery of the CRISPR/Cas9 system to

tumor cells for permanent dual disruption of the PD-L1/PVR immune checkpoints could be a promising strategy for combined ICB therapy.

To achieve this, different CRISPR/Cas9 formats, which are pDNA, mRNA and Cas9/sgRNA ribonucleoproteins (RNPs), can be selected and applied.[161] Delivery of pre-assembled RNPs is generally considered as the most straightforward and efficient strategy.[161] However, the receptor-specific intracellular delivery of Cas9 RNPs still remains a major challenge.[129] Sequence-defined oligo(ethylenamino) amides (OAAs) constructed out of natural and artificial amino acids have been developed as a versatile delivery platform for a variety of biomacromolecules, including pDNA,[162] siRNA,[163] mRNA,[164] proteins[165] and phosphorodiamidate morpholino oligomers (PMOs)[166]. Our previous study has identified a T-shape lipo-OAA containing hydroxystearic acid (T-OHSteA) as a particularly effective structure for Cas9 RNP delivery.[45] By incorporating an azido function into the OAA sequence, the platform can be further extended towards receptor-targeted nanocarriers via copper-free click chemistry with dibenzocyclooctyne (DBCO)-containing targeting ligands.[167] In the current work, we present a folate receptor α (FRα)-specific T-OHSteA-based Cas9 RNP nanocarrier targeting PD-L1 and PVR for dual immune checkpoint disruption at tumor sites (Scheme 1).

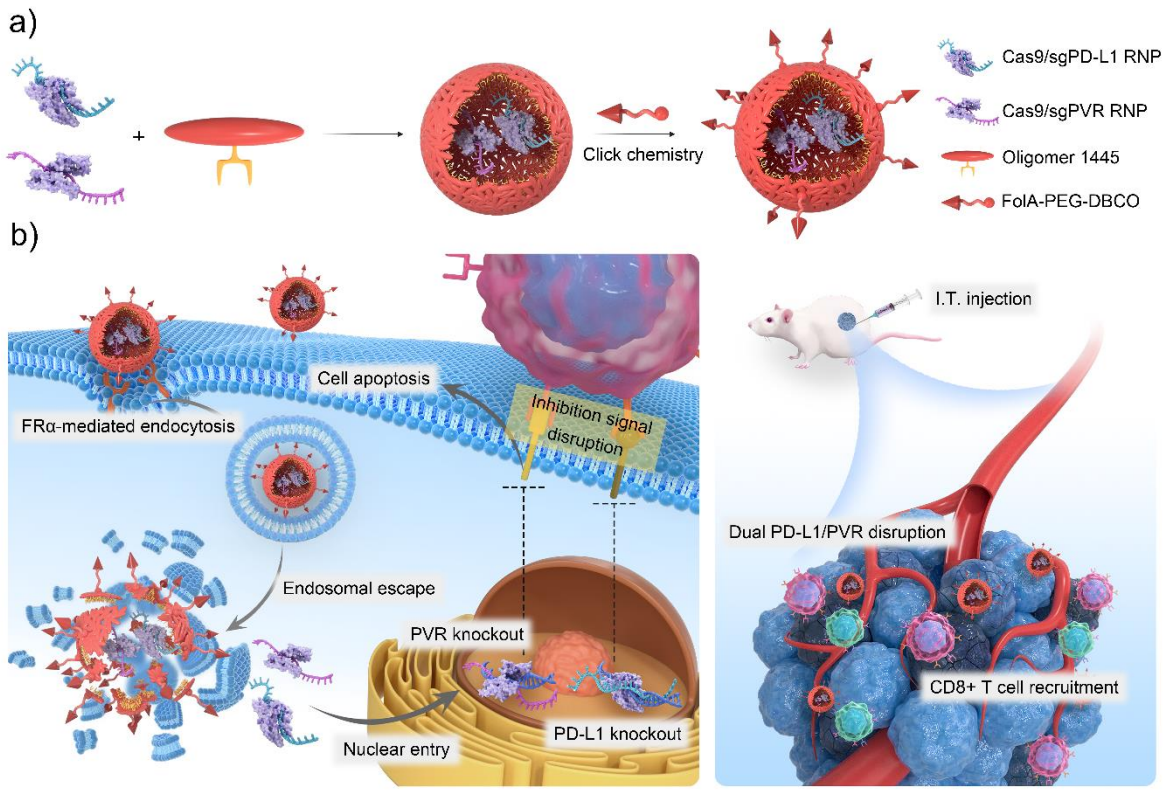

Scheme 1. FRα-specific Cas9 RNP nanocarriers for dual immune checkpoint disruption. a) Fabrication of folate receptor α (FRα)-specific Cas9 RNP nanocarriers targeting PD-L1 and PVR genes. Azide-containing T-shape oligomer #1445 is first complexed with Cas9/sgPD-L1 and Cas9/sgPVR RNPs and subsequently functionalized with folic acid (FolA)-PEG_{24}-DBCO via click chemistry to form the FRα-specific dual RNP-loaded FolA-PEG_{24}-1445 nanocarrier. b) Schematic illustration of FolA-PEG_{24}-1445 nanocarrier-mediated dual immune checkpoint disruption in FRα-overexpressing tumor cells. FRα mediates the endocytosis of FolA-PEG_{24}-1445 nanocarriers. Internalized FolA-PEG24-1445 nanocarriers escape from endosomes and release Cas9/sgPD-L1 and Cas9/sgPVR RNPs into the cytosol. The RNPs enter the nucleus for simultaneous disruption of PD-L1 and PVR immune checkpoint genes. PVR knockout induces cell apoptosis and inhibits cell proliferation. Consequently, intratumoral administration of FolA-PEG_{24}-1445 nanocarriers mediates combined PD-L1/PVR disruption in vivo and promotes CD8+ T cell recruitment in tumor tissues.

2.3 Materials and methods

2.3.1 Chemicals and solvents

Table 1. Chemicals and solvents in alphabetical order

Chemicals and solvents (abbreviations)	Manufacturer

1,2-Ethanedithiol (EDT)	Sigma-Aldrich, Munich, Germany
1,4-Dithiothreitol (DTT)	Sigma-Aldrich, Munich, Germany
1-Hydroxybenzotriazole (HOBt)	Sigma-Aldrich, Munich, Germany
2,5-Dihydroxybenzoic acid (DHB)	Sigma-Aldrich, Munich, Germany
2-Chlorotrityl chloride resin, 200–400 mesh, 1% DVB crosslinking	Iris Biotech, Marktredwitz, Germany
2-Hydroxy-5-methoxybenzoic acid	Sigma-Aldrich, Munich, Germany
3-(4,5-Dimethylthiazol-2-yl)-2,5-diphenyltetrazolium bromide (MTT)	Sigma-Aldrich, Munich, Germany
4′,6-Diamidino-2-phenylindole (DAPI)	Sigma-Aldrich, Munich, Germany
Acetonitrile (ACN)	VWR, Darmstadt, Germany
Agarose	Sigma-Aldrich, Munich, Germany
Aminoallyl-UTP-Cy3	Jena Bioscience, Jena, Germany
ATTO647N NHS-ester	ATTO-TEC, Siegen, Germany
(Benzotriazol-1-yloxy)tripyrrolidinophosphonium hexafluorophosphate (Pybop®)	Multisyntech, Witten, Germany
Chloramphenicol	Sigma-Aldrich, Munich, Germany
Chloroform-d	Sigma-Aldrich, Munich, Germany
Deuterium Oxide	Sigma-Aldrich, Munich, Germany
Dibenzocyclooctyne acid (DBCO)	Sigma-Aldrich, Munich, Germany
Dichloromethane (DCM)	Bernd Kraft, Duisburg, Germany
Dimethyl sulfoxide (DMSO)	Acros Organics, Geel, Belgium
Di-*tert*-butyl dicarbonate (Boc_2O)	Sigma-Aldrich, Munich, Germany
Ethylenediaminetetraacetic acid disodium salt dihydrate (EDTA)	Sigma-Aldrich, Munich, Germany
Fatty acids	Sigma-Aldrich, Munich, Germany
Fetal bovine serum (FBS)	Life Technologies, Carlsbad, USA
N-α-Fmoc-*L*-glutamic acid α-2-phenylisopropyl ester (Fmoc-Glu-O-2-PhiPr)	VWR, Darmstadt, Germany
Fmoc-N-amido-dPEG24-acid	Quanta Biodesign, Powell, Ohio, USA
Fmoc-Stp(Boc_3)-OH building block	In-house synthesis[1]
Fmoc-α-amino acids	Iris Biotech, Marktredwitz, Germany
GelRed™	VWR, Darmstadt, Germany
Glucose	Sigma-Aldrich, Munich, Germany
Hydrazine monohydrate	Sigma-Aldrich, Munich, Germany
Hydrochloric acid solution (1 M) (1 M HCl)	Bernd Kraft, Duisburg, Germany
Imidazole	Sigma-Aldrich, Munich, Germany
Isopropyl β-*D*-1-thiogalactopyranoside (IPTG)	Sigma-Aldrich, Munich, Germany
Kanamycin	Sigma-Aldrich, Munich, Germany
Magnesium chloride ($MgCl_2$)	Sigma-Aldrich, Munich, Germany
Methanol (MeOH)	Iris Biotech, Marktredwitz, Germany
Methyl *tert*-butyl ether (MTBE)	Brenntag GmbH, Essen, Germany

N-(2-hydroxyethyl)piperazine-N′-(2-ethanesulfonic acid) (HEPES)	Biomol GmbH, Hamburg, Germany
N,N-Diisopropylethylamine (DIPEA)	Iris Biotech, Marktredwitz, Germany
N,N-Dimethylformamide (DMF)	Iris Biotech, Marktredwitz, Germany
N^{10}-(Trifluoroacetyl)pteroic acid	Clauson-Kass A/S, Farum, Denmark
n-Hexane	Grüssing GmbH, Filsum, Germany
Paraformaldehyde (PFA)	Sigma-Aldrich, Munich, Germany
Penicillin	Biochrom, Berlin, Germany
Phenylmethylsulfonylfluorid (PMSF)	Carl Roth, Karlsruhe, Germany
Piperidine	Iris Biotech, Marktredwitz, Germany
Potassium chloride (KCl)	Sigma-Aldrich, Munich, Germany
Potassium phosphate monobasic (KH_2PO_4)	Sigma-Aldrich, Munich, Germany
Sodium chloride (NaCl)	Sigma-Aldrich, Munich, Germany
Sodium hydroxide (NaOH)	Sigma-Aldrich, Munich, Germany
Sodium phosphate dibasic (Na_2HPO_4)	Sigma-Aldrich, Munich, Germany
Streptomycin	Biochrom, Berlin, Germany
Sucrose	Sigma-Aldrich, Munich, Germany
Trifluoro acetic acid (TFA)	Iris Biotech, Marktredwitz, Germany
Triisopropylsilane (TIS)	Sigma-Aldrich, Munich, Germany
Triton X-100	Sigma-Aldrich, Munich, Germany
Trizma® base	Sigma-Aldrich, Munich, Germany

2.3.2 sgRNAs and oligonucleotides

The sgRNAs used for *in vitro* knockout experiments were synthesized by T7 *in vitro* transcription. The sgRNAs used for *in vivo* knockout experiments were chemically modified (2’ O-methyl modification on the first 3 and last 3 RNA bases) and purchased from Integrated DNA Technologies (IDT, USA). The sequences of ssDNA oligonucleotides for assembly of dsDNA template, sgRNAs after *in vitro* transcription, and chemically modified sgRNAs are shown below.

Table 2. ssDNA oligonucleotides for assembly of dsDNA templates (5’ → 3’)

F-sgGFP	GCGGCCTCTAATACGACTCACTATAGGACCAGGATGGGCACCACCCGTTTTAGAGCTAGAAATAGCA
F-sgCtrl	GCGGCCTCTAATACGACTCACTATAGGGTAACCGTGCGGTCGTACGTTTTAGAGCTAGAAATAGCA
F-sgFRα	TTCTAATACGACTCACTATAGAGGGTTTAACAAGTGCGCAGGTTTTAGAGCTAGA
F-sgPD-L1_1	GCGGCCTCTAATACGACTCACTATAGGTCCAGCTCCCGTTCTACAGTTTTAGAGCTAGAAATAGCA
F-sgPD-L1_2	GCGGCCTCTAATACGACTCACTATAGTATGGCAGCAACGTCACGAGTTTTAGAGCTAGAAATAGCA
F-sgPD-L1_3	GCGGCCTCTAATACGACTCACTATAGCTTGCGTTAGTGGTGTACTGTTTTAGAGCTAGAAATAGCA

F-sgPD-L1_4	GCGGCCTCTAATACGACTCACTATAGACTTGTACGTGGTGGAGTAGTTTTAGAGCTAGAAATAGCA
F-sgPVR_1	GCGGCCTCTAATACGACTCACTATAGCTACAATTCGACAGGCGTCTGTTTTAGAGCTAGAAATAGCA
F-sgPVR_2	GCGGCCTCTAATACGACTCACTATAGCAGCCATGACAGCGGGGAGGTTTTAGAGCTAGAAATAGCA
F-sgPVR_3	GCGGCCTCTAATACGACTCACTATAGCTTCTAATCTCCACCGTAGGTTTTAGAGCTAGAAATAGCA
R-sgRNA	AAAAAAAGCACCGACTCGGTGCCACTTTTTCAAGTTGATAACGGACTAGCCTTATTTTAACTTGCTATTTC TAGCTCTAAAAC

Table 3. sgRNAs after *in vitro* transcription (5' → 3')

sgGFP	GACCAGGAUGGGCACCACCCGUUUUAGAGCUAGAAAUAGCAAGUUAAAAUAAGGCUAGUCCGUU AUCAACUUGAAAAAGUGGCACCGAGUCGGUGCUUUUUUU
sgCtrl	GGGUAACCGUGCGGUCGUACGUUUUAGAGCUAGAAAUAGCAAGUUAAAAUAAGGCUAGUCCGUU AUCAACUUGAAAAAGUGGCACCGAGUCGGUGCUUUUUUU
sgFRα	GGGUUUAACAAGUGCGCAGUGUUUUAGAGCUAGAAAUAGCAAGUUAAAAUAAGGCUAGUCCGUU AUCAACUUGAAAAAGUGGCACCGAGUCGGUGCUUUUUUU
sgPD-L1_1	GGUCCAGCUCCCGUUCUACAGUUUUAGAGCUAGAAAUAGCAAGUUAAAAUAAGGCUAGUCCGUU AUCAACUUGAAAAAGUGGCACCGAGUCGGUGCUUUUUUU
sgPD-L1_2	GUAUGGCAGCAACGUCACGAGUUUUAGAGCUAGAAAUAGCAAGUUAAAAUAAGGCUAGUCCGUU AUCAACUUGAAAAAGUGGCACCGAGUCGGUGCUUUUUUU
sgPD-L1_3	GCUUGCGUUAGUGGUGUACUGUUUUAGAGCUAGAAAUAGCAAGUUAAAAUAAGGCUAGUCCGUU AUCAACUUGAAAAAGUGGCACCGAGUCGGUGCUUUUUUU
sgPD-L1_4	GACUUGUACGUGGUGGAGUAGUUUUAGAGCUAGAAAUAGCAAGUUAAAAUAAGGCUAGUCCGUU AUCAACUUGAAAAAGUGGCACCGAGUCGGUGCUUUUUUU
sgPVR_1	GCUACAAUUCGACAGGCGUCUGUUUUAGAGCUAGAAAUAGCAAGUUAAAAUAAGGCUAGUCCGU UAUCAACUUGAAAAAGUGGCACCGAGUCGGUGCUUUUUUU
sgPVR_2	GCAGCCAUGACAGCGGGGAGGUUUUAGAGCUAGAAAUAGCAAGUUAAAAUAAGGCUAGUCCGUU AUCAACUUGAAAAAGUGGCACCGAGUCGGUGCUUUUUUU
sgPVR_3	GCUUCUAAUCUCCACCGUAGGUUUUAGAGCUAGAAAUAGCAAGUUAAAAUAAGGCUAGUCCGUU AUCAACUUGAAAAAGUGGCACCGAGUCGGUGCUUUUUUU

Table 4. Chemically modified sgRNAs obtained from commercial source (5' → 3')

sgCtrl	mG*mG*mG*rUrArArCrCrGrUrGrCrGrGrUrCrGrUrArCrGrUrUrUrUrArGrArGrCrUrArGrArArArUrArGrCrAr ArGrUrUrArArArArUrArArGrGrCrUrArGrUrCrCrGrUrUrArUrCrArArCrUrUrGrArArArArArGrUrGrGrCrArCr CrGrArGrUrCrGrGrUrGrCmU*mU*mU*rU
sgPD-L1_4	mG*mA*mC*rUrUrGrUrArCrGrUrGrGrUrGrGrArGrUrArGrUrUrUrUrArGrArGrCrUrArGrArArArUrArGrCrAr ArGrUrUrArArArArUrArArGrGrCrUrArGrUrCrCrGrUrUrArUrCrArArCrUrUrGrArArArArArGrUrGrGrCrArCr CrGrArGrUrCrGrGrUrGrCmU*mU*mU*rU
sgPVR_3	mG*mC*mU*rUrCrUrArArUrCrUrCrCrArCrCrGrUrArGrGrUrUrUrUrArGrArGrCrUrArGrArArArUrArGrCrAr ArGrUrUrArArArArUrArArGrGrCrUrArGrUrCrCrGrUrUrArUrCrArArCrUrUrGrArArArArArGrUrGrGrCrArCr CrGrArGrUrCrGrGrUrGrCmU*mU*mU*rU

Table 5. Sequences of PCR primers (5' → 3')

PD-L1-F	TGGTTCCTTTTAAACAAGACTGGG
PD-L1-R	CGCACCACCGTAGCTGATTA

PVR-F	AGAGCCCTGGTATCGGATCT
PVR-R	ACCCACATCCCACTGCTAAG
FRα-F	GACCATGGAGCAGGAACC
FRα-R	CAGCTCCAGTTCTATTCGG

2.3.3 Buffers and solutions

Deionized water was purified in-house using a Millipore system (Simplicity Plus, Millipore Corp.) and was used for all experiments.

Kaiser test solutions: 80 % (w/v) phenol in EtOH; 5 % (w/v) ninhydrine in EtOH; 20 µM KCN in pyridine (2 mL of 1 mM KCN (aq) in 98 mL of pyridine).

HEPES buffered glucose (HBG): 20 mM HEPES, 5 % w/v glucose, pH 7.4.

Phosphate buffered saline (PBS): 136.89 mM sodium chloride, 2.68 mM potassium chloride, 8.10 mM sodium phosphate dibasic heptahydrate, 1.47 mM potassium dihydrogen phosphate, pH 7.4.

Tris/Borate/EDTA (TBE) 10 × buffer: 1.49 M tris base, 0.89 M boric acid, 20 mM EDTA, pH 8.0.

FACS buffer: PBS buffer containing 10 % FBS, pH 7.4.

2.3.4 Synthesis of hydroxystearic acid (OHSteA)

Firstly, oleic acid (2 g, 7.08 mmol) was dissolved in TFA/CH_2Cl_2 (2:1, 30 mL) and stirred for 3 days at room temperature. Afterwards, the solvent was removed by a nitrogen flow to obtain hydroxystearic acid TFA ester (2.67 g, 6.73 mmol, yield: 95.1 %). Secondly, the hydroxystearic acid TFA ester (2.67 g, 6.73 mmol) was dissolved in 1 M NaOH methanol/water (4:1, 30 mL) mixture and stirred overnight. 1 M HCl solution was added to the reaction to adjust pH to 1-2 and then the mixture was centrifuged. The supernatant was collected and evaporated to remove the solvent. The obtained light brown powder was dissolved in water and extracted 3 times with DCM. The DCM phase was combined and evaporated to generate the white powder hydroxystearic acid (1.58 g, 5.26 mmol, yield: 78.2%).

2.3.5 Solid-phase synthesis

Synthesis of oligomer 1445

The synthesis of the artificial amino acid Fmoc-Stp(Boc)$_3$-OH (Stp) was described previously by Schaffert et al.[168] Firstly, the 1445 backbone of C(Trt)-[Y(tBu)]$_3$-[Stp(Boc)$_3$]$_2$-K(Dde)-[Stp(Boc)$_3$]$_2$-[Y(tBu)]$_3$-C(Trt)-Lys(N_3) (C → N) was synthesized manually using standard Fmoc solid-phase peptide synthesis conditions. Coupling step was performed using 4 eq Fmoc-amino acid, 4 eq HOBt, 4 eq PyBOP, and 8 eq DIPEA in DCM/DMF (1:1, 5 mL g^{-1} resin) for 75 min. Fmoc deprotection step was carried out by 3 times incubation with 20 % piperidine in DMF (5 mL g^{-1} resin) for 15 min. After each coupling and deprotection step, the resin was washed 3 times with DMF and 3 times with DCM sequentially followed by a Kaiser test. After the last deprotection of Fmoc-Lys(N_3)-OH, the N-terminal NH_2-group was protected with 10 eq Boc_2O and 10 eq DIPEA in DCM/DMF (1:1, 5 mL g^{-1} resin). Dde deprotection step was accomplished by 15 times incubation with 2 % hydrazine in DMF for 2 min. Afterwards, the resin was washed 5 times with DMF, 5 times with 10 % DIPEA in DMF, and 3 times with DCM (5 mL g^{-1} resin each) sequentially. Subsequently, Fmoc-Lys(Fmoc)-OH was introduced followed by the coupling of hydroxystearic acid. The resin was washed 3 times with DMF and DCM sequentially and dried in vacuo.

Synthesis of DBCO agents

FolA-PEG$_{24}$-DBCO and PEG$_{24}$-DBCO were synthesized manually as described above using Fmoc-Lys(Dde)-OH and Fmoc-N-amido-dPEG$_{24}$-acid preloaded resin, respectively.[169] For FolA-PEG$_{24}$-DBCO, Fmoc-Glu-O-2-PhiPr and N^{10}-(trifluoroacetyl)pteroic acid were coupled in sequence to generate folic acid. Then, a Dde deprotection step was carried out as described above. To deprotect the trifluoroacetyl group of pteroic acid, the resin was incubated 4 times with 25 % aqueous ammonia solution/DMF (1:1, 5 mL g^{-1} resin) for 30 min. Afterwards, Fmoc-dPEG$_{24}$-OH was introduced followed by the coupling of DBCO acid. The resin was washed 3 times with DMF and DCM sequentially and dried in vacuo.

Cleavage and purification

The oligomer was cleaved off the resin by incubation with pre-cooled cleavage cocktail TFA/EDT/H$_2$O/TIS (94:2.5:2.5:1, 10 mL g^{-1} resin) for 60 min. The solution was immediately precipitated in pre-cooled MTBE/n-hexane (1:1, 45 mL). Afterwards, the oligomer was purified by a Äkta purifier system (GE Healthcare Bio-Sciences AB, Uppsala, Sweden) using 10 mM HCl/ACN (7:3) as the mobile phase. The collected fractions were snap frozen and lyophilized to obtain the final products.

DBCO agents were cleaved off the resin by incubation with pre-cooled cleavage cocktail DCM/TFA/TIS (92.5:5:2.5, 10 mL g^{-1} resin) for 60 min. The solution was immediately precipitated in pre-cooled MTBE/n-hexane (2:8, 45 mL). Afterwards, the precipitate was dissolved in 5 mL of 0.05 M NaOH solution, and the pH was adjusted to 7. The agents were purified by dialysis using a dialysis membrane (RC, MWCO: 1000 Da) against deionized water for 48 h. Deionized water was changed every 8 hours. The solution was snap frozen and lyophilized to obtain the final products.

2.3.6 Analytical methods

Proton ^{1}H NMR spectroscopy

All ^{1}H NMR spectra were recorded on an Advance III HD Bruker BioSpin (400 MHz) equipped with a Cryo Probe™ Prodigy probe head without TMS. The chemical shifts

were calibrated to the residual solvent signal and were reported in parts per million (ppm). The spectra were processed in MestReNova software (MestReLab Research, SL). Integration was performed manually.

MALDI mass spectrometry

Super-DHB consisting of 2,5-dihydroxybenzoic acid and 2-hydroxy-5-methoxybenzoic acid (9:1, m/m) in H_2O/ACN/TFA (69.93:30:0.07) was prepared as matrix solution. 1 µL of the solution was spotted on an MTP AnchorChip (Bruker Daltonics, Bremen, Germany). After drying of the matrix, 1 µL of sample solution (1 mg/mL in water) was added to the dried matrix. All mass spectra were recorded on an Autoflex II mass spectrometer (Bruker Daltonics, Bremen, Germany) in the positive ion mode.

2.3.7 Cas9 protein expression and purification

Cas9 protein expression and purification were performed as described previously.[45] In brief, a plasmid pET28a/Cas9-Cys (Addgene plasmid no. 53261; http://n2t.net/addgene:53261; RRID: Addgene_53261) was transformed into Rosetta 2(DE3)pLysS (Merck Millipore, Germany) as expression strain. An overnight culture was prepared from a monoclonal glycerol stock which was inoculated into LB medium containing kanamycin and chloramphenicol and incubated at 37 °C. Afterwards, the bacterial culture was diluted with LB medium (+kanamycin, +chloramphenicol) and incubated at 37 °C until an optical density at 600 nm (OD 600) of 0.5 − 0.7 was reached. Then, 1 mM isopropyl β-D-1-thiogalactopyranoside (IPTG) was added to the bacterial suspension to induce Cas9 protein expression, and the culture was incubated overnight at RT. On the next day, bacteria were harvested and resuspended in bacterial lysis buffer (20 mM trizma-base, 0.2 M NaCl, 20 % sucrose, 10 mM $MgCl_2$, pH 7.5) followed by the addition of 30 µg/mL DNase, 10 µg/mL RNase, 1 mg/mL lysozyme, and 1 mM phenylmethylsulfonylfluorid (PMSF). The lysed suspension was frozen in liquid nitrogen, thawed on ice, and sonicated 3 times on ice for 20 seconds. The bacterial lysate was ultra-centrifuged (20000 rpm) at 4 °C for 1 h followed by filtration using a syringe filter (0.45 µm).

The purification of Cas9 protein was performed by nickel chromatography (HisTrap HP column, GE Healthcare, Sweden). Afterwards, the collected fractions containing Cas9 were concentrated and further purified with an Äkta purifier using storage buffer (20 mM HEPES, 200 mM KCl, 10 mM $MgCl_2$, and 1 mM DTT) as the solvent. The fractions containing Cas9 were collected, and the concentration of Cas9 protein was measured with a Nanodrop photometer (Thermo Scientific, USA) using an extinction coefficient of ε/1.000 = 120 M^{-1} cm^{-1}. The Cas9 solution was aliquoted and stored at −80 °C.

2.3.8 ATTO647N-Cas9 preparation

ATTO647N-Cas9 was prepared as described previously.[45] In brief, Cas9 protein was diluted in HEPES (20 mM, pH 7.4) to a concentration of 1 mg/mL, and the pH was adjusted to 8.0 using 0.2 M sodium bicarbonate solution. Afterwards, 1.5-fold molar excess of ATTO647N NHS-ester dissolved in DMSO (10 mM) was added to the Cas9 solution. The resulting solution was stirred at RT for 1 h. ATTO647N-labelled Cas9 was purified with an Äkta purifier system (GE Healthcare Bio-Sciences AB, Sweden) using storage buffer (20 mM HEPES, 200 mM KCl, 10 mM $MgCl_2$, 1 mM DTT) as the solvent. The fractions containing ATTO647N-Cas9 were combined, and the concentration of ATTO647N-Cas9 was measured with a Nanodrop photometer (Thermo Scientific, USA) using an extinction coefficient of ε/1.000 = 120 M^{-1} cm^{-1}. The ATTO647N-Cas9 solution was aliquoted and stored at −80 °C.

2.3.9 *In vitro* transcription of sgRNAs

In vitro transcribed sgRNAs were prepared as described previously.[45] In brief, two single-stranded DNA (ssDNA) oligonucleotides were annealed, extended using T4 DNA polymerase (NEB, Germany), and then purified with a QIAquick PCR Purification Kit (QIAGEN, Germany). The obtained DNA template was transcribed using the HiScribe T7 High Yield RNA Synthesis Kit (NEB, Germany) followed by the purification of the generated sgRNA with a RNeasy Micro Kit (QIAGEN, Germany). The purified sgRNA was heated to 80 °C for 2 min, immediately snap frozen, and stored at −80 °C.

2.3.10 Formulation of Cas9 RNP nanocarriers

The Cas9 RNP complexes were formed by mixing the Cas9 protein with sgRNA at 1:1 molar ratio and incubation for 15 min at RT. The obtained RNP and the amount of oligomer 1445 corresponding to a N/P (nitrogen to phosphate) ratio of 24 were diluted separately with HBG to equal volumes. The RNP was added to the oligomer solution, mixed thoroughly by pipetting up and down and finally incubated for 15 min at RT to give the final formulation. In case of the shielded and targeted formulations, the RNP nanocarriers were further conjugated with different DBCO agents (PEG_{24}-DBCO or FolA-PEG_{24}-DBCO). Varied equivalents (defined as molar ratios of DBCO agent to oligomer) of DBCO agents diluted in one-fourth volume of the RNP nanocarriers were added to the non-shielded formulation, followed by 5 times pipetting up and down and 4 h incubation at RT.

2.3.11 Measurement of particle size and zeta potential

Dynamic and electrophoretic light scattering were applied for the determination of hydrodynamic particle size and zeta potential of Cas9 RNP nanocarriers. For the size measurements, 100 µL of RNP nanocarriers containing 1.25 µg Cas9 protein and 0.25 µg sgRNA (1:1 molar ratio) in HBG was measured 3 times with 13 sub-runs at a fixed scattering angle of 173°. Afterwards, 700 µL of HEPES buffer (20 mM, pH 7.4) was added to each sample, and zeta potential was analyzed 3 times with 12-15 sub-runs. All measurements were performed in folded capillary cells (DTS 1070) using a Zetasizer Nano ZS (Malvern Instruments, UK). The refractive index (RI) of the solvent was 1.330, the viscosity was 0.8872 mPa·s, and the temperature was set to 25 °C.

2.3.12 Transmission electron microscopy (TEM)

Non-shielded, FolA-PEG_{24}-DBCO or PEG_{24}-DBCO modified Cas9 RNP nanocarriers (modification ratio 0.75 eq) were formulated in distilled water as described in paragraph 2.1. The hydrophilized carbon coated copper grids (Ted Pella, Redding, CA, USA, 300 mesh, 3.0 mm OD) were placed on top of 10 µL of sample droplets for 20 s. Subsequently, the sample solution was removed using a filter paper, stained

with 1.0 % uranyl formate in water, and allowed to dry for 20 min. All samples were detected using a JEM-1100 electron microscope (JEOL, Tokyo, Japan) with 80 kV acceleration voltage.

2.3.13 Ribogreen assay

Encapsulation efficiency of Cas9/sgRNA RNP complexes was determined using a Quant-iTTM RiboGreen® RNA assay kit (Invitrogen, CA, USA). 50 µL of RNP nanocarriers containing 250 ng sgRNA was mixed with 50 µL of TE buffer in the presence or absence of 2 % (v/v) Triton X-100 (Sigma Aldrich, Gillingham, UK). A standard curve of the sgRNA was prepared in TE buffer as well. Afterwards, the samples were added to a 96-well plate followed by incubation for 10 min at 37 °C. Subsequently, 100 µL of Ribogreen solution (diluted 1:100 in TE buffer) was added to each well. The plate was incubated for another 5 min. Ribogreen fluorescence intensity of each well was detected using a microplate reader (Spectrafluor Plus, Tecan, Männedorf, Switzerland) with excitation and emission wavelength of 485 and 528 nm, respectively. The sgRNA concentration of RNP nanocarriers with or without Triton X-100 lysis was calculated based on the sgRNA standard curve. After subtraction of the blank wells, the encapsulation efficiency (in percentage) was calculated as $(1 - (\text{nanocarriers without lysis} / \text{nanocarriers with lysis})) \times 100$ %. All studies were performed in triplicate.

2.3.14 Agarose gel shift assay

A 2 % (w/v) agarose gel containing GelRed® (Biotium, Hayward, CA, USA) was prepared using 1 × TBE buffer. 20 µL of Cas9 RNP nanocarriers at a concentration of 75 nM RNP in HBG buffer was mixed with 4 µL of 6 × loading buffer followed by sample loading in the gel pockets. The electrophoresis was carried out at 100 V for 75 min.

2.3.15 Long-term stability

Cas9 RNP nanocarriers with or without ligand modification (0.75 eq) were prepared. Afterwards, the nanocarriers were aliquoted and directly stored at different temperatures (4 °C, -20 °C, or -80 °C), or first lyophilized and then stored at -80 °C. At determined time points, 100 µL of RNP nanocarriers was taken or reconstituted for size and zeta potential measurements.

2.3.16 Cell culture

CT26 WT, CT26 eGFP/luc, HeLa eGFP/tub, FRα-knockout HeLa eGFP/tub, and HeLa mRuby3/gal8 cells were grown in DMEM medium supplemented with 10 % FBS, 100 U/mL penicillin, and 100 µg/mL streptomycin. The cells were cultured in ventilated flasks in the cell incubator at 37 °C and 5 % CO2 in a humidified atmosphere. The cells were passaged at a confluency of approximately 80 %.

FRα-knockout HeLa eGFP/tub cells were generated by using Cas9/sgFRα ribonucleoproteins and a hydroxystearyl oligo(ethylenamino) amide #1105 as previously reported.[45] FRα-knockout single-cell derived lines were isolated by limiting dilution from the transfected pools. The detection of FRα was performed using allophycocyanin (APC)-conjugated α-FolR1 IgG1 antibody by FACS. The genomic DNA of the identified FRα-negative cells was extracted and the sgFRα target regions of FRα gene were amplified with the FRα-F and FRα-R primers. The knockout of FRα gene was further confirmed by sequencing the purified amplicons by Eurofins GATC Biotech (Germany) with the primer FRα-F.

2.3.17 eGFP reporter gene knockout by flow cytometry

One day prior to knockout experiments, CT26 eGFP/luc, HeLa eGFP/tub or FRα-knockout HeLa eGFP/tub cells were seeded into 96-well plates at a density of 5000 cells/well. On the next day, the medium in each well was replaced with 75 µL of fresh medium.

To optimize the FRα-specific gene knockout, 25 µL of RNP nanocarriers with or without different equivalents of FolA-PEG_{24}-DBCO or PEG_{24}-DBCO modification was

added into each well resulting in a final concentration of 75 nM RNP complexes. For the dose titration experiment, RNP nanocarriers with or without 0.75 eq (for CT26 eGFP/luc cells) or 0.5 eq (for HeLa eGFP/tub cells) ligand modification were formulated and then diluted to prepare a series of dilutions with different concentrations of RNP. 25 µL of dilutions were added to each well resulting in final concentrations of RNP ranging from 1 nM to 100 nM. To test the knockout efficiency after long-term storage, 25 µL of the samples was taken or reconstituted and then added into each well resulting in a final concentration of 75 nM RNP. After 4 h, the medium in each well was replaced with 100 µL of fresh medium and the cells were incubated for 44 h.

For optimizing the transfection time, RNP nanocarriers with or without 0.75 eq (for CT26 eGFP/luc cells) or 0.5 eq (for HeLa eGFP/tub cells) ligand modification were applied. The cells were incubated for different times (15 min, 30 min, 45 min, 1 h, 2 h, 4 h or 48 h). After replacement with fresh medium, the cells were further incubated to reach the total incubation time of 48 h.

Afterwards, the cells were trypsinized and transferred to 24-well plates. After another 3 days incubation, the cells were harvested and resuspended in 600 µL of FACS buffer. The samples were analyzed by flow cytometry on a CytoFLEX S flow cytometer (Beckman Coulter, CA, USA). Before the measurement, 1 ng/µL DAPI was added to differentiate between live and dead cells. The DAPI signal was detected with 405 nm excitation and 450 nm emission. The eGFP fluorescence was assayed with 488 nm excitation and 530 nm emission. Ten thousand of isolated live cells were counted and evaluated. The data were analyzed using FlowJo 7.6.5 by FlowJo, LLC (Becton, Dickinson and Company, USA). All studies were performed in triplicate.

2.3.18 Cell viability assay (MTT) after eGFP reporter gene knockout

MTT assay was performed to determine the cell viability after treatments of CT26 eGFP/luc, HeLa eGFP/tub, or FRα-knockout HeLa eGFP/tub cells with Cas9 RNP nanocarriers. After 48 h total incubation, 10 µL of MTT (5 mg/mL) was added to each well. The cells were incubated for 2 h in the incubator. Afterwards, the medium was discarded, and the plates were frozen at – 80 °C overnight. 100 µL of DMSO was then added to each well to dissolve the formed formazan product. The plates were

incubated for 30 min at 37 °C under shaking. The absorbance of each well was measured at 590 nm with background correction at 630 nm using a microplate reader (Tecan Spark 10M, Tecan, Männedorf, Switzerland). The relative cell viability (in percentage) was calculated relative to control wells treated with HBG buffer as ([A] test/[A] control) × 100 %. All experiments were conducted in triplicate.

2.3.19 Cellular uptake by flow cytometry

One day prior to the cellular uptake experiments, CT26 WT, HeLa WT, or FRα-knockout HeLa cells were seeded into 24-well plates at a density of 25000 cells/well. On the next day, the medium in each well was replaced with 375 µL of fresh medium. RNP nanocarriers with or without 0.75 eq (for CT26 WT cells) or 0.5 eq (for HeLa WT cells) ligand modification were prepared as described above using 20 % of ATTO647N-Cas9 and 20 % of Cy3-sgRNA. 125 µL of the nanocarriers was added to each well resulting in a final concentration of 75 nM RNP complexes. The cells were incubated for 45 min, 2 h or 4 h. Afterwards, the cells were harvested, prepared and analyzed by flow cytometry as described above. The DAPI signal was detected with 405 nm excitation and 450 nm emission. The ATTO647N fluorescence was assayed with 640 nm excitation and 670 nm emission. And the Cy3 fluorescence was detected with 550 nm excitation and 570 nm emission. All experiments were performed in triplicate.

2.3.20 Cellular uptake by confocal laser scanning microscopy (CLSM)

CT26 WT cells were seeded in 8-well Ibidi µ-slides (Ibidi GmbH, Germany) at a density of 15000 cells/well 24 h prior to the treatment. On the next day, the medium was replaced with 225 µL of fresh medium. 75 µL of RNP nanocarriers containing 20 % of ATTO647N-Cas9 and 20 % of Cy3-sgRNA was added to each well resulting in a final concentration of 75 nM RNP. After 4 h, the medium was discarded and the cells were washed twice with 300 µL of PBS. Subsequently, 300 µL of PBS containing heparin (500 IU/mL) was added to disassociate extracellular nanocarriers from the cell membrane. The cells were incubated on ice for 20 min. Afterwards, the cells were washed with PBS followed by 40 min of fixation with 4 % PFA at RT. The cells

were then washed with PBS, and the cell nuclei were stained with DAPI (2 µg/mL). After 20 min incubation, the DAPI solution was removed. 300 µL of PBS was added per well for CLSM imaging. Images were recorded on a Leica-TCS-SP8 confocal laser scanning microscope equipped with a HC PL APO 63× 1.4 objective (Germany). DAPI emission was recorded at 450 nm, ATTO647N-Cas9 at 670 nm, and Cy3-sgRNA at 570 nm. All images were analyzed using the LAS X software from Leica.

2.3.21 Gal8 endosomal escape assay

HeLa cells with stable expression of a mRuby3-galectin 8 fusion protein were generated by using a Super piggyBac Transposase expression vector (SBI, CA, USA) and a PB-CAG-mRuby3-Gal8-P2A-Zeo plasmid.[84] The PB-CAG-mRuby3-Gal8-P2A-Zeo plasmid was a gift from Jordan Green's lab (Addgene plasmid no. 150815; http://n2t.net/addgene:150815; RRID: Addgene_150815). HeLa mRuby3/gal8 cells were seeded in 8-well Ibidi µ-slides (Ibidi GmbH, Germany) at a density of 15000 cells/well 24 h prior to treatments. On the next day, the medium was replaced with 225 µL of fresh medium. 75 µL of RNP nanocarriers was added to each well resulting in a final concentration of 75 nM RNP. After 4 h, the cells were washed, fixed, stained and imaged as described above. DAPI emission was recorded at 450 nm, mRuby3 emission was recorded at 590 nm. Gal8 spots per cell were analyzed using the ImageJ software.

2.3.22 Determination of PD-L1/PVR gene knockout by flow cytometry

One day prior to the treatments, CT26 WT cells were seeded into 24-well plates at a density of 50000 cells/well. On the next day, the medium in each well was replaced with 375 µL of fresh medium. sgPD-L1/sgPVR loaded RNP nanocarriers with or without ligand modification (0.75 eq) were prepared as described above using sgPD-L1_4 and sgPVR_3 at a molar ratio of 1:1. 125 µL of RNP nanocarriers was added to each well resulting in a final concentration of 75 nM RNP in total. After 4 h, the medium in each well was replaced with 500 µL of fresh medium and the cells were incubated for 44 h. Afterwards, 100 ng/mL IFN-γ was added to each well to stimulate

PD-L1 expression. After further incubation for 24 h, the cells were harvested, stained with APC anti-mouse PD-L1 antibody and/or PE anti-mouse PVR antibody, and analyzed by flow cytometry. All experiments were performed in triplicate.

2.3.23 Cell viability assay (MTT) after PD-L1/PVR gene knockout

One day prior to the treatments, CT26 WT cells were seeded into 96-well plates at a density of 5000 cells/well. On the next day, the medium in each well was replaced with 75 µL of fresh medium. sgPD-L1/sgPVR loaded RNP nanocarriers were applied and cells were incubated for 4 h. Afterwards, the medium was removed and 100 µL of fresh medium was added in each well. After 48 h total incubation, 10 µL of MTT (5 mg/mL) was added to each well. The cells were incubated for 2 h in the incubator. Afterwards, the medium was discarded, and the plates were frozen at – 80 °C overnight. 100 µL of DMSO was then added to each well to dissolve the formed formazan product. The plates were incubated for 30 min at 37 °C under shaking. The absorbance of each well was measured at 590 nm with background correction at 630 nm using a microplate reader (Tecan Spark 10M, Tecan, Männedorf, Switzerland). The relative cell viability (in percentage) was calculated relative to control wells treated with HBG buffer as ([A] test/[A] control) × 100 %. All experiments were conducted in triplicate.

2.3.24 Determination of PD-L1/PVR gene knockout by CLSM

One day prior to the treatments, CT26 WT cells were seeded in 8-well Ibidi µ-slides (Ibidi GmbH, Germany) at a density of 50000 cells/well. On the next day, the medium was replaced with 225 µL of fresh medium. 75 µL of sgPD-L1/sgPVR loaded RNP nanocarriers was added to each well resulting in a final concentration of 75 nM RNP complexes. After 4 h, the medium in each well was replaced with 300 µL of fresh medium. The cells were further incubated for 44 h. Afterwards, 100 ng/mL IFN-γ was added to stimulate PD-L1 expression. After 24 h stimulation, the cells were stained using 2 µL of APC anti-mouse PD-L1 antibody and/or 2 µL of PE anti-mouse PVR antibody, washed, fixed and imaged by CLSM as described above.

2.3.25 Apoptosis assay after PVR gene knockout

Assessment of cell apoptosis after PVR gene knockout was performed using an Annexin V-FITC Apoptosis Detection Kit (BioVision, USA). CT26 WT cells were seeded into 24-well plates at a density of 50000 cells/well 24 h prior to the treatments. On the next day, the medium in each well was replaced with 375 µL of fresh medium. 125 µL of RNP nanocarriers containing sgPVR_3 or sgCtrl with or without ligand modification (0.75 eq) was added to each well resulting in a final concentration of 75 nM RNP complexes. After 4 h, the medium in each well was replaced with 500 µL of fresh medium and the cells were incubated for 20 h. Afterwards, the cells were harvested and resuspended in 500 µL of 1 × Annexin V-FITC binding buffer, followed by the addition of 5 µL of Annexin V-FITC and 5 µL of propidium iodide (PI, 50 µg/mL). The samples were incubated in the dark for 5 min at RT and then analyzed by flow cytometry. The FITC fluorescence was detected with 488 nm excitation and 520 nm emission. The PI fluorescence was assayed with 488 nm excitation and 640 nm emission. All experiments were performed in triplicate.

2.3.26 Cellwatcher study

CT26 WT cells were seeded into 48-well plates at a density of 20000 cells/well 24 h prior to the treatments. On the next day, the medium in each well was replaced with 150 µL of fresh medium. The dynamics of cell growth was real-time monitored up to 114 h using a Cellwatcher device (PHIO, Germany). At 1 h after recording, 50 µL of RNP nanocarriers containing sgPVR_3 or sgCtrl with or without ligand modification (0.75 eq) was added to each well resulting in a final concentration of 75 nM RNP complexes. The cell growth curves were generated based on the automated detection of cells and analysis algorithms.

2.3.27 Colony formation assay

CT26 WT cells were seeded in 24-well plates at a density of 25000 cells/well 24 h prior to the treatments. On the next day, the medium was replaced with 375 µL of fresh medium. 125 µL of RNP nanocarriers (75 nM) containing sgPVR_3 or sgCtrl with or without ligand modification (0.75 eq) was added to each well. After 4 h, the

cells were typsinized and counted using a cell counter (Z2 Coulter, Beckman Coulter, CA, USA). Afterwards, 250 treated cells were immediately re-plated in the 12-well plates and incubated in the incubator. The medium in each well was replaced with fresh medium every 3 days. After 3 weeks, the colonies were fixed with 4 % PFA, stained with crystal violet (0.5 % w/v) and counted under a microscope. At least 50 cells were counted as a colony. The relative colony formation ratio (in percentage) was calculated relative to control wells treated with HBG as (colony number of test / colony number of control) × 100 %. All experiments were performed in triplicate.

2.3.28 Sanger sequencing and TIDE analysis of dual PD-L1/PVR gene edits

Genomic DNA of CT26 WT cells was extracted 3 days after treatments with dual sgPD-L1/sgPVR loaded RNP nanocarriers using a QIAamp DNA Mini Kit. The target regions of PD-L1 and PVR genes were amplified, gel purified, sequenced, and analyzed by TIDE analysis.

2.3.29 Dual PD-L1/PVR gene knockout *in vivo*

All animal studies were performed according to guidelines of the German Animal Welfare Act and were approved by the animal experiments ethical committee of the “Regierung von Oberbayern”, District Government of Upper Bavaria, Germany. Experiments were performed by Ulrich Wilk, Jana Pöhmerer, Elisa Hörterer as part of their veterinary MD studies at Pharmaceutical Biotechnology, LMU.

Eight-week-old, female, BALB/c mice, (Janvier, Le Genest-Saint-Isle, France), were housed in isolated ventilated cages under pathogen-free condition with a 12 h light/dark interval and were acclimated for seven days prior to the treatments. Water and food were provided ad libitum. For the determination of the efficiency of dual immune checkpoint gene disruption in vivo, 5×10^5 CT26 WT cells were injected subcutaneously into the left flank. For the tumor growth inhibition study, 1×10^5 CT26 WT cells were injected subcutaneously into the left flank. The tumor volume was measured using a caliper and calculated as [0.5 × (longest diameter) × (shortest diameter)^2] and the body weight was recorded daily.

For dual gene knockout study, dual sgPD-L1/sgPVR loaded RNP nanocarriers containing 125 μg Cas9 protein, 12.5 μg sgPD-L1_4 and 12.5 μg sgPVR_3 with or without ligand modification (0.75 eq) were prepared in a total volume of 50 μL HBG. Control RNP nanocarriers containing 25 μg sgCtrl with FolA-PEG24-DBCO modification were prepared in the same way. The mice were randomly divided into 5 groups (n = 6) 7 days after the tumor implantation. The RNP nanocarriers were intratumorally injected every other day with a total of 3 injections. The mice were euthanized by cervical dislocation 7 days after the last injection.

For tumor growth inhibition study, sgCtrl (25 μg), sgPD-L1_4/sgCtrl (12.5 μg/12.5 μg), sgPVR_3/sgCtrl (12.5 μg/12.5 μg) or sgPD-L1_4/sgPVR_3 (12.5 μg/12.5 μg) loaded FolA-PEG_{24}-1445 RNP nanocarriers (125 μg Cas9 protein) were prepared in a total volume of 50 μL HBG. The mice were randomly divided into 5 groups (n = 5 for sgPD-L1/sgPVR group, n = 6 for other groups) 3 days after the tumor implantation. The RNP nanocarriers were intratumorally injected at day 4, 7, 11, 18, 21, and 25. The mice were euthanized by cervical dislocation when tumor reached the criteria of critical size (≥ 12 mm in diameter) or continuous weight loss occurred.

2.3.30 Flow cytometry analysis of tumor tissues

Tumor tissues were harvested, treated with FastPrep® homogenizer, passed through 100 μm subsequently 40 μm mesh and washed with PBS to obtain single-cell suspensions.

To evaluate dual PD-L1/PVR gene knockout in vivo, 5 μL of APC anti-mouse PD-L1 antibody and 5 μL of PE anti-mouse PVR antibody were added to each sample (n = 3). The samples were incubated for 60 min on ice in the dark. Afterwards, the samples were washed, resuspended, and analyzed by flow cytometry as described above.

To evaluate CD8+ T cells recruitment, 5 μL of PE anti-mouse CD45 antibody and 5 μL of APC anti-mouse CD8 antibody (BioLegend, San Diego, CA, USA) were added to each sample (n = 3). The samples were incubated for 60 min on ice in the dark. Afterwards, the samples were washed, resuspended, and analyzed by flow cytometry as described above.

2.3.31 Sanger sequencing and TIDE analysis of tumor tissues

Genomic DNA of tumor tissues was extracted using a QIAamp DNA Mini Kit. The target regions of PD-L1 and PVR genes were amplified, gel purified, sequenced, and analyzed by TIDE analysis as described above.

2.3.32 Statistical analysis

Data were analyzed with GraphPad prism 5 and presented as arithmetic mean ± standard deviation (SD) of at least triplicates. The statistical significance of the experiments was estimated using the two-tailed student's t-test, *** $p \leq 0.001$, ** $p \leq 0.01$, * $p \leq 0.05$.

2.4 Results and discussion

2.4.1 Preparation and characterization of Cas9 RNP nanocarriers

The hydroxystearyl oligo(ethylenamino) amide #1105 was previously identified as a potent structure for intracellular delivery of Cas9 RNP.[45] To enable the post-functionalization with receptor ligands, a #1105 analog with an azido lysine integrated at the N-terminus, oligomer #1445, was synthesized by solid-phase-supported synthesis (SPS, Figure 4a). The original procedure for the synthesis of hydroxystearyl oligomers from oleic acid containing precursors contained a prolonged hydrolysis step which had to be followed by treatment with a reducing agent, such as tris(2-carboxyethyl)phosphine (TCEP), to break the generated disulfide bonds between cysteines.[170] However, in case of oligomer #1445, an unwanted azide reduction was frequently observed during this process (data not shown). To circumvent this side-reaction, an optimized protocol was established: the hydroxystearic acid was directly synthesized in solution and then coupled as building block onto the backbone of the structure on solid-phase.

Three different formulations of Cas9 RNP nanocarriers were prepared based on oligomer #1445 as shown in Figure 4b. Non-shielded 1445 nanocarriers were produced by mixing pre-assembled Cas9/sgRNA RNP complexes with oligomer #1445 at nitrogen to phosphate (N/P) ratio of 24 followed by 15 min incubation. The obtained formulation was subsequently click-functionalized with FolA-PEG_{24}-DBCO or PEG_{24}-DBCO to generate FRα-specific FolA-PEG_{24}-1445 or shielded but non-targeted PEG_{24}-1445 nanocarriers, respectively. To explore the effect of ligand feed ratio on the physiochemical properties of the nanocarriers, different equivalents (eq) of DBCO ligands were added to the non-shielded 1445 nanocarriers and incubated for 4 h to accomplish the click reaction. The size, polydispersity (PDI), and zeta potential of the formulations were determined by dynamic light scattering (DLS) (Figure 4c and 4d). The non-shielded 1445 formulation without ligand modification displayed homogeneous nanoparticles with a z-average of 166 nm and a PDI of 0.11. Slightly bigger nanoparticles (180-260 nm) were detected after modification with increasing amounts of DBCO ligands from 0.05 to 0.75 eq. Further increase of the ligand modification ratio to 1 eq induced severe aggregation of the PEG_{24}-DBCO-

1445 nanocarriers (426 nm), while the FolA$_{24}$-DBCO-1445 nanocarriers maintained at smaller particle size (249 nm). Excess amounts of ligands (1 and 2 eq) aggravated the nanoparticle aggregation in both formulations.

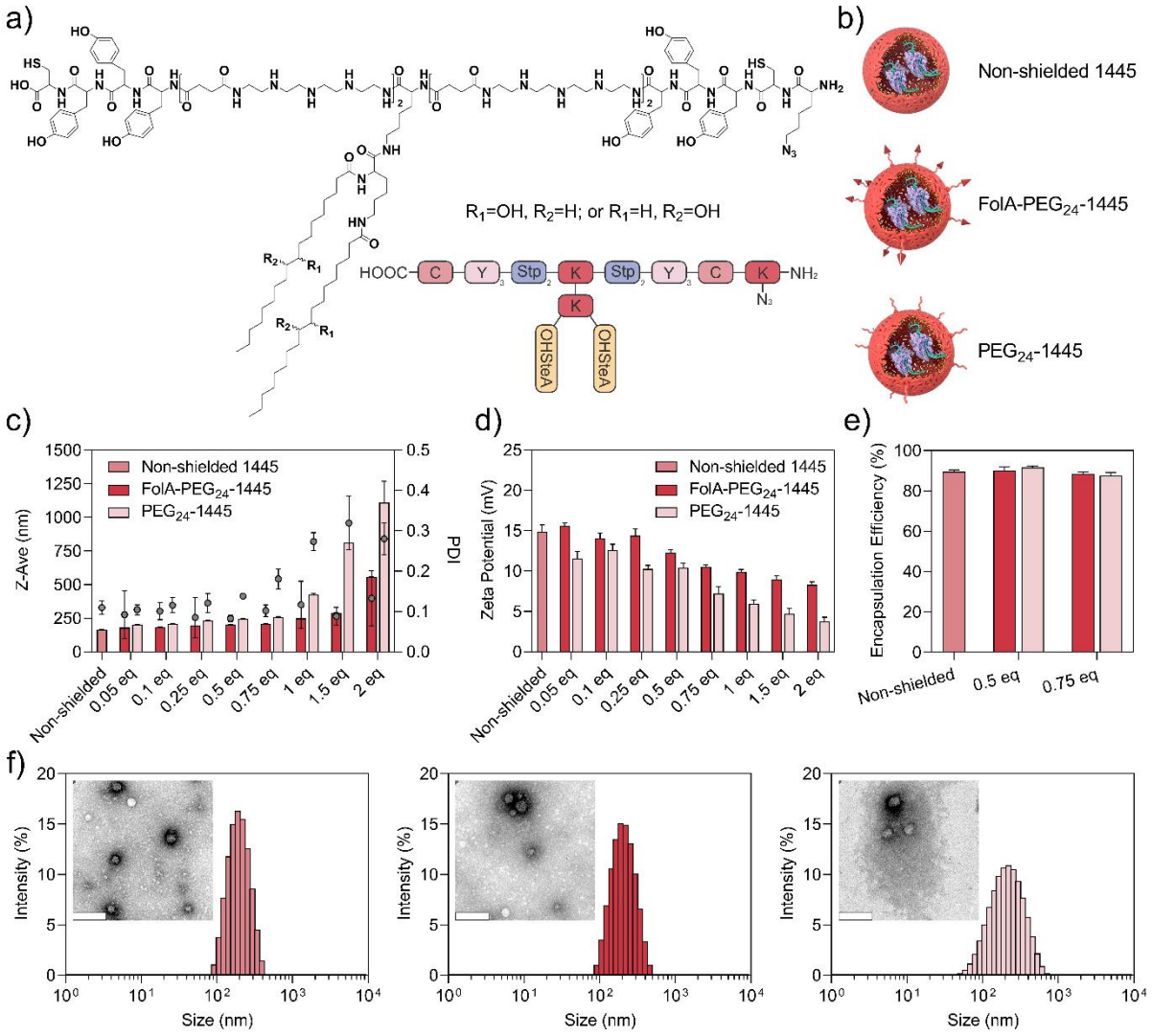

Figure 4. Characterization of Cas9 RNP nanocarriers. a) Chemical structure and sequence of T-shape oligomer #1445 with *N*-terminal azidolysine for functionalization with FRα-targeted FolA-PEG$_{24}$-DBCO or non-targeted PEG$_{24}$-DBCO via click chemistry. b) Schematic illustration of three different formulations of Cas9 RNP nanocarriers: non-shielded 1445, FRα-specific FolA-PEG$_{24}$-1445, and shielded but non-specific PEG$_{24}$-1445. c) Hydrodynamic particle size (z-average), polydispersity index (PDI) and d) zeta potential of Cas9 RNP nanocarriers at different FolA-PEG$_{24}$-DBCO or PEG$_{24}$-DBCO to oligomer ratios and at a RNP dose of 75 nM. Three technical replicates were measured. e) Cas9/sgRNA RNP encapsulation efficiency of nanocarriers at FolA-PEG$_{24}$-DBCO or PEG$_{24}$-DBCO to oligomer ratios of 0, 0.5, and 0.75 eq. Data were obtained by Ribogreen assay and are presented as mean ± SD (n=3). f) Intensity size distribution and transmission electron microscopy (TEM) images

(insert) of 3 different formulations of Cas9 RNP nanocarriers (from left to right: non-shielded 1445, FolA-PEG_{24}-1445, and PEG_{24}-1445). Scale bar: 100 nm.

At the same time, the zeta potential gradually decreased from + 15 mV to + 4 mV with increasing modification ratio, which is in accordance with the general finding that PEG shielding can lower the zeta potential of nanoparticles.[171] Particularly with 0.75 eq of ligand modification, zeta potential values of + 10 mV and + 7 mV were acquired with FolA-PEG_{24}-1445 and PEG_{24}-1445 nanocarriers, respectively. To stress the colloidal stability of the formulations, Cas9 RNP nanocarriers with or without 0.75 eq of ligand modification were prepared and directly stored at 4 °C, - 20 °C, - 80 °C or lyophilized and then stored at – 80 °C for up to two months. No significant particle aggregation was observed at any storage condition, only a slight size increase was detected with non-shielded 1445 and FolA-PEG_{24}-1445 nanocarriers stored at 4 °C (Figure 12).

In order to confirm the encapsulation of Cas9/sgRNA RNP in the nanocarriers, Ribogreen and agarose gel electrophoresis assays were performed in the next steps. A sgRNA encapsulation efficiency of 89.5 % was determined for the non-shielded 1445 nanoparticles by Ribogreen assay (Figure 4e), which indicates the efficient loading of RNP into the nanocarriers. Moreover, the modifications with 0.5 eq and 0.75 eq of DBCO ligands did not affect the RNP encapsulation or complex stability: 87.5 % - 91.6 % of encapsulation efficiency were determined for all formulations. Consistent results were obtained by electrophoretic mobility shift assays, where all formulations showed complete gel retardation of RNP while smear bands were observed with naked sgRNA and RNP (Figure 13). Transmission electron microscopy (TEM) measurements were further carried out to evaluate the appearance of the Cas9 RNP nanocarriers with or without 0.75 eq of ligand modification. All three formulations showed homogeneous and spherical particle shapes (Figure 4f). As expected the particle sizes (approximately 50 nm) acquired from TEM were lower than from DLS measurements due to the contribution of the dispersant to the hydrodynamic diameter in aqueous solution.[172]

2.4.2 Knockout evaluation and optimization

The overall *in vitro* gene editing efficiency of the Cas9 RNP nanocarriers with or without ligand modification was evaluated by eGFP knockout in two different cancer reporter cell lines: FRα-positive colon carcinoma CT26 eGFP/luc and cervix carcinoma HeLa eGFP/tub cells (Figure 5). Non-shielded 1445 mediated 72.2 % and 67.2 % of eGFP knockout after 4 h incubation at the RNP dose of 75 nM in CT26 eGFP/luc and HeLa eGFP/tub cells, respectively (Figure 5a). Numerous studies have shown that PEGylation can lower the transfection efficiency of polyplexes due to the PEG shielding and reduction of unspecific cellular uptake.[173] In the current study, a dramatic decrease of the knockout efficiency in CT26 eGFP/luc cells was observed with non-targeted PEG_{24}-1445 nanocarriers at the PEG ratio of 0.75 eq (Figure 5a, left), indicating that an efficient PEG shielding was achieved. In contrast, the knockout efficiency of FRα-specific FolA-PEG_{24}-1445 nanocarriers stayed at high levels despite surface modification with PEG.

In contrast to the significant knockout reduction due to PEGylation of PEG_{24}-1445, FolA-PEG_{24}-1445 still mediated efficient eGFP knockout of about 78.5 % at the modification ratio of 0.75 eq, which implies that folic acid modification could enhance the knockout efficiency of the well-shielded RNP nanocarriers. Similar tendency was also found in HeLa eGFP/tub cells, but 0.5 eq of PEG was already sufficient to achieve a distinct PEG shielding effect (Figure 5a, right). Therefore, 0.75 eq and 0.5 eq of ligand modification were selected for subsequent experiments in CT26 eGFP/luc and HeLa eGFP/tub cells, respectively.

To further investigate the effect of FRα-targeting on cellular delivery kinetics, the different Cas9 RNP formulations were incubated with the cells for increasing durations between 15 min to 48 h and eGFP knockout was determined 5 days after the transfections. A general dependency of knockout levels on the incubation time was observed with all 3 formulations. Notably, no significant differences were found between the longest incubation times of 4 h and 48 h in case of non-shielded 1445 and FolA-PEG_{24}-1445, which indicates that the uptake process is accomplished to a major extent within the first 4 h (Figure 5b). FRα-targeted FolA-PEG_{24}-1445 clearly showed the best knockout efficiencies in CT26 eGFP/luc cells while PEG_{24}-1445 was the worst and only achieved maximal eGFP knockout levels of 28.5 % after the longest incubation time of 48 h. Similar results were found in HeLa eGFP/tub cells.

Notably, FolA-PEG$_{24}$-1445 already reached similar eGFP knockout levels after 2 h incubation as non-shielded 1445 after 4 h and 48 h in HeLa eGFP/tub cells, which demonstrates that FRα-targeting accelerates cellular delivery. To confirm that the observed advantages of FolA-modification are indeed FRα-specific, a FRα-knockout cell line was generated from HeLa eGFP/tub by CRISPR/Cas9. The direct comparison of the HeLa eGFP/tub derivatives demonstrated that FolA-targeting mediates distinct enhancement of knockout levels in FRα-positive cells, whereas the advantage vanishes in FRα-negative cells. In the FRα-deficient cell line, non-shielded 1445 outperformed FolA-PEG$_{24}$-1445, which indicates that the advantages of FolA-PEG modification are highly specific and receptor-dependent.

Encouraged by the improved knockout and accelerated cellular delivery via FRα-targeting, systematic dose-titration experiments from 1 to 100 nM were carried out to assess the effects on the potency at different doses (Figure 5c). All three formulations exhibited a dose-dependent knockout behavior in all three cell lines, but a clear dependency of FolA-PEG$_{24}$-1445 on FRα-expression became obvious: the FolA-modified formulation has the highest potency in the cell lines which express the target receptor, but the potency drops in the FRα-knockout cells. In CT26 eGFP/luc cells, FolA-PEG$_{24}$-1445 showed approximately 80 % of eGFP knockout at RNP doses as low as 10 nM, while a sharp decrease of knockout efficiency from 76.8 % to 32.0 % was observed with non-shielded 1445 at a RNP dose of 25 nM.

The cytotoxicity of Cas9 RNP nanocarriers was investigated in parallel during the described knockout experiments and the formulations were generally well-tolerated (Figure 14-16). Besides, additional knockout experiments were performed to evaluate the effects of long-term storage on eGFP knockout efficiency in HeLa eGFP/tub cells (Figure 17). Cas9 RNP nanocarriers were prepared and stored as discussed previously. The overall knockout efficiency of all formulations did not significantly change over time.

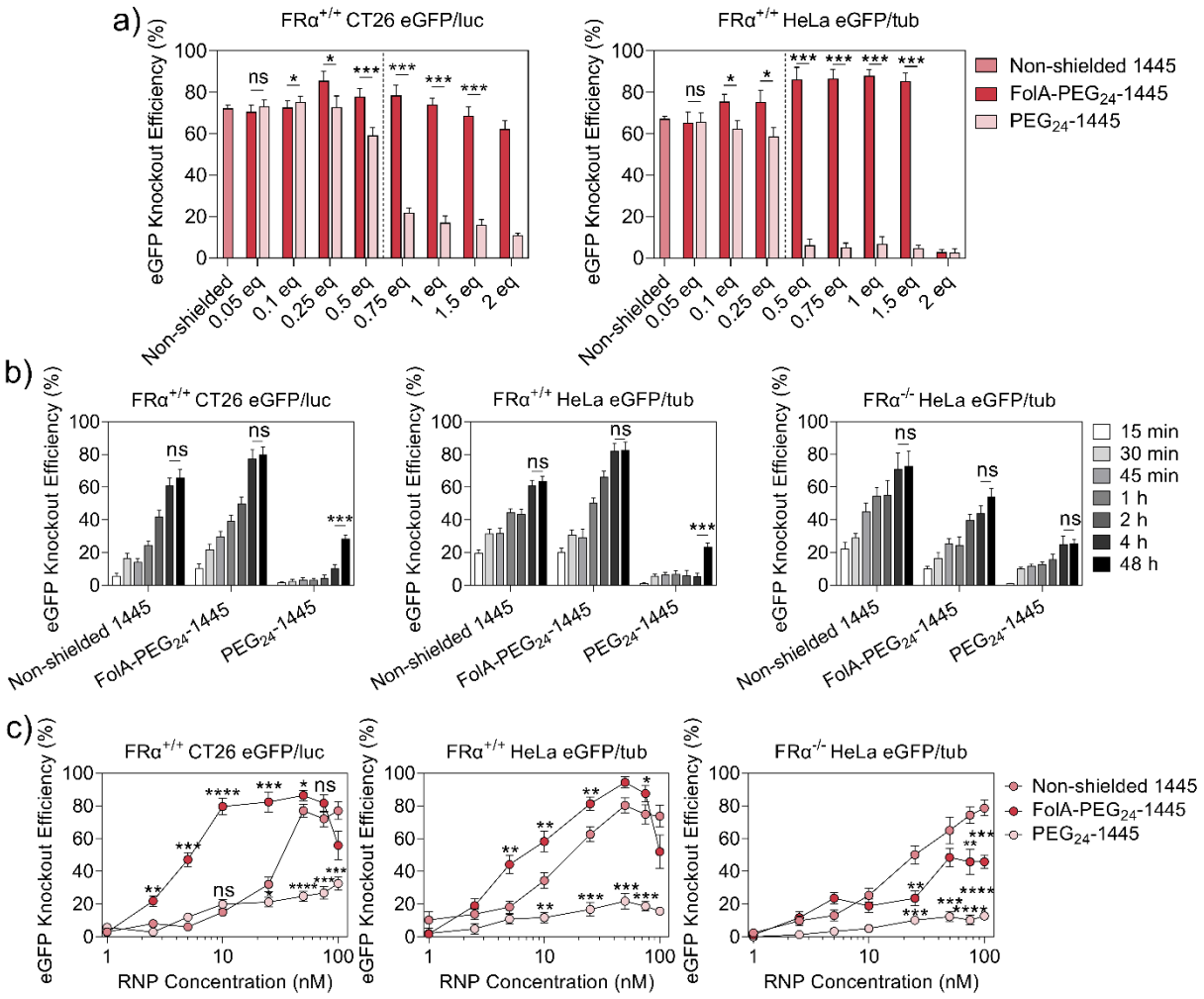

Figure 5. Knockout evaluation and optimization. a) eGFP knockout efficiency of Cas9 RNP nanocarriers at different FolA-PEG_{24}-DBCO or PEG_{24}-DBCO to oligomer ratios in FRα-positive CT26 eGFP/luc and HeLa eGFP/tub cells. Cas9/sgGFP RNP was used at 75 nM. Cell were incubated with the formulations for 4 h followed by a medium change and evaluation was performed 5 days after the treatment. b) eGFP knockout efficiency of Cas9 RNP nanocarriers incubated for different times in CT26 eGFP/luc cells with a FolA-PEG_{24}-DBCO or PEG_{24}-DBCO to oligomer ratio of 0.75 eq and in HeLa eGFP/tub and FRα-knockout HeLa eGFP/tub cells with a ratio of 0.5 eq. Cas9/sgGFP RNP was used at 75 nM. Evaluation was performed 5 days after the treatments. c) Dose titration of Cas9 RNP nanocarriers containing 1 to 100 nM Cas9/sgGFP RNP in CT26 eGFP/luc cells with a FolA-PEG_{24}-DBCO or PEG_{24}-DBCO to oligomer ratio of 0.75 eq and in HeLa eGFP/tub and FRα-knockout HeLa eGFP/tub cells with a ratio of 0.5 eq. Nanocarriers were incubated for 4 h and evaluation was performed 5 days after the treatment. Statistical significance was estimated using the two-tailed student's t-tests comparing the knockout efficiency to that of non-shielded1445 group at each concentration. **** $p \leq 0.0001$, *** $p \leq 0.001$, ** $p \leq 0.01$, * $p \leq 0.05$; ns, not significant; Data are presented as mean ± SD (n=3).

2.4.3 Cellular uptake and endosomal escape

The cellular delivery of Cas9 RNPs is a complex multileveled process. To elucidate the impact of the formulations on different stages, we investigated the cellular uptake and endosomal escape ability of Cas9 RNP nanocarriers with or without ligand modification. The cellular uptake after different time points (45 min, 2 h, and 4 h) was quantified by flow cytometry using ATTO647N-labeled Cas9 protein and Cy3-labeled sgRNA in FRα-positive CT26, HeLa and FRα-knockout HeLa cell lines (Figure 6a and Figure 18-19). FRα-specific FolA-PEG_{24}-1445 mediated the highest levels of cellular uptake in FRα-positive cells at each time point, while shielded but non-specific PEG_{24}-1445 showed the lowest. In contrast, non-shielded 1445 RNPs exhibited the strongest cellular uptake in FRα-knockout HeLa cells. All three formulations demonstrated time-dependent uptake characteristics. The maximal uptake levels in CT26 cells were obtained after 4 h, where the median Cas9 intensity (MFI) of FolA-PEG_{24}-1445 was 3-fold and 7-fold higher, and the sgRNA MFI was 5-fold and 13-fold higher than non-shielded 1445 and PEG_{24}-1445 nanocarriers, respectively. Confocal laser scanning microscopy (CLSM) was utilized to visualize the intracellular localization at this time point (Figure 6b). The most intense red (Cas9 protein) and green (sgRNA) signals were observed in FolA-PEG_{24}-1445 treated cells, which is in line with the flow cytometry results. These data all together show that the FolA-PEG modification strongly enhances the cellular internalization of RNP nanocarriers in FR-α expressing cancer cells, which is an essential requirement to realize FRα-specific genome editing.

To characterize the endosomal escape capability of RNP nanocarriers, a HeLa cell line with stable expression of a mRuby3/galectin-8 (gal8) fusion protein was established using the PiggyBac transposon system together with a mRuby3/gal8 encoding plasmid recently constructed by Jordan Green's lab.[84] The fluorescent galectin fusion proteins distribute in the cytosol when endosomal membranes are intact, and specifically bind to glycosylation moieties which are exposed when endosomes are ruptured.[174] Consequently, the recruitment of mRuby3/gal8 results in punctate red spots which are an indicator for damaged endosomes.

HeLa mRuby3/gal8 cells were visualized by CLSM 1 h and 4 h after treatment with Cas9 RNP nanocarriers (Figure 6c) and the number of punctuate spots was counted per cell to quantify the endosomal escape capability of different formulations (Figure

6d). The images reveal that the largest quantity of red spots appeared in FolA-PEG24-1445 treated cells, indicating the most efficient endosome disruption. Since each formulation contained the same oligomer backbone structure, the highest endosomal escape efficiency achieved by FolA-PEG_{24}-1445 could be due to the higher amount of internalized carrier material. It is important to note that the average number of punctuate spots detected for FolA-PEG_{24}-1445 after 1 h was comparable to non-shielded 1445 at the latest time point after 4 h (Figure 6d), which was very consistent with the previous knockout experiments, where 1 h incubation with FolA-PEG_{24}-1445 reached the same knockout level as 4 h incubation with non-shielded 1445 (Figure 5b).

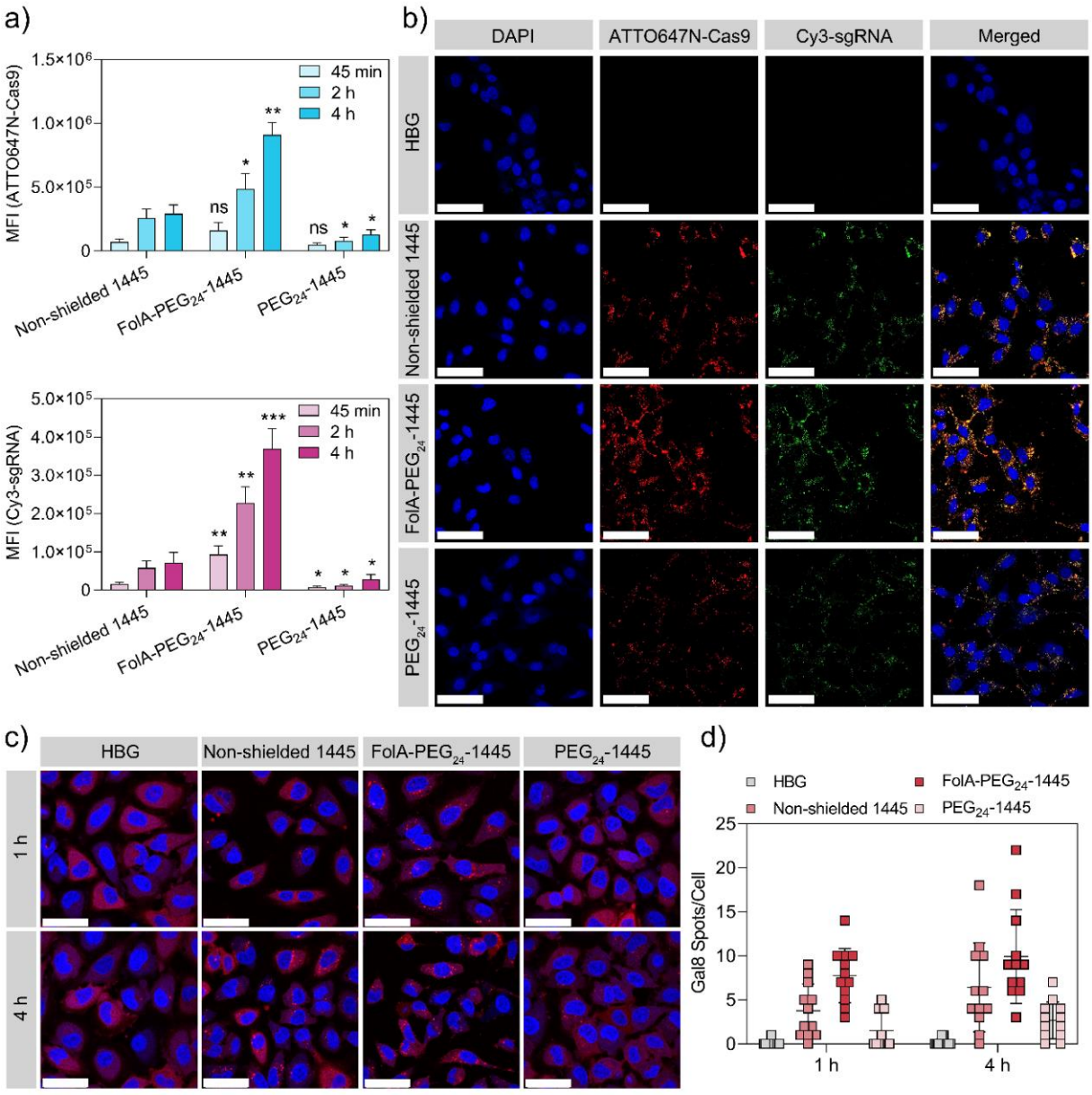

Figure 6. Cellular uptake and endosomal escape. a) Cellular uptake of Cas9 RNP nanocarriers (75 nM RNP, modification ratio 0.75 eq) containing 20 % of ATTO647N-Cas9/Cy3-sgRNA into CT26 WT cells. The median fluorescence intensity (MFI) was determined by flow cytometry 45 min, 2 h and 4 h after the treatment. Statistical significance was estimated using the two-tailed student's t-tests comparing the cellular uptake to that of non-shielded 1445 group at each time point. *** $p \leq 0.001$, ** $p \leq 0.01$, * $p \leq 0.05$; ns, not significant. Data are presented as mean ± SD (n=3). b) Confocal laser scanning microscopy (CLSM) images of CT26 WT cells 4 h after treatments with Cas9 RNP nanocarriers (75 nM RNP, modification ratio 0.75 eq) containing 20 % of ATTO647N-Cas9/Cy3-sgRNA. Nuclei were stained with DAPI (blue). The merged channel indicates co-localization (yellow) of ATTO647N-Cas9 (red) and Cy3-sgRNA (green). Scale bar: 70 µm. c) CLSM images of HeLa mRuby3/gal8 cells treated with Cas9 RNP nanocarriers (75 nM RNP, modification ratio 0.5 eq) for 1 h and 4 h. Nuclei were stained with DAPI (blue). Red punctuate mRuby3/gal8 spots indicate damaged endosomes. Scale bar: 50 µm. d) Endosomal disruption level at 1 h and 4 h of each group quantified

by the number of mRuby3/gal8 spots per cell using ImageJ software. Data are presented as means ± SD (n = 12).

2.4.4 Validation of PD-L1 disruption

After demonstration and optimization of FRα-specific Cas9 RNP delivery, we next assessed if the nanocarrier system could induce the disruption of endogenous immune checkpoint genes of interest. The disruption of PD-L1 gene was first evaluated by flow cytometry. Different concentrations of interferon-γ (IFN-γ) were added to stimulate the PD-L1 expression in CT26 cells and suitable expression could be achieved with 100 ng/mL IFN-γ (Figure 20). Four sgRNAs targeting PD-L1 were designed and tested with the nanocarriers at a RNP dose of 75 nM. sgPD-L1_4 that targets the exon 3 of murine PD-L1 gene (Figure 7a) was identified as the most efficient sgRNA sequence (Figure 21). After 4 h treatment, FolA-PEG_{24}-1445 containing sgPD-L1_4 induced 68.6 % of PD-L1 gene knockout, which was significantly higher than 38.2 % and 13.2 % of non-shielded 1445 and PEG_{24}-1445, respectively. The dose-titration experiments of the formulations revealed that FolA-PEG_{24}-1445 maintained high levels of PD-L1 knockout at RNP doses down to 25 nM, while the other two formulations immediately showed a dose-dependent reduction already at higher concentrations (Figure 7b). Moreover, the PD-L1 expression level was visualized by CLSM after staining with APC-labeled anti-PD-L1 antibody (red, Figure 7d and Figure 22). Compared to the buffer-treated cells, the PD-L1 expression of the cells treated with RNP nanocarriers was reduced to varying extents. Especially for FolA-PEG_{24}-1445, a majority of the cells did not show detectable PD-L1 expression after treatment. Despite slight toxicity observed with FolA-PEG_{24}-1445 at high RNP doses, an overall low cytotoxicity was confirmed in cytotoxicity studies (Figure 23).

To validate the PD-L1 disruption at the genomic level, the insertions and deletions (Indels) caused by non-homologous end-joining (NHEJ)-mediated DNA repair were investigated. Monoclonal cell lines were generated from CT26 cells 48 h after treatment by limiting dilution. The genomic DNA of the single cell-derived clones was extracted and the target region within PD-L1 exon 3 was amplified by PCR. After gel purification, the amplicons were determined by Sanger sequencing and the exemplary Indels are shown in Figure 7e. TIDE (Tracking of Indels by

Decomposition) analysis was further carried out to determine the Indel frequency in the heterogenous cell populations generated after treatments with the different formulations (Figure 7f). A total efficiency of 68.6 % was estimated in cells treated with FolA-PEG24-1445, which was higher than in case of treatments with non-shielded 1445 (40.7 %) or PEG_{24}-1445 (11.3 %). These results together with flow cytometry data indicated that FRα-specific FolA-PEG_{24}-1445 enabled efficient and robust PD-L1 disruption in FRα-expressing CT26 cells.

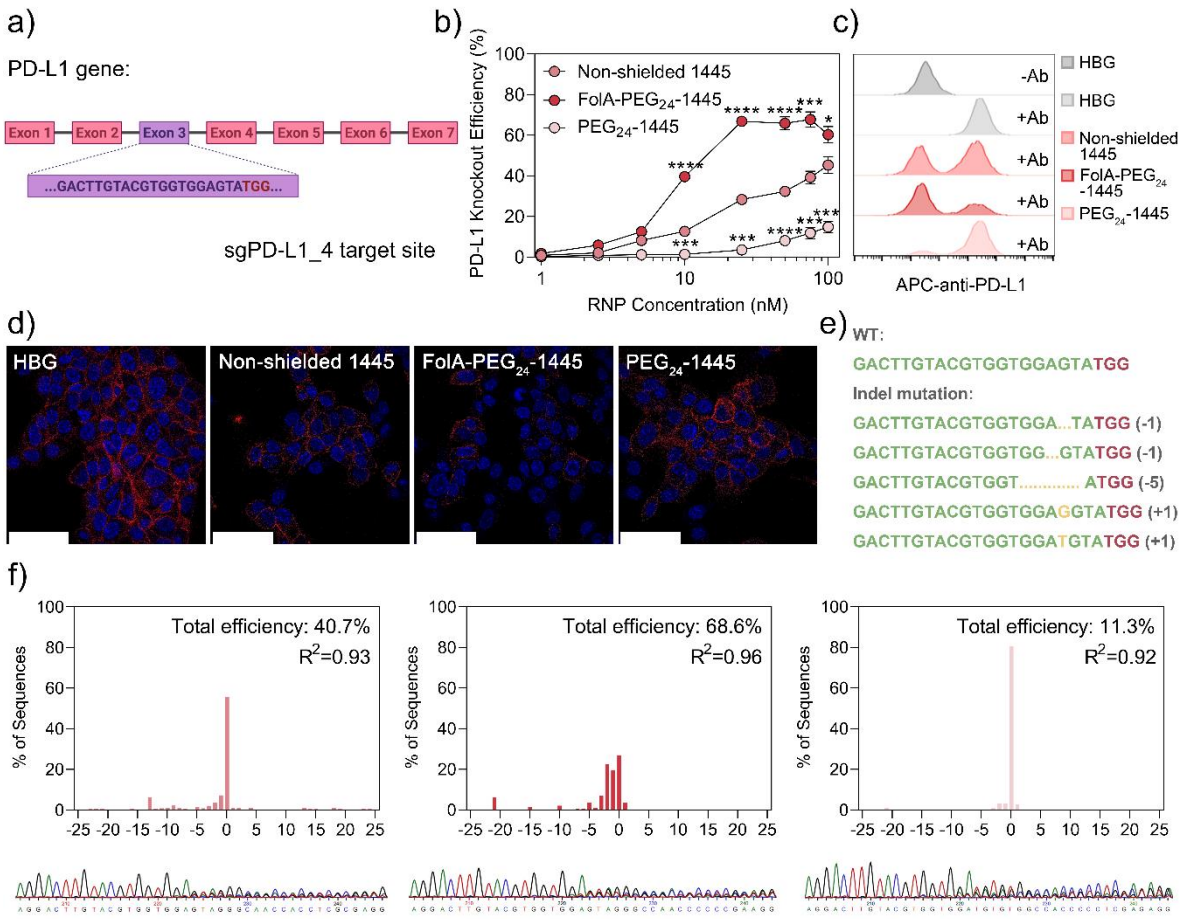

Figure 7. Validation of PD-L1 disruption. a) Exon map of the murine PD-L1 gene and the target region of sgPD-L1_4. b) PD-L1 knockout efficiency of the dose titration of Cas9 RNP nanocarriers containing 1 to 100 nM Cas9/sgPD-L1_4 RNP with or without modification at a ratio of 0.75 eq in CT26 WT cells. Nanocarriers were incubated with cells for 4 h followed by medium change and evaluation was performed 5 days after the treatment. Statistical significance was estimated using the two-tailed student's t-tests comparing the knockout efficiency to the non-shielded group at each concentration. **** $p \leq 0.0001$, *** $p \leq 0.001$, ** $p \leq 0.01$, * $p \leq 0.05$. Data are presented as mean ± SD (n=3). c) Scatter plots obtained by flow cytometry and d) CLSM images showing the PD-L1 expression of CT26 WT cells after 4 h treatment with HBG buffer, or Cas9 RNP nanocarriers (75 nM Cas9/sgPD-L1_4

RNP, modification ratio 0.75 eq) in CT26 WT cells. Evaluation was performed 5 days after the treatment. For the detection of PD-L1, cells were treated with an allophycocyanin (APC)-conjugated antibody (Ab) against PD-L1. Nuclei were stained with DAPI (blue). Scale bar: 50 µm. Additional CLSM data of the full set of the channels are provided in Figure S12 of the Supporting Information. e) Sequencing of monoclonal PD-L1 knockout cells. The green sequence indicates the sgPD-L1_4 target sequence in exon 3 of the PD-L1 gene next to the protospacer adjacent motive (PAM) sequence in red. Detected insertions and deletions (Indels) are highlighted in orange. f) TIDE analysis (top) and part of sequencing maps (bottom) of the sgPD-L1_4 target site of each group (from left to right: non-shielded 1445, FolA-PEG_{24}-1445 or PEG_{24}-1445). Sanger sequencing data were evaluated by the TIDE web tool (http://tide.deskgen.com/).

2.4.5 Validation of PVR disruption

Next, we studied whether FolA-PEG_{24}-1445 could also induce a FRα-specific enhancement of PVR gene knockout in CT26 cells. PVR, also known as CD155, is an immunological factor which is overexpressed in various types of tumors including colorectal cancer.[175] PVR has been reported to not only inhibit the function of T cells via TIGIT/PVR axis but also promote the proliferation and migration of tumor cells. It was recently found that PVR knockdown induces cell apoptosis and inhibits cell growth in colon cancer cells. To verify, if CRISPR/Cas9-mediated knockout can induce similar antitumoral effects, three sgRNAs targeting PVR gene were designed and tested with Cas9 RNP nanocarriers. The effect of PVR disruption on cell proliferation was first investigated by MTT assay and colony formation assay. The results of the MTT assay revealed that sgPVR_3 targeting the exon 5 of PVR gene (Figure 8a) outperformed the other 2 sgRNAs particularly at high RNP doses (Figure 8b and Figure 24). In contrast to the RNP formulation containing a control sgRNA without target sequence in the genome (sgCtrl), all formulations containing sgPVR_3 significantly affected cell viability and over 93 % reduction was achieved with FolA-PEG_{24}-1445 at RNP doses of 75 nM and 100 nM. At the same doses, around 84 % and 66 % reduction of viability were achieved with the non-shielded 1445 and PEG_{24}-1445, respectively. Similar findings were obtained by the colony formation assay, where both the size and number of colonies originating from FolA-PEG_{24}-1445 treated cells were the lowest (Figure 25). An Annexin V-FITC/PI assay was additionally performed to evaluate cell apoptosis induced by PVR knockout. Annexin V binds to phosphatidylserine (PS) exposed on the cell surface of early apoptotic

cells; PI is able to pass through the damaged cell membranes of late apoptotic and necrotic cells and causes staining of DNA in the nucleus. Thus, Annexin V-positive and PI-negative cell populations indicate early apoptotic cells, whereas Annex V-positive and PI-positive suggest late apoptotic cells. As depicted in Figure 8c, 24 h after transfection, FolA-PEG_{24}-1445 mediated the most frequent apoptosis events with a total of 57.4 % apoptotic cells (19.8 % early and 37.6 % late apoptotic), while only 45.5 % and 31.4 % of apoptotic cells were detected in case of non-shielded 1445 and PEG_{24}-1445, respectively. To explore the time-resolved effects on proliferation and cell numbers, the cellular growth dynamics were investigated with a Cellwatcher real-time camera system (Figure 8d, Figure 26). CT26 cells were constantly monitored up to 114 h by the Cellwatcher system (t = 0 h to 144 h), which automatically identified the individual cells as indicated by the colored marks (Figure 26). Different Cas9 RNP formulations were added 1 h after the start of recording (t = 1 h) and cell growth curves were generated based on the increasing cell confluency detected by the device (Figure 8d). The cells treated with buffer or sgCtrl RNP formulations all showed continuous cell proliferation until the end of the experiment, although at slightly different growth rates. In contrast, a flat curve was observed in case of the sgPVR containing formulations after a certain time point which indicates a stop of proliferation. Especially for FolA-PEG_{24}-1445-treated cells, an initial cellular growth was found in the first 12 h, which was followed by a rapid drop of the curve to a constant unchanging level. At the end point of recording (t = 114 h), FolA-PEG_{24}-1445+sgPVR treatment showed the lowest cell confluency (Figure 8d and Figure 26).

We next characterized the PVR expression levels after PVR knockout via RNP nanocarriers. The cells were treated with different formulations for 4 h and the evaluation was performed by flow cytometry at day 3 and day 4. PE-labeled anti-PVR antibody was used to stain expressed PVR on the cell surface. The two populations representing PVR-knockout and PVR-positive cells were already observed at day 3, but the two sub-populations were not well separated (Figure 27). A more reliable quantification was possible at day 4, where 62.6 % PVR knockout was detected in case of FolA-PEG_{24}-1445 treated cells while 50.3 % and 32.5 % were found for non-shielded 1445 and PEG_{24}-1445, respectively (Figure 8e and Figure 28). Accordingly, the enhanced disruption of PVR mediated by FolA-PEG_{24}-1445 was also confirmed by CLSM experiments (Figure 8f and Figure 29).

Similar to the validation of PD-L1 disruption, PVR knockout was also evaluated at the genomic level. Since PVR disruption inhibits the cell proliferation and induces apoptosis, the generation of monoclonal cell lines is sophisticated in this case.

Thus, the genomic DNA of the heterogenous cell population was directly extracted 3 days after treatments. The genomic target site was amplified by PCR and analyzed by sequencing. TIDE analysis was carried out to determine the frequency of Indels induced by different formulations (Figure 8g). The total efficiency of 43.7 % and 28.2 % were achieved with non-shielded 1445 and PEG_{24}-1445, respectively. FolA-PEG_{24}-1445 mediated the highest frequency of Indels of 61.7 %, which was very consistent with the PVR knockout efficiency determined by flow cytometry. Taken together, all these data demonstrate that the FRα-specific Cas9 RNP nanocarrier enabled the most efficient PVR disruption in CT26 cells, which leads to suppression of cell proliferation, induction of apoptosis and cell killing.

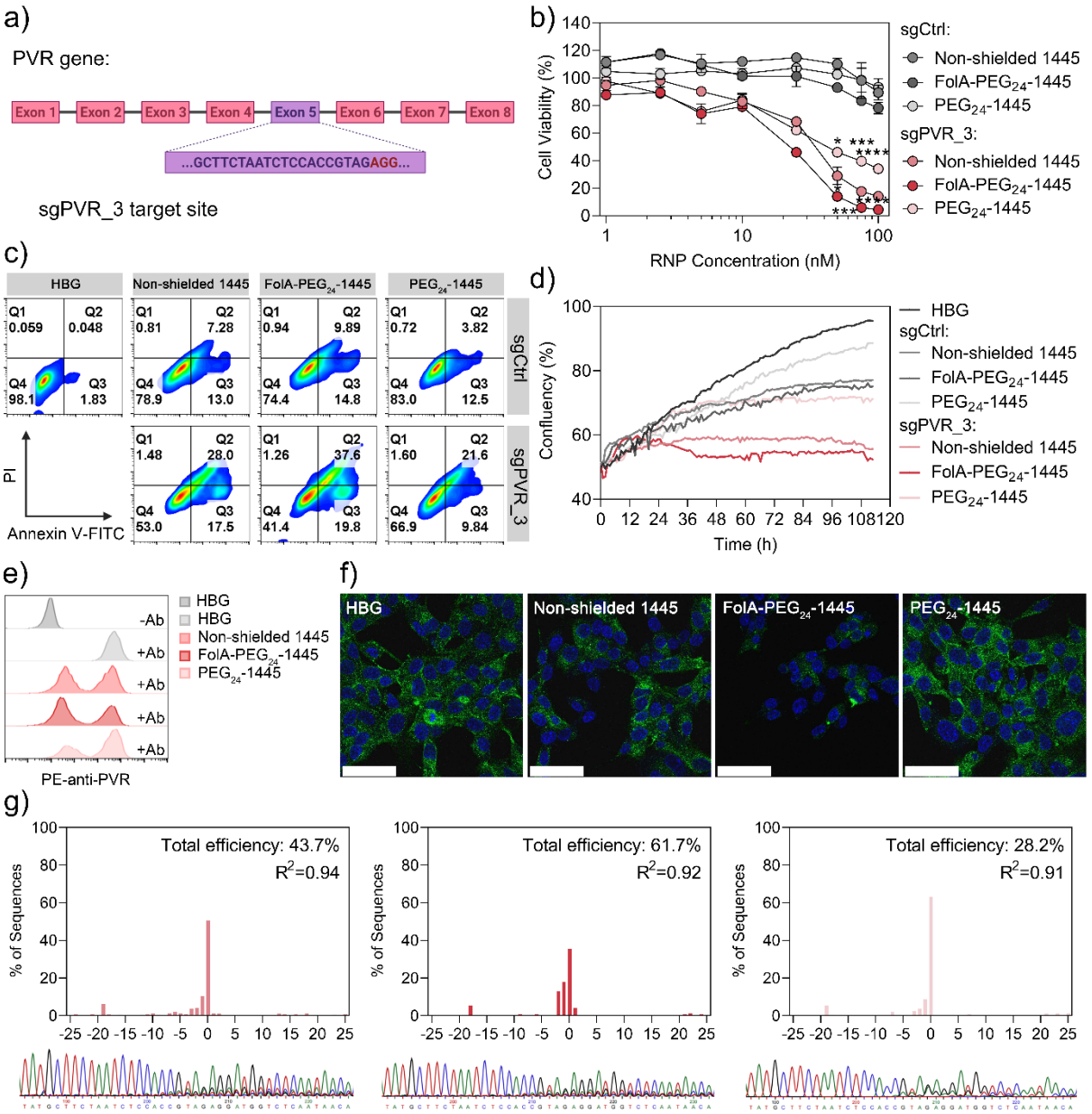

Figure 8. Validation of PVR disruption. a) Exon map of the murine PVR gene and the target region of sgPVR_3. b) Cell viability of CT26 WT cells treated with Cas9 RNP nanocarriers containing 1 to 100 nM Cas9/sgPVR_3 or sgCtrl RNP with or without modification at a ratio of 0.75 eq. Nanocarriers were incubated with the cells for 4 h followed by medium changes and evaluation was performed 48 h after the treatment. Statistical significance was estimated using the two-tailed student's t-tests comparing the knockout efficiency to that of non-shielded group at each concentration. **** $p \leq 0.0001$, *** $p \leq 0.001$, ** $p \leq 0.01$, * $p \leq 0.05$. Data are presented as mean ± SD (n=3). c) Annexin V-FITC/PI double-staining flow cytometry analysis to determined apoptosis in CT26 WT cells treated with HBG buffer, or Cas9 RNP nanocarriers (75 nM Cas9/sgPVR_3 or sgCtrl RNP, modification ratio 0.75 eq). Q1: necrotic cells; Q2: late apoptotic cells; Q3: early apoptotic cells; Q4: live cells. d) Cell growth dynamics of CT26 WT cells treated with HBG buffer, or Cas9 RNP nanocarriers (75 nM Cas9/sgPVR_3 or sgCtrl RNP, modification ratio 0.75 eq) determined by a Cellwatcher system. Cas9 RNP nanocarriers were

added 1 h after start of recording. Additional Cellwatcher study data are provided in Figure S16 and Video S1-S5 of the Supporting Information. e) Histograms of flow cytometry and f) CLSM images showing the PVR expression of CT26 WT cells after 4 h treatment with HBG buffer, or Cas9 RNP nanocarriers (75 nM Cas9/sgPVR_3 RNP, modification ratio 0.75 eq) in CT26 WT cells. Evaluation of flow cytometry and CLSM were performed 4 and 3 days after transfection, respectively. For the detection of PVR status, cells were treated with a phycoerythrin (PE)-conjugated antibody (Ab) against PVR. Nuclei were stained with DAPI (blue). Scale bar: 50 µm. Additional flow cytometry and CLSM data are provided in Figure S17-S19 of the Supporting Information. g) TIDE analysis (top) and part of sequencing maps (bottom) of the sgPVR_3 target site of each group (from left to right: non-shielded 1445, FolA-PEG_{24}-1445 or PEG_{24}-1445). Sanger sequencing data were evaluated by the TIDE web tool (http://tide.deskgen.com/).

2.4.6 Dual PD-L1/PVR disruption *in vitro*

After confirmation of single PD-L1 and PVR knockouts in CT26 cells, the dual PD-L1/PVR disruption by Cas9 RNP nanocarriers was evaluated. Different formulations of the nanocarriers were prepared using Cas9/sgPD-L1_4 and Cas9/sgPVR_3 RNPs at an equimolar ratio (1:1) and a total RNP dose of 75 nM. The cells were treated for 4 h and the cell viability was evaluated by MTT assay 48 h after the treatments. Despite the lower dose of Cas9/sgPVR_3 RNP, FolA-PEG_{24}-1445 still reduced cell viability to 23 %, which was significantly lower than the effects mediated by non-shielded 1445 and PEG_{24}-1445 (Figure 9a). Next, the expression of PD-L1 and PVR was determined by flow cytometry 72 h after treatments. On average, 54.43 % of cells treated with FolA-PEG modified RNP nanocarriers exhibited a dual PD-L1/PVR knockout and a total of 59.38 % of cells showed any editing event (Figure 9b). In comparison, non-shielded 1445 mediated dual gene knockout at a frequency of 29.61 % (37.59 % total efficiency), and the shielded but non-specific PEG_{24}-1445 induced the lowest gene editing levels with a dual knockout efficiency of 19.30 % (27.9 % total efficiency). Interestingly, with all three formulations the frequency of single knockouts of either PD-L1 or PVR was much lower than the dual knockout, which suggests that the developed RNP nanocarriers enable a robust encapsulation of multiple RNPs and have a great potential for multiplexed genome editing. Figure 9c illustrates representative histograms obtained by flow cytometry of the treated cells, where dual knockout events are plotted at the bottom left while single PD-L1 and single PVR knockouts are found at the top left and bottom right, respectively.

The inhibited expression of PD-L1 (red) and PVR (green) induced by different formulations was also confirmed by CLSM experiments (Figure 9d). To further determine the dual knockout efficiency at the genomic level, TIDE analysis of the two target sequences was performed. The genomic DNA was isolated 3 days after treatments, and both PD-L1 and PVR target regions were amplified and analyzed by sequencing. As shown in Figure 9e and Figure 30, 60.7 % of PD-L1 and 58.7 % of PVR Indel frequencies were determined in case of cells treated with FRα-specific FolA-PEG$_{24}$-1445 nanocarriers, while 18.3 % and 21.9 % were observed for shielded and un-targeted PEG$_{24}$-1445 nanocarriers. Non-shielded 1445 mediated medium level of dual gene knockout with Indel frequencies of 37.7 % for PD-L1 and 30.6 % for PVR.

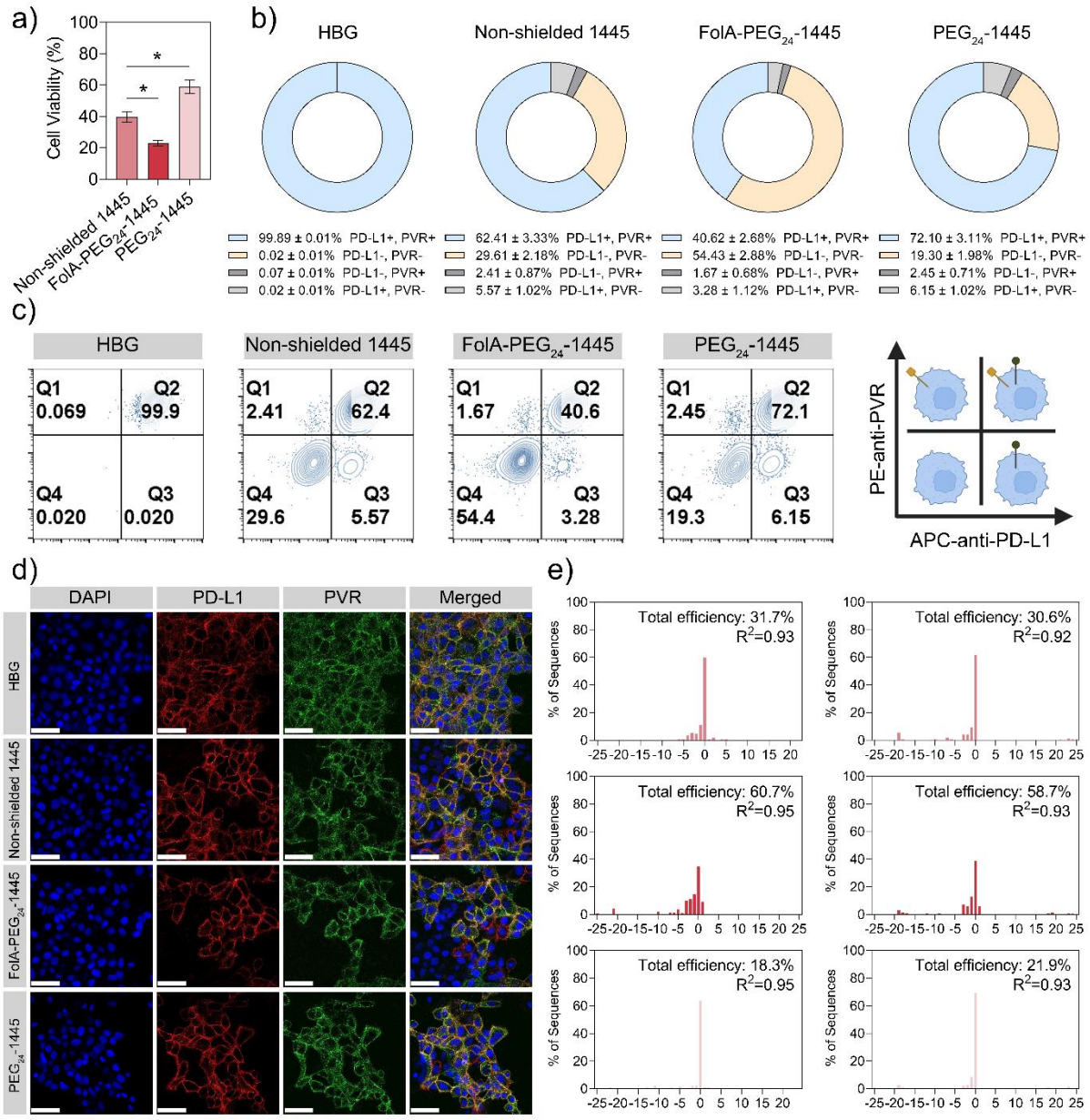

Figure 9. Dual PD-L1/PVR disruption *in vitro*. a) Cell viability and b) dual PD-L1/PVR knockout efficiency in CT26 WT cells treated with HBG buffer or Cas9 RNP nanocarriers containing 37.5 nM Cas9/sgPD-L1_4 and 37.5 nM Cas9/sgPVR_3 RNPs with or without modification at a ratio of 0.75 eq. Cas9 RNP nanocarriers were incubated with the cells for 4 h followed by medium change. MTT assay and flow cytometry were performed 48 h and 72 h after the treatment, respectively. Statistical significance was estimated using the two-tailed student's t-tests. * $p \leq 0.05$. Data are presented as mean ± SD (*n* = 3). c) Scatter plots obtained by flow cytometry and d) CLSM images showing the PD-L1 and PVR expression of CT26 WT cells after 4 h treatment with HBG buffer, or Cas9 RNP nanocarriers (37.5 nM Cas9/sgPD-L1_4 and 37.5 nM Cas9/sgPVR_3 RNPs, modification ratio 0.75 eq). Evaluation was performed 3 days after the treatment. Nuclei were stained with DAPI (blue). PD-L1 was stained with APC-anti-PD-L1 (red). PVR was stained with PE-anti-PVR (green). Scale bar: 70 µm. e) TIDE analysis of sgPD-L1_4 (left) and sgPVR_3 (right) target loci of each group (from top to

bottom: non-shielded 1445, FolA-PEG$_{24}$-1445 or PEG$_{24}$-1445). Sanger sequencing data were evaluated by the TIDE web tool (http://tide.deskgen.com/).

2.4.7 Dual PD-L1/PVR Disruption *in vivo*

Next, the capability of Cas9 RNP nanocarriers to enable FRα-specific dual immune checkpoint disruption *in vivo* was assessed (Figure 10a). CT26 WT cells were inoculated subcutaneously into BALB/c mice. Three days later, HBG buffer, sgCtrl (25 µg sgCtrl per mouse), and sgPD-L1_4/sgPVR_3 (12.5 µg of each sgRNA per mouse) containing RNP nanocarriers with or without 0.75 eq of ligand modification were injected intratumorally every other day with a total of 3 injections. Since the in vivo concentration differs from in vitro conditions, particle sizes of the nanocarriers were checked before the injections (Figure 31). Mice were euthanized 7 days after the last injection and tumor tissues were harvested for the next steps. Single-cell tumor suspensions were prepared and PD-L1/PVR were double stained with antibodies for quantification by flow cytometry (Figure 10b and 10c). FRα-specific FolA-PEG$_{24}$-1445 nanocarriers achieved around 25 % of dual knockout and a total of 40 % editing in the PD-L1 or PVR target loci in the tumors, while around 16 % dual knockout and 25 % total gene editing were mediated by non-shielded 1445. Notably, only 4 % of tumor cells were edited by un-targeted PEG$_{24}$-1445, which indicates that the surface PEGylation successfully suppresses unspecific cellular interactions and FolA-modification significantly enhances editing in FRα-expressing tumor cells in vivo. The TIDE analysis of the genomic DNA from the tumor tissues confirmed that Indel frequencies of 33.2 % in PD-L1 and 29.8 % in PVR target loci were induced by FolA-PEG$_{24}$-1445 (Figure 10d and Figure 32). Since the fundamental aim of immune checkpoint blockade therapy is the stimulation of the immune system against cancers, we investigated whether the dual PD-L1/PVR disruption can recruit cytotoxic T cells into the tumor microenvironment. The gating strategy of CD8+ T cells is shown in Figure 33.

Notably, the efficient dual PD-L1/PVR gene disruption by FolA-PEG$_{24}$-1445 significantly enhanced infiltration of CD8+ T cells into the tumors compared to all other groups. A slight increase of the CD8+/CD45+ ratio was achieved by non-shielded nanocarriers, but tumors treated with PEG$_{24}$-1445 exhibited comparable levels as the control groups treated with HBG or sgCtrl-containing FolA-PEG$_{24}$-1445.

As a proof of concept, these results demonstrate that FolA-PEG$_{24}$-1445 Cas9 RNP nanocarriers can enable FRα-specific dual immune checkpoint disruption and CD8+ T cell recruitment in FRα-expressing tumors *in vivo*.

Last, we investigated the antitumor effect of PD-L1/PVR dual immune checkpoint disruption in a separate therapeutic *in vivo* trial (Figure 11). CT26 WT cells were inoculated subcutaneously into BALB/c mice and RNP nanocarriers containing 25 µg sgRNA (sgCtrl, sgPD-L1_4/sgCtrl 1:1, sgPVR_3/sgCtrl 1:1 or sgPD-L1_4/sgPVR_3 1:1) and 0.75 eq of FolA-PEG modification were injected intratumorally at day 4, 7, 11, 18, 21, and 25 (Figure 11a). Tumor size and weight of the mice were measured daily and animals were euthanized when a tumor reached the critical size (≥ 12 mm in diameter) or when continuous weight loss was observed.

Tumors of animals without treatment or treated with sgCtrl, sgPD-L1_4/sgCtrl or sgPVR_3/sgCtrl showed continuous tumor growth beginning from day 8 (Figure 11b). Several mice from those groups had to be euthanized after day 20 due to exceeding tumor sizes or serious weight loss (Figure 11b and 11c). Compared with the un-treated group, neither sgCtrl nor single sgPD-L1 or sgPVR treatment showed significant deceleration of tumor growth (Figure 11b), which indicates that the single immune checkpoint disruptions are not sufficient to induce effective antitumoral effects in the tumor model. In contrast, the tumor growth of dual sgPD-L1_4/sgPVR_3 treated mice was delayed (day 14) and strongly inhibited throughout the entire experiment. At day 20, the mean tumor size of the sgPD-L1_4/sgPVR_3 group was 2.9-, 3.7-, and 5-fold smaller than those from the sgCtrl, sgPD-L1_4/sgCtrl, and sgPVR_3/sgCtrl groups, respectively. Besides, rather constant body weights were observed in the dual sgPD-L1_4/sgPVR_3 treated group. The Kaplan - Meier plot illustrates the dramatically improved survival rate of the dual sgPD-L1_4/sgPVR_3 treatment, where all mice survived at day 40 while at least 5 out of 6 animals were euthanized in all other groups (Figure 11d). Overall, the in vivo antitumor results demonstrate that dual PD-L1/PVR immune checkpoint disruption mediated by FRα-specific FolA-PEG$_{24}$-1445 Cas9 RNP nanocarriers can significantly suppress tumor growth in vivo, providing a promising strategy for cancer immunotherapy.

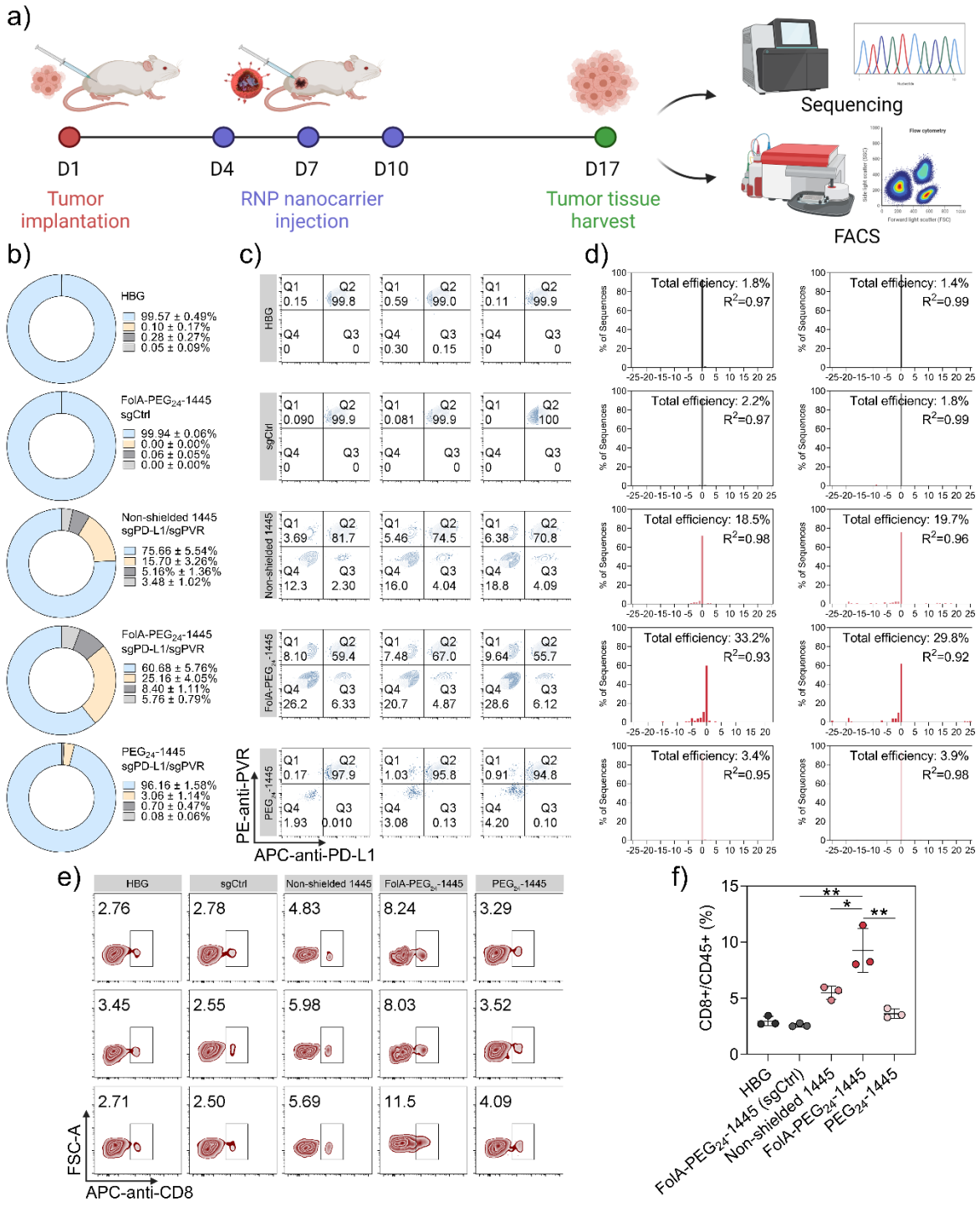

Figure 10. Dual PD-L1/PVR disruption *in vivo*. a) Schematic illustration of the experimental workflow. Different formulations of Cas9 RNP nanocarriers were administered intratumorally (i.t.) every other day with a total of 3 injections. Dual PD-L1/PVR knockout and CD8+ T cell recruitment at the tumor sites were evaluated 7 days after the last injection. b) Dual PD-L1/PVR knockout efficiency and c) scatter plots obtained by flow cytometry of the CT26 tumors treated with HBG buffer and Cas9 RNP nanocarriers containing Cas9/sgCtrl or Cas9/sgPD-L1_4 and Cas9/sgPVR_3 (1:1) with or without modification at a ratio of 0.75 eq. Data are presented as mean ± SD (*n* = 3). d) TIDE analysis of sgPD-L1_4 (left) and sgPVR_3 (right) target loci of each group (from top to bottom: HBG buffer, FolA-PEG$_{24}$-

1445 containing Cas9/sgCtrl, non-shielded 1445 containing Cas9/sgPD-L1_4 and Cas9/sgPVR_3, FolA-PEG$_{24}$-1445 containing Cas9/sgPD-L1_4 and Cas9/sgPVR_3, and PEG$_{24}$-1445 containing Cas9/sgPD-L1_4 and Cas9/sgPVR_3). Sanger sequencing data were evaluated by the TIDE web tool (http://tide.deskgen.com/). e) Scatter plots obtained by flow cytometry and f) derived CD8+/CD45+ ratio showing the CD8+ T cell recruitment at the CT26 tumor sites (*n* = 3) after different treatments. Statistical significance was estimated using the two-tailed student's t-tests. ** p ≤ 0.01, * p ≤ 0.05; Data are presented as mean ± SD (*n* = 3). Animal treatments were performed by Ulrich Wilk and Elisa Hörterer as part of their veterinary MD studies at Pharmaceutical Biotechnology, LMU.

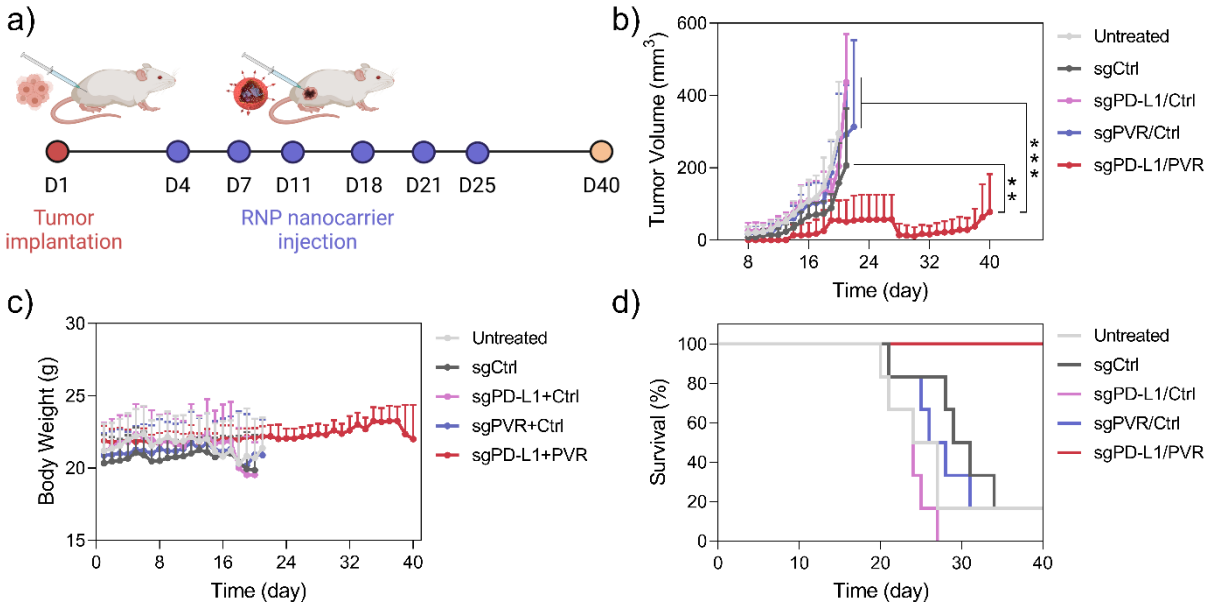

Figure 11. Antitumoral activity *in vivo*. a) Treatment schedule of Cas9 RNP nanocarriers in the syngeneic CT26 in Balb/c tumor model. Different formulations of Cas9 RNP nanocarriers were administered intratumorally (i.t.) at day 4, 7, 11, 18, 21, and 25. b) Tumor volume of subcutaneous CT26 tumors during the study. ** p ≤ 0.01, ***p ≤ 0.001; Data are presented as mean ± SD (*n* = 5 for sgPD-L1+PVR group, *n* = 6 for other groups). c) Body weight of mice throughout the experiment. Data are presented as mean ± SD (*n* = 5 for sgPD-L1+PVR group, *n* = 6 for other groups). d) Kaplan-Meier survival curve of mice receiving different treatments. (*n* = 5 for sgPD-L1+PVR group, *n* = 6 for other groups). Animal treatments were performed by Ulrich Wilk and Jana Pöhmerer as part of their veterinary MD studies at Pharmaceutical Biotechnology, LMU.

2.5 Conclusion

In summary, we developed an efficient and FRα-specific Cas9 RNP nanocarrier based on a hydroxystearyl oligoamino amide (#1445) to permanently disrupt PD-L1 and PVR immune checkpoint genes in tumors. FolA-PEG modified Cas9 RNP nanocarriers mediated enhanced cellular uptake and endosomal escape compared to unmodified and PEG modified nanocarriers, resulting in more efficient and specific gene knockout in FRα-positive CT26 and HeLa cells. Besides, the highest levels of PD-L1 and PVR gene knockout was achieved with this formulation in CT26 cells, and PVR disruption was found to strongly inhibit cell proliferation, induce apoptosis and cell killing. The dual disruption of PD-L1 and PVR genes mediated by FolA-PEG_{24}-1445 was confirmed in CT26 cells in vitro as well as after intratumoral injection into subcutaneous CT26 tumors in vivo. Remarkably, FolA-PEG_{24}-1445 facilitated ~25 % of dual PD-L1/PVR knockout, a total of ~40 % gene editing events, induced CD8+ T cell recruitment and a significant tumor growth inhibition. Thus, the presented strategy has potential for the development of new CRISPR/Cas9 based ICB and cancer therapeutics. Furthermore, the developed nanocarriers are suggested to constitute a platform for receptor-specific delivery of Cas9 RNPs with numerous potential applications, also beyond cancer.

2.6 Acknowledgements

The authors acknowledge support by the UPGRADE (Unlocking Precision Gene Therapy) project that has received funding from the European Union's Horizon 2020 research and innovation programme under grant agreement No 825825. This work was also supported by the German Research Foundation (DFG) SFB1032 (project-ID 201269156) sub-project B4. Y.L. and H.M. appreciate the fellowship of the China Scholarship Council that supports their Ph.D. studies. U.L. appreciates support by the Galenus Foundation (Vienna, Austria). We thank Özgür Öztürk for performing TEM measurements, and Teoman Benli-Hoppe for performing MALDI-TOF mass spectrometry measurements. TOC figure and some graphical elements were created with Biorender.com.

2.7 Supporting information figures

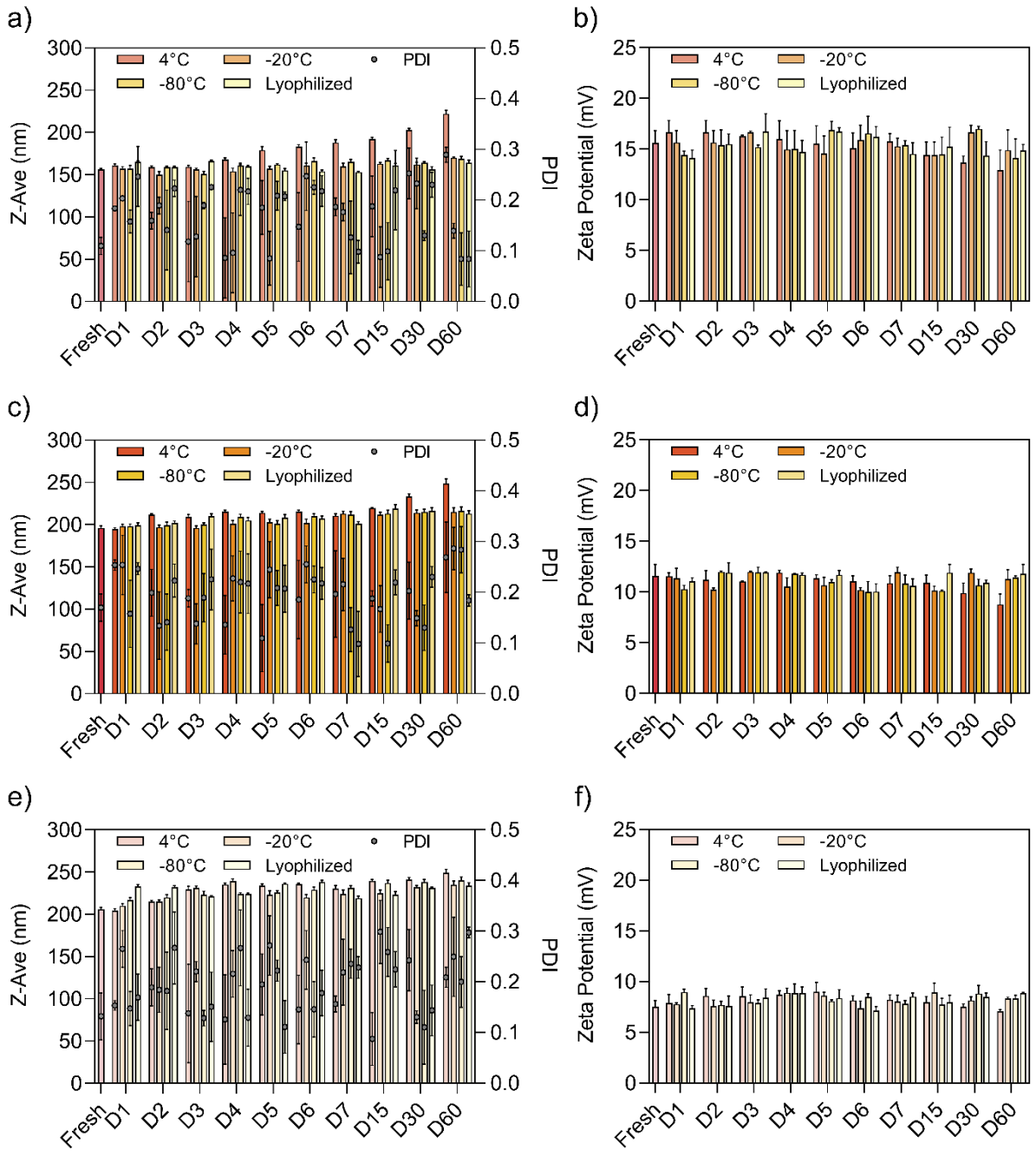

Figure 12. Long-term storage stability of nanoparticles determined by dynamic light scattering (DLS). a) Hydrodynamic particle size (Z-average) and polydispersity index (PDI) of a) non-shielded RNP nanocarriers, c) FolA-PEG$_{24}$-DBCO modified RNP nanocarriers, and e) PEG$_{24}$-DBCO modified RNP nanocarriers. Zeta potential of b) non-shielded RNP nanocarriers, d) FolA-PEG$_{24}$-DBCO modified RNP nanocarriers, and f) PEG$_{24}$-DBCO modified RNP nanocarriers. Three technical replicates were measured.

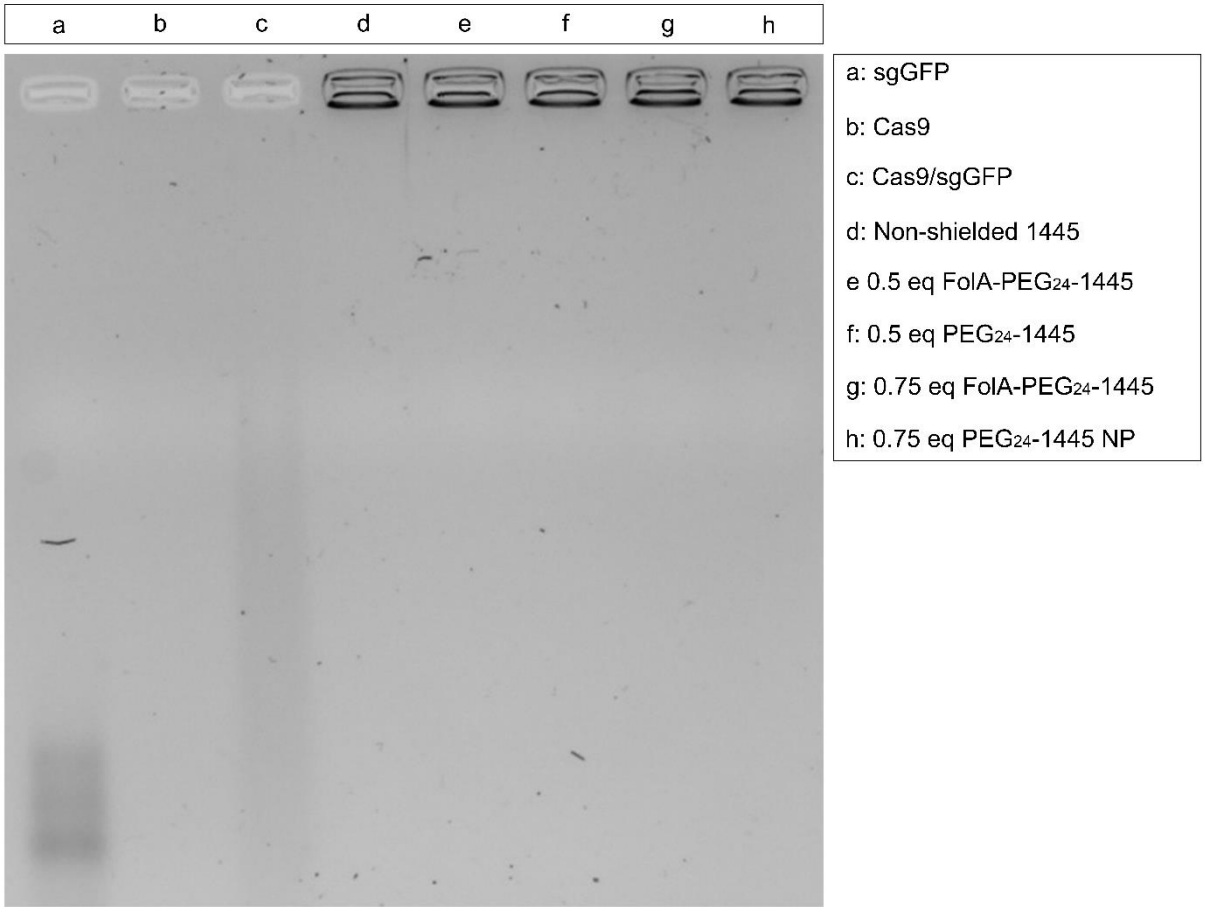

Figure 13. Agarose gel shift assay of Cas9 RNP nanocarriers. Different formulations of Cas9 RNP nanocarriers with or without 0.5 eq or 0.75 eq of ligand modification were prepared using 1.25 μg Cas9 protein and 0.25 μg sgGFP. Free sgGFP, free Cas9 protein, and free Cas9/sgGFP RNP were used as controls.

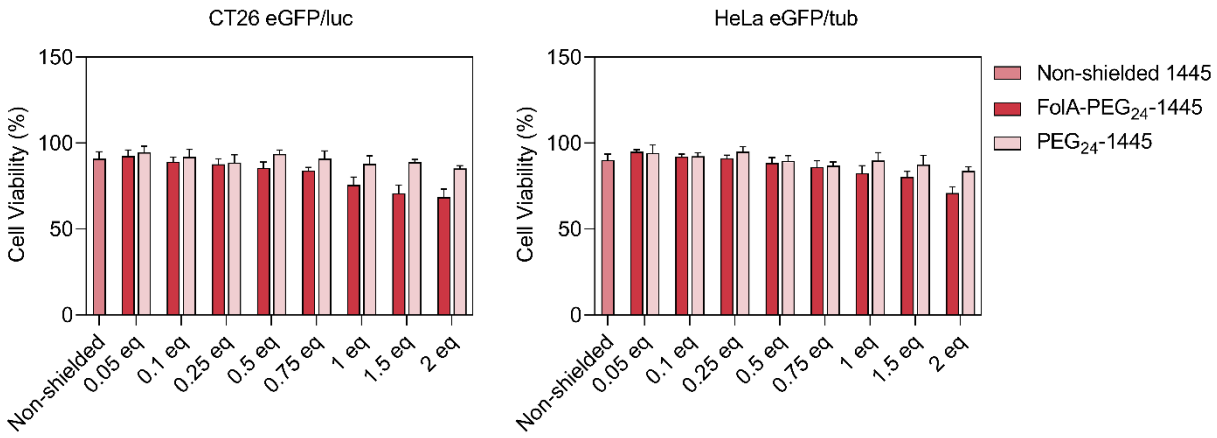

Figure 14. Viability of CT26 eGFP/luc and HeLa eGFP/tub cells after treatments with Cas9/sgGFP RNP nanocarriers with or without ligand modification at different equivalents. CT26 eGFP/luc and HeLa eGFP/tub cells were treated with the Cas9 RNP nanocarriers at the RNP dose of 75 nM for 4 h. Metabolic activity of the cells was determined using a MTT assay 48 h after transfection. Data are presented as % cell viability with respect to the control cells ± SD (n = 3).

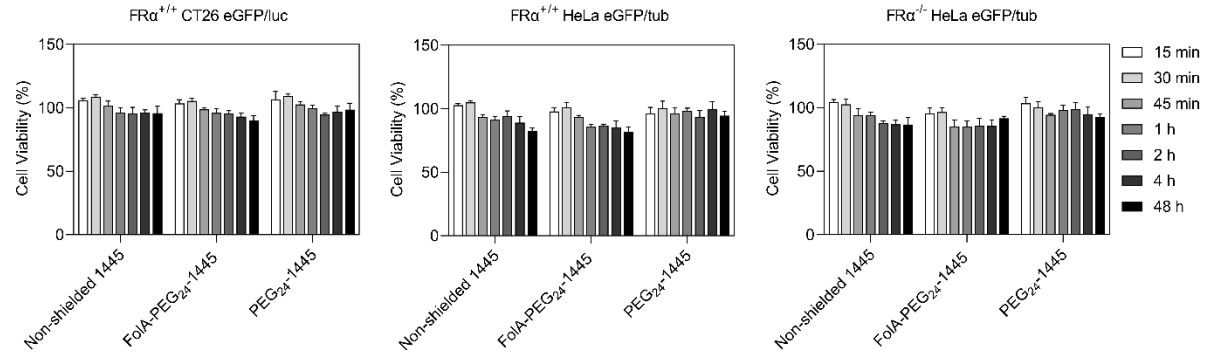

Figure 15. Viability of CT26 eGFP/luc, HeLa eGFP/tub, and FRα-knockout HeLa eGFP/tub cells after treatments with Cas9/sgGFP RNP nanocarriers with or without ligand modification (0.75 eq for CT26 cells and 0.5 eq for HeLa cells) for different times. CT26 eGFP/luc, HeLa eGFP/tub, and FRα-knockout HeLa eGFP/tub cells were treated with the Cas9 RNP nanocarriers at the RNP dose of 75 nM for 15 min, 30 min, 45 min, 1 h, 2 h, 4 h, or 48 h. Metabolic activity of the cells was determined using a MTT assay 48 h after transfection. Data are presented as % cell viability with respect to the control cells ± SD (n=3).

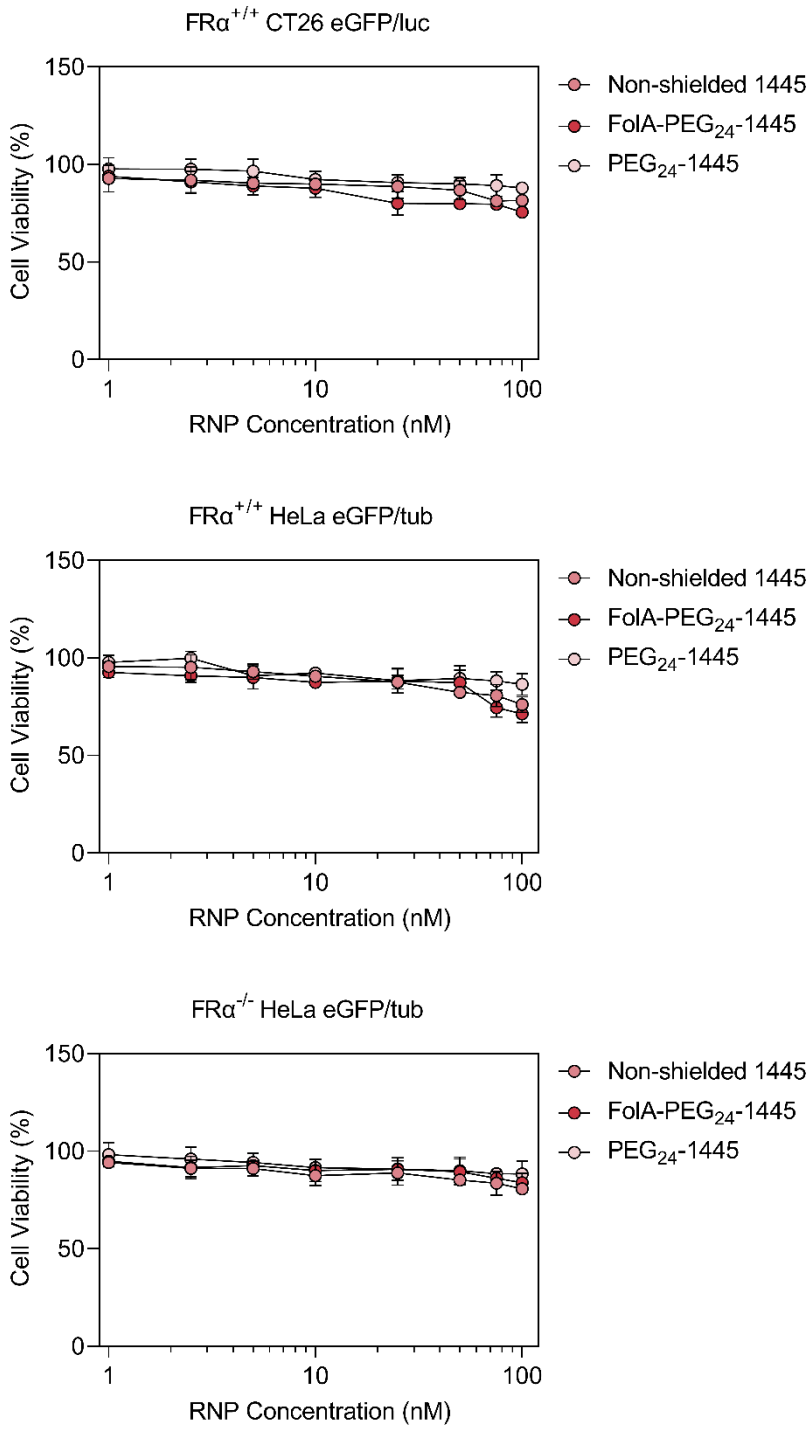

Figure 16. Viability of CT26 eGFP/luc, HeLa eGFP/tub, and FRα-knockout HeLa eGFP/tub cells after treatments with Cas9/sgGFP RNP nanocarriers with or without ligand modification (0.75 eq for CT26 cells and 0.5 eq for HeLa cells) at different RNP doses. CT26 eGFP/luc, HeLa eGFP/tub, and FRα-knockout HeLa eGFP/tub cells were treated with the Cas9 RNP nanocarriers at RNP doses ranging from 1 nM to 100 nM for 4 h. Metabolic activity of the cells was determined using a MTT assay 48 h after transfection. Data are presented as % cell viability with respect to the control cells ± SD (n=3).

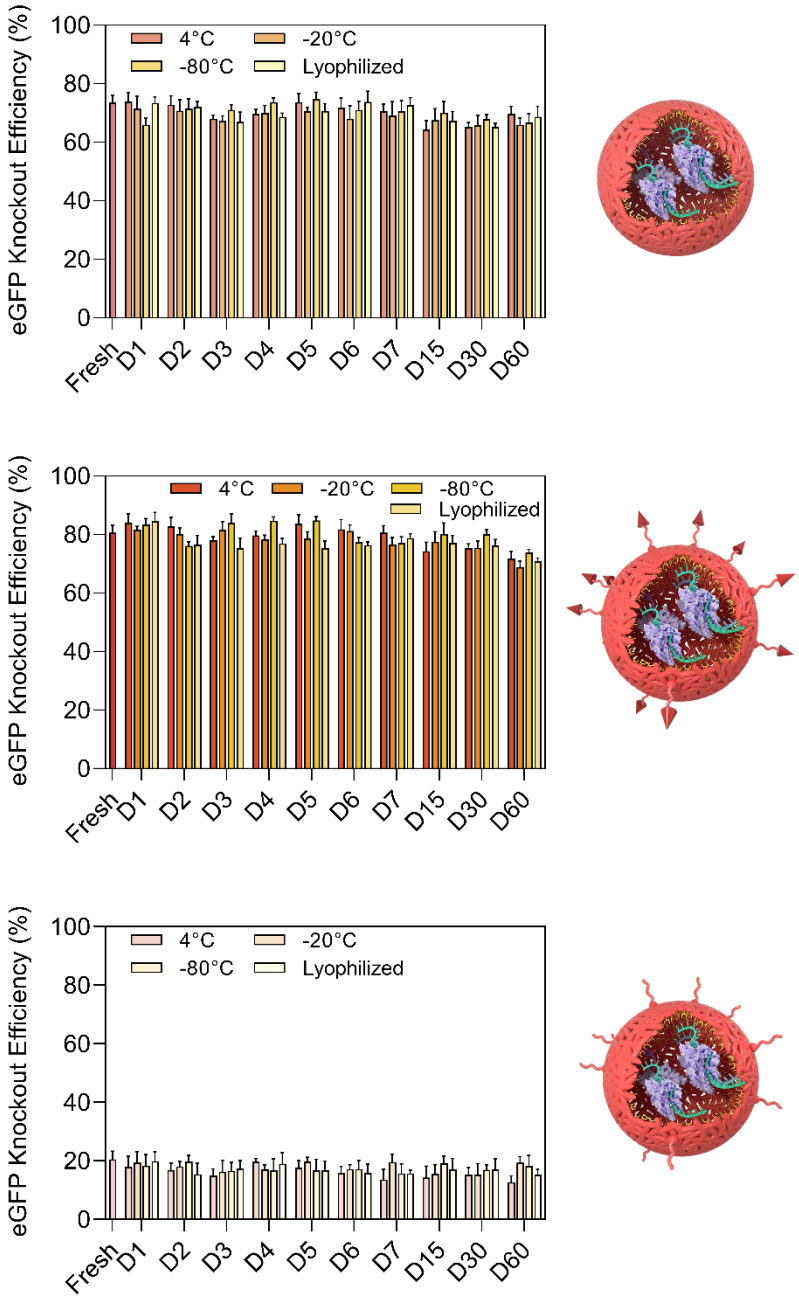

Figure 17. Effect of different long-term storage conditions on the eGFP knockout efficiency in HeLa eGFP/tub cells. Cas9/sgGFP RNP nanocarriers with or without 0.5 eq of ligand modification were prepared and stored under four conditions (4 °C, -20 °C, -80 °C or -80 °C after lyophilization) before use. HeLa eGFP/tub cells were incubated with the Cas9 RNP nanocarriers at the RNP dose of 75 nM for 4 h after different storage times. Flow cytometry was conducted 48 h after transfection. From top to bottom: non-shielded 1445, FolA-PEG$_{24}$-1445, and PEG$_{24}$-1445. Data are presented as the mean ± SD (n=3).

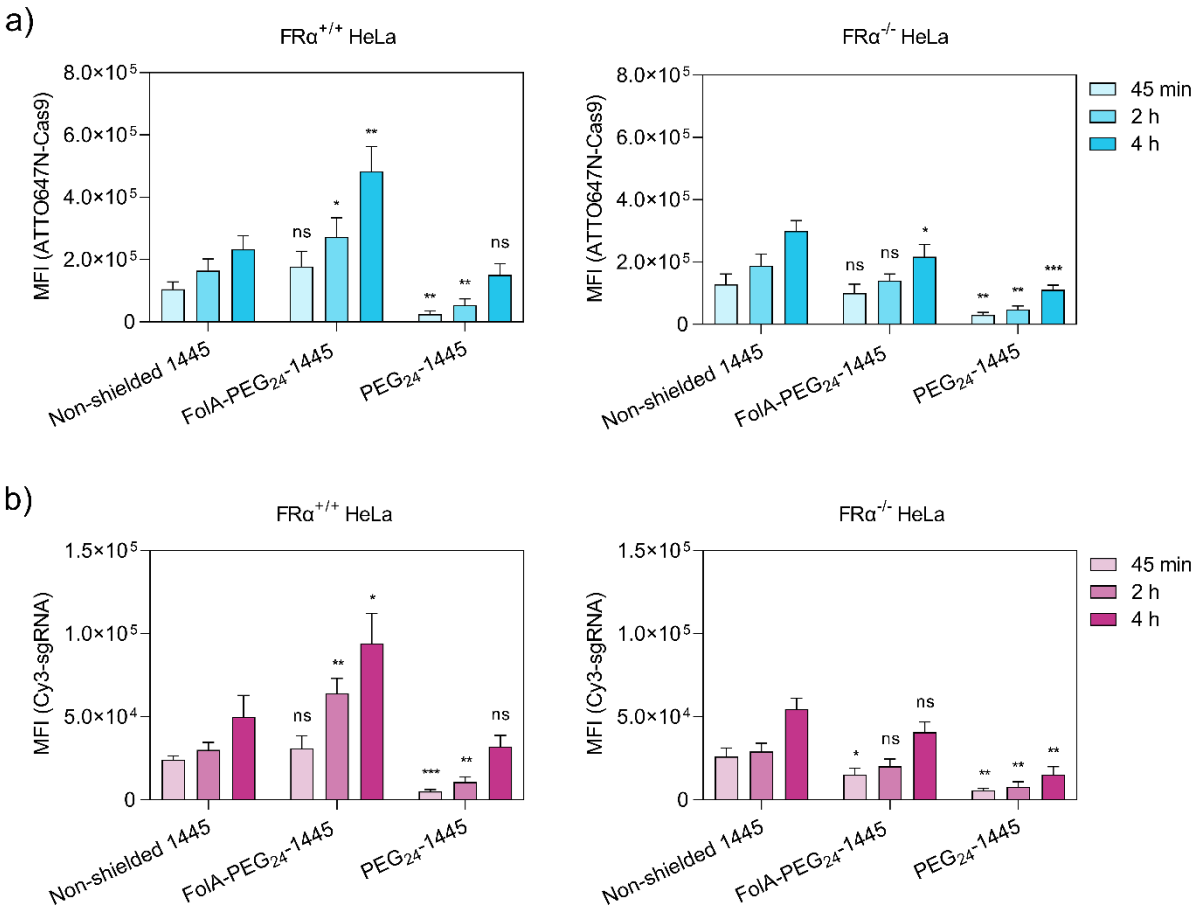

Figure 18. Cellular uptake of Cas9 RNP nanocarriers with or without ligand modification (0.5 eq) determined by flow cytometry. FRα-positive or FRα-knockout HeLa cells were incubated with the Cas9 RNP nanocarriers containing 20 % ATTO647N-labeled Cas9 protein and 20 % Cy3-labeled sgRNA at the RNP dose of 75 nM. Flow cytometry was conducted 45 min, 2 h, or 4 h after RNP treatment. a) Comparison of the measured median fluorescence intensities (MFI) of Cas9 protein. b) Comparison of the measured median fluorescence intensities (MFI) of sgRNA. The data are presented as the mean ± SD (n = 3).

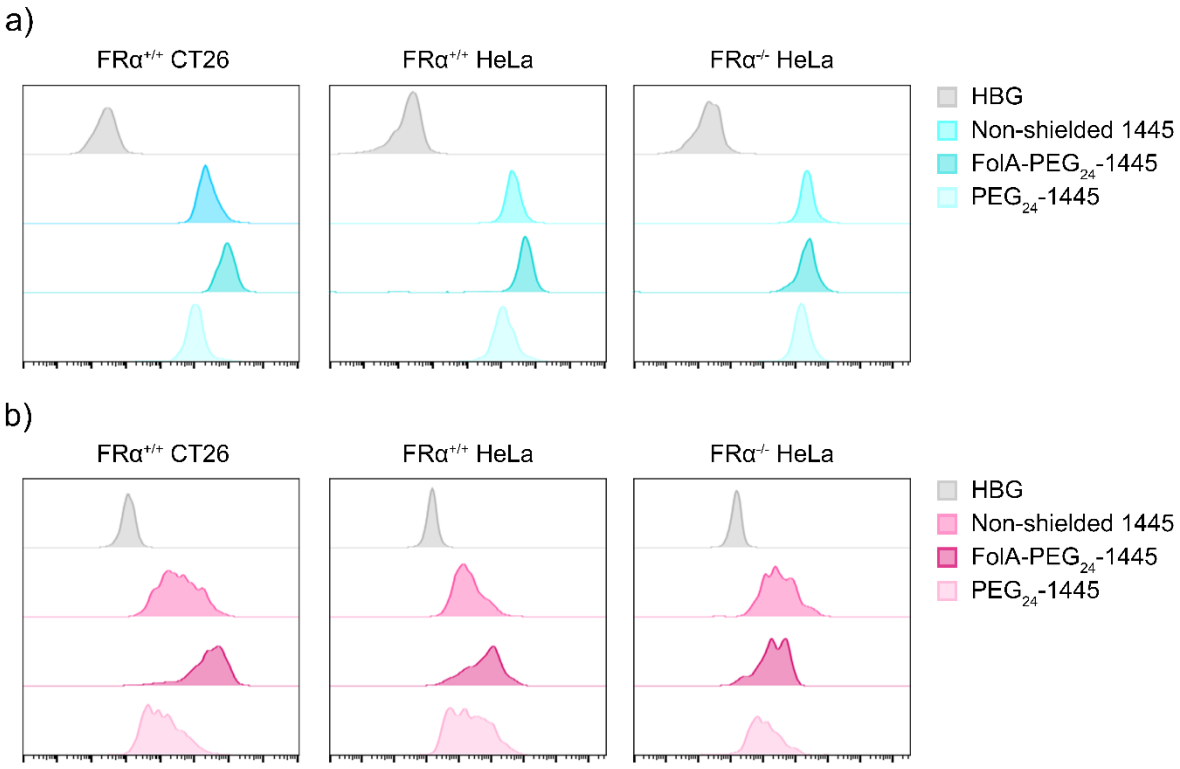

Figure 19. Cellular uptake of Cas9 RNP nanocarriers with or without ligand modification (0.75 eq for CT26 cells and 0.5 eq for HeLa cells) determined by flow cytometry. CT26, HeLa, and FRα-knockout HeLa cells were incubated with the Cas9 RNP nanocarriers containing 20 % ATTO647N-labeled Cas9 protein and 20 % Cy3-labeled sgRNA at the RNP dose of 75 nM. Flow cytometry was conducted 4 h after RNP transfection. a) Flow cytometry histograms of Cas9 protein uptake of each sample. b) Flow cytometry histograms of sgRNA uptake of each sample.

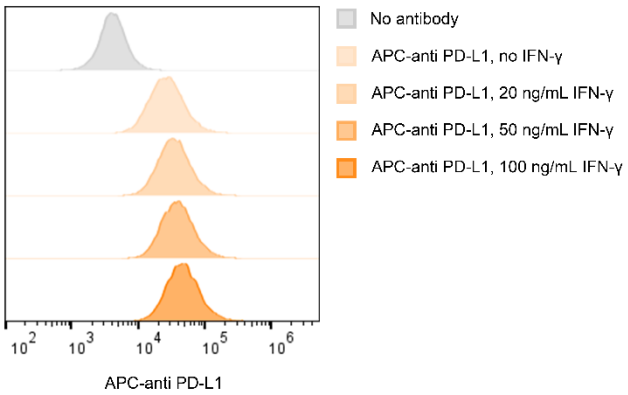

Figure 20. PD-L1 expression of CT26 WT cells stimulated by different concentrations of interferon-γ (IFN-γ). CT26 WT cells were incubated with or without 20, 50 or 100 ng/mL IFN-γ for 24 h. The flow cytometry experiment was conducted after PD-L1 was stained with APC-anti-PD-L1 antibody. The figure shows a flow cytometry histogram plot of each sample.

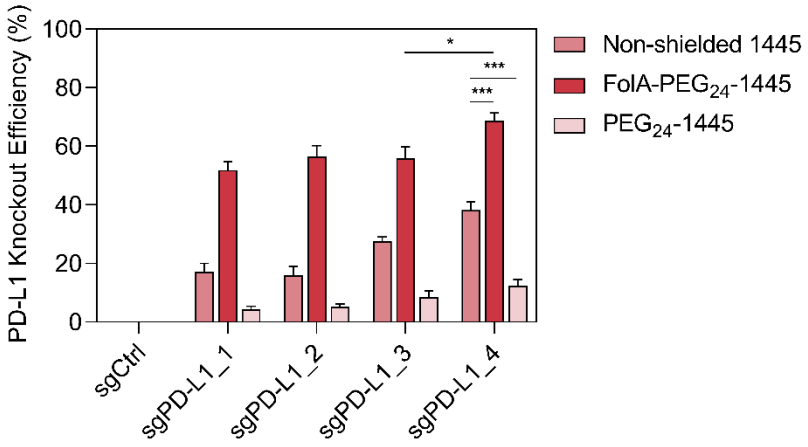

Figure 21. Screening of sgPD-L1. CT26 WT cells were incubated with Cas9 RNP nanocarriers containing 4 different sgPD-L1 sequences with or without 0.75 eq of ligand modification at the RNP dose of 75 nM for 4 h. Flow cytometry was conducted 48 h after transfection. The figure shows the PD-L1 knockout efficiency of Cas9 RNP nanocarriers containing 4 different sgPD-L1 sequences. Data are presented as the mean ± SD (n = 3).

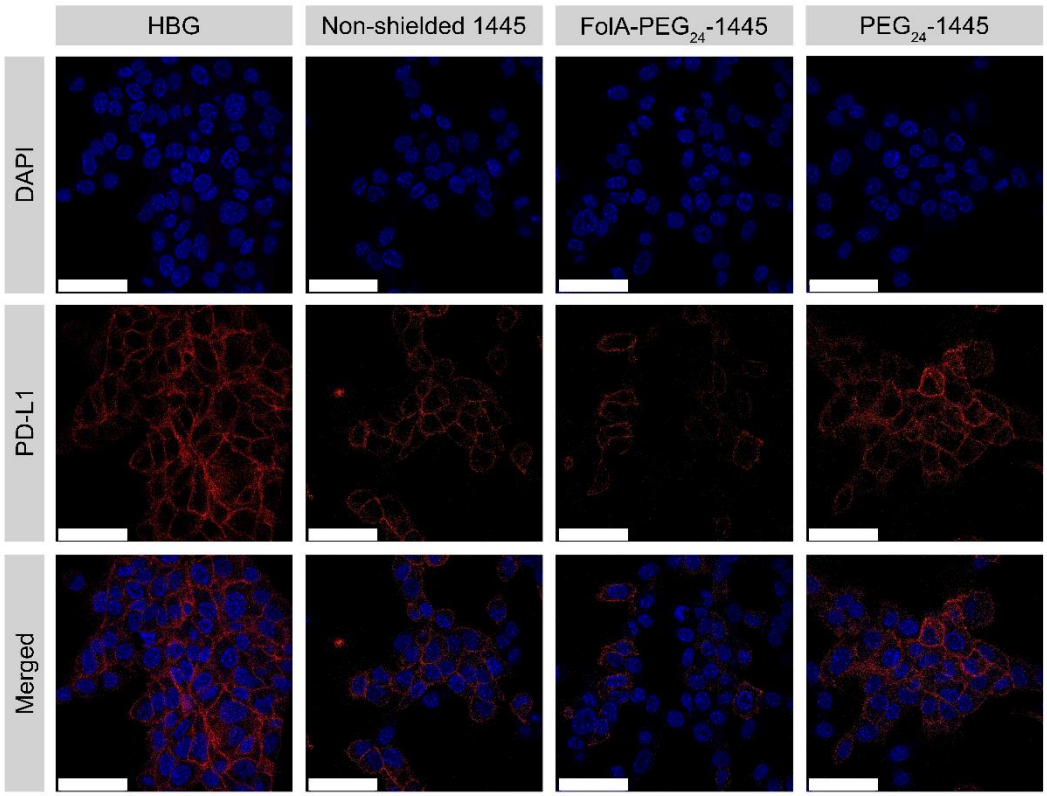

Figure 22. Confocal laser scanning microscopy (CLSM) images of CT26 WT cells after treatments with Cas9/sgPD-L1_4 RNP nanocarriers. CT26 WT cells treated with the Cas9 RNP nanocarriers containing 75 nM Cas9/sgPD-L1_4 RNP with or without 0.75 eq of ligand modification were recorded. First row: nuclear staining with DAPI; second row: fluorescence of APC-anti-PD-L1 antibody; third column: merge of two channels. A subset of the data is shown in Figure 4d of the main manuscript. Scale bar: 50 µm.

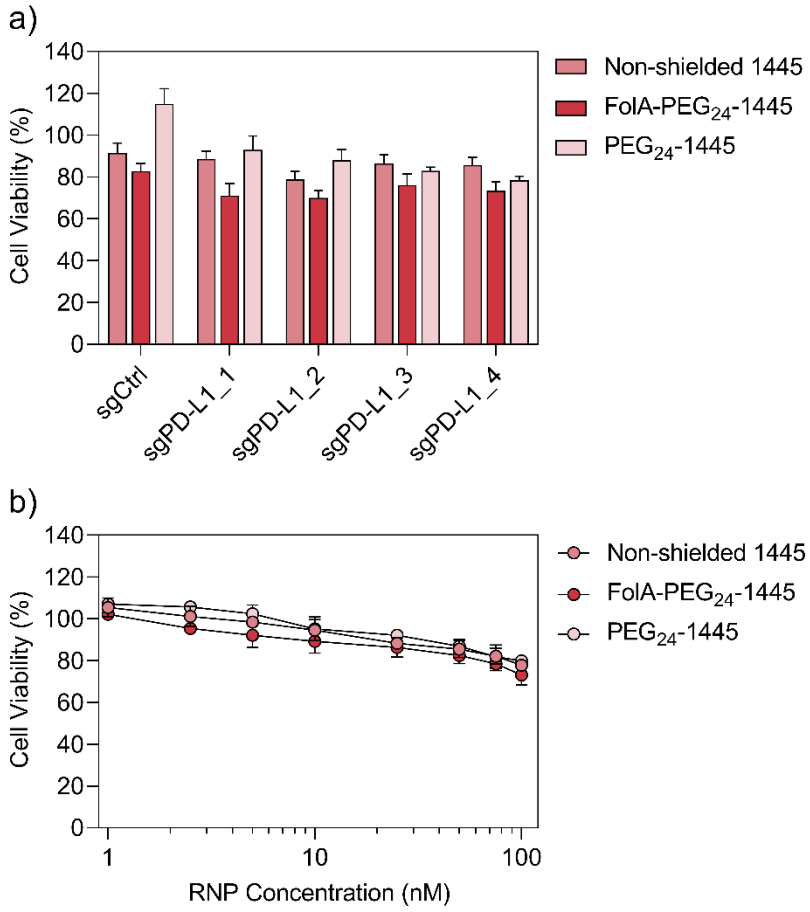

Figure 23. Viability of CT26 WT cells after treatments with Cas9/sgPD-L1 RNP nanocarriers with or without 0.75 eq of ligand modification. CT26 WT cells were incubated with the Cas9 RNP nanocarriers containing 4 different sgPD-L1 sequences at the RNP dose of 75 nM or the Cas9 RNP nanocarriers containing sgPD-L1_4 at various RNP doses ranging from 1 nM to 100 nM for 4 h. Metabolic activity of the cells was determined using a MTT assay 48 h after transfection. Data are presented as % cell viability with respect to the control cells ± SD (n = 3).

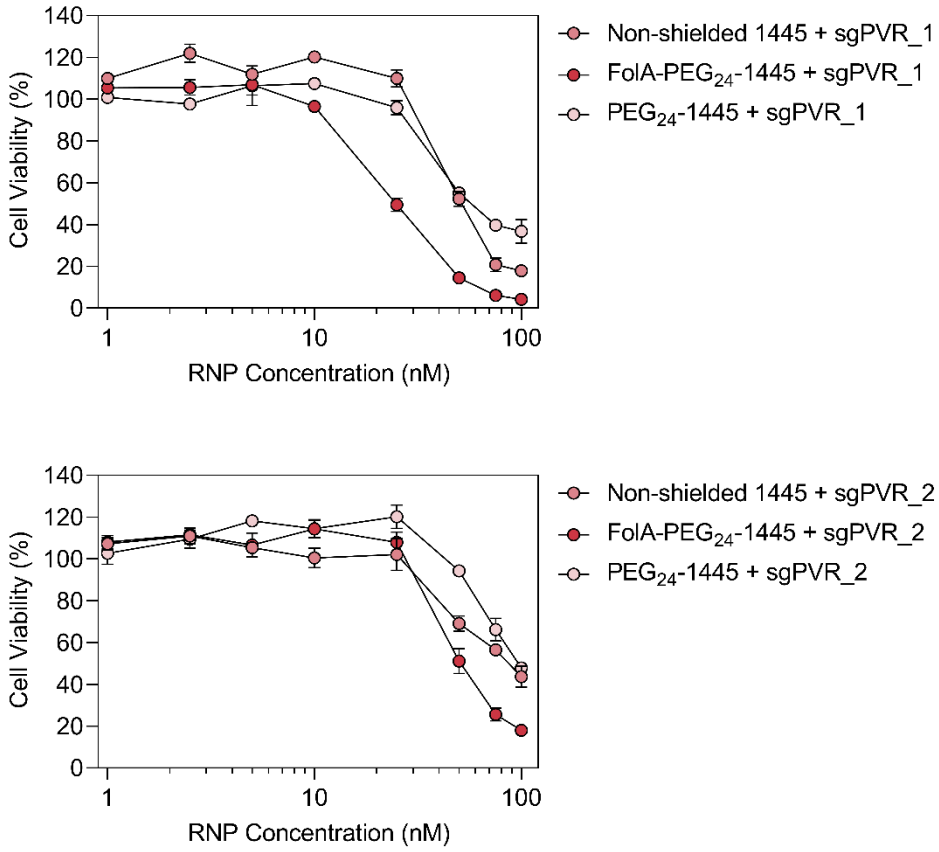

Figure 24. Viability of CT26 WT cells after treatments with Cas9/sgPVR RNP nanocarriers with or without 0.75 eq of ligand modification. CT26 WT cells were incubated with the Cas9 RNP nanocarriers containing sgPVR_1 or sgPVR_2 at various RNP doses ranging from 1 nM to 100 nM for 4 h. Metabolic activity of the cells was determined using a MTT assay 48 h after transfection. Data are presented as % cell viability with respect to the control cells ± SD (n=3).

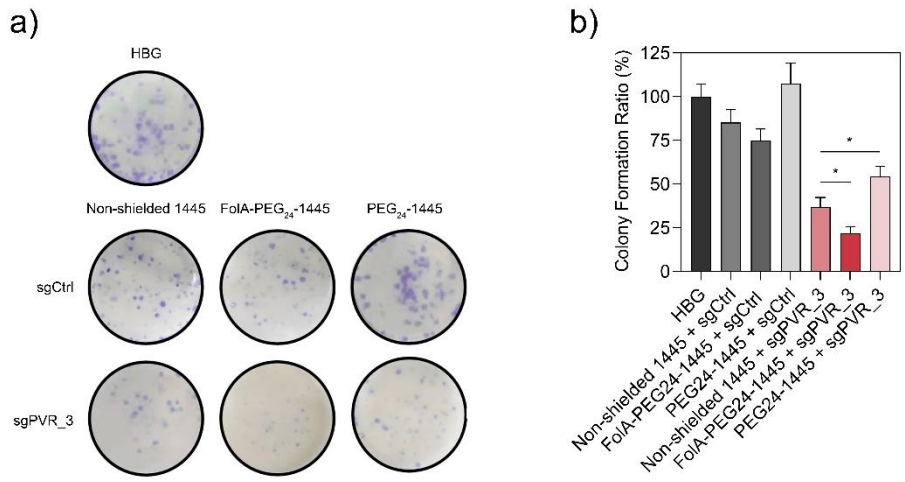

Figure 25. PVR knockout effect on CT26 WT cells evaluated by colony formation assay. CT26 WT cells were incubated with Cas9 RNP nanocarriers containing sgPVR_3 or sgCtrl with or without 0.75 eq of ligand modification at the RNP dose of 75 nM for 4 h. 250 cells of each group were subsequently re-plated and crystal violet staining was performed 3 weeks after re-plating. a) Representative colony formation images of CT26 WT cells treated with different RNP nanocarriers. b) Colony formation ratio of CT26 WT cells treated with different RNP nanocarriers. Data are presented as % colony formation ratio with respect to the control cells treated with HBG buffer ± SD (n=3).

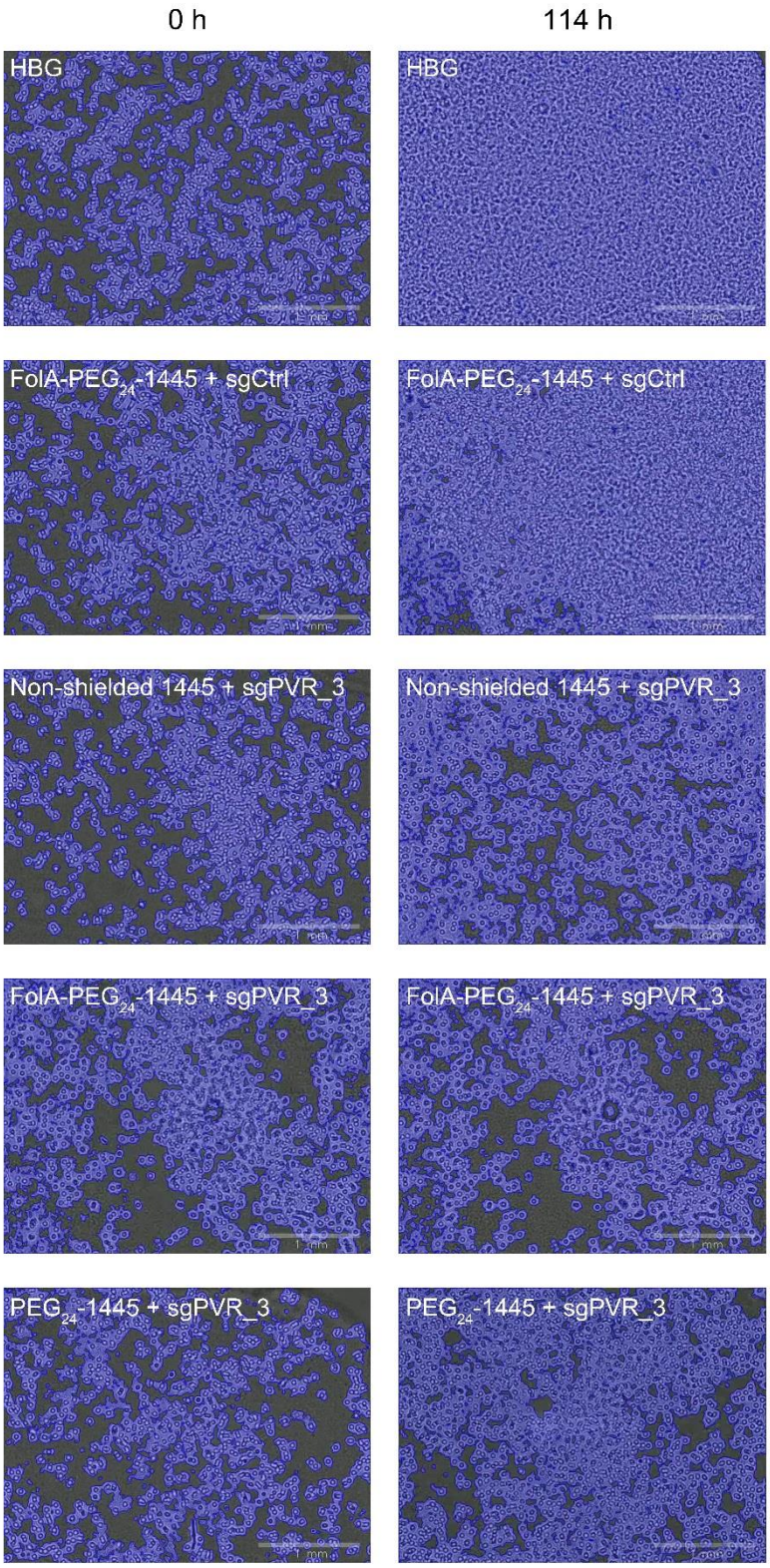

Figure 26. Cellwatcher images of CT26 WT cells treated with Cas9/sgPVR_3 RNP nanocarriers at starting and terminal time points. Cell growth kinetics were recorded from 0 h to 114 h. The RNP nanocarriers with or without 0.75 eq of ligand modification at the RNP dose of 75 nM were added to the cells 1 h after recording.

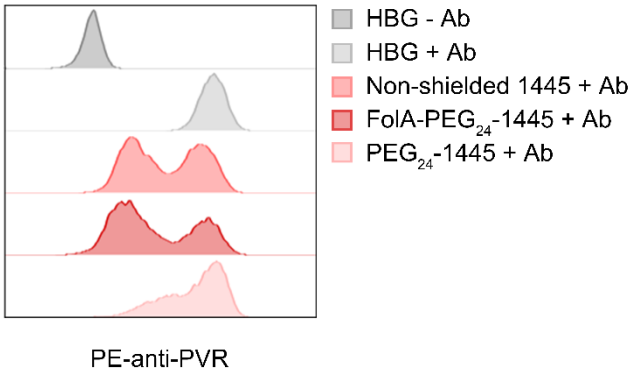

Figure 27. PVR knockout evaluation of CT26 WT cells treated with Cas9/sgPVR_3 RNP nanocarriers by flow cytometry. CT26 WT cells were incubated with the Cas9 RNP nanocarriers with or without 0.75 eq of ligand modification at the RNP dose of 75 nM for 4 h. Flow cytometry was conducted after PVR was stained with PE-anti-PVR antibody 3 days after transfection. The figure shows a flow cytometry histogram plot of each sample.

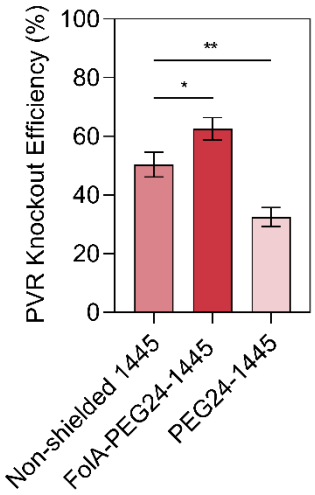

Figure 28. PVR knockout efficiency of Cas9/sgPVR_3 RNP nanocarriers in CT26 WT cells. CT26 WT cells were incubated with the Cas9 RNP nanocarriers with or without 0.75 eq of ligand modification at the RNP dose of 75 nM for 4 h. PVR knockout efficiency of each group was determined by flow cytometry 4 days after treatment. Data are presented as the mean ± SD (n=3).

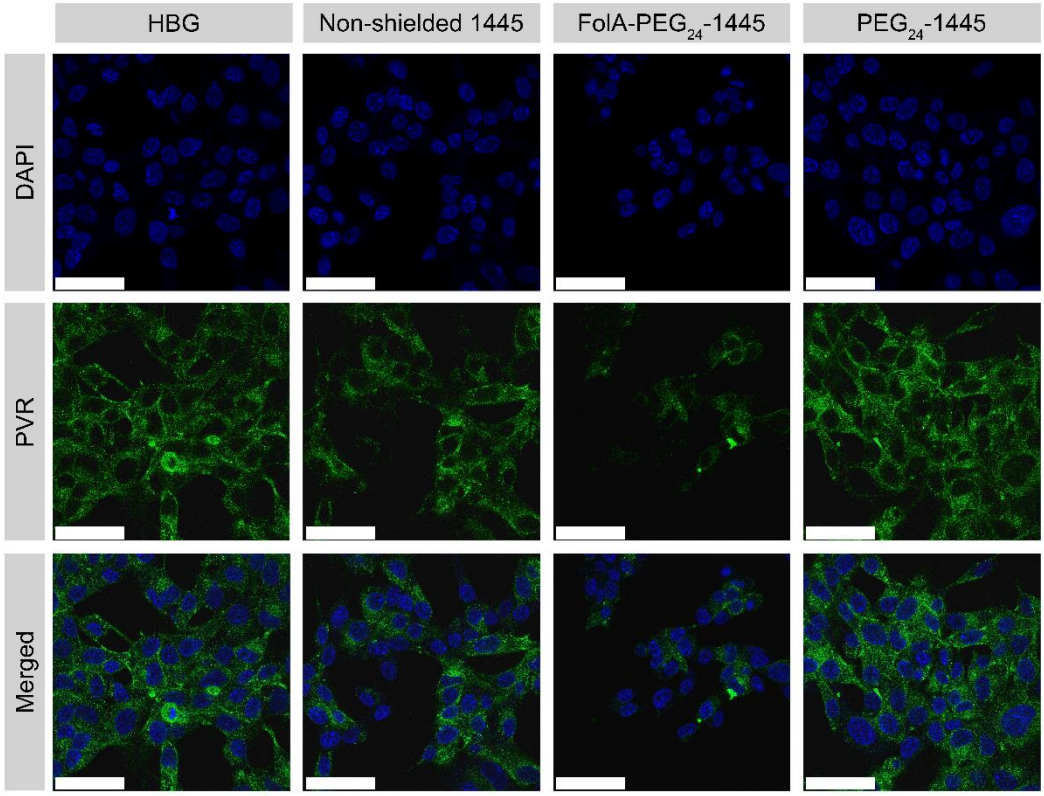

Figure 29. Confocal laser scanning microscopy (CLSM) images of CT26 WT cells after treatments with different Cas9/sgPVR_3 RNP nanocarriers. CT26 WT cells treated with the Cas9 RNP nanocarriers containing 75 nM Cas9/sgPVR_3 RNP with or without 0.75 eq of ligand modification were imaged. First row: nuclear staining with DAPI; second row: fluorescence of PE-anti-PVR antibody; third column: merge of two channels. A subset of the data is shown in Figure 5e of the main manuscript. Scale bar: 50 µm.

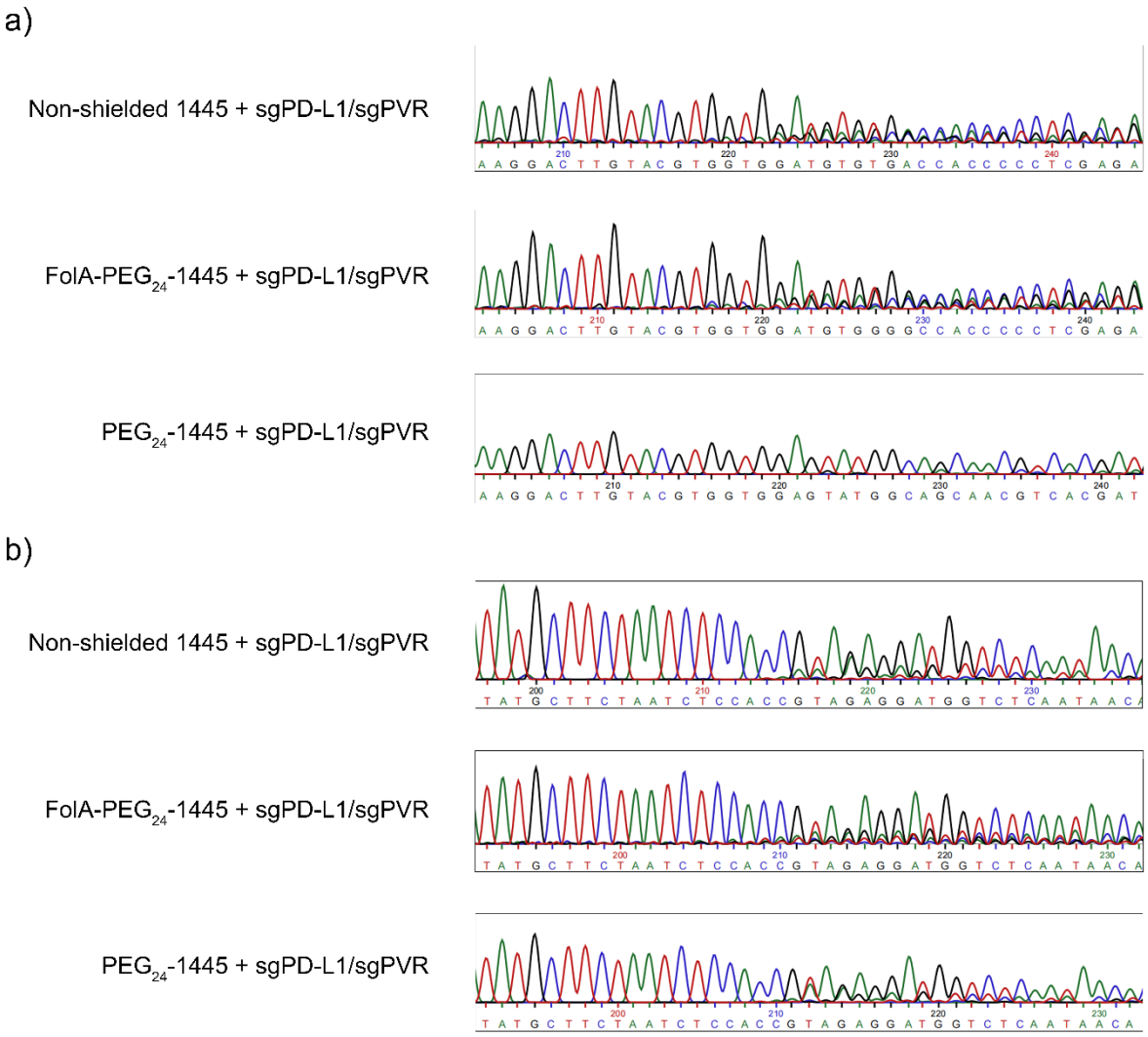

Figure 30. Sanger sequencing maps of PD-L1 and PVR genes at the target loci. Sanger sequencing maps of a) PD-L1 target locus and b) PVR target locus of genomic DNA isolated from CT26 WT cells treated with sgPD-L1_4/sgPVR_4 dual loaded Cas9 RNP nanocarriers.

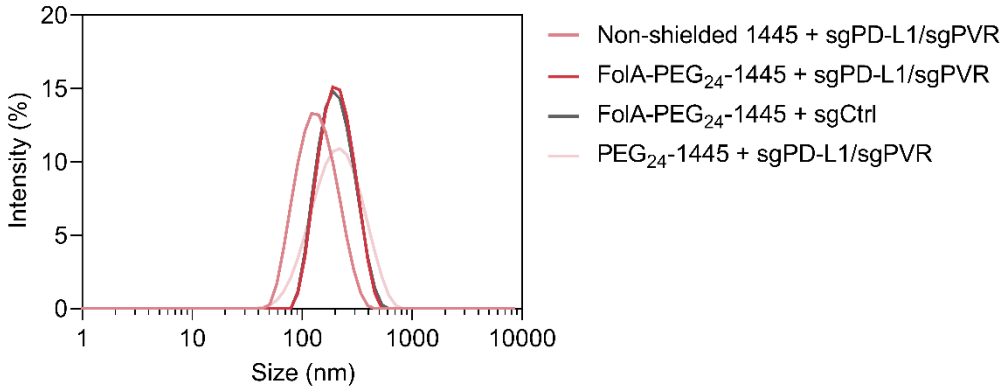

Figure 31. Particle size of Cas9 RNP nanocarriers for *in vivo* studies determined by DLS. sgPD-L1/sgPVR dual loaded or sgCtrl Cas9 RNP nanocarriers containing 125 µg Cas9 protein, 12.5 µg sgPD-L1_4, and 12.5 µg sgPVR_3 or 25 µg sgCtrl were prepared in 50 µL of HBG for each mouse. The figure shows the intensity size distribution of each sample.

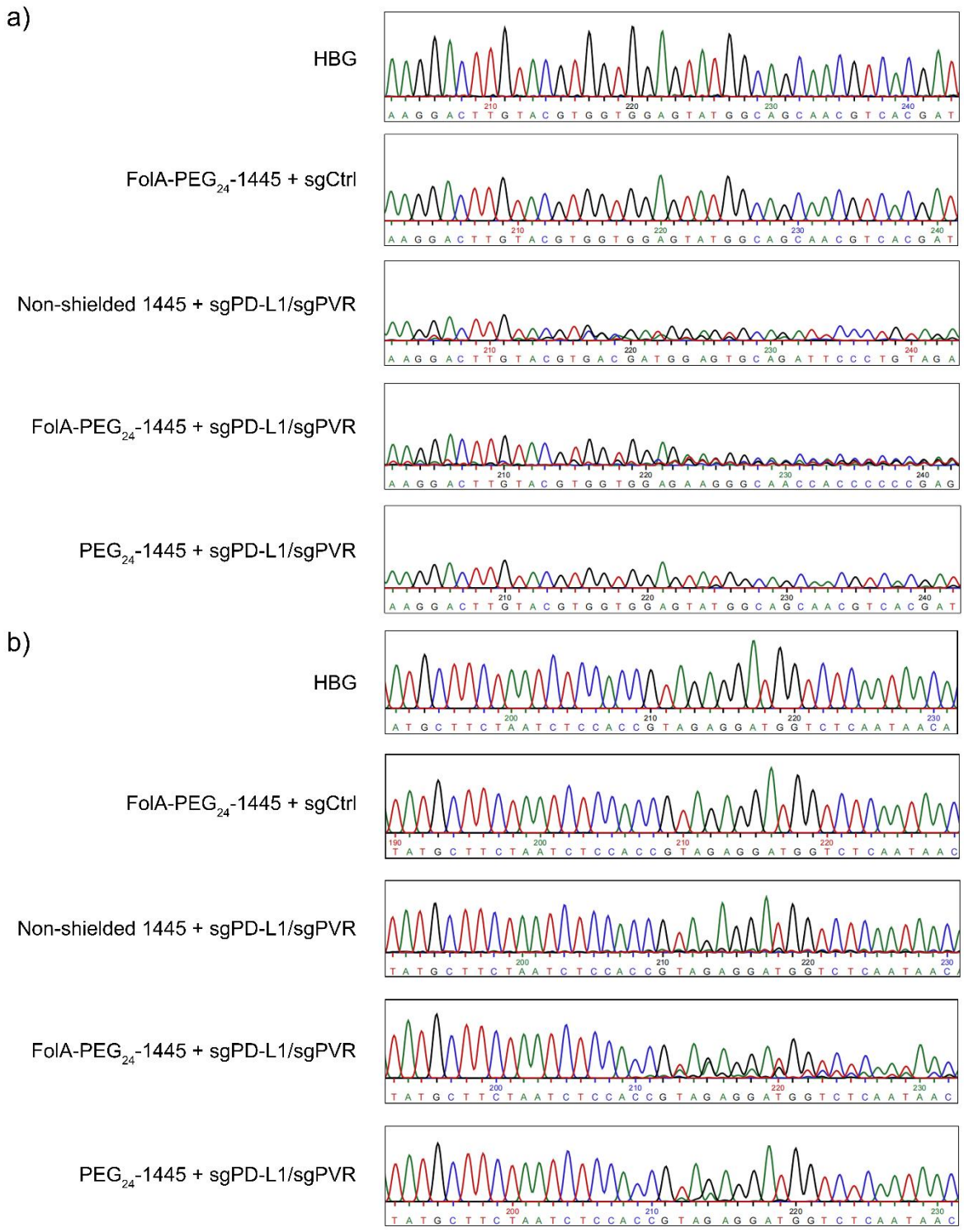

Figure 32. Sanger sequencing maps of PD-L1 and PVR at the target loci from CT26 tumor tissues. Sanger sequencing maps of a) PD-L1 target locus and b) PVR target locus of genomic DNA isolated from CT26 tumor tissues treated with HBG, sgCtrl-containing FolA-PEG$_{24}$-1445, sgPD-L1_4/sgPVR_3 dual loaded non-shielded 1445, sgPD-L1_4/sgPVR_3 dual loaded FolA-PEG$_{24}$-1445, and sgPD-L1_4/sgPVR_3 dual loaded PEG$_{24}$-1445.

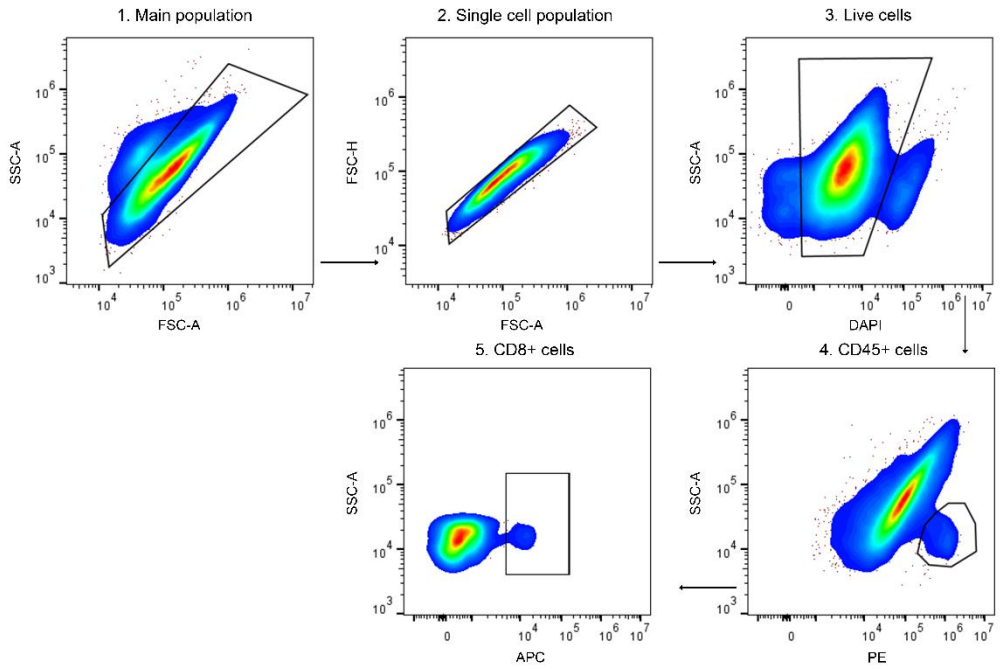

Figure 33. Gating strategy to determine CD8+ T cells in single cell tumor suspensions.

3 Chapter II:

Hydrophobic balance of artificial lipopeptides greatly promotes NHEJ and HDR gene editing by Cas9 ribonucleoproteins

Yi Lin[1], Xianjin Luo[1], Tobias Burghardt[1], Sarah Dörrer[1], Miriam Höhn[1], Ernst Wagner[1], and Ulrich Lächelt[1,2]

[1]Department of Pharmacy and Center for NanoScience (CeNS), LMU Munich, 81377 Munich, Germany
[2]Department of Pharmaceutical Sciences, University of Vienna, 1090 Vienna, Austria

The following sections are adapted from the manuscript.

Sections may have been moved for consistency.

3.1 Abstract

Introduction of the CRISPR/Cas9 system into cells in form of the Cas9/sgRNA ribonucleoprotein (RNP) is considered a straightforward strategy and potent vectors are in high demand. Here, we report a series of lipopeptides based on artificial amino acids that are able to deliver Cas9 RNP into cells. Systematic variation of hydrophobic properties revealed a correlation between the lipopeptide $logD_{7.4}$ and eGFP knockout EC50 values and $logD_{7.4}$ optima were found for different lipopeptide sequence architectures. The optimized lipopeptides enable ~88 % eGFP knockout at a RNP dose of only 1 nM, and up to 40 % homology-directed repair (HDR) in eGFP/BFP switchable HeLa cells by co-delivery with a ssDNA template. Mechanistic studies demonstrated that hydrophobically balanced lipopeptides are more resistant to ionic stress and concentration dependent dissociation and promote endocytosis by both clathrin-mediated and macropinocytosis pathways. These findings highlight impactful structure-activity relationships and can provide a new chemical guide for the design and optimization of non-viral Cas9 RNP nanocarriers.

3.2 Introduction

The CRISPR/Cas9 system has become a fundamental gene editing technology in modern biomedical research.[2,3,6] Introduction of the system into cells by plasmid DNA (pDNA) encoding Cas9 protein and sgRNA was initially the most widely used format, but is currently not preferred due to its low editing efficiency, rare but harmful insertional mutagenesis, and higher risk of off-target events.[53,55] Delivery of transiently expressed Cas9 mRNA is an alternative and the delivery technology of lipid nanoparticle (LNP) is more mature since the success of mRNA-based vaccines.[138,176,177] Instead of introducing these genetic “blue prints”, delivery of pre-assembled Cas9/sgRNA ribonucleoprotein (RNP) is generally considered the most efficient strategy and has gained much attention.[161] It bypasses the transcription and translation processes, and can be immediately functional once it is delivered into the cells. Similar to mRNA, RNP has a short exposure time to the cellular genome and can be rapidly eliminated, which decrease the potential off-target effects to the utmost extent.[53] Encouraged by the advantages of Cas9 RNP, numerous delivery strategies were developed, including polymer-based,[85] lipid-based,[43] peptide-based,[45,113] bio-derived vesicle-based,[119] DNA nanostructure-based,[127] inorganic and inorganic/organic hybrid delivery systems.[99,100]

Peptide-mediated delivery can be achieved either by covalent conjugation to the Cas9 protein[108,109] or by non-covalent ionic interaction with negatively charged Cas9 RNP.[45,113] In case of the peptide-Cas9 conjugates, Cas9 RNP is exposed to the cells without any protection which may result in the rapid degradation of both protein and sgRNA. Besides, the production of the conjugates by conjugation chemistry or protein engineering is complex and time-consuming,[75] and final products still face the risk of unpredictable loss of function.[178,179] In contrast, the complexation of Cas9 RNP with amphiphilic peptides containing cationic and hydrophobic domains such as hydrophobic amino acids or lipid chains via electrostatic interaction is more feasible.[45,116]

Herein, we report the synthesis of novel “T-shape” lipopeptides constructed from a series of artificial amino acids that are extremely potent for the intracellular delivery of Cas9 RNP. Through systematic variation of peptide sequences and fine tuning the hydrophobicity of artificial amino acids we have modulated the octanol-water

distribution coefficient ($logD_{7.4}$) of the sequence-defined lipopeptides and investigated the relationship between the $logD_{7.4}$ value and eGFP knockout EC50, which is defined as the concentration of delivered Cas9 RNP required to provoke 50 % eGFP knockout in HeLa cells.

3.3 Materials and methods

3.3.1 Materials

Tetraethylenepentamine (TEPA), triethylenetetramine (TETA), 3,3'-ethylenediiminodipropylamine (EIPA), 2-chlorotrityl chloride resin (200-400 mesh, 1 % DVB crosslinking), 1-hydroxybenzotriazole (HOBT), di-tert-butyl dicarbonate (Boc2O), stearic acid (SteA), oleic acid (OleA), linoleic acid (LinA), linolenic acid (LenA), 5β-cholanic acid (CholA), chloroform-d, deuterium oxide and Triton X-100 were purchased from Sigma-Aldrich (Munich, Germany). Succinic anhydride, glutaric anhydride, diglycolic anhydride, phthalic anhydride, 1,1-cyclohexanediacetic anhydride, hexahydrophthalic anhydride, and naphthalic anhydride were purchased from Sigma-Aldrich (Munich, Germany). (Benzotriazol-1-yloxy)tripyrrolidinophosphonium hexafluorophosphate (Pybop®) was purchased from Multisyntech (Witten, Germany). All fmoc-α-amino acids were obtained from Iris Biotech (Marktredwitz, Germany). Kaiser test solution was prepared using 80 % (w/v) phenol, 5 % (w/v) ninhydrine in ethanol, and 20 µM potassium cyanide in pyridine. All chemical reagents and solvents were used as received without further purification. Cas9 protein was produced in house. Single guide RNA (sgRNA, 2' O-methyl modification on the first 3 and last 3 RNA bases) and single stranded DNA (ssDNA) were purchased from Integrated DNA Technologies (IDT, USA), the sequences of sgRNA and ssDNA are shown below. Dulbecco's Modified Eagle's Medium (DMEM), penicillin/streptomycin and fetal bovine serum (FBS) were purchased from Life Technologies (Carlsbad, USA). 3-(4,5-Dimethylthiazol-2-yl)-2,5-diphenyltetrazolium bromide (MTT), 4′,6-diamidino-2-phenylindole (DAPI), and paraformaldehyde (PFA) were obtained from Sigma-Aldrich (Munich, Germany). HEPES buffered glucose solution (HBG, pH 7.4) was prepared using 20 mM HEPES and 5 % (w/v) glucose.

Deionized water was purified in-house using a Millipore system (Simplicity Plus, Millipore Corp.) and was used for all experiments.

sgGFP1 sequence (5' → 3'):
mG*mA*mC*rCrArGrGrArUrGrGrGrCrArCrCrArCrCrCrGrUrUrUrUrArGrArGrCrUrArG
rArArArUrArGrCrArArGrUrUrArArArArUrArArGrGrCrUrArGrUrCrCrGrUrUrArUrCrArAr
CrUrUrGrArArArArArGrUrGrGrCrArCrCrGrArGrUrCrGrGrUrGrCmU*mU*mU*rU

sgGFP2 sequence (5' → 3'):
mG*mC*mU*rGrArArGrCrArCrUrGrCrArCrGrCrCrGrUrGrUrUrUrUrArGrArGrCrUrArG
rArArArUrArGrCrArArGrUrUrArArArArUrArArGrGrCrUrArGrUrCrCrGrUrUrArUrCrArAr
CrUrUrGrArArArArArGrUrGrGrCrArCrCrGrArGrUrCrGrGrUrGrCmU*mU*mU*rU

ssDNA sequence (5' → 3'):
G*C*CACCTACGGCAAGCTGACCCTGAAGTTCATCTGCACCACCGGCAAGCTGC
CCGTGCCCTGGCCCACCCTCGTGACCACCCTGAGCCACGGCGTGCAGTGCTTC
AGCCGCTACCCCGACCACAT*G*A

sgGFP1 was used in all eGFP knockout experiments. sgGFP2 was used in all homology-directed repair (HDR) mediated eGFP to BFP conversion experiments.

3.3.2 ^{1}H Nuclear magnetic resonance (1H NMR) spectroscopy

^{1}H NMR spectra were recorded on an Advance III HD Bruker BioSpin (400 MHz) in chloroform-d ($CDCl_3$), deuterium oxide (D_2O) or methanol-d4 (CD_3OD) without TMS. Chemical shifts were calibrated to the residual solvent signal and were reported in parts per million (ppm). The spectra were processed in MestReNova software (MestReLab Research, SL). Integration was performed manually.

3.3.3 Electrospray ionization mass spectroscopy (ESI-MS)

ESI mass spectra of artificial building blocks were recorded with a Thermo Scientific LTQ FT Ultra fourier transform ion cyclotron and an IonMax source in chloroform or methanol.

3.3.4 Matrix-assisted laser desorption/ionization mass spectrometry (MALDI-MS)

MALDI mass spectra of lipopeptides were recorded on an Autoflex II mass spectrometer (Bruker Daltonics, Bremen, Germany) in the positive ion mode. Super-DHB in H_2O/ACN/TFA (69.93:30:0.07) was used as matrix solution. 1 µL of the matrix solution was spotted on an MTP AnchorChip (Bruker Daltonics, Bremen, Germany). After drying of the matrix, 1 µL of lipopeptide solution (1 mg/mL in water) was added to the dried matrix.

3.3.5 Size-exclusion chromatography (SEC)

Purification of lipopeptides was carried out by SEC using a Äkta purifier system (GE Healthcare Bio-Sciences AB, Uppsala, Sweden) equipped with a P-900 solvent pump module, a UV-900 UV/VIS multi-wavelength detector, a pH/C-900 conductivity module and a Frac-950 automated fraction collector. Sephadex G-10 (MWCO 700 Da) was used as the gel filtration resin and 10 mM HCl solution/acetonitrile (v/v, 7/3) as the mobile phase.

3.3.6 Analytical reverse phase high-performance liquid chromatography (RP-HPLC)

The octanol/water distribution of lipopeptides was analyzed by RP-HPLC on a VWR Hitachi Chromaster HPLC system equipped with a 5160 pump module, a 5260 auto sampler, a 5310 column oven, and a 5430 diode array detector. 50 µL of lipopeptides in octanol or water were analyzed using a YMC C18 column (HS-302, HS12S05-1546WT, 5 µm, 4.6 x 150 mm, 12 nm, YMC Europe GmbH, Dinslaken, Germany) and a water/acetonitrile gradient (95:5 - 0:100) containing 0.1 % TFA. The extinction at 280 nm was monitored.

3.3.7 Dynamic light scattering (DLS) and zeta potential analysis

The hydrodynamic particle size and zeta potential of nanoparticles were measured in folded capillary cells (DTS 1070) using a Zetasizer Nano ZS (Malvern Instruments,

UK). The scattering angle of 173° was fixed, the refractive index (RI) of the solvent was 1.330, the viscosity was 0.8872 mPa·s, and the temperature was set to 25 °C. All samples were measured 3 times with 12-15 sub-runs.

3.3.8 Ribogreen assay

sgRNA amount in naked Cas9/sgRNA ribonucleoproteins (Cas9 RNPs) or Cas9 RNP nanocarriers were determined using a Quant-iTTM RiboGreen® RNA assay kit (Invitrogen, CA, USA). 50 µL of naked Cas9 RNPs or Cas9 RNP nanocarriers containing 250 ng Cas9 protein and 50 ng sgRNA were mixed with 50 µL of TE buffer and were added to the 96-well plate. The plate was incubated for 10 min. Afterwards, 100 µL of Ribogreen solution (diluted 1:100 in TE buffer) was added to each well. The plate was incubated for another 5 min. Ribogreen fluorescence intensity was detected using a microplate reader (Spectrafluor Plus, Tecan, Männedorf, Switzerland) with excitation and emission wavelength of 485 and 528 nm, respectively.

3.3.9 Cell culture

HeLa WT, HeLa eGFP/tub, and HeLa GFPd2 (destabilized eGFP) cells were grown in DMEM medium supplemented with 10 % FBS, 100 U/mL penicillin, and 100 µg/mL streptomycin. The cells were cultured in ventilated flasks in the cell incubator at 37 °C and 5 % CO_2 in a humidified atmosphere. The cells were passaged at a confluency of approximately 80 %.

3.3.10 Flow cytometry

Cells were harvested and resuspended in 600 µL of FACS buffer (PBS buffer containing 10 % FBS). The samples were analyzed by flow cytometry on a CytoFLEX S flow cytometer (Beckman Coulter, CA, USA). For eGFP knockout and cellular uptake experiments, 0.6 µL of 1 µg/µL DAPI was added to each sample for differentiating live and dead cells before the measurement. The DAPI signal and BFP fluorescence were detected with 405 nm excitation and 450 nm emission. The eGFP

and ATTO488 fluorescence was assayed with 488 nm excitation and 530 nm emission. The ATTO647N fluorescence was assayed with 640 nm excitation and 670 nm emission. Ten thousand of isolated live cells were counted and evaluated. The data were analyzed using FlowJo 7.6.5 by FlowJo, LLC (Becton, Dickinson and Company, USA).

3.3.11 MTT assay

Cell viability was determined using an MTT assay. After different treatments, 10 µL of MTT (5 mg/mL) were added to each well. Cells were incubated for 2 h. Afterwards, medium was removed and the plate was frozen at – 80 °C for 4 h. 100 µL of DMSO were added to each well. The plate was incubated for another 30 min at 37 °C under constant shaking. The absorbance was measured at 590 nm with background correction at 630 nm using a microplate reader (Tecan Spark 10M, Tecan, Männedorf, Switzerland). The relative cell viability (%) was calculated relative to control wells treated with HBG buffer as ([A] test/[A] control) × 100 %.

3.3.12 Confocal Laser Scanning Microscopy (CLSM)

CLSM images were recorded on a Leica-TCS-SP8 confocal laser scanning microscope equipped with a HC PL APO 63× 1.4 objective (Germany). DAPI emission was recorded at 450 nm, Rhodamine at 540 nm, mRuby3 at 590 nm, ATTO647N-Cas9 at 670 nm, and ATTO488-sgRNA at 520 nm. All images were processed using the LAS X software from Leica.

3.4 Experimental

3.4.1 Synthesis of *N*-(*tert*-Butoxycarbonyl)iminodiacetic acid (Boc-IDA)

N-(*tert*-Butoxycarbonyl)iminodiacetic acid (Boc-IDA) was synthesized as previously reported with slight variations.[180] In brief, 13.3 g of iminodiacetic acid (0.1 mol, 1 eq) and 200 mL 1,4-dioxane were added into a 1 L round-bottom flask. 200 mL NaOH

solution (1 M) were added and the mixture was stirred until a clear solution formed. 24.0 g of di-*tert*-butyl dicarbonate (0.11 mol, 1.1 eq) dissolved in 50 mL 1,4-dioxane were added and the mixture was stirred at RT for 72 h. Afterwards, the mixture was concentrated to approximately 200 mL under reduced pressure, washed twice with 150 mL diethyl ether. 100 mL 10 % HCl were then added to acidify the mixture. The product was extracted with ethyl acetate (3 x 150 mL). The organic phases were collected and dried over anhydrous sodium sulfate. The ethyl acetate was filtrated and evaporated to obtain 21.8 g of Boc-IDA (0.094 mol, 94 %) as white crystals.

3.4.2 Synthesis of *N*-(*tert*-Butoxycarbonyl)iminodiacetic acid anhydride (Boc-IDA anhydride)

5.0 g of Boc-IDA (21.5 mmol, 1 eq) and 250 mL DCM were added into a 500 mL round-bottom flask. 4.45 g of dicyclohexylcarbodiimid (21.5 mmol, 1 eq) dissolved in 50 mL DCM were then added and the mixture was stirred at RT overnight. Afterwards, the mixture was concentrated to approximately 100 mL under reduced pressure. The insoluble dicyclohexyl urea was removed by filtration. The obtained solution was evaporated to yield 4.3 g of Boc-IDA anhydride (19.9 mmol, 93 %) as a solid.

3.4.3 Synthesis of *N*-(Trifluoroethyl)iminodiacetic acid (TFE-IDA)

TFE-IDA was synthesized analog to the synthesis of methyliminodiacetic acid reported by Berchet with modification.[181] 20.0 g of chloroacetic acid (211.6 mmol, 2 eq) were put into a 500 mL round-bottom flask. 20 mL H_2O were added and the flask was cooled in an ice bath. 93 mL cold NaOH (21.1 g, 529 mmol, 5 eq) solution were added slowly under stirring. Afterwards, the cooling bath was removed and 14.3 g of trifluoroethylamine hydrochloride (105.8 mmol, 1 eq) dissolved in 65 mL H_2O were added dropwise. After complete addition, the mixture was stirred overnight. The next day 45 g of $BaCl_2$ dihydrate in 100 mL boiling H_2O were added and the mixture was heated for 1.5 hours. The solid was filtered off and dried to yield 20.5 g of TFE-IDA barium salt (58.6 mmol). The TFE-IDA barium salt was put into a 500 mL round-bottom flask. 50 mL H_2O were added and heated to boiling. 23.4 mL H_2SO_4 solution

(2.5 M, 58.6 mmol) were added slowly under constant heating to boiling. After cooling to RT, the mixture was centrifuged to remove the solid $BaSO_4$. The supernatant was freeze-dried to yield 16.1 g of TFE-IDA (55.7 mmol, 53 %) as colorless crystals.

3.4.4 Synthesis of *N*-(Trifluoroethyl)iminodiacetic acid anhydride (TFE-IDA anhydride)

5.0 g TFE-IDA (23.2 mmol) and 140 mL DCM were put into a 250 mL round-bottom flask. 4.8 g dicyclohexylcarbodiimid (23.2 mmol, 1 eq) dissolved in 30 mL DCM were added into the flask. The mixture was stirred at RT overnight. The next day the mixture was concentrated to approximately 80 mL under reduced pressure. The insoluble dicyclohexyl urea was removed by filtration. The obtained solution was evaporated to yield 4.2 g TFE-IDA anhydride (21.3 mmol, 92 %) as a solid.

3.4.5 Synthesis of artificial amino acid building blocks

The synthesis procedures of artificial amino acid building blocks are shown in Scheme 4. Fmoc-Stp(Boc_3)-OH, Fmoc-Boc-IDAtp(Boc_3)-OH, Fmoc-dGtp(Boc_3)-OH, Fmoc-Gtp(Boc_3)-OH, Fmoc-Htp(Boc_3)-OH, Fmoc-chGtp(Boc_3)-OH, Fmoc-TFE-IDAtp(Boc_3)-OH, Fmoc-Gtt(Boc_2)-OH, Fmoc-GEIPA(Boc_2)-OH, Fmoc-Ptp(Boc_3)-OH, and Fmoc-Ntp(Boc_3)-OH were synthesized analogously as previously reported.[168] In brief, the primary amines of TETA, TEPA or EIPA were firstly protected with ethyl trifluoroacetate. The secondary amines were then Boc-protected with di-tert-butyl dicarbonate (Boc_2O) in a one-pot reaction. The bis-tfa-TETA(Boc_2) or bis-tfa-TEPA(Boc_3) were obtained after purification and recrystallization. Subsequently, the primary amines were deprotected with NaOH solution (H_2O/EtOH, v/v, 55/45) to give the compound TETA(Boc_2), TEPA(Boc_3), or EIPA(Boc_2). Last, the two primary amines were successively substituted by a cyclic anhydride (as shown in Scheme 4) and Fmoc-OSu. Purification of the final compounds was performed by dry column vacuum chromatography (DCVC).

3.4.6 Synthesis of hydroxystearic acid (OHSteA)

4 g oleic acid (14.16 mmol) were added into a 250 mL round-bottom flask. 60 mL TFA/DCM solution (v/v, 2/1) were added and the mixture was stirred at RT for 72 h. Subsequently, the solvent was removed by a nitrogen flow to yield 5.45 g of hydroxystearic acid TFA ester (13.74 mmol, 97 %). In the next step, 5.45 g hydroxystearic acid TFA ester (13.74 mmol) was dissolved in 60 mL NaOH methanol/water solution (v/v, 4/1, 1 M) and the mixture was stirred overnight. The next day 1 M HCl solution was added slowly to the mixture to adjust pH to 1-2. The mixture was centrifuged. The supernatant was evaporated to obtain light brown powder. The products were dissolved in H_2O and extracted 3 times with DCM. The organic phases were combined and evaporated to yield 3.57 g of hydroxystearic acid (11.9 mmol, 84 %) as white powder.

3.4.7 Solid-phase synthesis of lipopeptides

All lipopeptides were synthesized manually on 2-chlorotrityl chloride resin using standard Fmoc-based solid-phase peptide synthesis.[168] For standard Fmoc-α-amino acids, Fmoc-Stp(Boc_3)-OH, Fmoc-Boc-IDAtp(Boc_3)-OH, Fmoc-dGtp(Boc_3)-OH, Fmoc-Gtp(Boc_3)-OH, Fmoc-TFE-IDAtp(Boc_3)-OH, Fmoc-Gtt(Boc_2)-OH, or Fmoc-GEIPA(Boc_2)-OH, the coupling step was performed using 4 eq Fmoc-amino acid, 4 eq HOBt, 4 eq PyBOP, and 8 eq DIPEA in DCM/DMF (1/1, 5 mL g^{-1} resin) for 75 min. For Fmoc-Htp(Boc_3)-OH or Fmoc-chGtp(Boc_3)-OH, the coupling step was performed using 4 eq Fmoc-amino acid, 4 eq HOBt, 4 eq PyBOP, and 8 eq DIPEA in DCM/DMF (1/1, 5 mL g^{-1} resin) containing 1 % Triton X-100 overnight. For Fmoc-Ptp(Boc_3)-OH or Fmoc-Ntp(Boc_3)-OH, the coupling step was performed using 4 eq Fmoc-amino acid, 4 eq Oxyma, and 4 eq DIC in NMP (5 mL g^{-1} resin) overnight. Fmoc deprotection step was performed by 3 times incubation with 20 % piperidine in DMF (5 mL g^{-1} resin) containing 1 % Triton X-100 for 15 min. The resin was washed 3 times with DMF and 3 times with DCM after each coupling and deprotection step. A Kaiser test was then carried out. After the last deprotection of Fmoc-Lys(N_3)-OH, the N-terminal amino group was protected with 10 eq Boc_2O and 10 eq DIPEA in DCM/DMF (1/1, 5 mL g^{-1} resin). Dde deprotection of Fmoc-Lys(Dde)-OH was accomplished by 15 times incubation with 2 % hydrazine in DMF for 2 min.

Subsequently, the resin was washed 5 times with DMF, 5 times with 10 % DIPEA in DMF, and 3 times with DCM (5 mL g−1 resin each). Afterwards, Fmoc-Lys(Fmoc)-OH was introduced followed by the coupling of different fatty acids. The resin was washed 3 times with DMF and DCM and dried in vacuo. The lipopeptides were cleaved off the resin by incubation with pre-cooled cleavage cocktail TFA/EDT/H_2O/TIS (94/2.5/2.5/1, 10 mL g^{-1} resin) for 30 min. The cleavage solution was then immediately precipitated in pre-cooled MTBE/n-hexane (1/1, 40 mL). Afterwards, the lipopeptides were purified by a Äkta purifier system (GE Healthcare Bio-Sciences AB, Uppsala, Sweden) using 10 mM HCl solution/acetonitrile (v/v, 7/3) as solvent and Sephadex G-10 (MWCO 700 Da) as the gel filtration resin. The fractions were combined and snap frozen and lyophilized to obtain the final products.

3.4.8 $LogD_{7.4}$ determination of lipopeptides

Octanol–water partition coefficient D at pH 7.4 ($logD_{7.4}$) was determined as previously reported with slight modification.[182] Briefly, 10 µL of 10 mg/mL lipopeptides in water were diluted with 90 µL HEPES buffer (20 mM, pH 7.4) in 1.5 mL reaction tubes. 100 µL *n*-octanol were then added. The tubes were shaken at 1400 rpm for 24 h. Afterwards, the tubes were centrifuged followed by storage at 4 °C for 1 h to separate n-octanol and water phases. 70 µL of each phase were injected for HPLC analysis. The extinction at 280 nm was monitored and the peak area (A) of the lipopeptides was calculated. $LogD_{7.4}$ was calculated as $\log(A_{octanol} / A_{water})$. All experiments were performed in triplicate.

3.4.9 Preparation of Cas9 RNP and Cas9 RNP/ssDNA nanocarriers

Cas9 protein and sgRNA were mixed at 1:1 molar ratio and incubated at RT for 15 min to form the Cas9/sgRNA ribonucleoprotein (RNP) complexes. Afterwards, Cas9 RNP was added into the lipopeptide solution in HBG buffer (pH 7.4) at an N/P (nitrogen to phosphate of sgRNA) ratio of 24. The solution was mixed thoroughly by pipetting up and down and incubated at RT for another 15 min to generate the final Cas9 RNP nanocarriers. In case of preparing Cas9 RNP/ssDNA nanocarriers for HDR experiments, Cas9 RNP was mixed with ssDNA HDR template at 1:1 molar

ratio and then added into the lipopeptide solution in HBG buffer (pH 7.4) at an N/P (nitrogen to phosphate of sgRNA plus ssDNA) ratio of 12. The solution was mixed and incubated for 40 min to generate the Cas9 RNP/ssDNA nanocarriers.

3.4.10 Characterization of Cas9 RNP nanocarriers

The hydrodynamic size, PDI and zeta potential of Cas9 RNP nanocarriers were measured by DLS using a Zetasizer Nano ZS (Malvern Instruments, UK). Cas9 RNP nanocarriers were prepared as described above. The hydrodynamic size of Cas9 RNP nanocarriers containing 1.25 µg Cas9 protein and 0.25 µg sgRNA (Cas9/sgRNA, 1:1 molar ratio) in 100 µL HBG was measured. Afterwards, 700 µL HEPES buffer (20 mM, pH 7.4) were added to each sample and the solution was mixed for the zeta potential measurement. For the dilution stability study, Cas9 RNP nanocarriers were prepared at an RNP concentration of 375 nM (6.25 µg Cas9 protein and 1.25 µg sgRNA) and then diluted with HBG buffer to a series of RNP concentrations (75, 50, 25, 10, 5, 2.5, 1, 0.5, and 0.1 nM). The size and zeta potential of diluted samples were measured as described above.

3.4.11 Heparin competition assay

Heparin competition assay was performed to evaluate the nanocarrier stability against anions. 50 µL TE buffer containing different amounts of Heparin were added to the 96-well plate. 50 µL of Cas9 RNP nanocarriers containing 250 ng Cas9 protein and 50 ng sgRNA were prepared and added to each well. The final amounts of Heparin were 0, 0.25, 0.5, 1, 2.5, 5 IU per µg of sgRNA. The plate was incubated at 37 °C for 30 min. Afterwards, 100 µL Ribogreen solution were added and a Ribogreen assay was performed as described above. HBG buffer and naked Cas9 RNP at the same conditions were prepared as the controls. After subtraction of the blank wells (HBG buffer), the fraction of dye exclusion was calculated as [1 − fraction of Ribogreen intercalation (normalized to Ribogreen intercalation of naked Cas9/sgRNA RNP)]. All experiments were performed in triplicate.

3.4.12 Nanocarrier stability in salt conditions

Nanocarrier stability against salt was studied using NaCl solutions. 50 µL TE buffer containing different concentrations of NaCl were added to the 96-well plate. 50 µL of Cas9 RNP nanocarriers containing 250 ng Cas9 protein and 50 ng sgRNA were prepared and added to each well. The final concentrations of NaCl were 0, 0.05, 0.15, 0.25, 0.5, 5 M. The plate was incubated at 37 °C for 30 min. Afterwards, 100 µL Ribogreen solution were added and a Ribogreen assay was performed. HBG buffer and naked Cas9 RNP at the same conditions were prepared as the controls. After subtraction of the blank wells (HBG buffer), the fraction of dye exclusion was calculated as [1 − fraction of Ribogreen intercalation (normalized to Ribogreen intercalation of naked Cas9/sgRNA RNP)]. All experiments were performed in triplicate.

3.4.13 Cellular uptake of Cas9 RNP nanocarriers

Cellular uptake of Cas9 RNP nanocarriers was evaluated by flow cytometry and confocal laser scanning microscopy (CLSM). For flow cytometry experiments, HeLa WT cells were seeded into 24-well plates at a density of 25000 cells/well one day prior to the treatments. On the next day, the medium was replaced with 400 µL of fresh medium. Cas9 RNP nanocarriers were prepared as described above using 20 % of ATTO647N-Cas9 and 20 % of ATTO488-sgRNA. 100 µL of RNP nanocarriers were added to each well resulting in a final concentration of 75 nM Cas9 RNP followed by incubation of the cells for 4 h. Afterwards, the medium was removed and 500 µL PBS containing 2000 IU heparin were added to disassociate the nanocarriers attached on the cell membrane. The cells were incubated on ice for 30 min. Subsequently, the cells were collected and prepared for flow cytometry analysis as described above. All experiments were performed in triplicate.

For CLSM experiments, HeLa WT cells were seeded in 8-well Ibidi µ-slides (Ibidi GmbH, Germany) at a density of 15000 cells/well one day prior to the treatments. On the next day, the medium was replaced with 240 µL of fresh medium. 60 µL of dye-labeled RNP nanocarriers were added to each well resulting in a final concentration of 75 nM Cas9 RNP followed by incubation of the cells for 4 h. The medium was removed and 300 µL PBS containing 1200 IU heparin were added. The cells were

incubated on ice for 30 min. Subsequently, the cells were washed twice with PBS and fixed with 4 % PFA in PBS at RT for 40 min. The cells were then washed twice with PBS and the cell nuclei were stained with 2 µg/mL DAPI in PBS at RT for 20 min. Afterwards, the DAPI solution was removed and 300 µL fresh PBS were added to each well. The slides were stored at 4 °C in the dark until the measurement.

3.4.14 Endocytosis pathway study

Potential endocytosis pathways of Cas9 RNP nanocarriers with varied hydrophobicity were investigated by using different endocytosis inhibitors. One day prior to the treatments, HeLa WT cells were seeded into 24-well plates at a density of 25000 cells/well. On the next day, the medium was replaced with 500 µL of serum-free medium containing different endocytosis inhibitors (15.4 mM sodium azide, 10 µM chlorpromazine, 450 mM sucrose, 54 µM nystatin, or 1 mM amiloride). The cells were incubated at 37 °C for 2 h. Afterwards, the medium was replaced with 400 µL of fresh medium. 100 µL of dye-labeled RNP nanocarriers were added to each well resulting in a final concentration of 75 nM Cas9 RNP followed by incubation of the cells for 4 h. For 4 °C group, the cells were placed on ice for 2 h prior to the treatment of 75 nM Cas9 RNP in ice-cold medium. Afterwards, the medium was removed and 500 µL PBS containing 2000 IU heparin were added followed by incubation of the cells on ice for 30 min. The cells were then collected and prepared for flow cytometry analysis. All experiments were performed in triplicate.

3.4.15 Endosomal escape of Cas9 RNP nanocarriers

Endosomal escape of Cas9 RNP nanocarriers were studied by CLSM using a HeLa reporter cell line stably expressing mRuby3-galectin 8 fusion protein.[84] The PB-CAG-mRuby3-Gal8-P2A-Zeo plasmid was a gift from Jordan Green's lab (Addgene plasmid no. 150815; http://n2t.net/addgene:150815; RRID: Addgene_150815). HeLa mRuby3/gal8 cells were seeded in 8-well Ibidi µ-slides (Ibidi GmbH, Germany) at a density of 15000 cells/well one day prior to the treatments. On the next day, the medium was replaced with 240 µL of fresh medium. 60 µL of RNP nanocarriers were added to each well resulting in a final concentration of 75 nM Cas9 RNP followed by

incubation of the cells for 4 h. Next, the cells were washed twice with PBS and then fixed with 4 % PFA at RT for 40 min. Afterwards, the cells were washed and incubated with 2 µg/mL DAPI (for staining cell nuclei) for 30 min. Then, the staining solution was removed and 300 µL fresh PBS were added. The slides were stored at 4 °C in the dark until the measurement.

3.4.16 eGFP knockout study

One day prior to the treatments, HeLa eGFP/tub cells were seeded into 96-well plates at a density of 5000 cells/well. On the next day, the medium was replaced with 80 µL of fresh medium. 20 µL of Cas9 RNP nanocarriers were added to each well resulting in a series of concentrations of RNP (100, 75, 50, 25, 10, 5, 2.5, 1, 0.5, and 0.1 nM). The cells were incubated for 48 h. Afterwards, the cells were trypsinized and transferred to 24-well plates, and incubated for another 72 h. Then, the cells were harvested and prepared for flow cytometry analysis. All experiments were performed in triplicate.

3.4.17 eGFP to BFP conversion (HDR) study

One day prior to the treatments, HeLa GFPd2 cells were seeded into 96-well plates at a density of 5000 cells/well. On the next day, the medium was replaced with 80 µL of fresh medium. 20 µL of Cas9 RNP/ssDNA nanocarriers containing different molar ratios of RNP/ssDNA were added to each well resulting in a series of concentrations of RNP (100, 75, 50, 25, 10, 5, 2.5, 1, 0.5, and 0.1 nM). The cells were incubated for 48 h. Afterwards, the cells were trypsinized and transferred to 24-well plates, and incubated for another 72 h. Then, the cells were harvested and prepared for flow cytometry analysis. All experiments were performed in triplicate.

3.4.18 Cell viability assay (MTT)

Treatments were performed as described in eGFP knockout and HDR studies. The cells were incubated for 48 h and an MTT assay was then carried out as mentioned above. All experiments were performed in triplicate.

3.4.19 Statistical analysis

Half maximal effective concentration (EC50) values were calculated by GraphPad prism 5. EC50-log$D_{7.4}$ correlation was analyzed with a second order polynomial equation by GraphPad prism 5. All other data were analyzed with GraphPad prism 5 and presented as arithmetic mean ± standard deviation (SD) of at least triplicates. The statistical significance of the experiments was estimated using the two-tailed student's t-test, **** $p \leq 0.0001$, *** $p \leq 0.001$, ** $p \leq 0.01$, * $p \leq 0.05$.

3.5 Results and discussion

We have previously identified an artificial "T-shape" lipopeptide, Stp2-C-OHSteA (Scheme 2) generated by solid-phase peptide synthesis (SPSS), as an efficient RNP delivery carrier. The artificial amino acid, succinoyl-tetraethylenepentamine (Stp) , serves as an ionizable unit to complex negatively charged Cas9 RNP and facilitate cellular delivery.[162-170] The hydrophobic tyrosine (Y) tripeptide motif enhances nanoparticle stability via hydrophobic interactions and improves transfection efficiency.[183] In our previous work, the fatty acid modification has been identified as an essential element which critically impacts delivery efficiency. In this work, the lead structure Stp2-C-OHSteA has been varied systematically to elucidate structure-activity relationships and evolve the next generation of RNP carriers. Structural variations including 1) presence of cysteine (C), 2) presence of histidine (H), 3) number of Stp units, and 4) type of fatty acid were introduced into the peptide sequence (Scheme 2). The Cas9 RNP nanocarriers were prepared by straightforward complexation of the lipopeptides with Cas9 RNP at an N/P ratio of 24. The hydrodynamic size, polydispersity index (PDI), and zeta potential of each nanocarrier were then determined by dynamic light scattering (DLS, Table 7 and Figure 38). Most lipopeptides generated RNP nanoparticles with a size between 150 – 250 nm and PDI of 0.15 – 0.40, except Stp2 and Stp2-H structures, which led to larger complexes (250 – 500 nm). Besides, all nanoparticles exhibited a positive surface charge with a zeta potential between 10 – 19 mV.

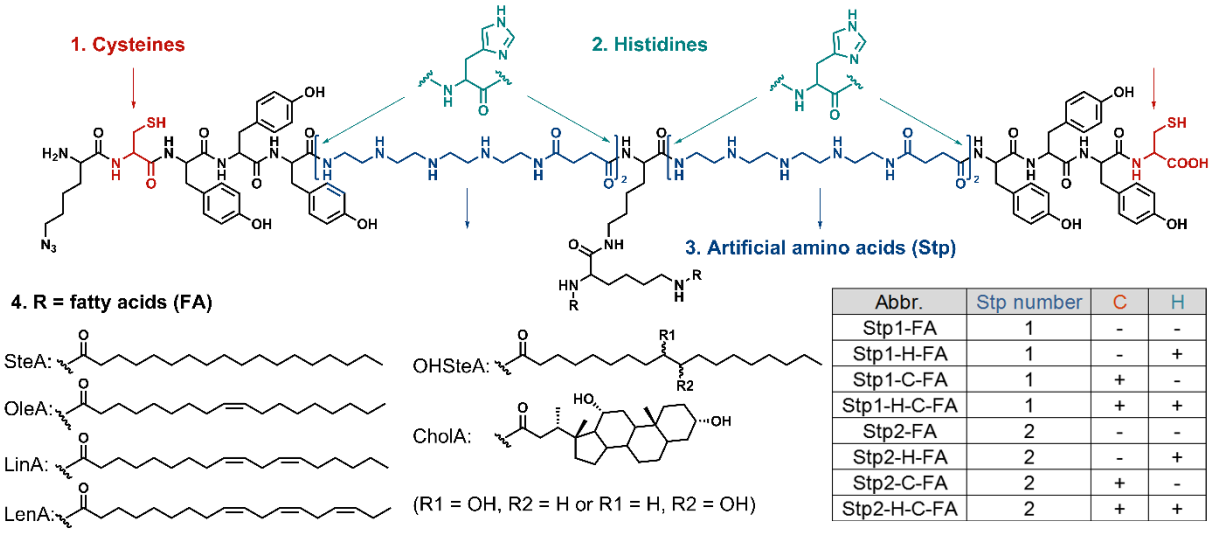

Abbr.	Stp number	C	H
Stp1-FA	1	-	-
Stp1-H-FA	1	-	+
Stp1-C-FA	1	+	-
Stp1-H-C-FA	1	+	+
Stp2-FA	2	-	-
Stp2-H-FA	2	-	+
Stp2-C-FA	2	+	-
Stp2-H-C-FA	2	+	+

Scheme 2. Chemical structure of T-shape lipopeptides for Cas9 RNP delivery.

The gene knockout efficiency and cytotoxicity of the nanocarriers were investigated in HeLa eGFP/tub cells after treatment with 75 nM RNP for 48 h (Figure 34A). The systematic evaluation demonstrated the effect of each variation. Firstly, cysteine showed benefits in lipopeptides containing 2 Stp units at each side beyond the lysine (Stp2 structures), but rather decreased the transfection efficiency in Stp1-based sequences. Secondly, histidine which has been previously shown to facilitate endosomal escape of polyplexes did not induce significant improvement in case of RNP nanocarriers. Thirdly, Stp1 structures in general demonstrated a better knockout performance than Stp2 structures. Lastly, in all cases unsaturated (OleA, LinA, LenA) or hydroxyl-modified fatty acids (OHSteA) were essential to mediate significant gene editing; saturated stearic acid (SteA) as well as the steroid cholanic acid almost completely interrupted any knockout efficiency. Seven lipopeptides exhibited better or comparable knockout efficiency than the initial Stp2-C-OHSteA and especially the Stp1 series outperformed the preceding lead structure. Over 90 % of eGFP knockout was achieved with these structures at the dose of 75 nM RNP. To differentiate the potency of the nanocarriers more in depth, a dose titration experiment was conducted in the concentration range of 1 nM – 100 nM RNP (Figure 34B). The lead structure Stp2-C-OHSteA showed a clear dose-dependent activity and eGFP knockout levels dropped below 40% at concentrations of 10 nM RNP or lower.

The new lipopeptide analogs Stp1-LinA, Stp1-LenA and Stp1-H-LinA turned out to be much more potent and induced ~80 % eGFP knockout even at the lowest RNP dose of 1 nM. Cell viability studies showed that all nanocarriers were generally well-tolerated except Stp1-C-OHSteA (Figure 34B).

Due to the generally more hydrophobic nature of the identified outperformers with lower content of ionizable artificial amino acid than the initial Stp2-C-OHSteA, we hypothesized that the hydrophobicity of the lipopeptides may be an important parameter to achieve efficient Cas9 RNP delivery. Consequently, the potency could be improved even further by fine tuning the hydrophobic properties of the artificial amino acid units. To validate this hypothesis, a series of artificial amino acid building blocks with varied hydrophilic or hydrophobic structural elements and suitable protective groups for SPPS was synthesized (Scheme 3A and Scheme 4).

Eight more hydrophobic Stp analogs were obtained by replacing tetraethylenepentamine (tp) by oligoamines with lower number of ionizable nitrogens (triethylenetetramine, tt or 3,3'-ethylenediiminodipropylamine, EIPA), and by including more hydrophobic dicarboxylic acids instead of succinic acid. Two more hydrophilic analogs were generated by replacing succinic acid by more hydrophilic dicarboxylic acids containing an amine or ether group (Scheme 3A). For a systematic evaluation of the new building blocks, the backbone sequences of the two best-performers Stp1-LinA and Stp1-H-LinA, as well as the initial lead structure Stp2-C-OHSteA were selected as lipopeptide architectures (Scheme 3B). The combination of 11 building blocks with 3 architectures resulted in a total of 33 lipopeptides which were synthesized by SPPS (Table 6 and 7).

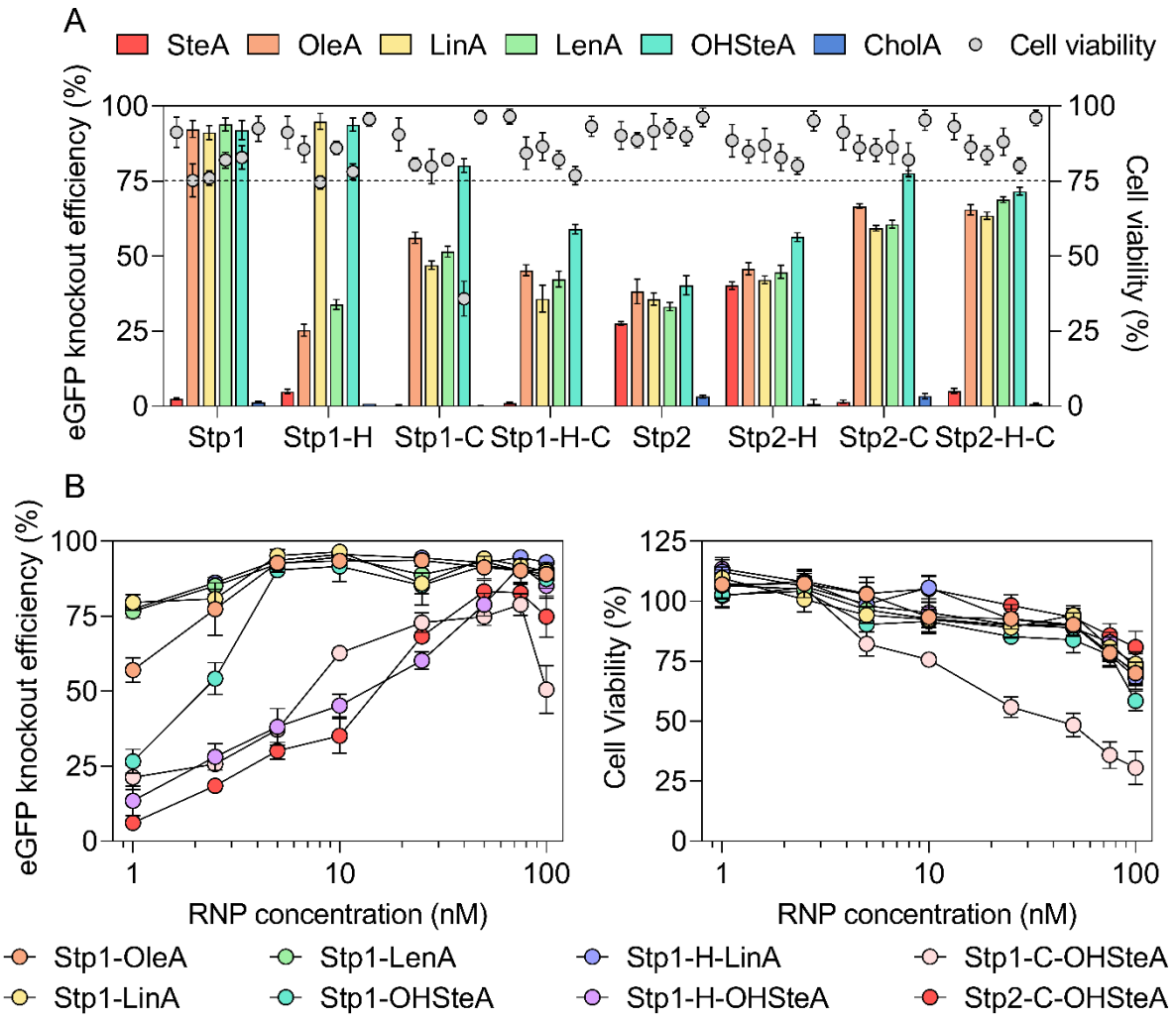

Figure 34. Reporter gene knockout efficiency and cytotoxicity of Stp-based lipopeptides. A) eGFP knockout efficiency and cell viability of HeLa eGFP/tub cells after 48 h treatment with Cas9 RNP nanocarriers at 75 nM RNP dose. B) eGFP knockout efficiency (left) and cell viability (right) of HeLa eGFP/tub cells after 48 h treatment with Cas9 RNP nanocarriers at a series of RNP concentrations ranging from 1 nM to 100 nM. Data are presented as mean ± SD (n = 3).

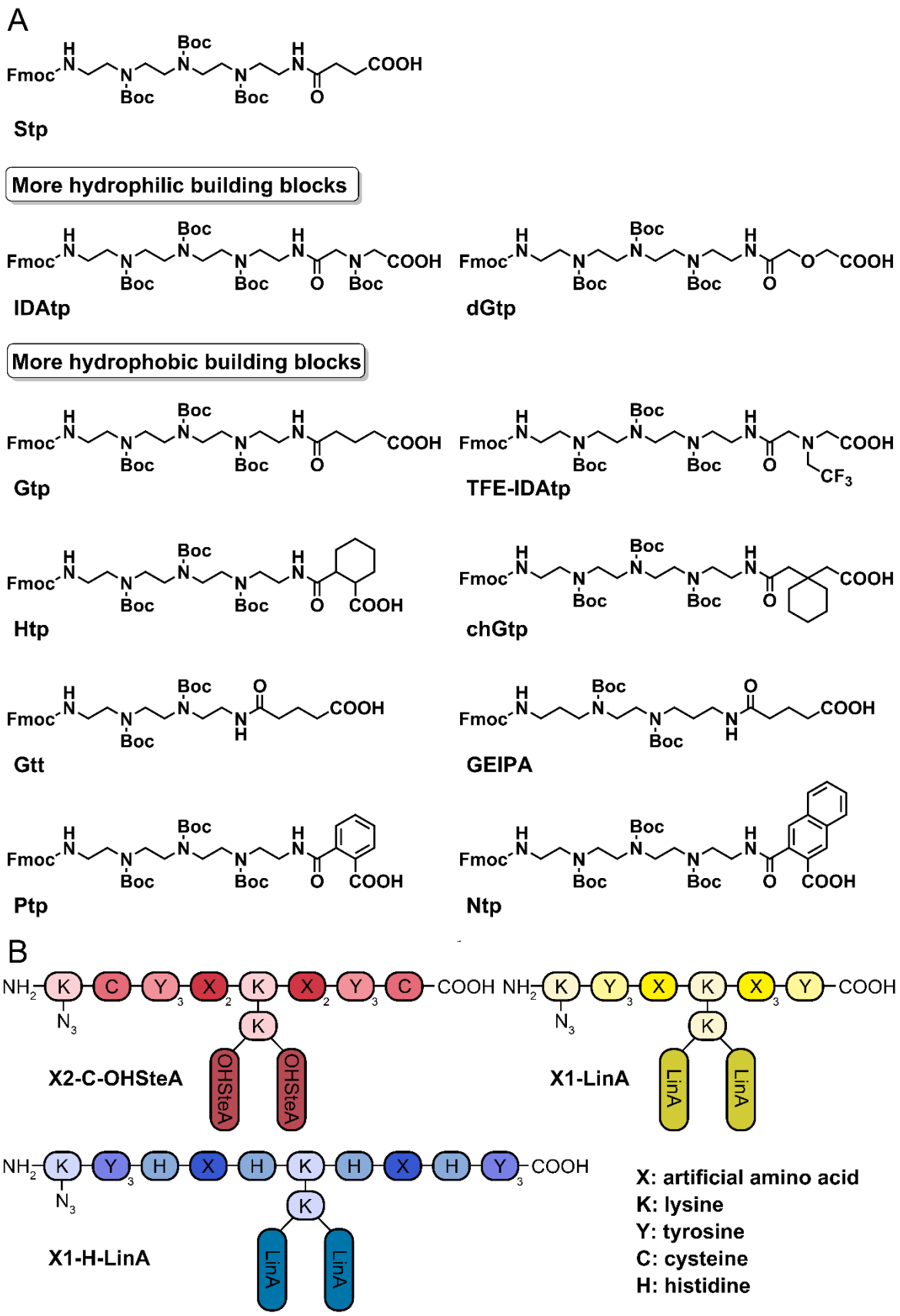

Scheme 3. Chemical structures of Stp analogs with varied hydrophobicity. A) Artificial amino acid building blocks with protective groups for use in solid-phase peptide synthesis (SPPS). B) Lipopeptide architectures selected for the construction of hydrophobically balanced lipopeptides.

$LogD_{7.4}$ of each lipopeptide was determined by quantifying the compound concentration in octanol and water phases by reversed-phase HPLC after mixing and phase separation.[182] The determined $logD_{7.4}$ values (Table 6) indicated the following order of artificial amino acids with increasing hydrophobicity: IDAtp < dGtp < Stp < Gtp < TFE-IDAtp < Htp < chGtp < Gtt < GEIPA < Ptp < Ntp. Cas9 RNP nanocarriers were then formulated with the lipopeptides (N/P = 24), and the size, PDI and zeta potential were determined by DLS. All lipopeptides formed homogeneous nanoparticles with Cas9 RNP with a size of 140 – 190 nm, PDI of 0.15 – 0.38, and zeta potential of 10.5 – 17.2 mV (Table 7). A dose titration study in the RNP concentration range between 0.1 nM – 100 nM was performed and the eGFP knockout EC50 of each lipopeptide was calculated (Table 6 and Figure 35A).

In general, structures based on the X1-LinA architecture exhibited the best knockout efficiency, where 6 out of 11 lipopeptides achieved ~75 - 80 % eGFP knockout at 1 nM RNP dose and 3 out of 11 lipopeptides even induced over 50 % eGFP disruption at 0.5 nM. X1-H-LinA based structures also demonstrated very high potency, but slightly lower efficacy than X1-LinA derivatives at very low doses of RNP (0.5 nM). Notably, the performance of X2-C-OHSteA structures was significantly boosted by introducing more hydrophobic artificial amino acids (Gtt, GEIPA, Htp, chGtp, TFE-IDAtp). The best performers of each lipopeptide series were identified as Gtt2-C-OHSteA, GEIPA1-H-LinA, and TFE-IDAtp1-LinA. Especially, TFE-IDAtp1-LinA achieved up to 99 % eGFP knockout at RNP concentrations down to 5 nM, ~88 % knockout at 1 nM, and still enabled ~61 % eGFP disruption at 0.5 nM. Cell viability studies revealed that Htp and chGtp containing structures were toxic at high RNP concentrations (25 – 100 nM) while all other artificial amino acids-containing lipopeptides were well-tolerated (Figure 39).

Table 6. Summary of octanol-water distribution coefficient at pH 7.4 ($logD_{7.4}$) of lipopeptides and eGFP knockout EC50 of lipopeptide-based Cas9 RNP nanocarriers.

ID	Abbreviation	$logD_{7.4}$	EC50 (nM)[a]
1445	Stp2-C-OHSteA	-1.33	14.50
1631	Gtp2-C-OHSteA	-1.30	15.38
1633	Htp2-C-OHSteA	-1.12	3.08
1634	Ptp2-C-OHSteA	-0.64	18.75
1635	Ntp2-C-OHSteA	-0.49	40.23
1636	Gtt2-C-OHSteA	-0.85	1.60
1637	GEIPA2-C-OHSteA	-0.80	3.18
1733	chGtp2-C-OHSteA	-1.00	4.15
1734	dGtp2-C-OHSteA	-1.41	35.03
1735	TFE-IDAtp2-C-OHSteA	-1.21	2.20
1736	IDAtp2-C-OHSteA	-1.47	17.67
1396	Stp1-H-LinA	-1.08	0.71
1647	Gtp1-H-LinA	-1.02	0.69
1649	Htp1-H-LinA	-0.89	0.67
1650	Ptp1-H-LinA	-0.48	12.24
1651	Ntp1-H-LinA	-0.29	18.59
1652	Gtt1-H-LinA	-0.68	0.75
1653	GEIPA1-H-LinA	-0.63	0.51
1741	chGtp1-H-LinA	-0.82	0.64
1742	dGtp1-H-LinA	-1.12	6.97
1743	TFE-IDAtp1-H-LinA	-0.99	0.65
1744	IDAtp1-H-LinA	-1.51	5.44
1392	Stp1-LinA	-0.83	0.44
1639	Gtp1-LinA	-0.79	0.80
1641	Htp1-LinA	-0.58	0.55
1642	Ptp1-LinA	-0.31	2.52
1643	Ntp1-LinA	-0.24	2.97
1644	Gtt1-LinA	-0.37	7.36
1645	GEIPA1 -LinA	-0.33	3.36
1737	chGtp1-LinA	-0.48	0.53
1738	dGtp1-LinA	-0.89	0.41
1739	TFE-IDAtp1-LinA	-0.70	0.38
1740	IDAtp1-LinA	-1.11	5.35

[a] EC50 (nM) is defined as the concentration of delivered Cas9 RNP required to provoke halfway eGFP knockout in HeLa eGFP/tub cells. Cas9 RNP nanocarriers were prepared by complexing lipopeptide with Cas9 RNP at an N/P ratio of 24.

To correlate the obtained structure-activity relationships with hydrophobic characteristics, the $logD_{7.4}$ was plotted versus eGFP knockout EC50 values for each lipopeptide series (Figure 35B). A clear correlation between the $logD_{7.4}$ and EC50 was found, and optimal $logD_{7.4}$ ranges were identified for each sequence-defined lipopeptide series. The efficacy of structures with $logD_{7.4}$ values beyond the optimal range (too hydrophililc or too hydrophobic) dramatically dropped.

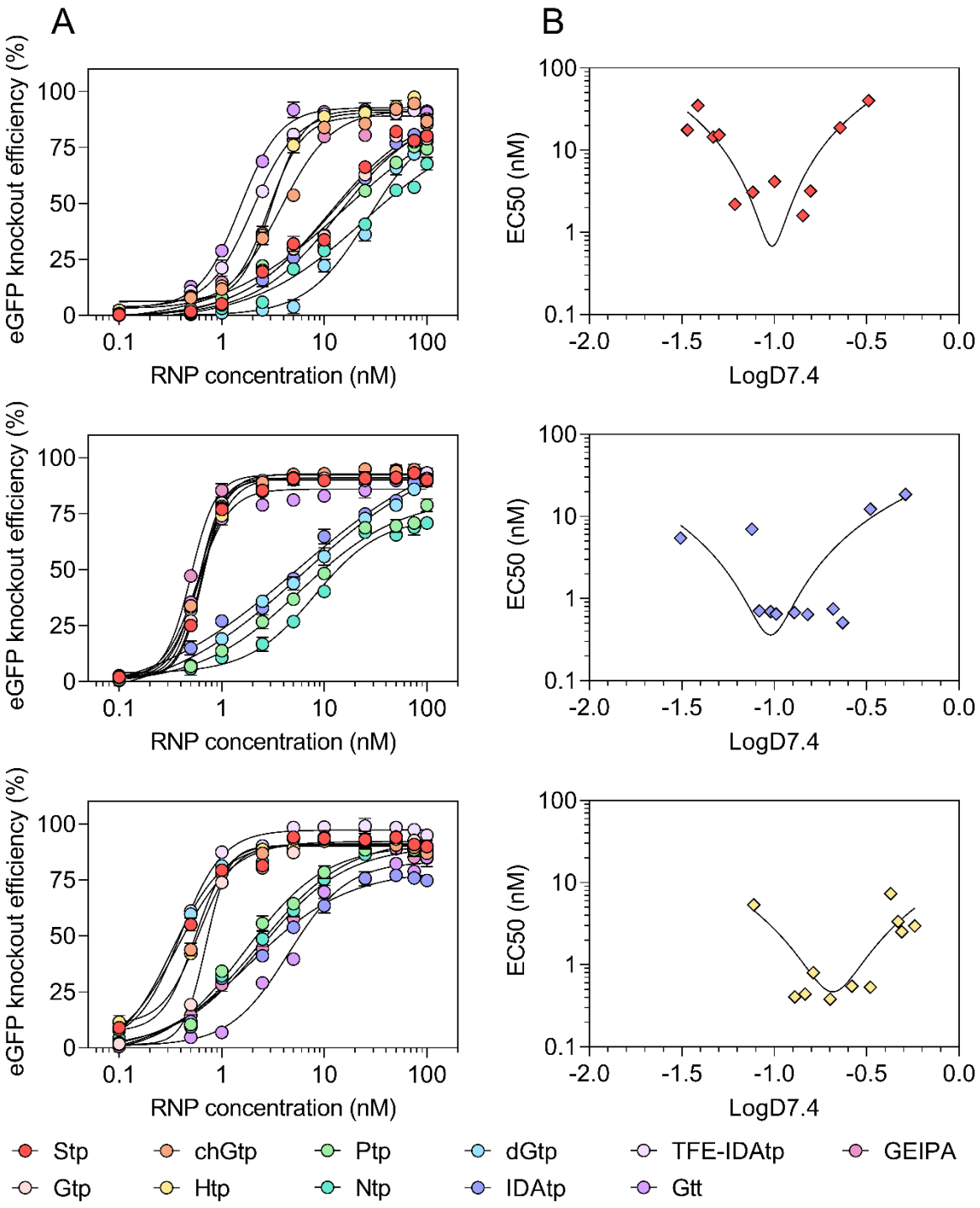

Figure 35. Dose-titration of artificial lipopeptides and logD7.4 correlation with eGFP knockout efficiencies. (A) eGFP knockout efficiency in HeLa eGFP/tub cells after 48 h treatment with Cas9 RNP nanocarriers at a series of RNP concentrations ranging from 0.1 nM to 100 nM; From top to bottom: X2-C-OHSteA, X1-H-LinA, X1-LinA; Data are presented as mean ± SD (n = 3). (B) Plot of eGFP knockout EC50 values versus lipopeptide logD7.4 values of each lipopeptide series; From top to bottom: X2-C-OHSteA, X1-H-LinA, X1-LinA.

To explore the reason why hydrophobically balanced lipopeptides are more potent, especially at low RNP concentrations, a group of representatives covering the spectrum from most hydrophilic to most hydrophobic were selected for investigation of the impact on critical carrier characteristics. The set of lipopeptides consisted of IDAtp-, Stp-, TFE-IDAtp-, Gtt-, GEIPA-, and Ntp-based structures. Firstly, the integrity of the nanocarriers upon dilution was investigated (Figure 36A). The nanocarriers were prepared at a high RNP concentration of 375 nM and then sequentially diluted to concentrations ranging from 0.1 nM to 75 nM. The size of IDAtp2-C-OHSteA and Stp2-C-OHSteA, the two most hydrophilic X2-C-OHSteA structures, immediately increased upon dilution and was not detectable at a RNP concentration of 1 nM or lower. In contrast, the more hydrophobic analogs exhibited improved dilution stability. A similar tendency was observed with the more hydrophobic X1-H-LinA and X1-LinA architectures that were generally more resistant towards dilution. Nanoparticles generated with the most hydrophobic structure, Ntp1-LinA, retained a stable size between 180 – 220 nm at 2.5 – 375 nM of RNP and were still detectable at 0.1 nM. In addition, the stability of the nanocarriers against excessive amounts of ions was investigated by the detection of RNA release with the intercalating dye Ribogreen (Figure 36B and 36C). Sodium chloride (NaCl) and the polyanion, heparin, were selected as ionic stress factors in this study. At isotonic NaCl concentration (0.15 M), all the nanocarriers showed robust encapsulation of Cas9 RNP. With increasing NaCl concentrations, higher Ribogreen fluorescence was detected indicating lower dye exclusion and release of Cas9 RNP from dissociated nanocarriers (Figure 36B). Notably, the more hydrophobic lipopeptides of each series exhibited better resistance against NaCl. Similar trends were found in the heparin competition assay, where hydrophobic artificial amino acids remarkably enhanced the nanocarrier stability against polyanionic stress (Figure 36C).

To examine the cellular uptake of hydrophobically balanced Cas9 RNP nanocarriers, flow cytometry experiments were performed with ATTO647N-labeled Cas9 and ATTO488-labeled sgRNA (Figure 36D). The results demonstrated a general correlation of higher cellular uptake with increasing hydrophobic properties. A representative example are the hydrophobic Ntp-based structures, where Ntp2-C-OHSteA and Ntp1-LinA achieved 4.4- and 7.3-fold enhanced sgRNA uptake compared to the Stp-based analogs. CLSM studies further confirmed the observation

that Ntp2-C-OHSetA and Ntp1-LinA leads to higher Cas9 RNP uptake, indicated by the brighter intracellular fluorescence in HeLa cells (Figure 36F). Furthermore, the endocytosis pathways of Stp2-C-OHSteA, Ntp2-C-OHSteA, Stp1-LinA, and Ntp1-LinA nanocarriers were probed by pretreating the cells with different inhibitors or incubation at 4 °C (Figure 36E). Low temperature and sodium azide inhibited the uptake of all 4 nanocarriers by 85-90 % and 65-77 % respectively, indicating an energy-dependent internalization mechanism. Chlorpromazine and sucrose were the only other inhibitors that significantly reduced the uptake of the more hydrophilic Stp2-C-OHSteA nanocarrier, suggesting a dominant role of clathrin-mediated endocytosis. Interestingly, the Cas9 RNP uptake mediated by the more hydrophobic lipopeptides Ntp2-C-OHSteA, Stp1-LinA, and Ntp1-LinA could also be blocked by pretreatment with amiloride, which indicates a contribution of macropinocytosis in addition to the clathrin-mediated pathway. Notably, the macropinosomes are reported more leaky than other endosomes, which may be beneficial for the translocation of nanoparticles into the cytosol.[184] Following the intracellular delivery pathway stepwise, an endosomal escape reporter cell line HeLa mRuby3/gal8[84] was used to evaluate the endosomal escape capability of the selected nanocarriers (Figure 36G). In this model, the rupture of endosomal membranes results in recruitment of a mRuby3/galectin-8 (gal8) fusion protein which is visible by intracellular punctate red spots. After 4 h treatment, the Ntp-based structures were found to induce a higher number of endosomolytic events than their Stp counterparts, especially at a low RNP concentration (5 nM). Notably, the peptide architecture played an additional fundamental role in the endosomal escape process, since the X1-LinA sequences showed much better endosomal escape efficiency than the X2-C-OHSteA lipopeptides.

Taken the above results together, the mechanistic effects can be explained as follows: hydrophobic lipopeptides form Cas9 RNP nanocarriers, which 1) are more resistant towards dilution-mediated dissociation and remain intact at low concentrations; 2) are more resistant towards ionic stress and avoid premature cargo release; 3) mediate more efficient cellular internalization that is driven by both clathrin-mediated endocytosis and macropinocytosis; and 4) possess a higher endosomal escape capacity. The fact, that optimal logD7.4 ranges and a requirement of finding the right balance have been observed can be explained, since in certain

cases ‘more is not always better’: in particular, too stable nanoparticles may result in insufficient cargo release in the right place at the right time.

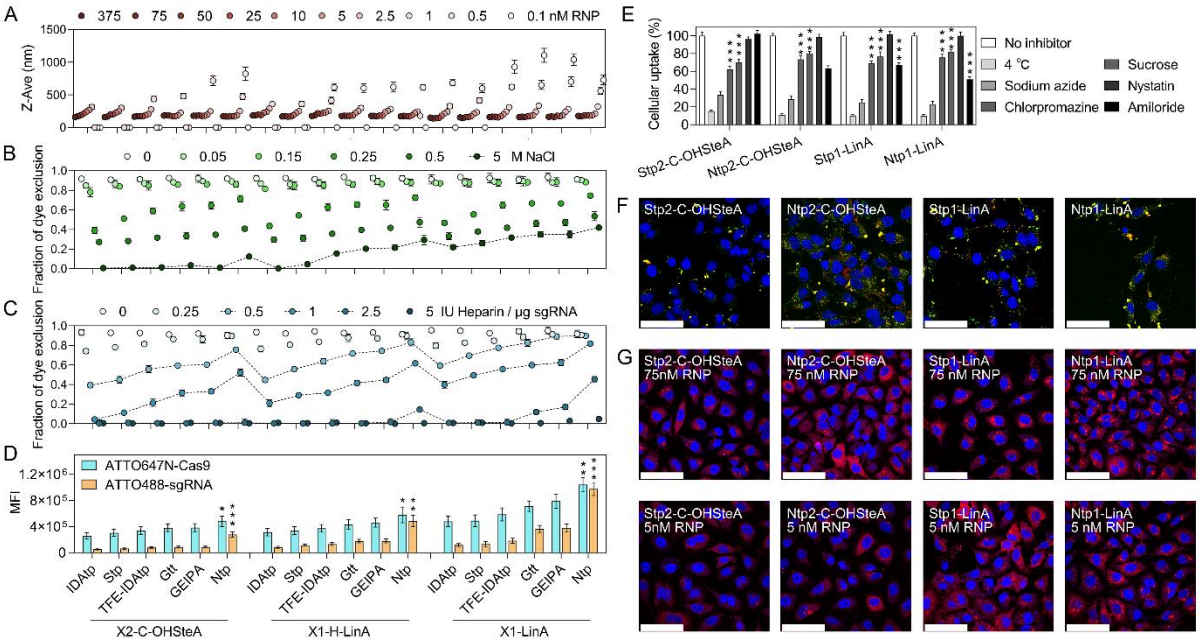

Figure 36. A) Effect of dilution on the nanocarrier size determined by DLS; value = 0 indicates “not detectable”. B) Nanocarrier stability against different concentrations of NaCl (0, 0.05, 0.15, 0.25, 0.5, and 5 M); Ribogreen was used for the detection of free Cas9 RNP. C) Nanocarrier stability against different concentrations of heparin (0, 0.25, 0.5, 1, 2.5, and 5 IU / µg sgRNA); Ribogreen was used for the detection of free Cas9 RNP. D) Cellular uptake of Cas9 RNP (75 nM) containing 20 % ATTO647N-Cas9 and 20 % ATTO488-sgRNA into HeLa cells determined by flow cytometry after 4 h incubation. E) Endocytosis pathway study with different inhibitors; sodium azide: energy-dependent endocytosis, chlorpromazine: clathrin-mediated endocytosis, sucrose: clathrin-mediated endocytosis, nystatin: caveolae-mediated endocytosis, amiloride: macropinocytosis. **** $p \leqslant 0.0001$, *** $p \leqslant 0.001$, ** $p \leqslant 0.01$, * $p \leqslant 0.05$. Data are presented as mean ± SD (n = 3). F) Confocal laser scanning microscopy (CLSM) images of HeLa WT cells 4 h after treatment with the selected Cas9 RNP nanocarriers (75 nM RNP) containing 20 % of ATTO647N-Cas9 and 20 % ATTO488-sgRNA. Nuclei were stained with DAPI (blue). The merged channel indicates co-localization (yellow) of ATTO647N-Cas9 (red) and ATTO488-sgRNA (green). Scale bar: 50 µm. G) CLSM images of HeLa mRuby3/gal8 cells treated with the selected Cas9 RNP nanocarriers (75 and 5 nM RNP) for 4 h. Nuclei were stained with DAPI (blue). Red punctuate mRuby3/gal8 spots indicate endosome membrane damage. Scale bar: 50 µm.

Having demonstrated that hydrophobically balanced lipopeptides are potent nanocarriers for delivering Cas9 RNP to mediate gene knockouts via non-

homologous end joining (NHEJ), we sought to extend the scope of application: the top 5 lipopeptides of each series were selected for the co-delivery of Cas9 RNP and a ssDNA template to mediate gene knockins via homology directed repair (HDR). A HeLa cell line expressing destabilized eGFP (HeLa GFPd2) was used in this study. The 66th amino acid in the eGFP sequence, tyrosine (code: TAC), can be replaced by histidine (code: CAT) via HDR-mediated DNA repair, which results in the conversion of eGFP into BFP.[185] Three cell populations can be expected after such treatments: 1) eGFP positive cells, representing non-edited cells; 2) eGFP and BFP negative cells representing cells with NHEJ-mediated gene knockout; and 3) BFP positive and eGFP negative cells representing HDR-mediated gene corrected cells (Figure 37A). In the first step, TFE-IDAtp1-LinA, which performed best in gene knockout experiments, was used for finding the most suitable RNP/ssDNA ratios. The nanocarriers for HDR were prepared by complexing TFE-IDAtp1-LinA with different RNP/ssDNA ratios ranging from 1/0.5 to 1/20 at an N/P ratio of 12. HeLa GFPd2 cells were treated with the Cas9 RNP/ssDNA nanocarriers for 48 h followed by cell population analysis via flow cytometry. As shown in Figure 37B and Figure 42, the best knockout and total editing efficiencies were achieved at high RNP concentrations (10 – 100 nM) and high RNP/ssDNA ratios (1/0.5 – 1/3), while the highest HDR levels were induced at moderate to low RNP concentrations (10 – 1 nM) and moderate RNP/ssDNA ratios (1/3 – 1/8). At RNP/ssDNA ratios below 1/10, almost all editing events were blocked, presumably due to severe cytotoxicity (Figure 43). The highest HDR efficiency of ~28 % was achieved at a dose of 10 nM RNP and 1/8 RNP/ssDNA ratio. Notably, a general trend of increasing percentage of HDR events in relation to total editing was observed with decreasing RNP concentration, which is explainable by the competition between NHEJ and HDR repair pathways (Figure 44). Next, the HDR induction efficiency of the other selected lipopeptides was investigated at an RNP/ssDNA ratio of 1/4 to circumvent cytotoxicity (Figure 37C). Surprisingly, the X2-C-OHSteA series that was the least efficient in gene knockout experiments, achieved the highest maximum HDR levels. Especially the hydrophobically balanced Gtt2-C-OHSteA, enabled HDR induction up to 40 % at a 25 nM RNP dose. Nevertheless, X1-LinA lipopeptides still showed the highest potency and best HDR efficiency at low concentrations. For instance, TFE-IDAtp1-LinA nanocarriers induced ~23 % and ~11 % HDR in HeLa GFPd2 cells treated with 1 nM or 0.5 nM RNP doses, respectively.

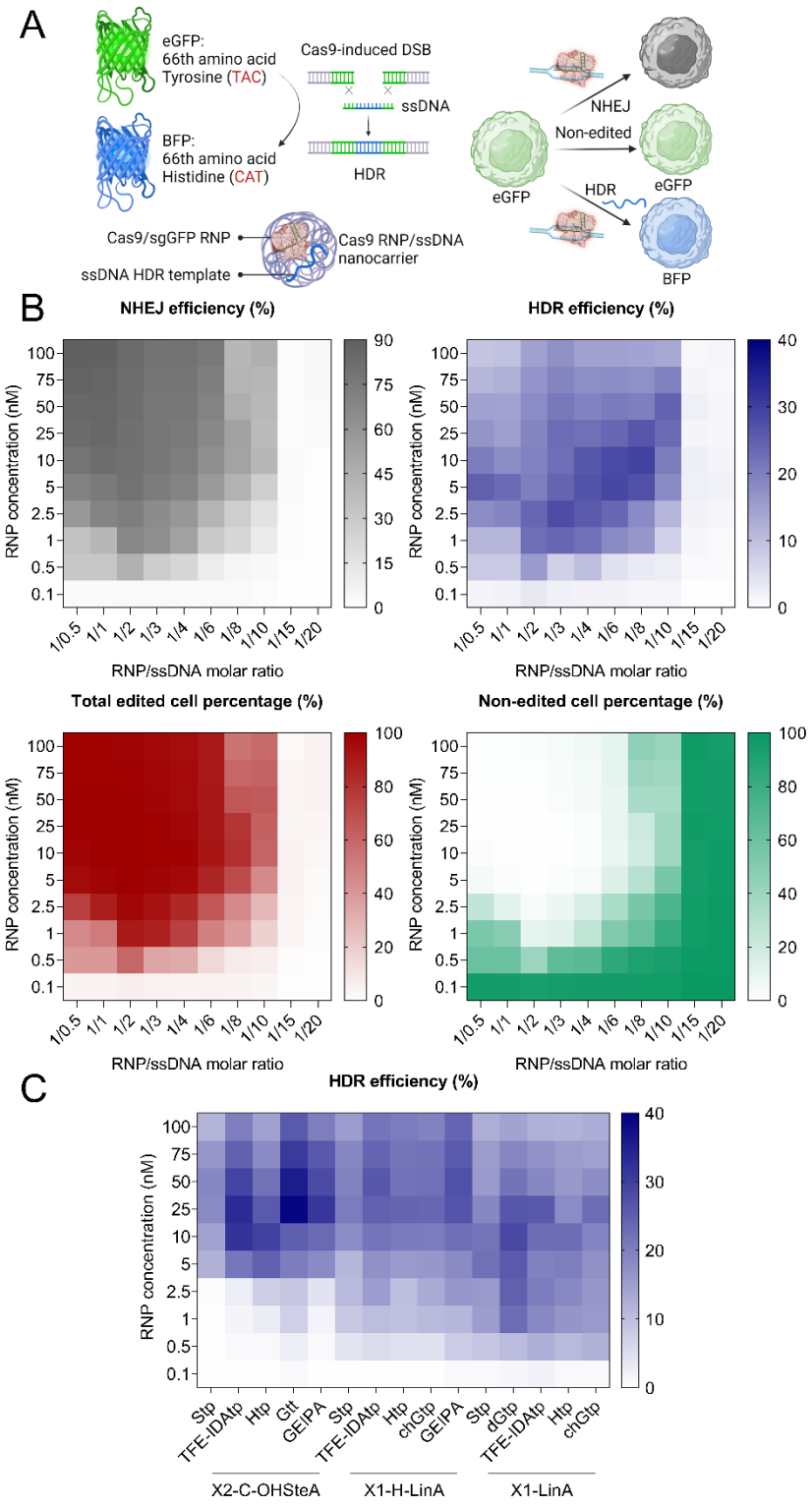

Figure 37. A) Schematic illustration of eGFP to BFP conversion by co-delivery of Cas9 RNP and a ssDNA template into eGFP expressing cells. B) Heat maps of NHEJ, HDR, total edited, and non-edited percentages in HeLa GFPd2 cells 48 h after treatment with Cas9 RNP/ssDNA nanocarriers (TFE-IDAtp1-LinA) at varied RNP concentrations and RNP/ssDNA ratios. C) Heat map of HDR

percentages in HeLa GFPd2 cells 48 h after treatment with different lipopeptide-based Cas9 RNP/ssDNA (fixed at 1/4) nanocarriers at varied RNP concentrations.

3.6 Conclusions

In summary, we have designed and synthesized a series of artificial amino acids and derived lipopeptides for the intracellular delivery of Cas9 RNP. Systematic biological evaluation revealed that the hydrophobic characteristics play a decisive role for potent gene editing, especially at low concentrations. The fluorinated lipopeptide TFE-IDAtp1-LinA was found to be a particularly potent nanocarrier which can achieve 88 % NHEJ gene knockout and 23 % HDR knockin at just 1 nM RNP concentration. The identified relationships between $logD_{7.4}$ values, carrier characteristics and impact on cellular delivery are suggested to serve as a guide for the future design of Cas9 RNP nanocarriers. The new artificial amino acids and lipopeptide architectures provide a versatile platform for the creation of highly potent and tunable cellular delivery agents.

3.7 Acknowledgements

The authors acknowledge support by the UPGRADE (Unlocking Precision Gene Therapy) project that has received funding from the European Union's Horizon 2020 research and innovation programme under grant agreement No 825825. This work was also supported by the German Research Foundation (DFG) SFB1032 (project-ID 201269156) sub-project B4. Y.L. and X.L. appreciate the fellowship of the China Scholarship Council that supports their Ph.D. studies. U.L. appreciates support by the Galenus Foundation (Vienna, Austria). We thank Teoman Benli-Hoppe for performing MALDI-TOF mass spectrometry measurements. Some figures and schemes were created with Biorender.com.

3.8 Supporting information figures and tables

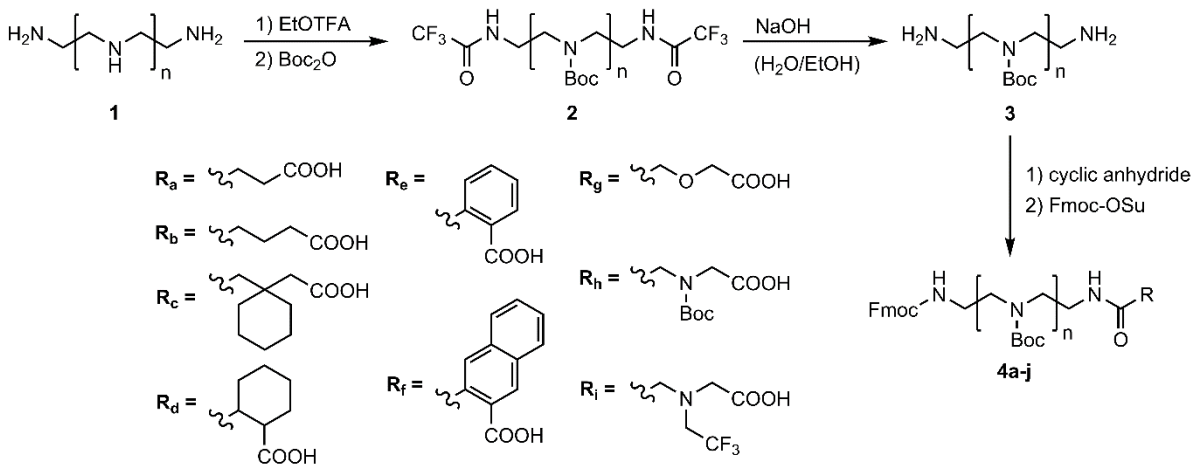

Fmoc-Stp(Boc_3)-OH: n=3, R=R_a
Fmoc-Gtp(Boc_3)-OH: n=3, R=R_b
Fmoc-Gtt(Boc_2)-OH: n=2, R=R_b
Fmoc-chGtp(Boc_3)-OH: n=3, R=R_c
Fmoc-Htp(Boc_3)-OH: n=3, R=R_d
Fmoc-Ptp(Boc_3)-OH: n=3, R=R_e
Fmoc-Ntp(Boc_3)-OH: n=3, R=R_f
Fmoc-dGtp(Boc_3)-OH: n=3, R=R_g
Fmoc-Boc-IDAtp(Boc_3)-OH: n=3, R=R_h
Fmoc-TFE-IDAtp(Boc_3)-OH: n=3, R=R_i

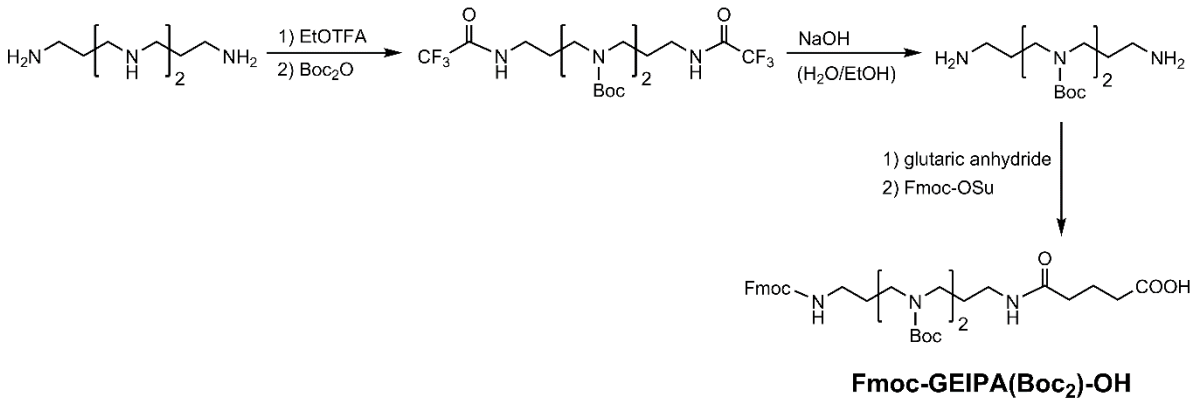

Fmoc-GEIPA(Boc_2)-OH

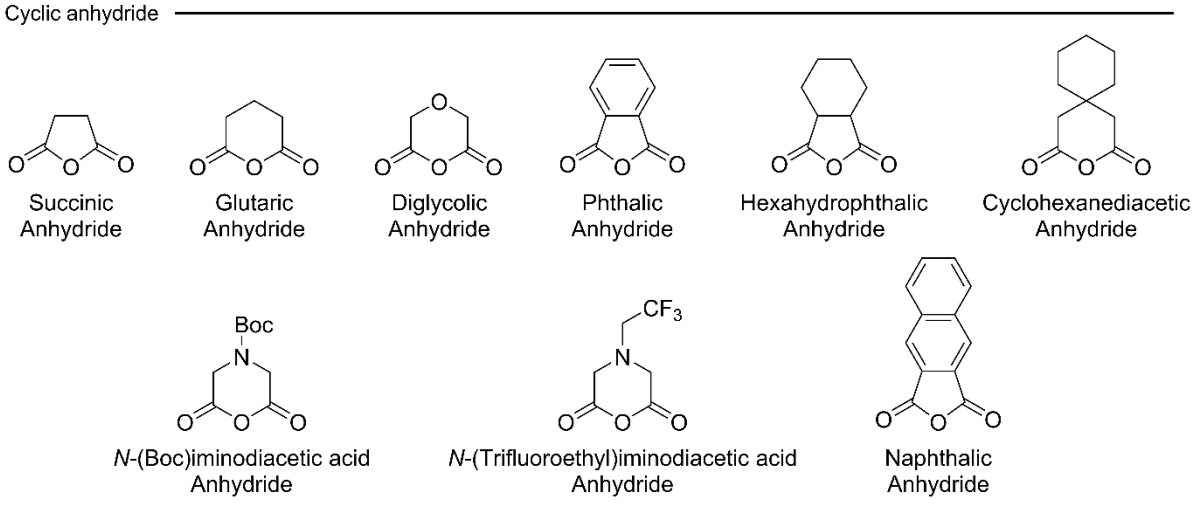

Scheme 4. A general synthetic route of artificial amino acid building blocks, and all cyclic anhydrides used in this study.

Table 7. Compound ID number, sequence, MALDI-MS of all lipopeptides and hydrodynamic size, PDI, zeta potential of Cas9 RNP nanocarriers formed with the lipopeptides.

ID	Sequence (N → C)	Size[a]	PDI[a]	Zeta potential[a]
1468	K(N3)-Y3-Stp-K(K(SteA)2)-Stp-Y3	201.5 ± 2.8	0.26 ± 0.03	15.2 ± 1.1
1391	K(N3)-Y3-Stp-K(K(OleA)2)-Stp-Y3	152.3 ± 3.8	0.29 ± 0.03	12.6 ± 1.9
1392	K(N3)-Y3-Stp-K(K(LinA)2)-Stp-Y3	159.3 ± 1.5	0.20 ± 0.04	12.8 ± 0.4
1393	K(N3)-Y3-Stp-K(K(LenA)2)-Stp-Y3	173.9 ± 4.0	0.27 ± 0.03	11.7 ± 0.9
1394	K(N3)-Y3-Stp-K(K(CholA)2)-Stp-Y3	194.4 ± 1.0	0.38 ± 0.03	14.4 ± 1.3
1469	K(N3)-Y3-Stp-K(K(OHSteA)2)-Stp-Y3	161.2 ± 4.1	0.26 ± 0.03	13.4 ± 0.2
1470	K(N3)-Y3-H-Stp-H-K(K(SteA)2)-H-Stp-H-Y3	204.9 ± 5.7	0.16 ± 0.04	14.9 ± 1.9
1395	K(N3)-Y3-H-Stp-H-K(K(OleA)2)-H-Stp-H-Y3	200.2 ± 3.5	0.19 ± 0.02	11.0 ± 1.4
1396	K(N3)-Y3-H-Stp-H-K(K(LinA)2)-H-Stp-H-Y3	194.9 ± 3.8	0.22 ± 0.03	10.3 ± 1.3
1397	K(N3)-Y3-H-Stp-H-K(K(LenA)2)-H-Stp-H-Y3	185.7 ± 0.9	0.35 ± 0.03	12.2 ± 1.5
1398	K(N3)-Y3-H-Stp-H-K(K(CholA)2)-H-Stp-H-Y3	167.1 ± 5.7	0.15 ± 0.03	16.1 ± 1.2
1471	K(N3)-Y3-H-Stp-H-K(K(OHSteA)2)-H-Stp-H-Y3	193.8 ± 4.4	0.22 ± 0.02	16.0 ± 0.6
1581	K(N3)-C-Y3-Stp-K(K(SteA)2)-Stp-Y3-C	190.3 ± 5.2	0.31 ± 0.01	15.2 ± 1.6
1577	K(N3)-C-Y3-Stp-K(K(OleA)2)-Stp-Y3-C	156.2 ± 3.9	0.40 ± 0.05	13.2 ± 1.7
1578	K(N3)-C-Y3-Stp-K(K(LinA)2)-Stp-Y3-C	147.0 ± 3.4	0.16 ± 0.02	14.0 ± 0.2
1579	K(N3)-C-Y3-Stp-K(K(LenA)2)-Stp-Y3-C	151.5 ± 6.8	0.29 ± 0.03	11.5 ± 0.2
1580	K(N3)-C-Y3-Stp-K(K(CholA)2)-Stp-Y3-C	190.1 ± 6.0	0.19 ± 0.03	14.1 ± 0.8
1582	K(N3)-C-Y3-Stp-K(K(OHSteA)2)-Stp-Y3-C	180.2 ± 4.3	0.24 ± 0.02	12.2 ± 1.2
1587	K(N3)-C-Y3-H-Stp-H-K(K(SteA)2)-H-Stp-H-Y3-C	245.1 ± 10.3	0.27 ± 0.02	14.1 ± 0.1
1583	K(N3)-C-Y3-H-Stp-H-K(K(OleA)2)-H-Stp-H-Y3-C	195.3 ± 5.8	0.15 ± 0.01	12.3 ± 1.9
1584	K(N3)-C-Y3-H-Stp-H-K(K(LinA)2)-H-Stp-H-Y3-C	235.8 ± 9.5	0.23 ± 0.04	12.8 ± 1.7
1585	K(N3)-C-Y3-H-Stp-H-K(K(LenA)2)-H-Stp-H-Y3-C	202.4 ± 8.7	0.39 ± 0.04	13.4 ± 0.7
1586	K(N3)-C-Y3-H-Stp-H-K(K(CholA)2)-H-Stp-H-Y3-C	199.0 ± 8.6	0.36 ± 0.03	16.1 ± 0.6
1588	K(N3)-C-Y3-H-Stp-H-K(K(OHSteA)2)-H-Stp-H-Y3-C	190.1 ± 6.0	0.20 ± 0.03	12.9 ± 0.7
1361	K(N3)-Y3-Stp2-K(K(SteA)2)-Stp2-Y3	377.5 ± 56.6	0.37 ± 0.01	17.5 ± 1.4
1208	K(N3)-Y3-Stp2-K(K(OleA)2)-Stp2-Y3	379.2 ± 70.5	0.29 ± 0.03	14.1 ± 0.4
1399	K(N3)-Y3-Stp2-K(K(LinA)2)-Stp2-Y3	345.5 ± 33.8	0.29 ± 0.01	13.1 ± 0.9
1400	K(N3)-Y3-Stp2-K(K(LenA)2)-Stp2-Y3	385.0 ± 47.5	0.35 ± 0.03	14.3 ± 1.6
1364	K(N3)-Y3-Stp2-K(K(CholA)2)-Stp2-Y3	501.6 ± 52.6	0.41 ± 0.01	13.0 ± 1.9
1573	K(N3)-Y3-Stp2-K(K(OHSteA)2)-Stp2-Y3	440.3 ± 33.2	0.24 ± 0.01	14.3 ± 0.3
1321	K(N3)-Y3-(H-Stp)2-H-K(K(SteA)2)-H-(Stp-H)2-Y3	340.2 ± 31.2	0.16 ± 0.04	14.3 ± 1.5
1209	K(N3)-Y3-(H-Stp)2-H-K(K(OleA)2)-H-(Stp-H)2-Y3	338.3 ± 28.0	0.28 ± 0.05	14.9 ± 0.5
1401	K(N3)-Y3-(H-Stp)2-H-K(K(LinA)2)-H-(Stp-H)2-Y3	478.7 ± 8.1	0.16 ± 0.02	11.1 ± 1.5
1402	K(N3)-Y3-(H-Stp)2-H-K(K(LenA)2)-H-(Stp-H)2-Y3	288.5 ± 17.5	0.45 ± 0.04	11.9 ± 0.5
1403	K(N3)-Y3-(H-Stp)2-H-K(K(CholA)2)-H-(Stp-H)2-Y3	366.8 ± 37.7	0.40 ± 0.04	13.9 ± 1.0
1574	K(N3)-Y3-(H-Stp)2-H-K(K(OHSteA)2)-H-(Stp-H)2-Y3	256.4 ± 11.5	0.37 ± 0.03	12.4 ± 0.3
1337	K(N3)-C-Y3-Stp2-K(K(SteA)2)-Stp2-Y3-C	201.4 ± 10.6	0.29 ± 0.03	16.7 ± 1.9
1338	K(N3)-C-Y3-Stp2-K(K(OleA)2)-Stp2-Y3-C	166.6 ± 5.8	0.25 ± 0.03	16.6 ± 0.4
1199	K(N3)-C-Y3-Stp2-K(K(LinA)2)-Stp2-Y3-C	159.3 ± 5.9	0.23 ± 0.02	15.9 ± 1.3
1200	K(N3)-C-Y3-Stp2-K(K(LenA)2)-Stp2-Y3-C	160.6 ± 4.3	0.17 ± 0.03	16.8 ± 1.2
1340	K(N3)-C-Y3-Stp2-K(K(CholA)2)-Stp2-Y3-C	203.4 ± 6.9	0.28 ± 0.03	15.4 ± 0.8
1445	K(N3)-C-Y3-Stp2-K(K(OHSteA)2)-Stp2-Y3-C	177.7 ± 5.9	0.25 ± 0.04	16.5 ± 1.7
1278	K(N3)-C-Y3-(H-Stp)2-H-K(K(SteA)2)-H-(Stp-H)2-Y3-C	205.1 ± 12.9	0.20 ± 0.04	15.1 ± 1.1
1214	K(N3)-C-Y3-(H-Stp)2-H-K(K(OleA)2)-H-(Stp-H)2-Y3-C	185.5 ± 5.7	0.26 ± 0.05	18.5 ± 1.5
1389	K(N3)-C-Y3-(H-Stp)2-H-K(K(LinA)2)-H-(Stp-H)2-Y3-C	178.5 ± 10.2	0.30 ± 0.02	16.8 ± 1.2
1390	K(N3)-C-Y3-(H-Stp)2-H-K(K(LenA)2)-H-(Stp-H)2-Y3-C	188.8 ± 9.9	0.28 ± 0.02	15.8 ± 0.6
1575	K(N3)-C-Y3-(H-Stp)2-H-K(K(CholA)2)-H-(Stp-H)2-Y3-C	200.7 ± 10.3	0.33 ± 0.03	14.7 ± 1.4
1576	K(N3)-C-Y3-(H-Stp)2-H-K(K(OHSteA)2)-H-(Stp-H)2-Y3-C	191.6 ± 6.3	0.33 ± 0.07	14.6 ± 0.6
1639	K(N3)-Y3-Gtp-K(K(LinA)2)-Gtp-Y3	156.3 ± 2.9	0.15 ± 0.04	13.1 ± 0.8
1641	K(N3)-Y3-Htp-K(K(LinA)2)-Htp-Y3	165.3 ± 2.7	0.22 ± 0.05	12.1 ± 0.9
1642	K(N3)-Y3-Ptp-K(K(LinA)2)-Ptp-Y3	168.1 ± 3.2	0.33 ± 0.01	10.9 ± 1.9
1643	K(N3)-Y3-Ntp-K(K(LinA)2)-Ntp-Y3	175.6 ± 1.1	0.26 ± 0.02	11.3 ± 1.3
1644	K(N3)-Y3-Gtt-K(K(LinA)2)-Gtt-Y3	165.3 ± 10.0	0.22 ± 0.03	11.5 ± 0.9
1645	K(N3)-Y3-GEIPA-K(K(LinA)2)-GEIPA-Y3	169.3 ± 9.1	0.28 ± 0.04	11.6 ± 0.8
1737	K(N3)-Y3-chGtp-K(K(LinA)2)-chGtp-Y3	176.3 ± 3.5	0.31 ± 0.05	12.5 ± 1.9
1738	K(N3)-Y3-dGtp-K(K(LinA)2)-dGtp-Y3	173.5 ± 1.3	0.20 ± 0.03	13.9 ± 2.9
1739	K(N3)-Y3-(TFE-IDAtp)-K(K(LinA)2)-(TFE-IDAtp)-Y3	166.3 ± 6.1	0.29 ± 0.03	12.5 ± 1.1
1740	K(N3)-Y3-IDAtp-K(K(LinA)2)-IDAtp-Y3	138.9 ± 9.0	0.31 ± 0.03	13.6 ± 3.1
1647	K(N3)-Y3-H-Gtp-H-K(K(LinA)2)-H-Gtp-H-Y3	165.6 ± 3.2	0.28 ± 0.01	12.1 ± 1.3
1649	K(N3)-Y3-H-Htp-H-K(K(LinA)2)-H-Htp-H-Y3	178.5 ± 3.2	0.25 ± 0.02	11.9 ± 0.3
1650	K(N3)-Y3-H-Ptp-H-K(K(LinA)2)-H-Ptp-H-Y3	180.3 ± 6.1	0.38 ± 0.03	10.5 ± 2.1
1651	K(N3)-Y3-H-Ntp-H-K(K(LinA)2)-H-Ntp-H-Y3	178.5 ± 3.2	0.35 ± 0.05	10.9 ± 1.6
1652	K(N3)-Y3-H-Gtt-H-K(K(LinA)2)-H-Gtt-H-Y3	180.5 ± 1.2	0.28 ± 0.02	11.6 ± 1.3
1653	K(N3)-Y3-H-GEIPA-H-K(K(LinA)2)-H-GEIPA-H-Y3	179.3 ± 2.3	0.25 ± 0.01	13.1 ± 3.2
1741	K(N3)-Y3-H-chGtp-H-K(K(LinA)2)-H-chGtp-H-Y3	175.4 ± 3.6	0.31 ± 0.02	11.8 ± 1.3
1742	K(N3)-Y3-H-dGtp-H-K(K(LinA)2)-H-dGtp-H-Y3	169.6 ± 3.9	0.22 ± 0.01	13.2 ± 1.4
1743	K(N3)-Y3-H-(TFE-IDAtp)-H-K(K(LinA)2)-H-(TFE-IDAtp)-H-Y3	185.6 ± 4.7	0.25 ± 0.03	12.8 ± 0.6
1744	K(N3)-Y3-H-IDAtp-H-K(K(LinA)2)-H-IDAtp-H-Y3	189.1 ± 4.2	0.19 ± 0.02	13.7 ± 1.2
1631	K(N3)-C-Y3-Gtp2-K(K(OHSteA)2)-Gtp2-Y3-C	168.3 ± 3.9	0.29 ± 0.02	16.0 ± 2.0
1633	K(N3)-C-Y3-Htp2-K(K(OHSteA)2)-Htp2-Y3-C	183.6 ± 4.5	0.36 ± 0.01	15.4 ± 1.2

1634	K(N3)-C-Y3-Ptp2-K(K(OHSteA)2)-Ptp2-Y3-C	190.3 ± 5.1	0.33 ± 0.02	14.1 ± 3.6
1635	K(N3)-C-Y3-Ntp2-K(K(OHSteA)2)-Ntp2-Y3-C	167.2 ± 3.0	0.29 ± 0.02	14.8 ± 2.8
1636	K(N3)-C-Y3-Gtt2-K(K(OHSteA)2)-Gtt2-Y3-C	189.8 ± 9.1	0.34 ± 0.05	13.2 ± 1.8
1637	K(N3)-C-Y3-GEIPA2-K(K(OHSteA)2)-GEIPA2-Y3-C	179.8 ± 5.3	0.28 ± 0.02	13.4 ± 2.1
1733	K(N3)-C-Y3-chGtp2-K(K(OHSteA)2)-chGtp2-Y3-C	185.6 ± 6.6	0.26 ± 0.03	15.9 ± 1.1
1734	K(N3)-C-Y3-dGtp2-K(K(OHSteA)2)-dGtp2-Y3-C	175.5 ± 3.6	0.23 ± 0.03	16.3 ± 1.3
1735	K(N3)-C-Y3-(TFE-IDAtp)2-K(K(OHSteA)2)-(TFE-IDAtp)2-Y3-C	173.3 ± 4.1	0.28 ± 0.03	15.5 ± 2.1
1736	K(N3)-C-Y3-IDAtp2-K(K(OHSteA)2)-IDAtp2-Y3-C	175.1 ± 2.2	0.31 ± 0.02	17.2 ± 1.6

[a] Cas9 RNP nanocarriers were prepared at a N/P ratio of 24 and an RNP concentration of 75 nM. The hydrodynamic size (z-average, nm), PDI and zeta potential of the nanocarriers were measured by DLS using a Zetasizer Nano ZS (Malvern Instruments, UK).

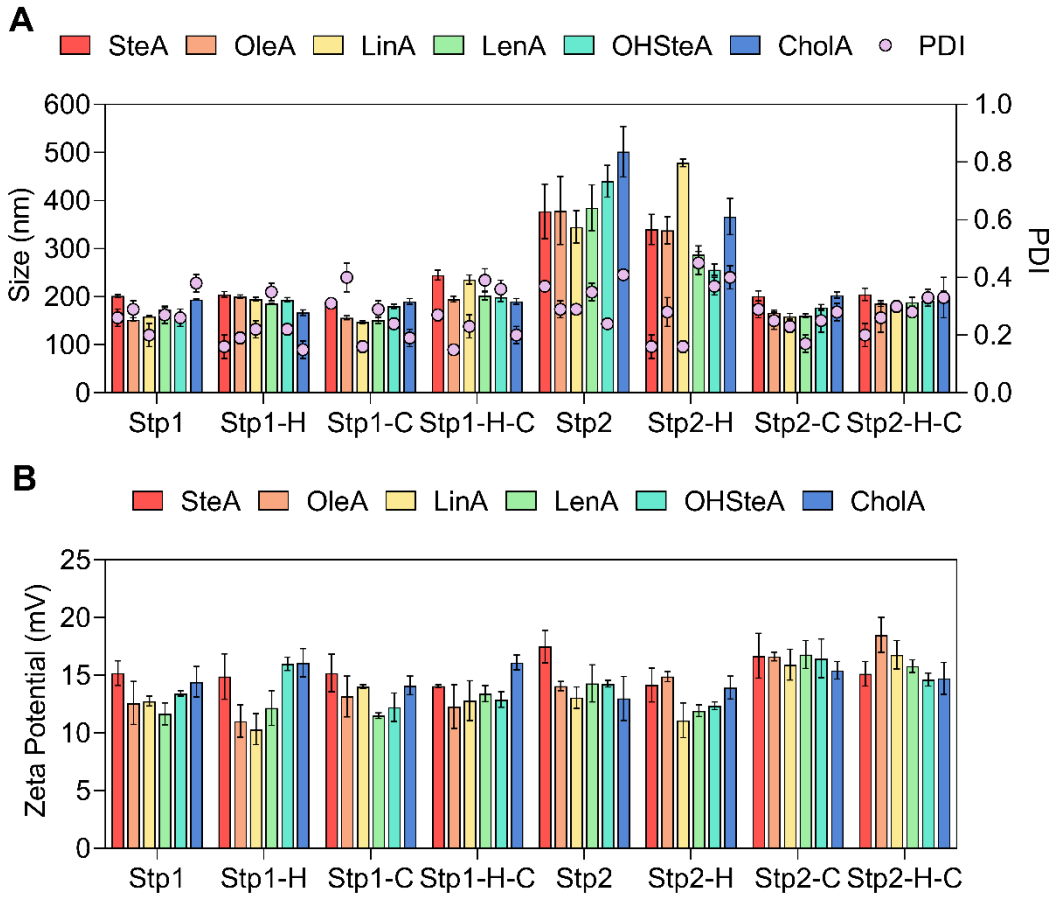

Figure 38. A) Hydrodynamic particle size (z-average), polydispersity index (PDI) and B) zeta potential of Cas9 RNP nanocarriers of different lipopeptides at an RNP dose of 75 nM (N/P = 24). Three technical replicates were measured.

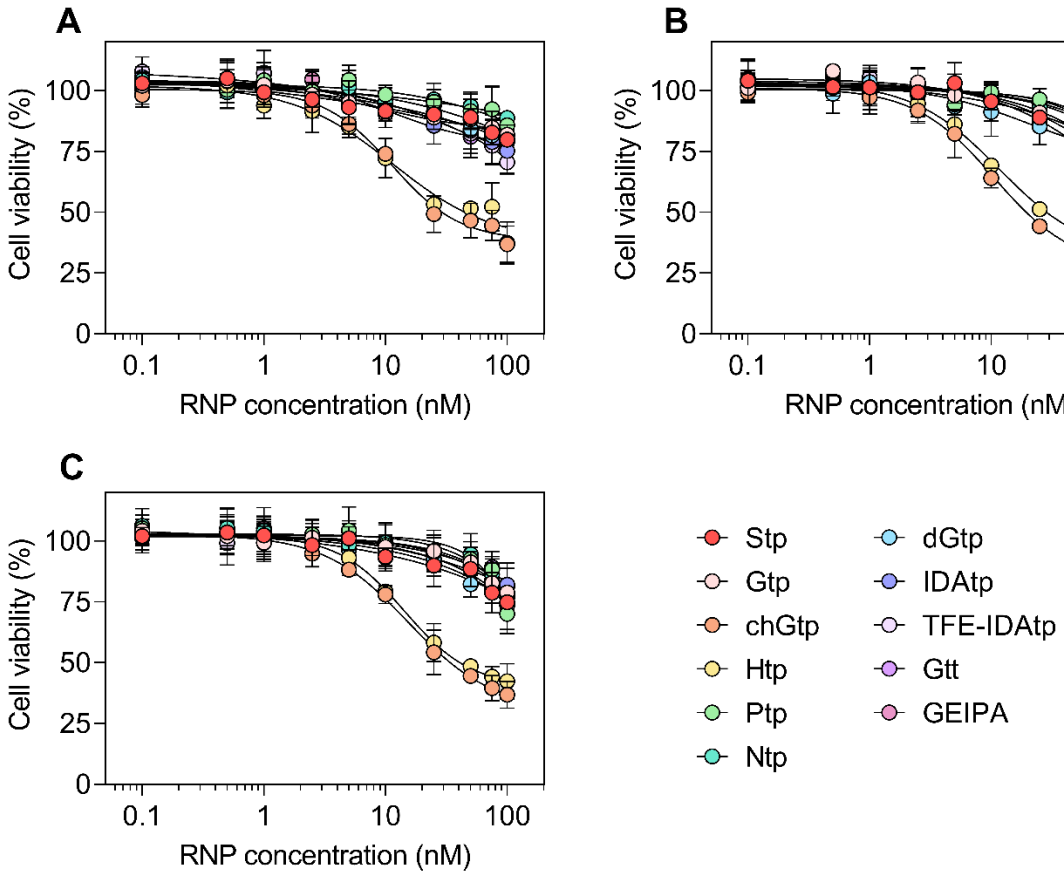

Figure 39. Cell viability of HeLa cells treated with A) X2-C-OHSteA, B) X1-H-LinA, and C) X1-LinA based nanocarriers at different concentrations of Cas9 RNP for 48 h. Metabolic activity of the cells was determined using a MTT assay. Data are presented as % cell viability with respect to the control cells ± SD (n = 3).

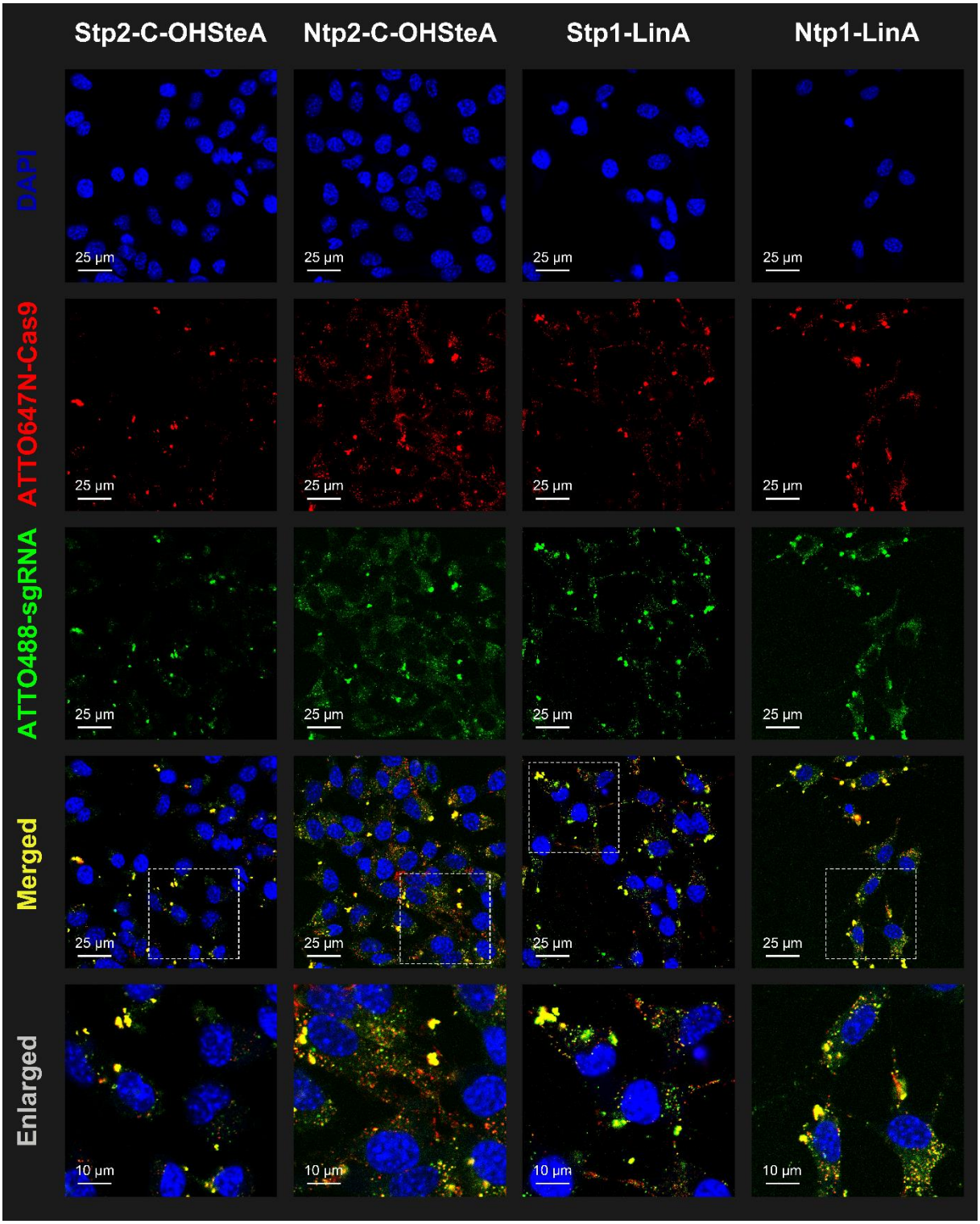

Figure 40. Confocal laser scanning microscopy (CLSM) images of HeLa WT cells 4 h after treatments with different Cas9 RNP nanocarriers containing 20 % of ATTO647N-Cas9/ATTO488-sgRNA at an RNP concentration of 75 nM. Nuclei were stained with DAPI (blue).

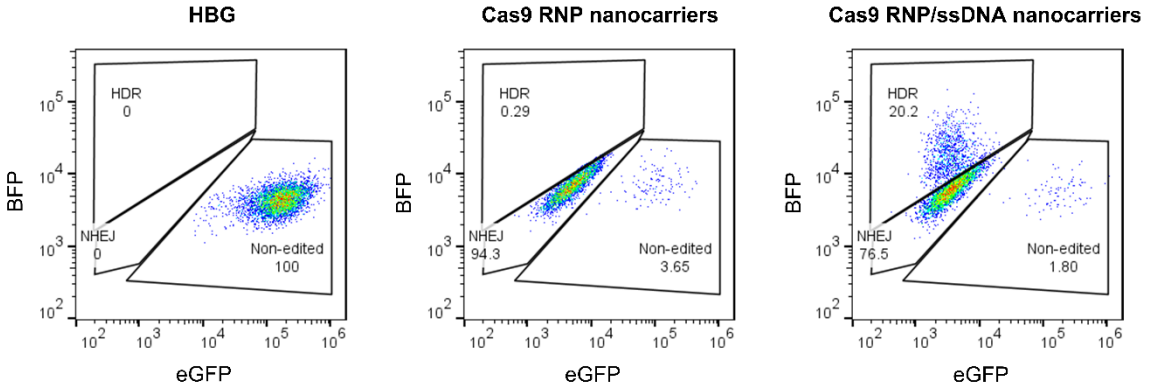

Figure 41. Gating strategy to differentiate non-edited (eGFP positive), NHEJ (eGFP negative), and HDR (BFP positive) cell populations.

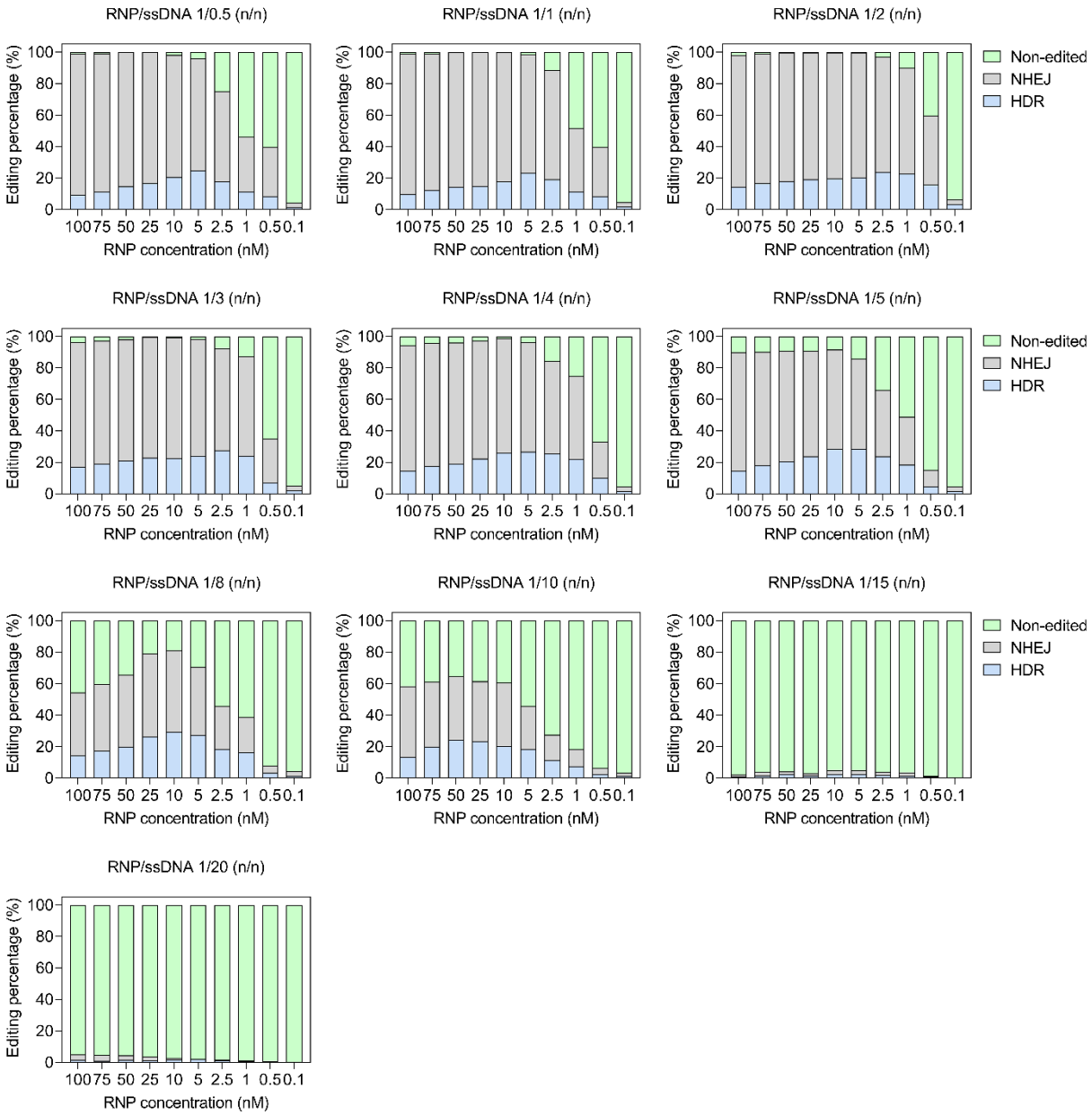

Figure 42. Editing percentage of NHEJ and HDR in HeLa GFPd2 cells treated with TFE-IDAtp1-LinA Cas9 RNP/ssDNA nanocarriers at various concentrations and ratios of RNP/ssDNA.

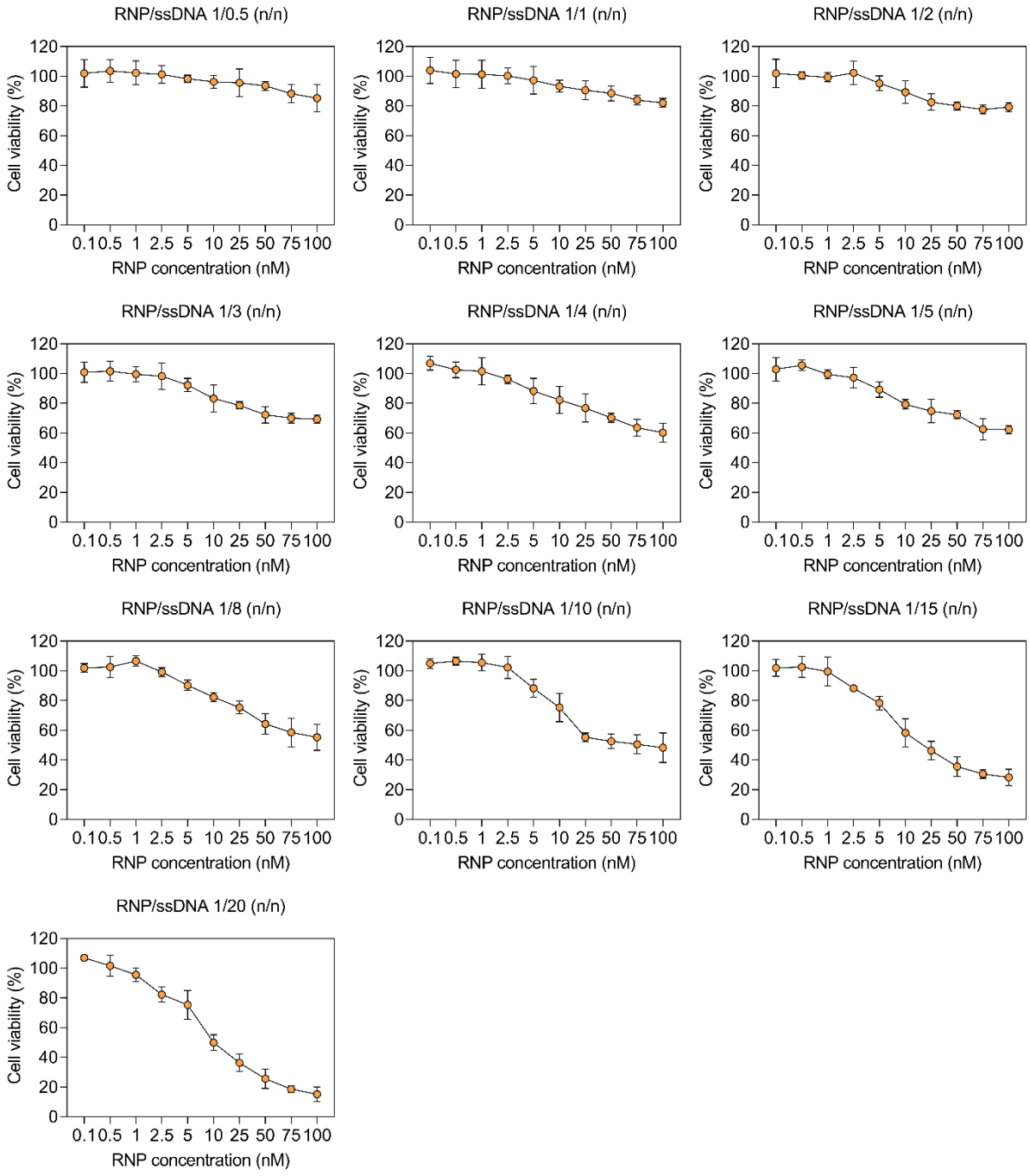

Figure 43. Cell viability of HeLa GFPd2 cells treated with TFE-IDAtp1-LinA Cas9 RNP/ssDNA nanocarriers at various concentrations and ratios of RNP/ssDNA.

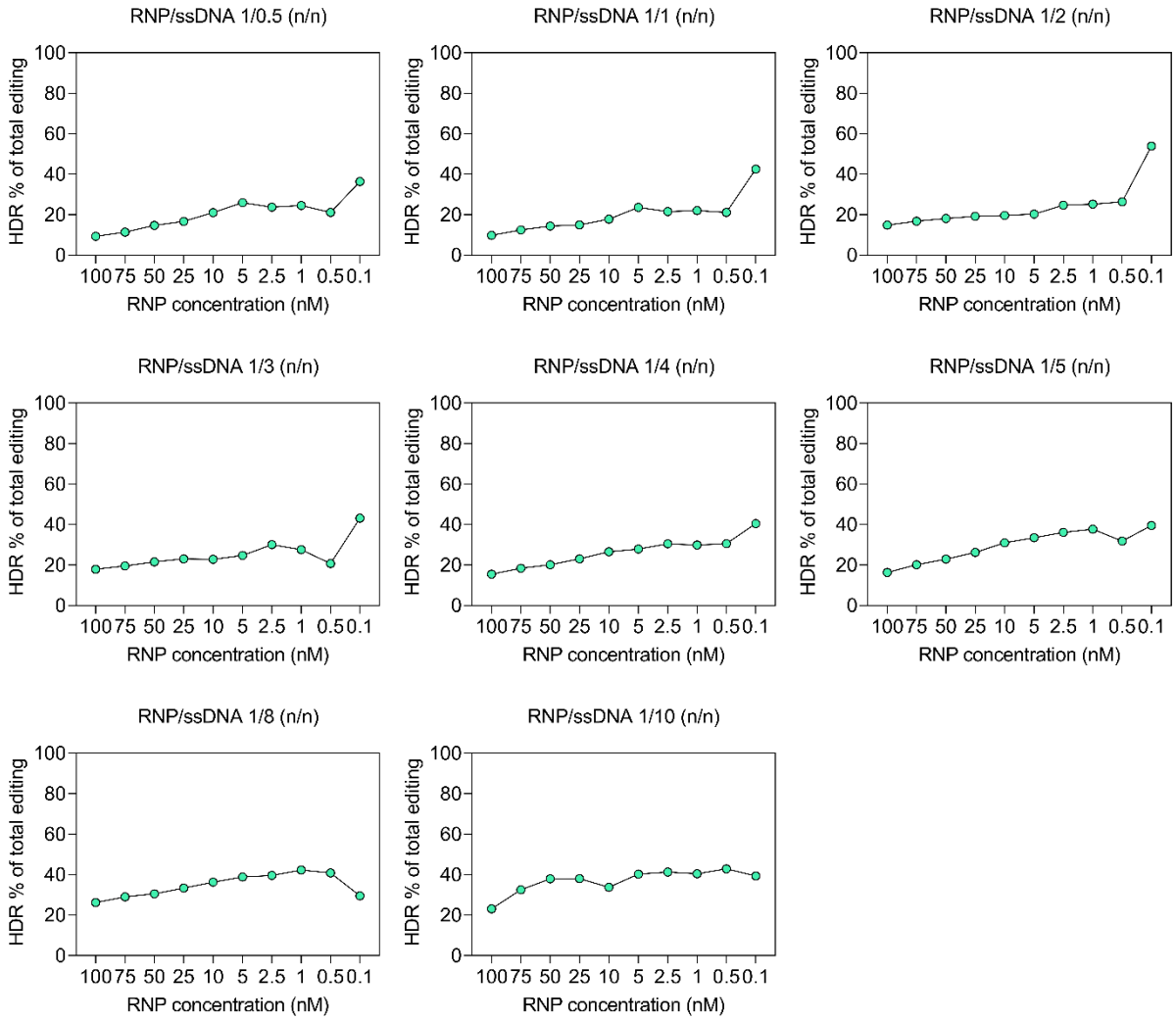

Figure 44. HDR percentage of total editing events in HeLa GFPd2 cells treated with TFE-IDAtp1-LinA Cas9 RNP/ssDNA nanocarriers at various concentrations and ratios of RNP/ssDNA.

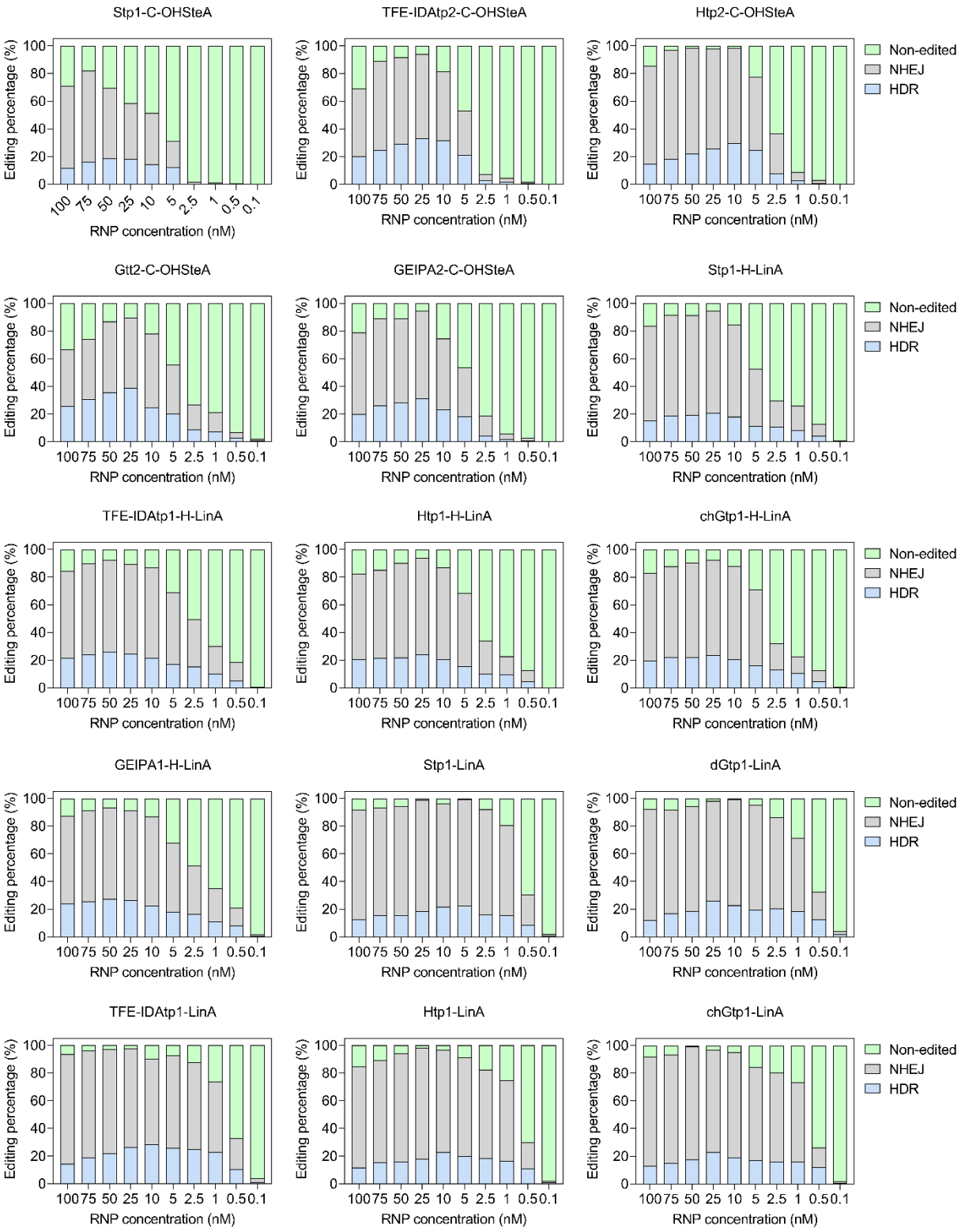

Figure 45. Editing percentage of NHEJ and HDR in HeLa GFPd2 cells treated with different Cas9 RNP/ssDNA nanocarriers at various concentrations (RNP/ssDNA = 1/4).

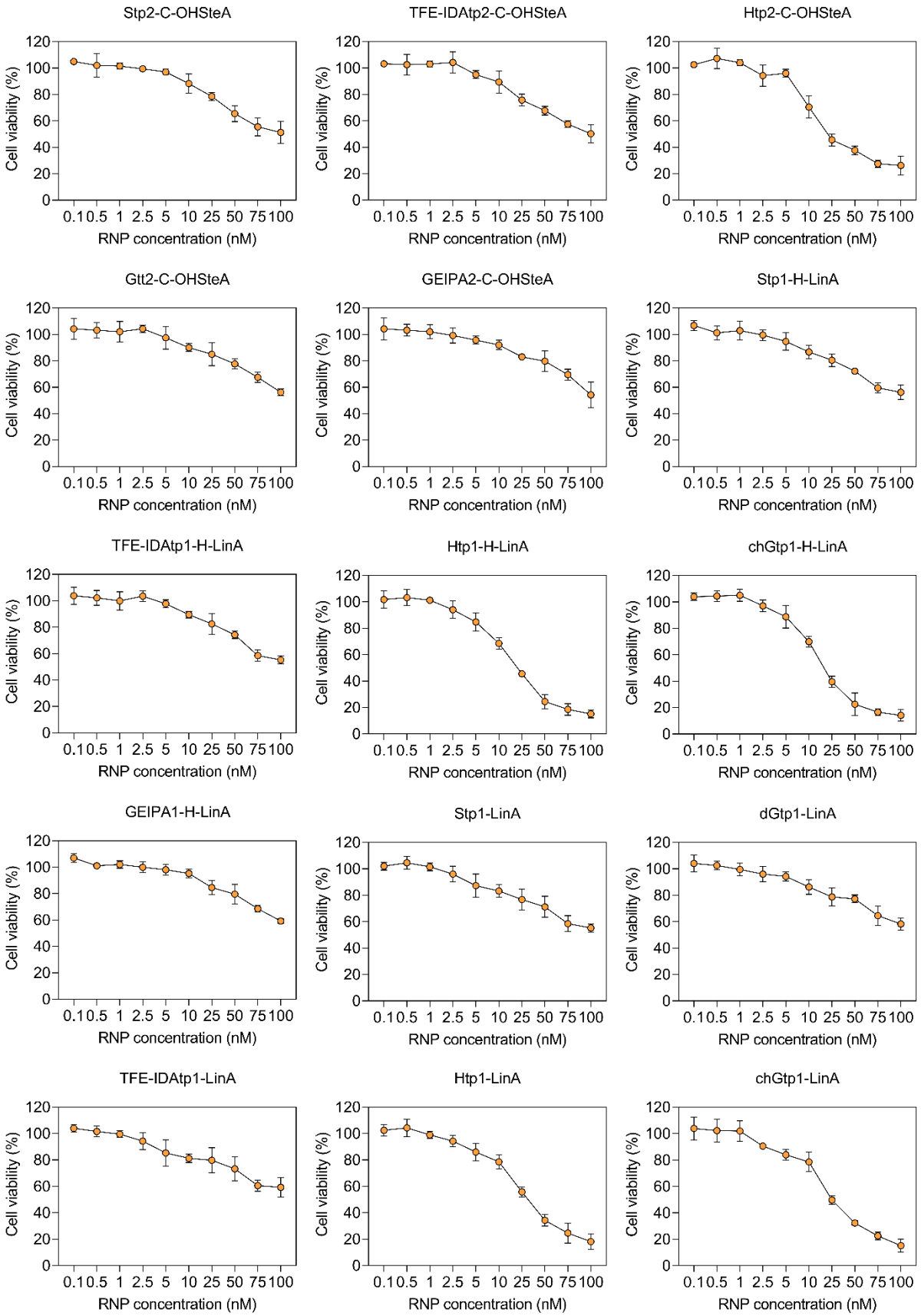

Figure 46. Cell viability of HeLa GFPd2 cells treated with different Cas9 RNP/ssDNA nanocarriers at various concentrations (RNP/ssDNA = 1/4).

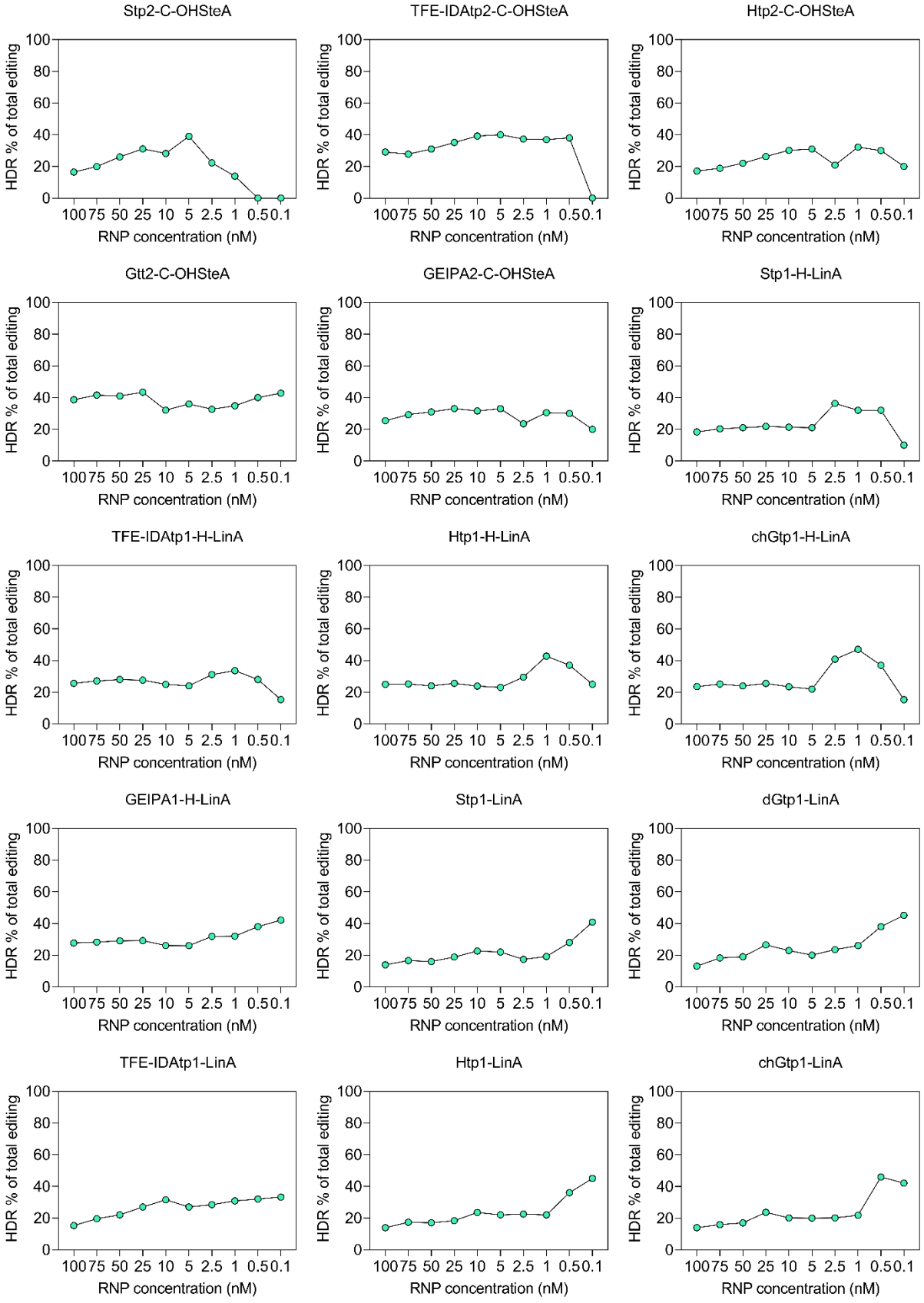

Figure 47. HDR percentage of total editing events in HeLa GFPd2 cells treated with different Cas9 RNP/ssDNA nanocarriers at various concentrations (RNP/ssDNA = 1/4).

4 Summary

In the first part, a folate receptor α (FRα)-specific Cas9 ribonucleoprotein (RNP) nanocarrier was developed for the effective intracellular transport of Cas9 RNP and PD-L1/PVR dual immune checkpoint disruption in FRα overexpressing CT26 cells. Cas9 RNP was first complexed with a hydroxystearic acid-containing lipopeptide 1445 to form the Cas9 RNP nanocarriers and then further conjugated with folic acid (FolA) and polyethylene glycol (PEG) to generate the FRα-specific nanocarriers. Knockout efficiency was firstly optimized in FRα overexpressing HeLa and CT26 eGFP reporter cells by varing the modification degree with FolA-PEG. *In vitro* studies showed that FolA-modified nanocarriers significantly enhanced eGFP knockout efficiency and improved the cellular uptake and endosomal escape capacity compared to PEG-shielded and unmodified nanocarriers. Moreover, the highest of PD-L1/PVR dual gene knockout was achieved with this formulation in CT26 cells, and the disruption of PVR was found to strongly inhibit the cell proliferation and induce cell apoptosis. *In vivo* knockout studies further confirmed that FolA-PEG modification of the nanocarriers enabled enhanced gene disruption with ~25 % dual PD-L1/PVR knockout, and a total of ~40 % gene editing events in CT26-bearing mice. Notably, the efficient knockout of dual PD-L1/PVR gene induced CD8+ T cell recruitment and a significant tumor growth inhibition. FolA-PEG_{24}-1445 Cas9 RNP nanocarriers are therefore considered as a promising platform for receptor-specific delivery of Cas9 RNPs for ICB-based cancer immunotherapy.

In the second part, enhanced Cas9 RNP delivery efficiency via lipopeptides was achieved by screening of effective lipopeptide sequence and fine tuning the hydrophobicity of artificial amino acids in lipopeptides. A series of lipopeptides with structural variations including cysteines, histidines, number of Stp units and type of fatty acids were synthesized and the ability to deliver Cas9 RNP was investigated. The structures containing less Stp and unsaturated or hydroxyl-modified fatty acids outperformed the others. Ten artificial amino acids with varied hydrophobicity were then synthesized, and introduced into the lead structures to generate a new series of hydrophobically varied lipopeptides. $LogD_{7.4}$ value and eGFP knockout EC50 of these lipopeptides were determined. A correlation between the lipopeptide $logD_{7.4}$ and eGFP knockout EC50 was found, with an optimal $logD_{7.4}$ range for each

lipopeptide architecture. The optimized lipopeptides achieved ~88 % eGFP knockout at 1 nM dose of RNP and up to 40 % homology-directed repair (HDR) by co-delivery with ssDNA template. The structure-activity relationship and mechanism studies demonstrate that hydrophobically balanced lipopeptides are more resistant to ionic competition, remain integrated at low concentrations, and facilitate stronger endocytosis by both clathrin-mediated and macropinocytosis pathways. These findings indicate that the hydrophobicity is an important characteristic of lipopeptides for the delivery of Cas9 RNP, and it may provide a new guide for the future design of non-viral nucleic acid nanocarriers, also beyond Cas9 RNP.

5 Appendix

5.1 Abbreviations

cgRNA	Control guide RNA
CRISPR	Clustered, regularly interspaced, short palindromic repeats
Cas	CRISPR-associated
DIPEA	*N,N*-Diisopropylethylamine
DMEM	Dulbecco's modified Eagle's medium
FCS	Fetal calf serum
FRα	Folate receptor α
HBG	Hepes-buffered glucose
HEPES	*N*-(2-Hydroxethyl) piperazine-N'-(2-ethansulfonic acid)
PD-L1	Programmed death-ligand 1
PD-1	Programmed cell death protein 1
MTT	3-(4,5-Dimethylthiazol-2-yl)-2,5-diphenyltetrazolium bromide
N/P	(Protonatable) nitrogen to phosphates ratio
TIGIT	T cell immunoreceptor with Ig and ITIM domains
PVR	Poliovirus receptor
PDI	Polydispersity index
RNP	Ribonucleoprotein
RT	Room temperature
SEC	Size-exclusion chromatography
FolA	Folic acid

5.2 Analytical Data

5.2.1 MALDI-TOF mass spectrometry of lipopeptides

MALDI-TOF MS of 1445

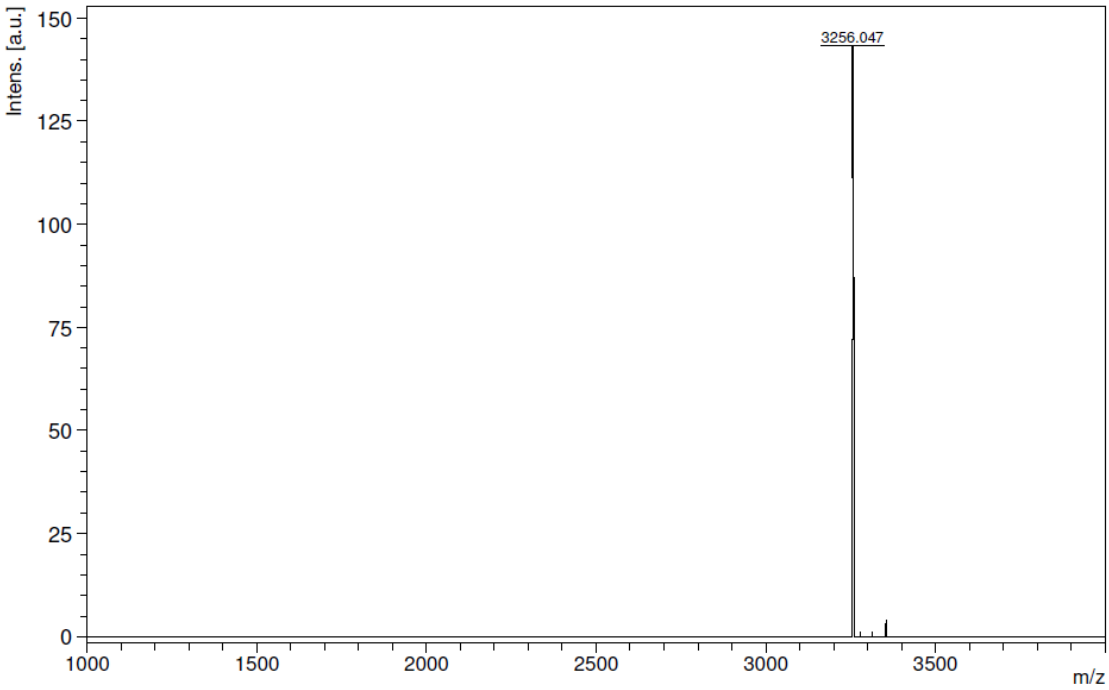

MALDI-TOF MS of FolA-PEG$_{24}$-DBCO

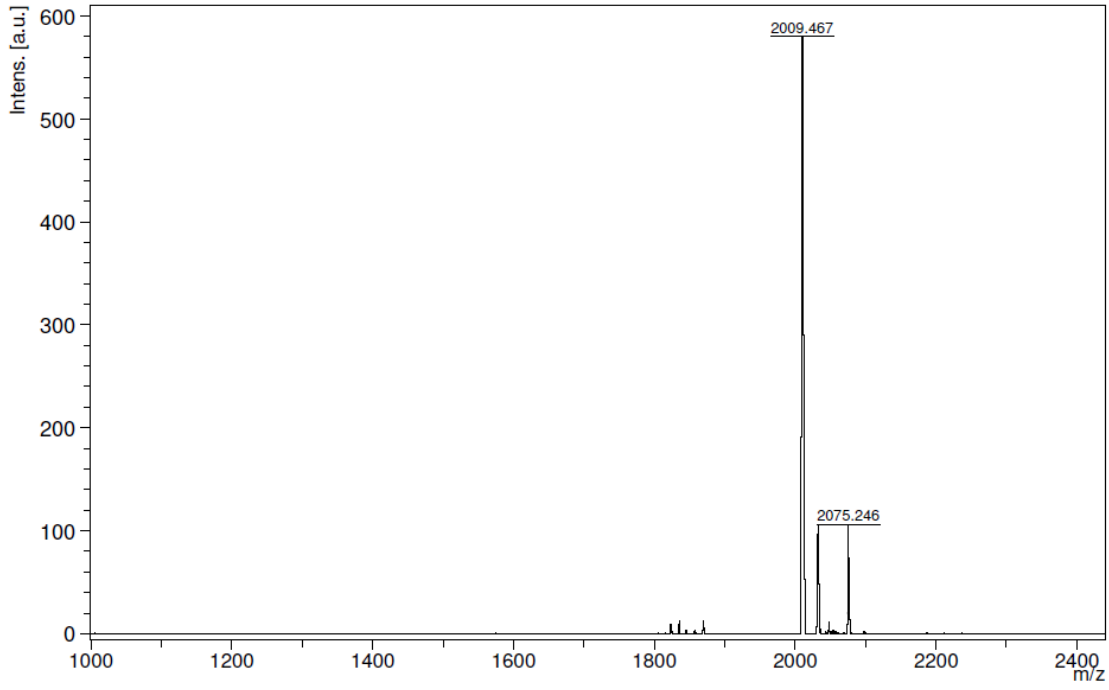

MALDI-TOF MS of PEG_{24}-DBCO

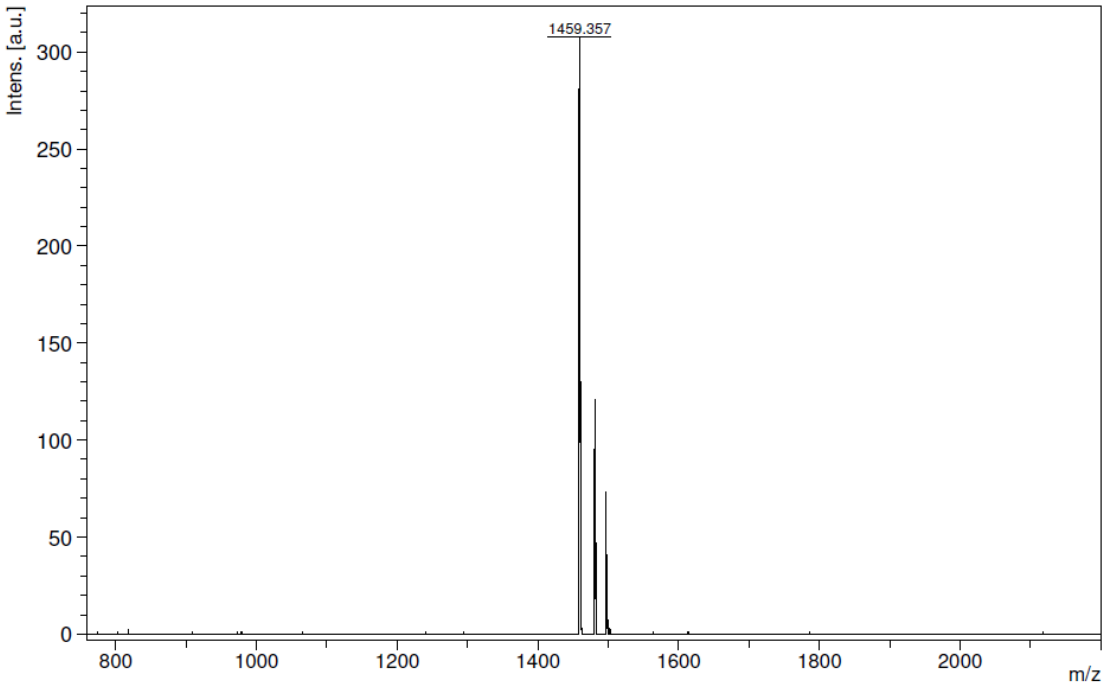

MALDI-TOF MS of FolA-PEG_{24}-1445

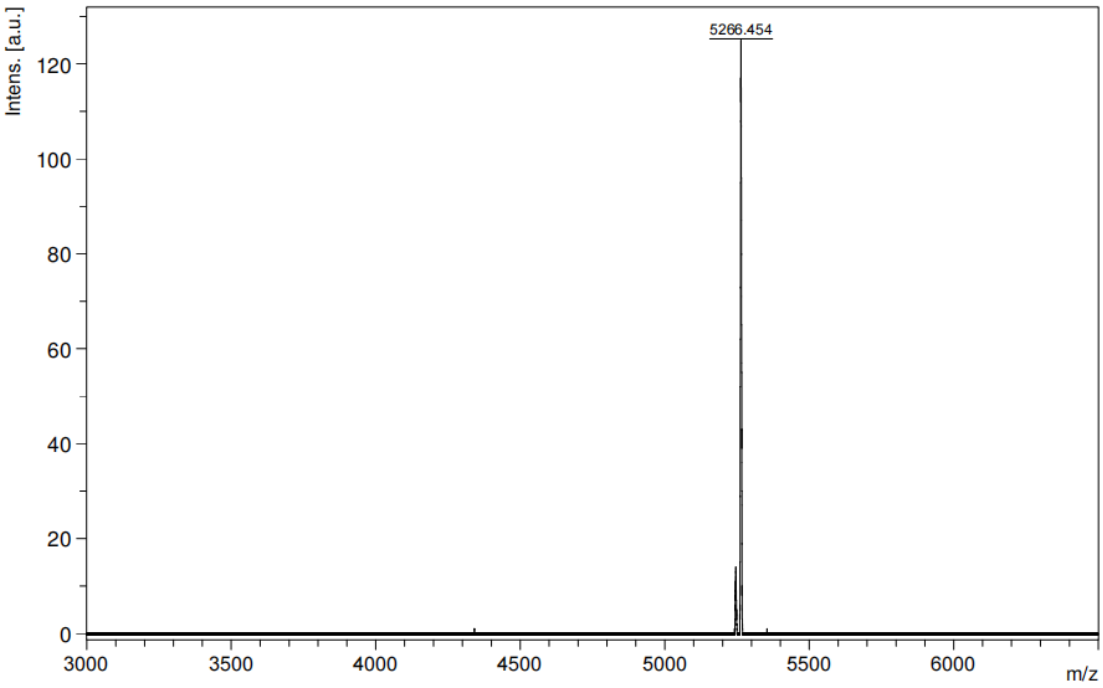

MALDI-TOF MS of PEG_{24}-1445

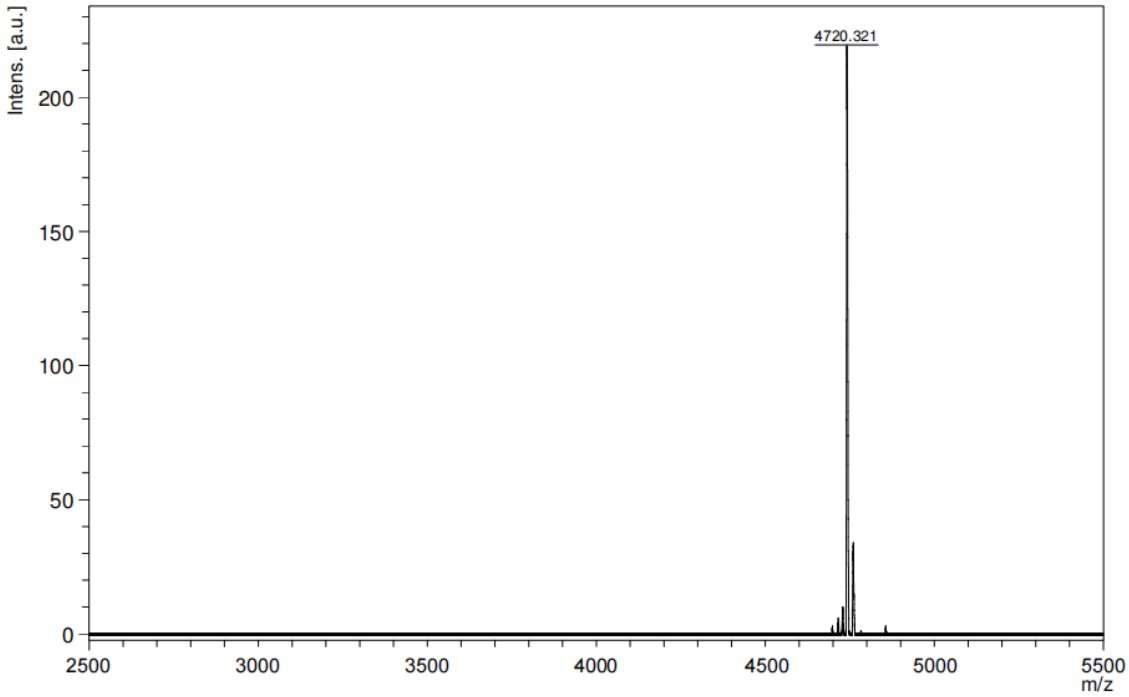

5.2.2 ESI mass spectrometry

ESI-MS of BOC-IDA

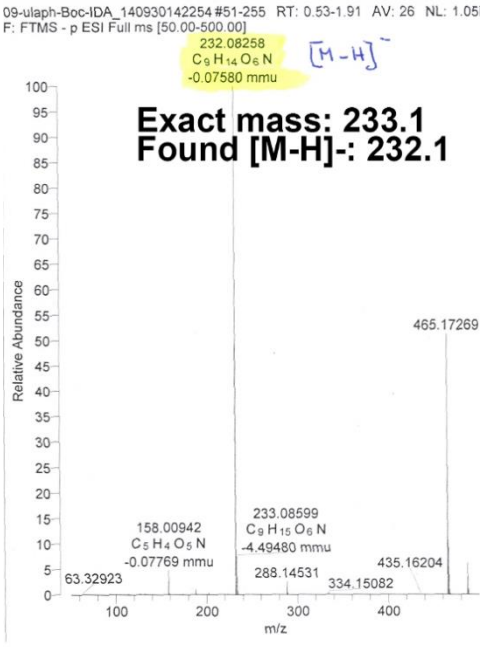

ESI-MS of TFE-IDA

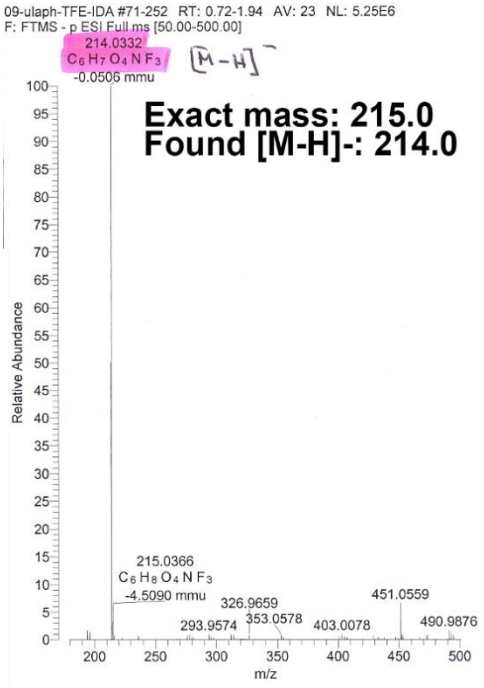

ESI-MS of OHSteA

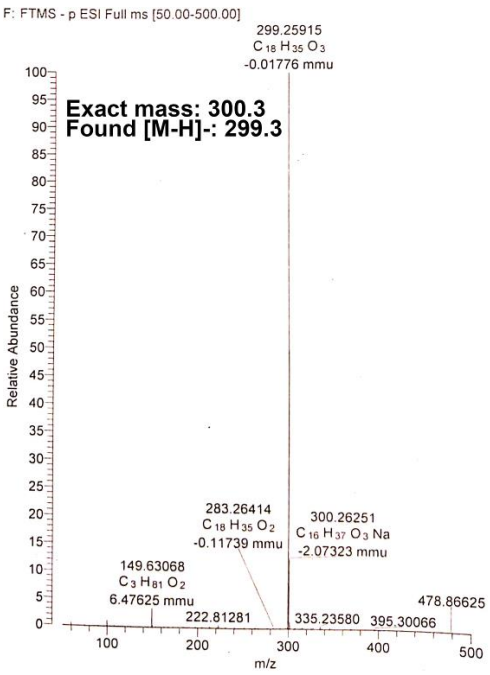

ESI-MS of artificial amino acids

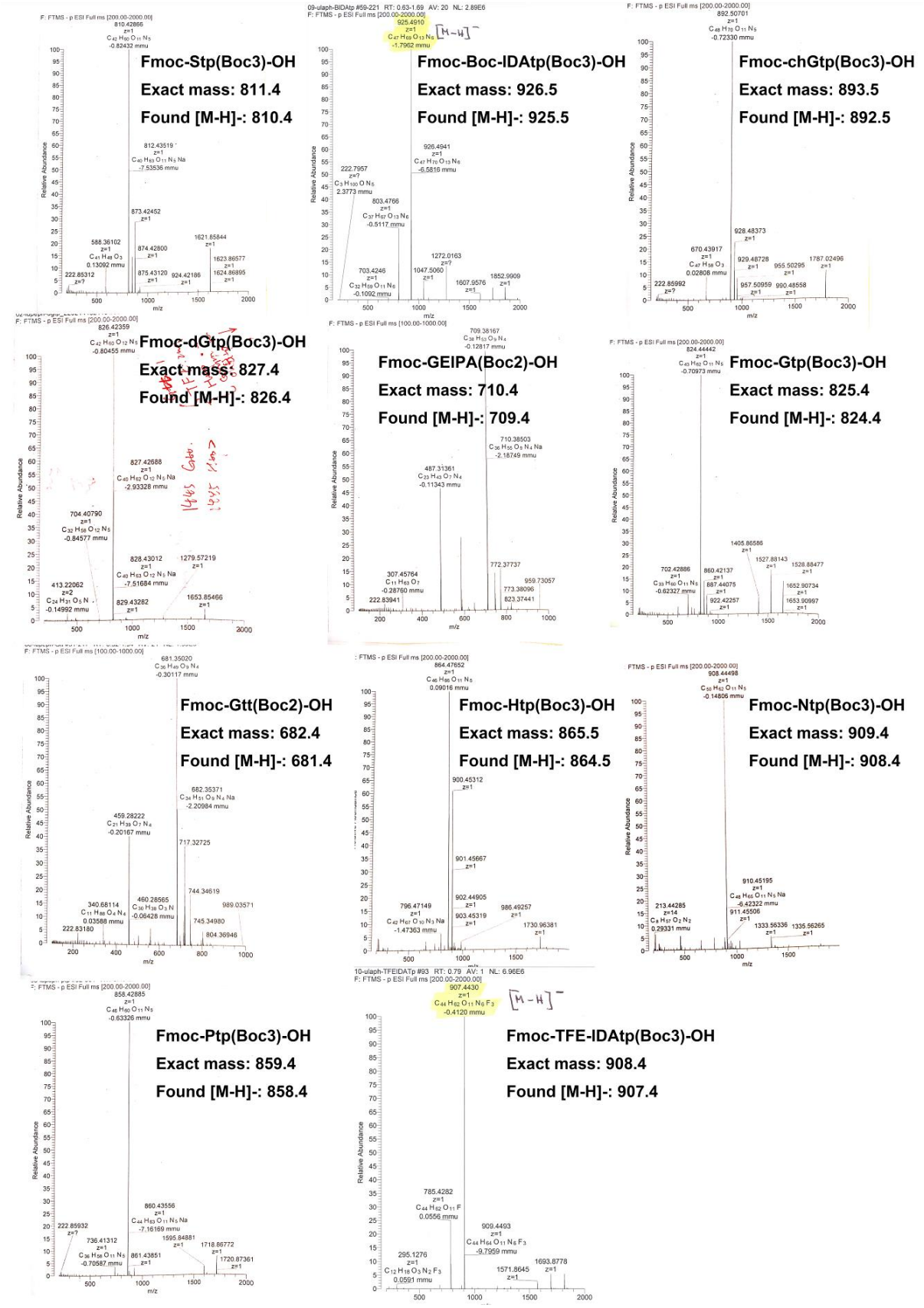

5.2.3 ^{1}H NMR spectra

Boc-IDA

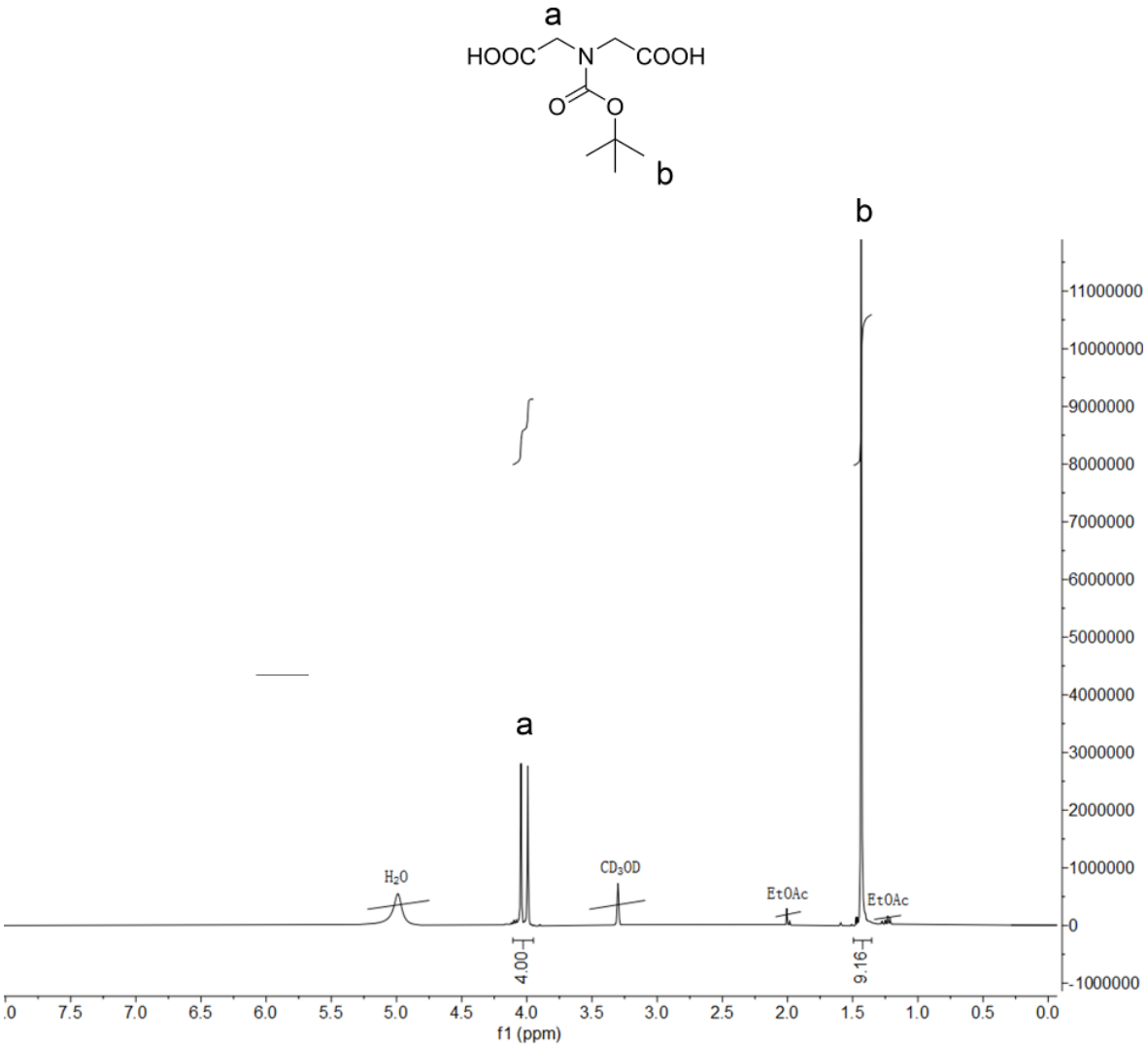

^{1}H NMR (400 MHz, CD_3OD) δ (ppm) = 4.10 - 3.95 (m, 4H, C**H₂**), 1.49 - 1.36 (s, 9H, C**H₃**-*tert*-but).

TFE-IDA

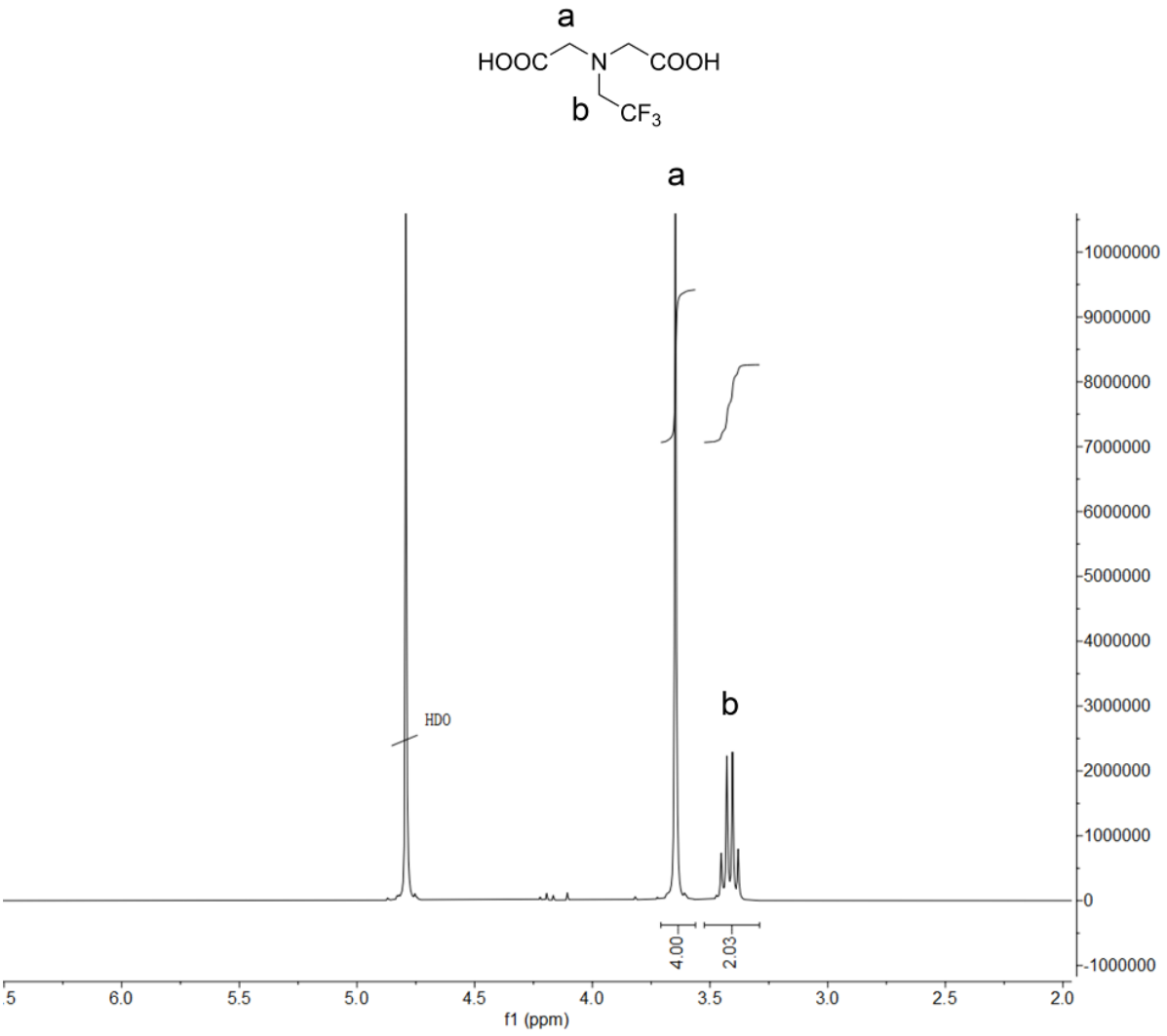

^{1}H NMR (400 MHz, D_2O) δ (ppm) = 3.70 - 3.56 (m, 4H, C**H₂**), 3.52 - 3.29 (q, 2H, C**H₂**CF_3).

Fmoc-Stp(Boc$_3$)-OH

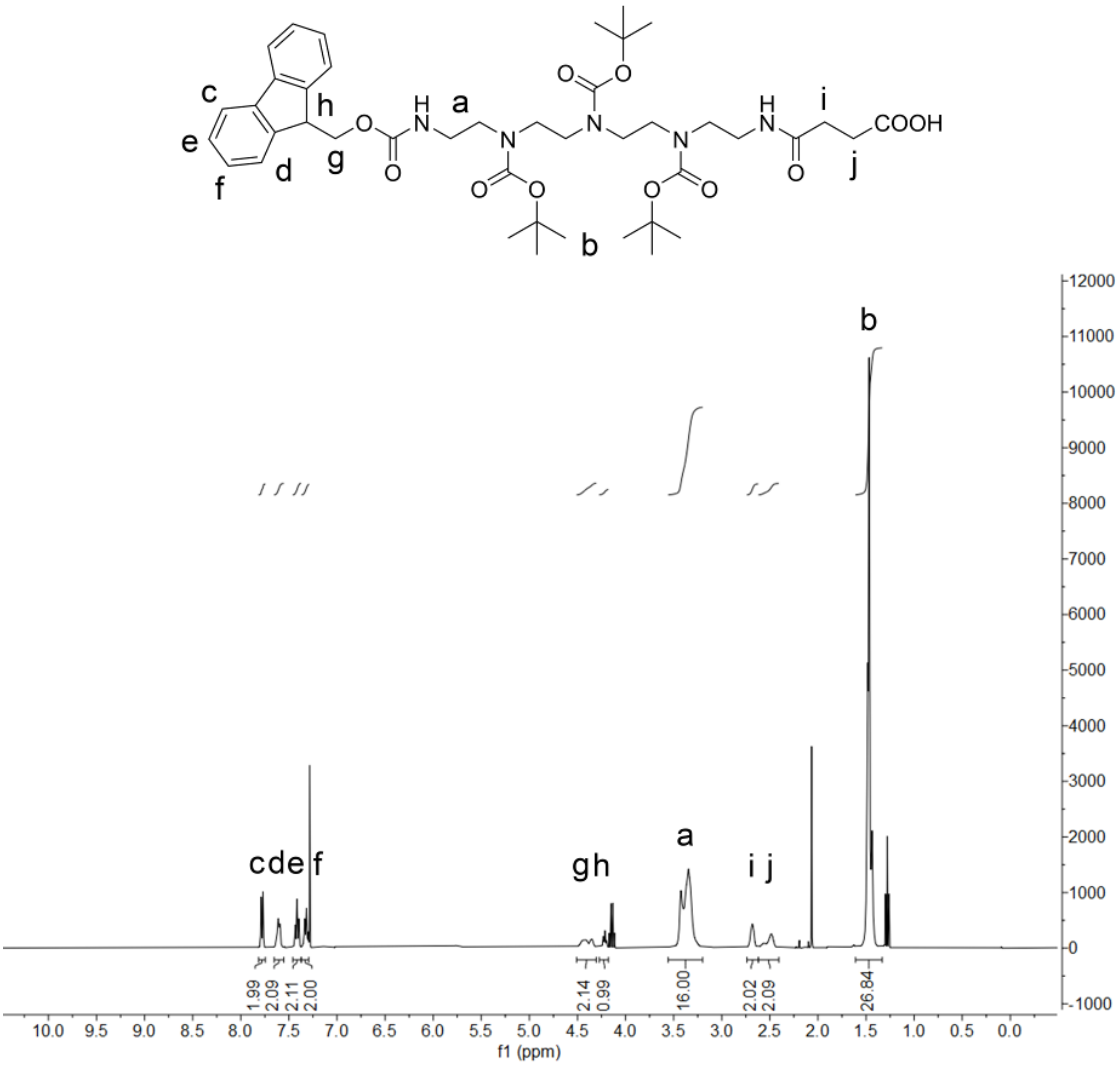

^{1}H NMR (400 MHz, $CDCl_3$) δ (ppm) = 7.78 (d, 2H, Ar**H**-Fmoc), 7.61 (d, 2H, Ar**H**-Fmoc), 7.41 (t, 2H, Ar**H**-Fmoc), 7.31 (t, 2H, Ar**H**-Fmoc), 4.40 (m, 2H, C**H$_2$**-Fmoc), 4.21 (m, 1H, C**H**-Fmoc), 3.47 - 3.20 (m, 16H, C**H$_2$**-Tepa), 2.67 (t, 2H, C**H$_2$**CONH-Suc), 2.48 (m, 2H, C**H$_2$**COOH-Suc), 1.46 (s, 27H, C**H$_3$**-*tert*-but).

Fmoc-Gtp(Boc$_3$)-OH

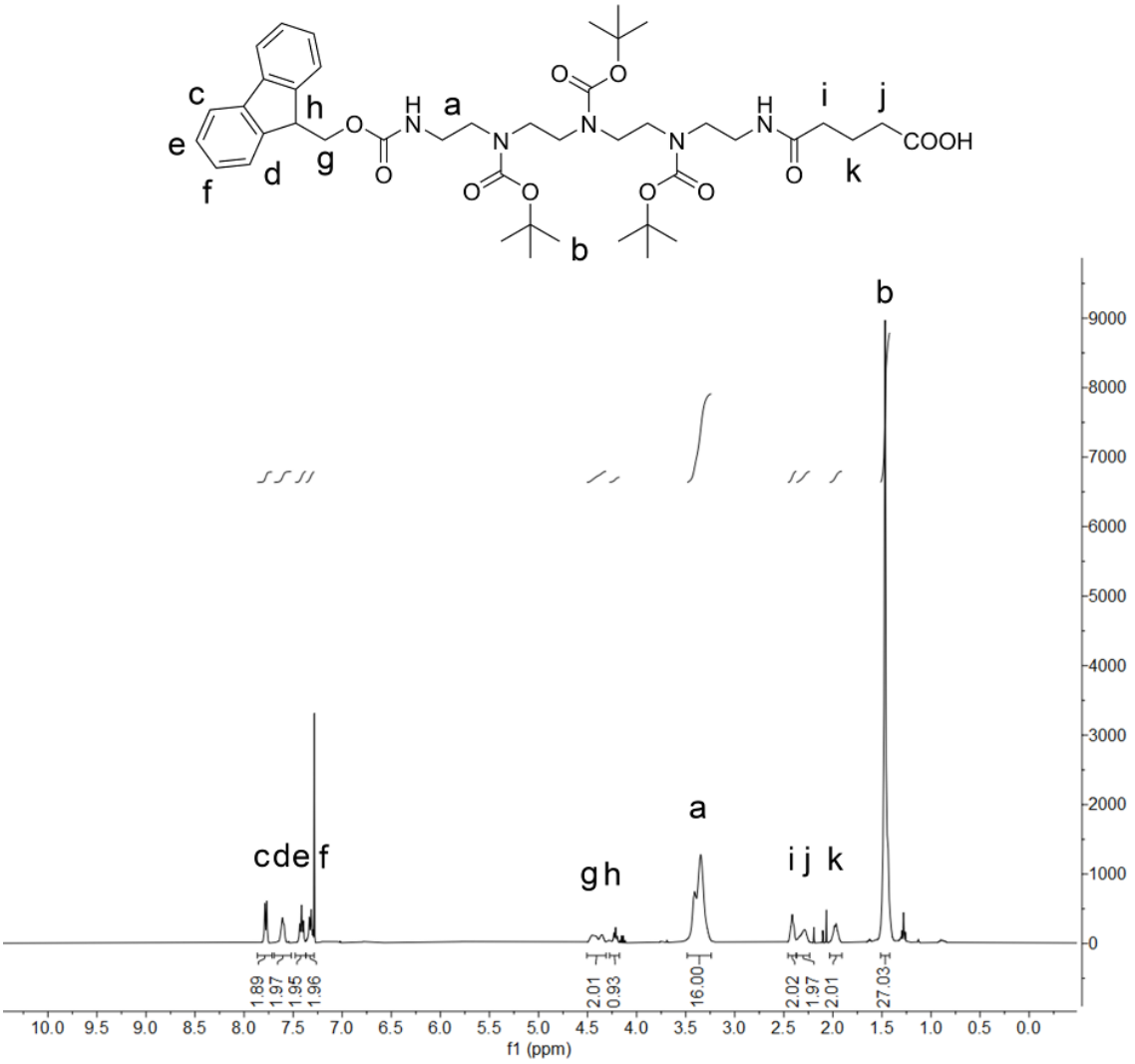

^{1}H NMR (400 MHz, $CDCl_3$) δ (ppm) = 7.79 (d, 2H, Ar**H**-Fmoc), 7.60 (d, 2H, Ar**H**-Fmoc), 7.41 (t, 2H, Ar**H**-Fmoc), 7.32 (t, 2H, Ar**H**-Fmoc), 4.41 (m, 2H, C**H$_2$**-Fmoc), 4.22 (m, 1H, C**H**-Fmoc), 3.48 - 3.24 (m, 16H, C**H$_2$**-Tepa), 2.42 (t, 2H, C**H$_2$**CONH-Glu), 2.29 (t, 2H, C**H$_2$**COOH-Glu), 1.97 (m, 2H, CH_2C**H$_2$**CH_2COOH-Glu), 1.47 (s, 27H, C**H$_3$**-*tert*-but).

Fmoc-Boc-IDAtp(Boc$_3$)-OH

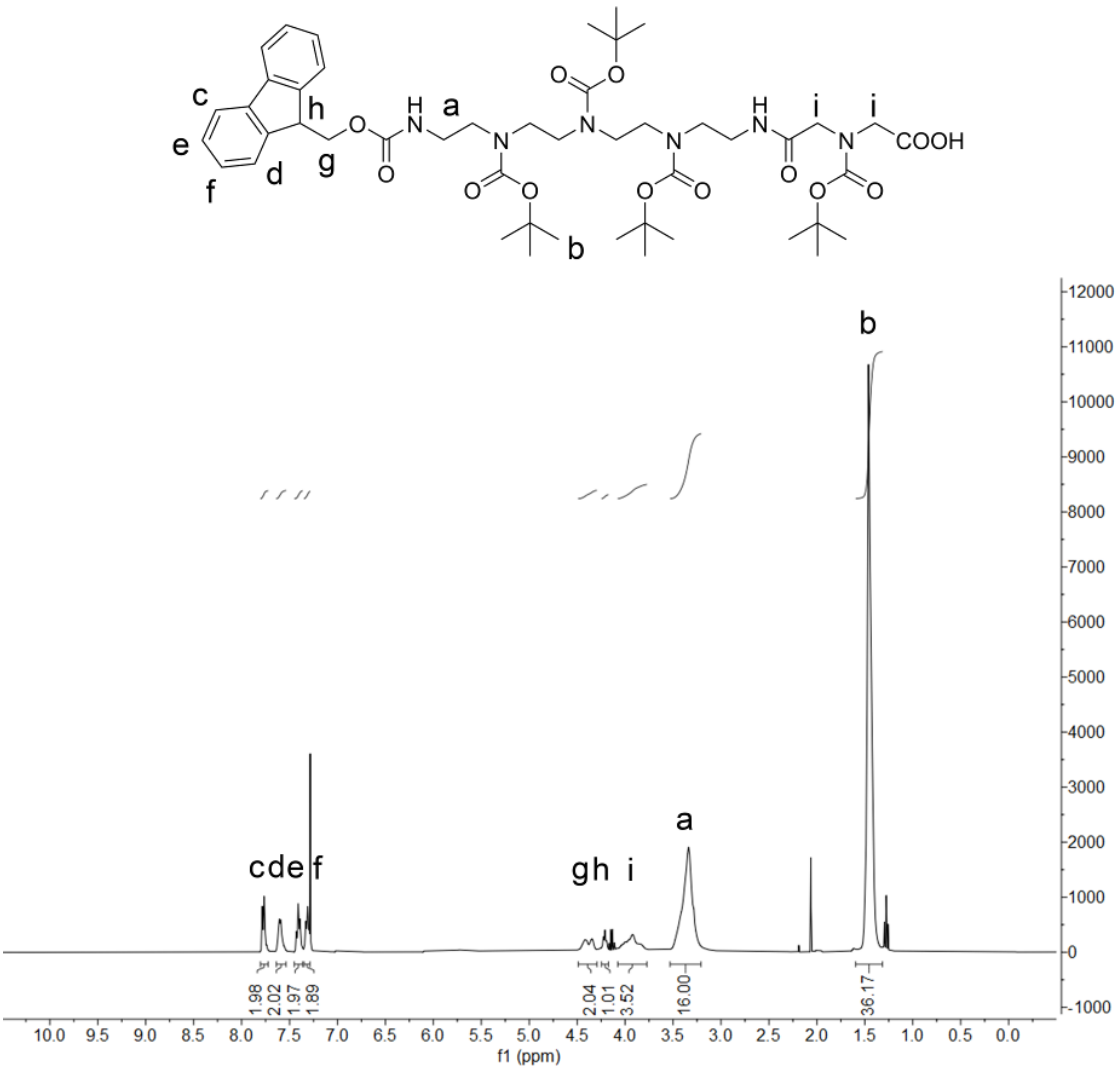

^{1}H NMR (400 MHz, $CDCl_3$) δ (ppm) = 7.77 (d, 2H, Ar**H**-Fmoc), 7.59 (d, 2H, Ar**H**-Fmoc), 7.40 (t, 2H, Ar**H**-Fmoc), 7.31 (t, 2H, Ar**H**-Fmoc), 4.40 (m, 2H, C**H$_2$**-Fmoc), 4.20 (m, 1H, C**H**-Fmoc), 3.91 (s, 4H, C**H$_2$**-IDA) 3.48 - 3.19 (m, 16H, C**H$_2$**-Tepa), 1.43 (s, 36H, C**H$_3$**-*tert*-but).

Fmoc-dGtp(Boc$_3$)-OH

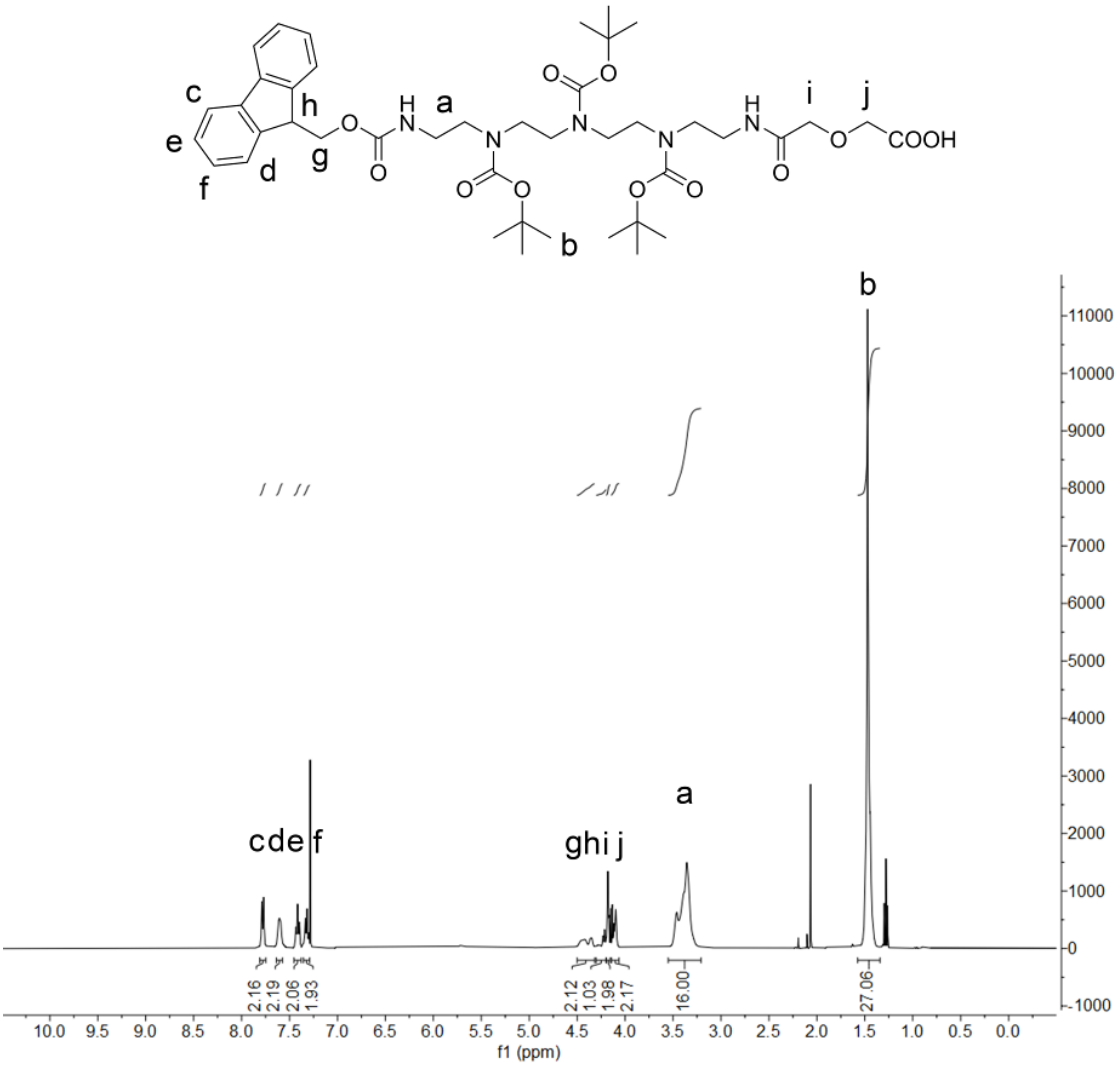

^{1}H NMR (400 MHz, $CDCl_3$) δ (ppm) = 7.77 (d, 2H, Ar**H**-Fmoc), 7.60 (d, 2H, Ar**H**-Fmoc), 7.42 (t, 2H, Ar**H**-Fmoc), 7.32 (t, 2H, Ar**H**-Fmoc), 4.41 (m, 2H, C**H$_2$**-Fmoc), 4.23 (m, 1H, C**H**-Fmoc), 4.17 (d, 2H, C**H$_2$**CONH-diglycolic acid), 4.10 (d, 2H, C**H$_2$**COOH- diglycolic acid), 3.51 - 3.18 (m, 16H, C**H$_2$**-Tepa), 1.45 (s, 27H, C**H$_3$**-*tert*-but).

Fmoc-GEIPA(Boc$_2$)-OH

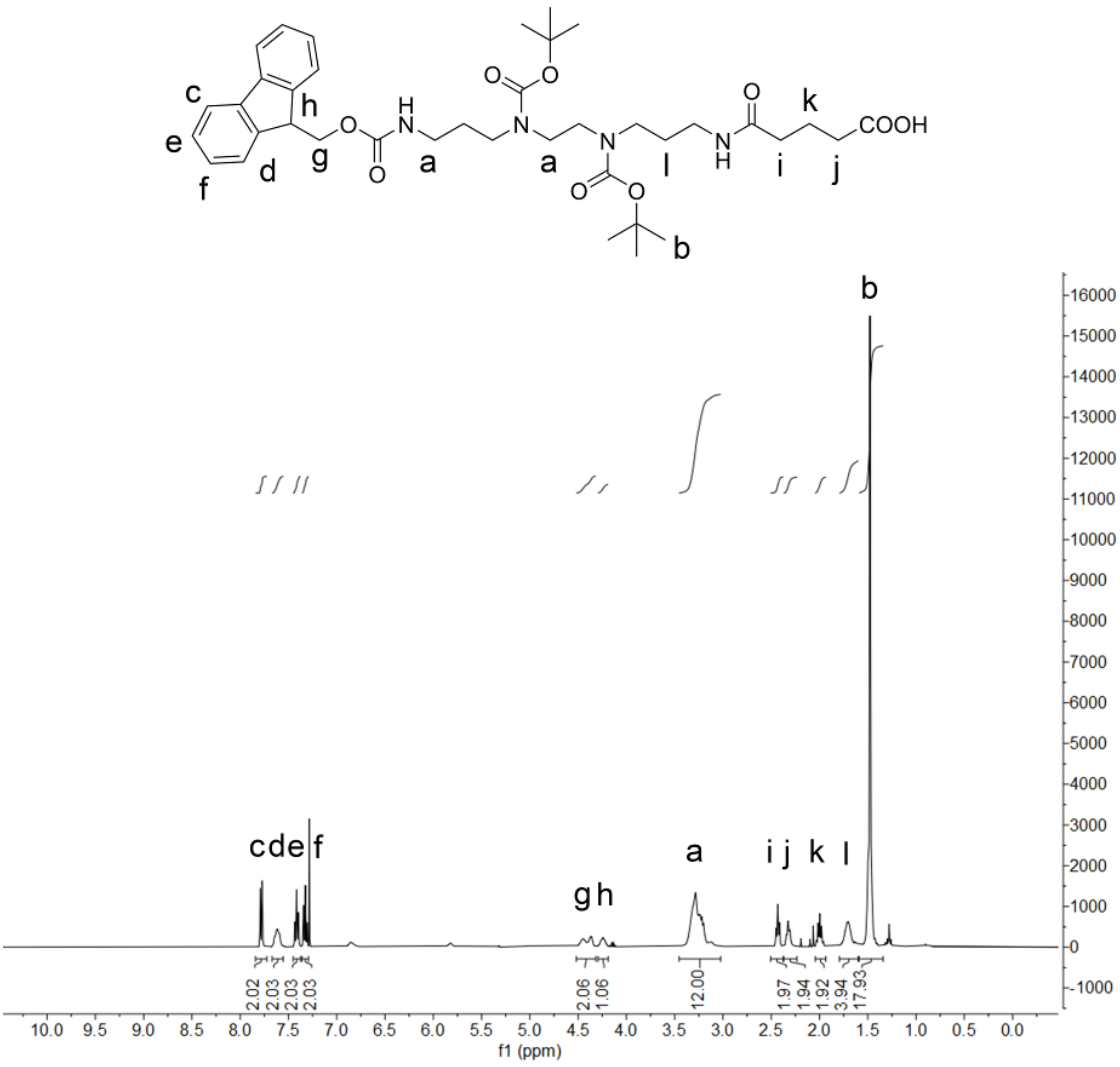

^{1}H NMR (400 MHz, $CDCl_3$) δ (ppm) = 7.78 (d, 2H, Ar**H**-Fmoc), 7.62 (d, 2H, Ar**H**-Fmoc), 7.41 (t, 2H, Ar**H**-Fmoc), 7.32 (t, 2H, Ar**H**-Fmoc), 4.42 (m, 2H, C**H$_2$**-Fmoc), 4.23 (m, 1H, C**H**-Fmoc), 3.43 - 3.03 (m, 12H, C**H$_2$**CH_2C**H$_2$**-GEIPA, C**H$_2$**C**H$_2$**-GEIPA), 2.44 (t, 2H, C**H$_2$**CONH-Glu), 2.30 (t, 2H, C**H$_2$**COOH-Glu), 1.99 (m, 2H, CH_2C**H$_2$**CH_2COOH-Glu), 1.71 (m, 4H, CH_2C**H$_2$**CH_2-GEIPA), 1.47 (s, 18H, C**H$_3$**-*tert*-but).

Fmoc-Gtt(Boc$_2$)-OH

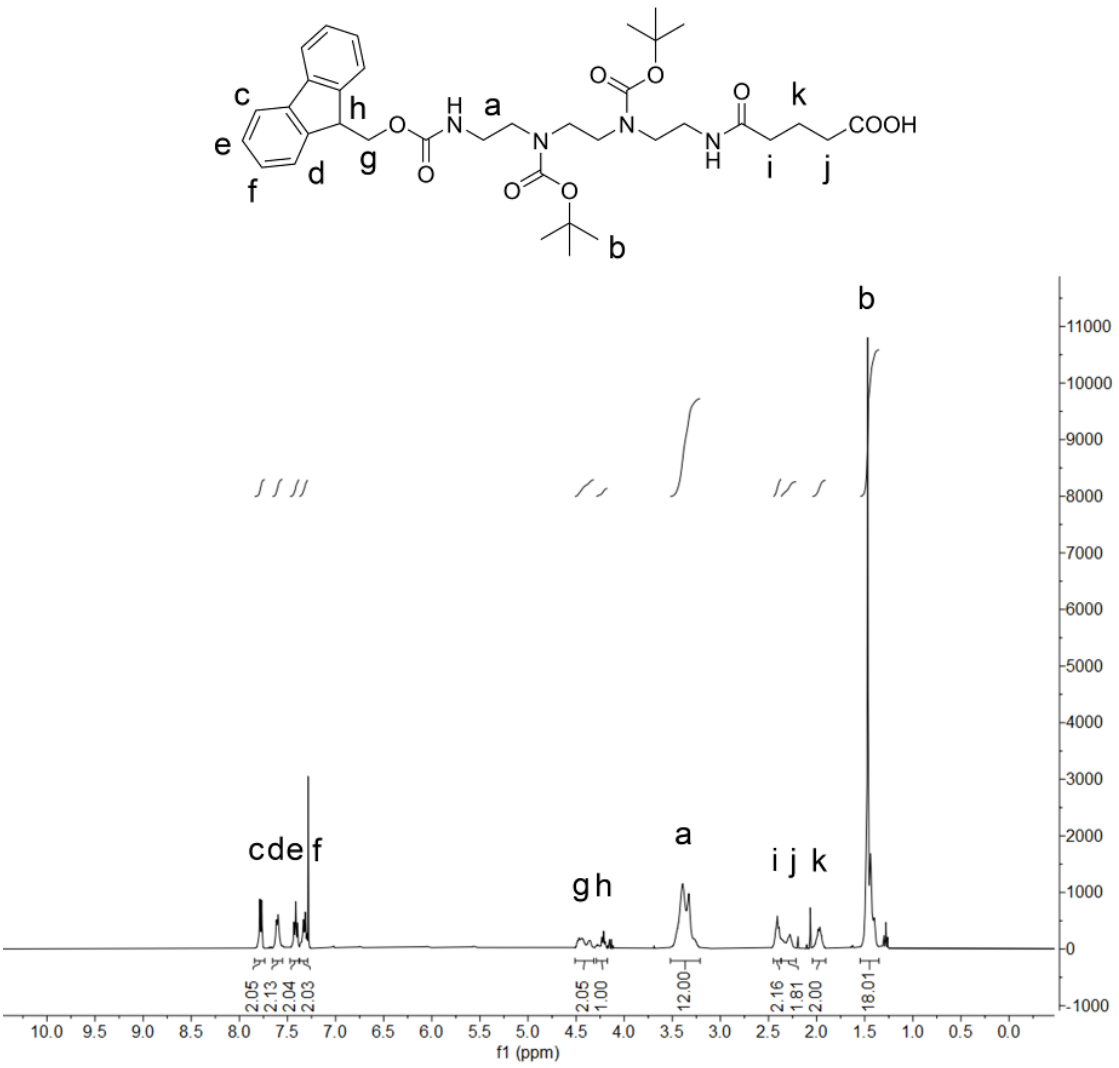

^{1}H NMR (400 MHz, $CDCl_3$) δ (ppm) = 7.79 (d, 2H, Ar**H**-Fmoc), 7.61 (d, 2H, Ar**H**-Fmoc), 7.42 (t, 2H, Ar**H**-Fmoc), 7.32 (t, 2H, Ar**H**-Fmoc), 4.42 (m, 2H, C**H$_2$**-Fmoc), 4.22 (m, 1H, C**H**-Fmoc), 3.52 - 3.21 (m, 12H, C**H$_2$**-Teta), 2.41 (t, 2H, C**H$_2$**CONH-Glu), 2.28 (t, 2H, C**H$_2$**COOH-Glu), 1.98 (m, 2H, CH_2C**H$_2$**CH_2COOH-Glu), 1.45 (s, 18H, C**H$_3$**-*tert*-but).

Fmoc-Htp(Boc$_3$)-OH

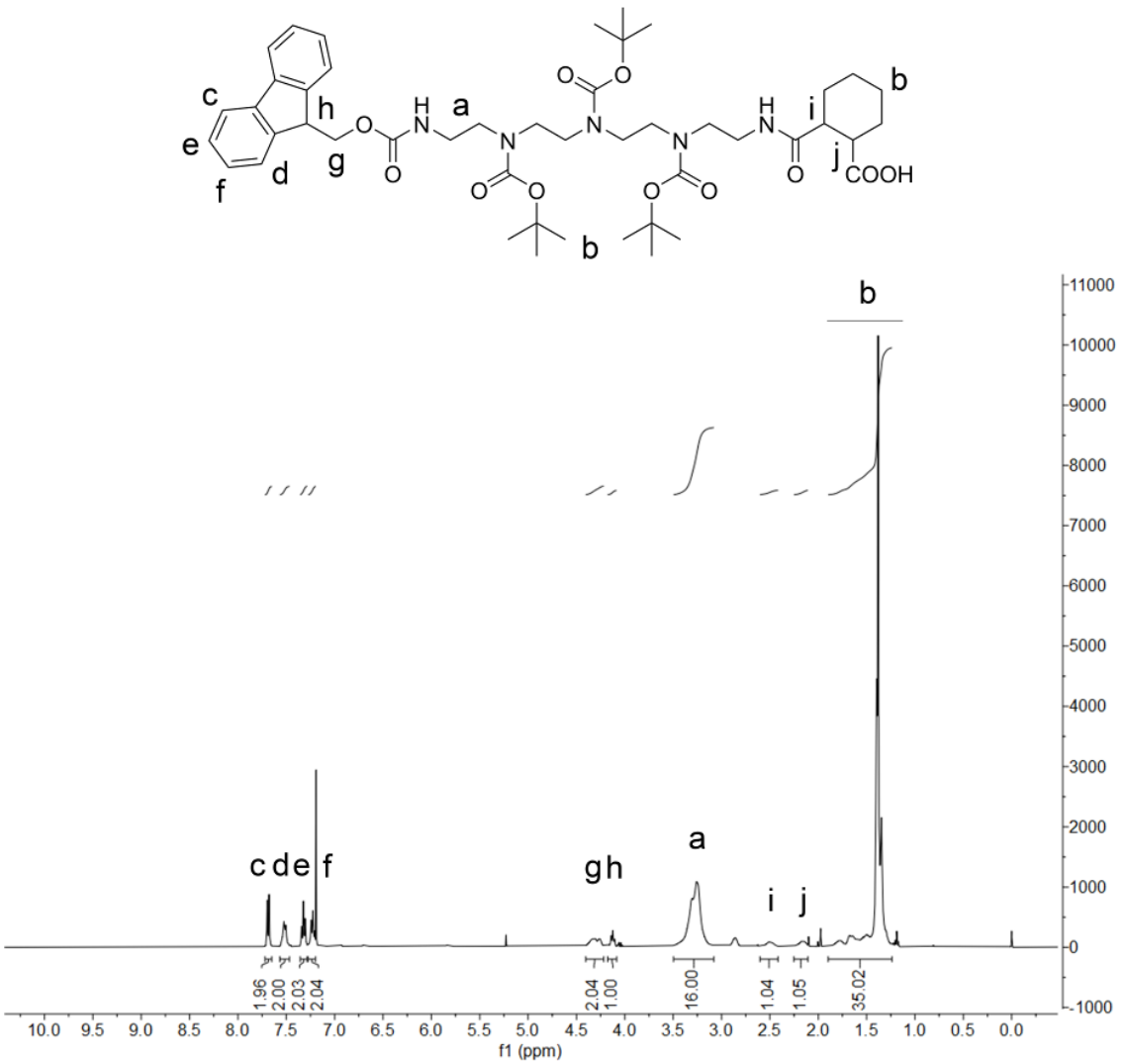

^{1}H NMR (400 MHz, $CDCl_3$) δ (ppm) = 7.69 (d, 2H, Ar**H**-Fmoc), 7.51 (d, 2H, Ar**H**-Fmoc), 7.32 (t, 2H, Ar**H**-Fmoc), 7.23 (t, 2H, Ar**H**-Fmoc), 4.30 (m, 2H, C**H$_2$**-Fmoc), 4.12 (m, 1H, C**H**-Fmoc), 3.48 - 3.08 (m, 16H, C**H$_2$**-Tepa), 2.50 (d, 1H, C**H**CONH-Hexahydrophthalic acid), 2.16 (s, 1H, C**H**COOH-Hexahydrophthalic acid), 1.89 - 1.24 (m, 35H, C**H$_2$**-Hexahydrophthalic acid, C**H$_3$**-*tert*-but).

Fmoc-Ptp(Boc$_3$)-OH

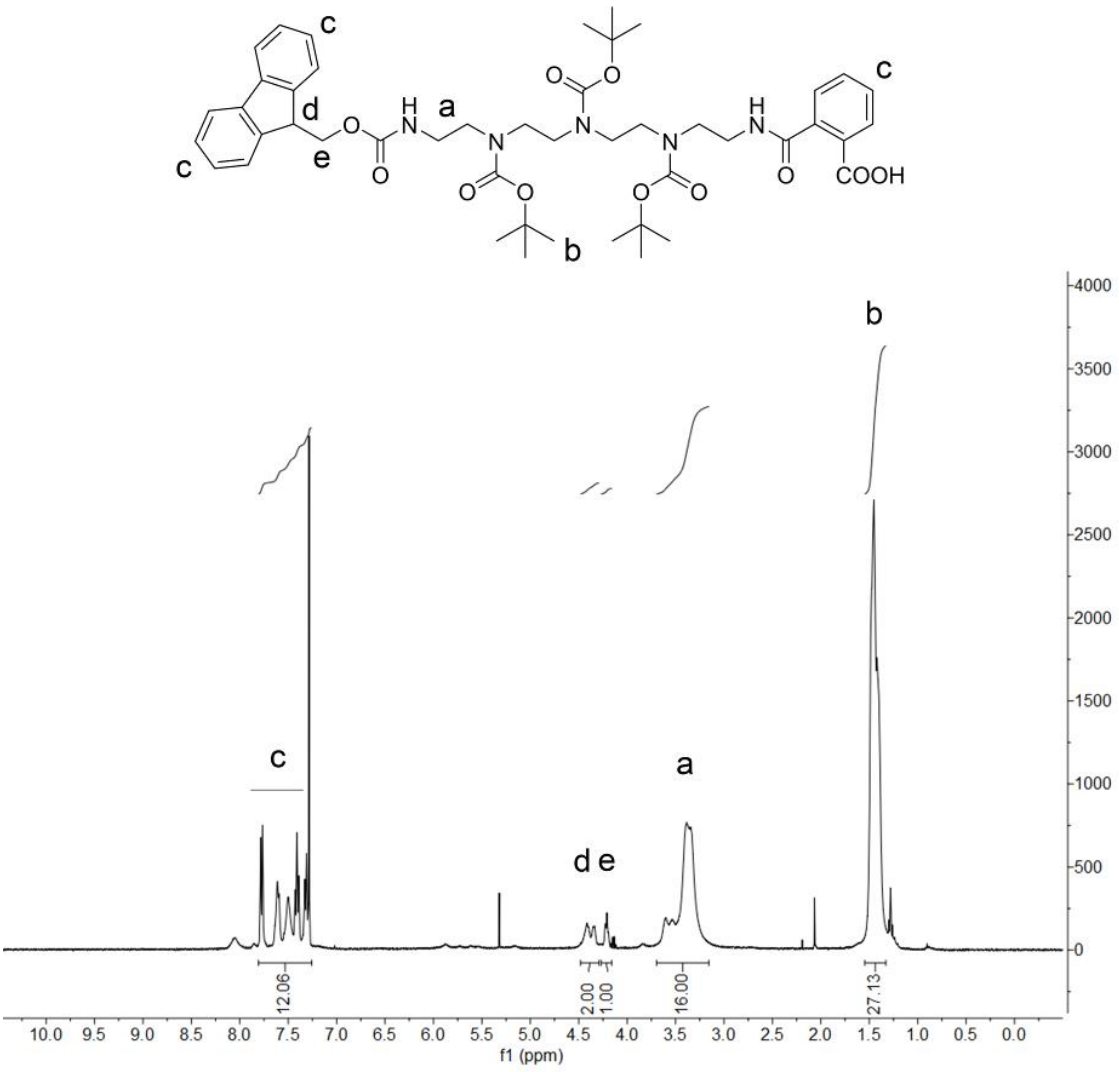

^{1}H NMR (400 MHz, $CDCl_3$) δ (ppm) = 7.81 - 7.25 (m, 12H, Ar**H**-Fmoc, Ar**H**-Phthalic acid), 4.41 (m, 2H, C**H$_2$**-Fmoc), 4.22 (m, 1H, C**H**-Fmoc), 3.69 - 3.17 (m, 16H, C**H$_2$**-Tepa), 1.44 (s, 27H, C**H$_3$**-*tert*-but).

Fmoc-Ntp(Boc$_3$)-OH

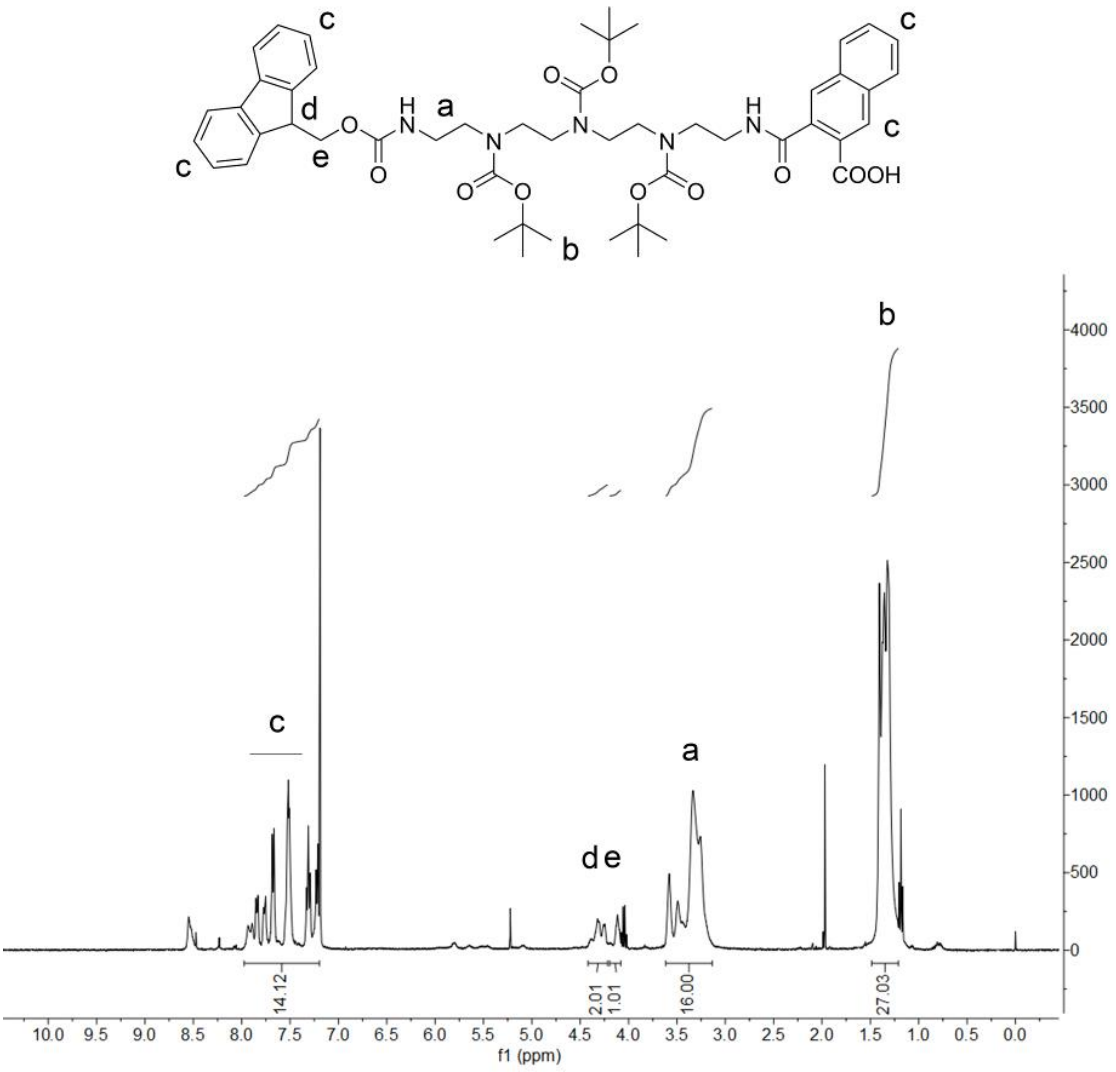

^{1}H NMR (400 MHz, $CDCl_3$) δ (ppm) = 7.98 - 7.17 (m, 14H, Ar**H**-Fmoc, Ar**H**-Naphthalenedicarboxylic acid), 4.29 (m, 2H, C**H$_2$**-Fmoc), 4.12 (m, 1H, C**H**-Fmoc), 3.62 - 3.12 (m, 16H, C**H$_2$**-Tepa), 1.34 (s, 27H, C**H$_3$**-*tert*-but).

Fmoc-TFE-IDAtp(Boc$_3$)-OH

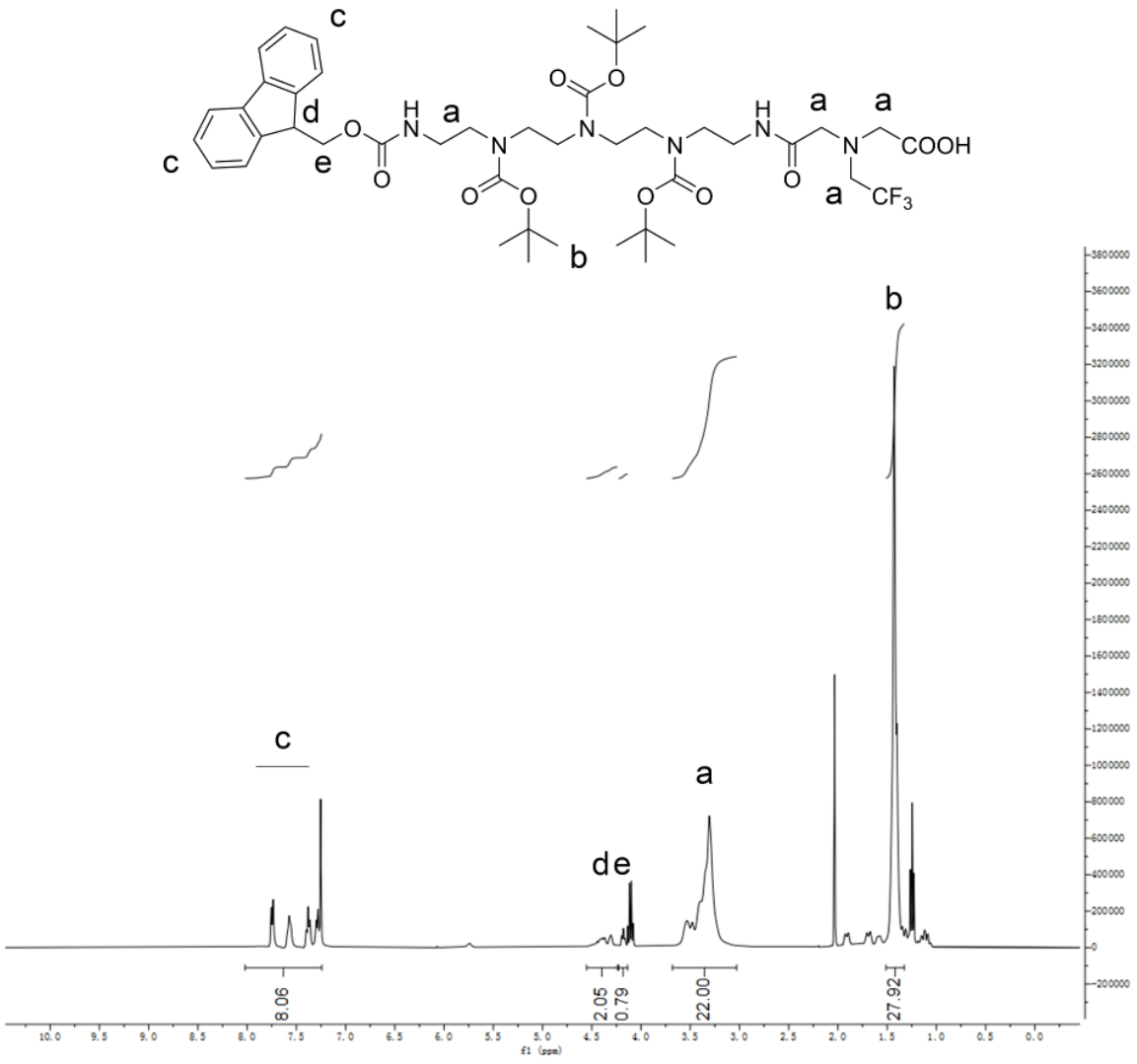

^{1}H NMR (400 MHz, $CDCl_3$) δ (ppm) = 8.03 - 7.25 (m, 8H, Ar**H**-Fmoc), 4.39 (m, 2H, C**H$_2$**-Fmoc), 4.18 (m, 1H, C**H**-Fmoc), 3.67 - 3.04 (m, 22H, C**H$_2$**-TFE-IDA), 1.43 (s, 27H, C**H$_3$**-*tert*-but).

Hydroxylstearic acid (OHSteA)

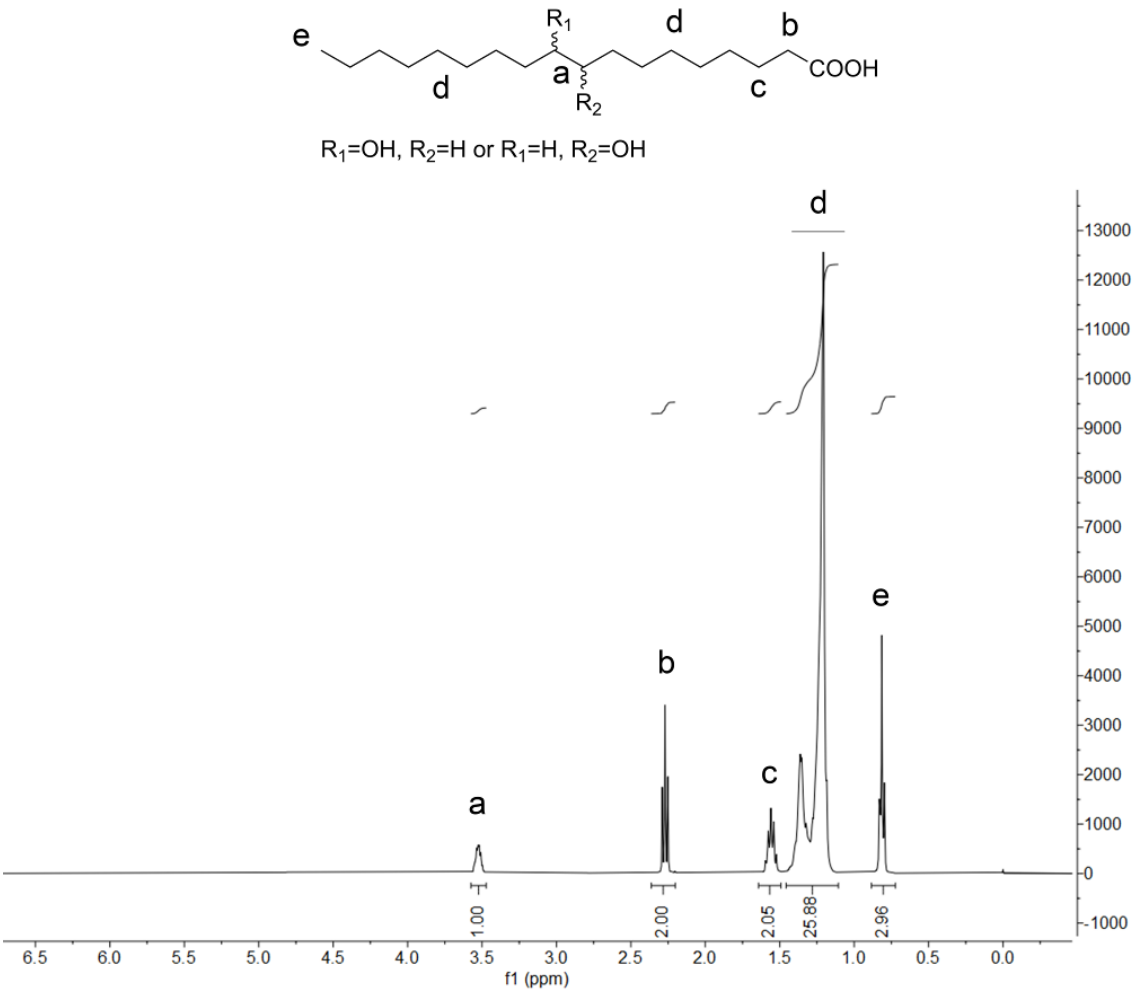

^{1}H NMR (400 MHz, $CDCl_3$) δ (ppm) = 3.57 - 3.48 (q, 1H, C**H**-OH), 2.35 - 2.21 (t, 2H, C**H$_2$**COOH), 1.63 - 1.49 (q, 2H, C**H$_2$**CH$_2$COOH), 1.44 - 1.11 (m, 26H, -C**H$_2$**-), 0.87 - 0.72 (t, 3H, C**H$_3$**).

T-OHSteA (1445)

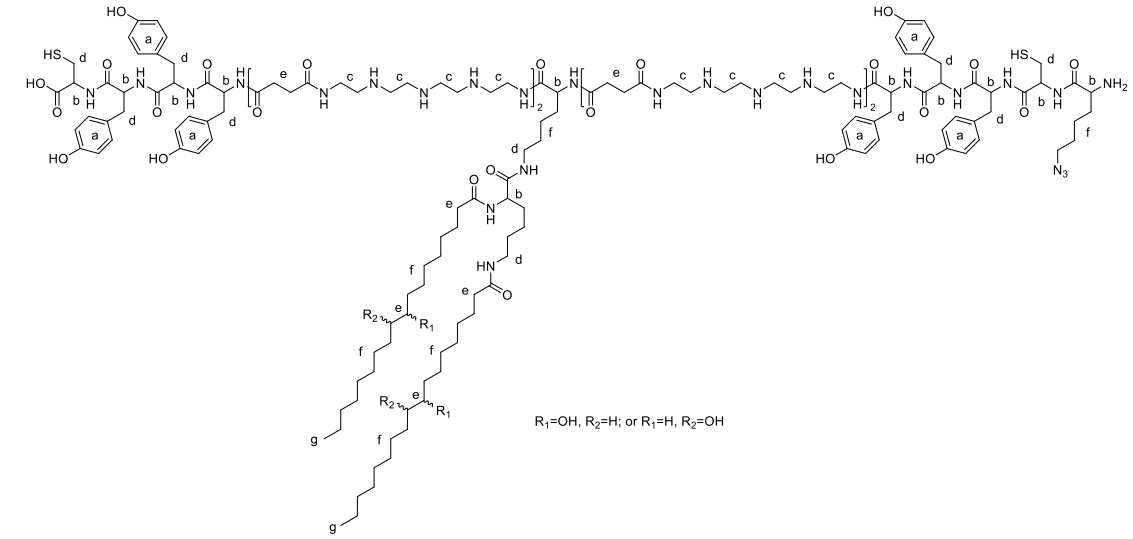

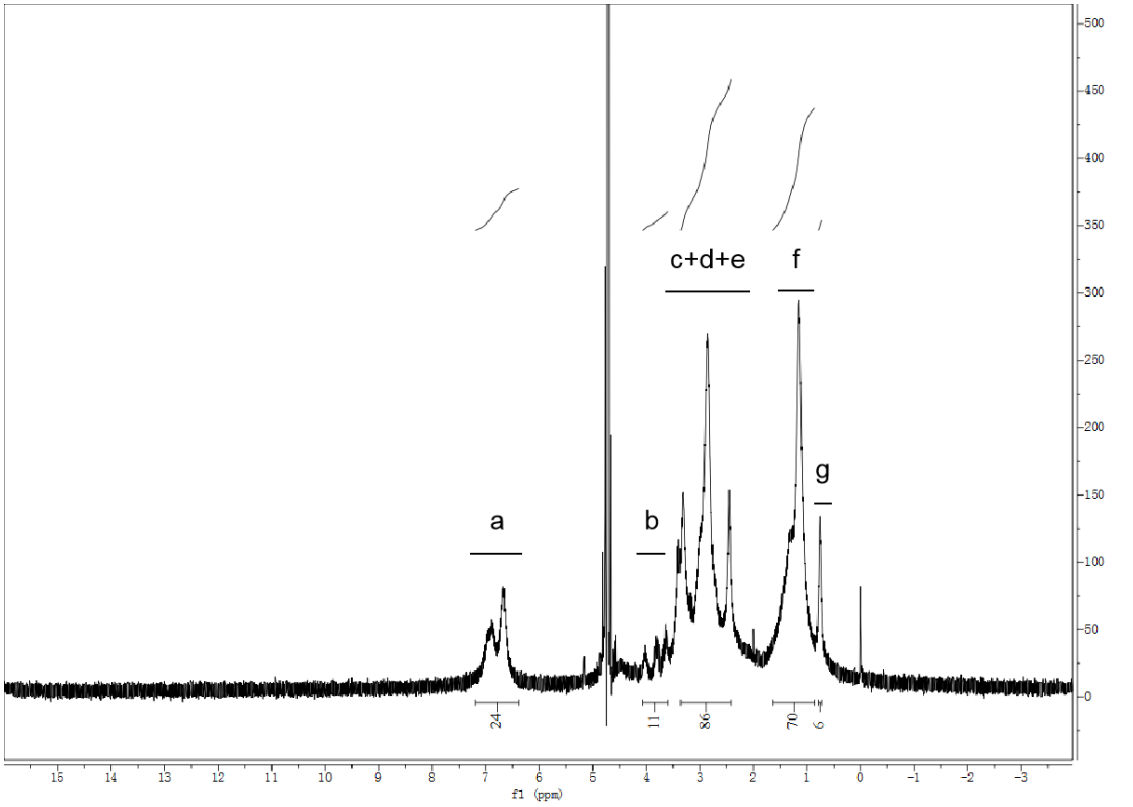

^{1}H NMR (400 MHz, D_2O) δ (ppm) = 7.20 - 6.38 (m, 24H, -C**H**- tyrosine), 4.12 - 3.57 (m, 11H, α**H** amino acids), 3.38 - 2.33 (m, 86H, -C**H₂**- Tp, ε**H** lysine, ε**H** tyrosine, ε**H** cysteine, -CO-C**H₂**-C**H₂**-CO-Stp, -CO-C**H₂**-hydroxystearic acid, =C**H**-OH-hydroxystearic acid), 1.64 - 0.86 (m, 70H, βγδ**H** lysine, βγδ**H** azidolysine, -C**H₂**-hydroxystearic acid), 0.81 - 0.66 (s, 6H, -C**H₃** hydroxystearic acid).

6 References

1. Mojica, F.J., Díez-Villaseñor, C., García-Martínez, J. and Soria, E., 2005. Intervening sequences of regularly spaced prokaryotic repeats derive from foreign genetic elements. *Journal of Molecular Evolution*, *60* (2), pp.174-182.
2. Jinek, M., Chylinski, K., Fonfara, I., Hauer, M., Doudna, J.A. and Charpentier, E., 2012. A programmable dual-RNA-guided DNA endonuclease in adaptive bacterial immunity. *Science*, *337* (6096), pp.816-821.
3. Charpentier, E. and Doudna, J.A., 2013. Rewriting a genome. *Nature*, *495* (7439), pp.50-51.
4. Sander, J.D. and Joung, J.K., 2014. CRISPR-Cas systems for editing, regulating and targeting genomes. *Nature Biotechnology*, *32* (4), pp.347-355.
5. Gaj, T., Gersbach, C.A. and Barbas III, C.F., 2013. ZFN, TALEN, and CRISPR/Cas-based methods for genome engineering. *Trends in Biotechnology*, *31* (7), pp.397-405.
6. Cong, L., Ran, F.A., Cox, D., Lin, S., Barretto, R., Habib, N., Hsu, P.D., Wu, X., Jiang, W., Marraffini, L.A. and Zhang, F., 2013. Multiplex genome engineering using CRISPR/Cas systems. *Science*, *339* (6121), pp.819-823.
7. Miller, J.B., Zhang, S., Kos, P., Xiong, H., Zhou, K., Perelman, S.S., Zhu, H. and Siegwart, D.J., 2017. Non‐viral CRISPR/Cas gene editing in vitro and in vivo enabled by synthetic nanoparticle co‐delivery of Cas9 mRNA and sgRNA. *Angewandte Chemie International Edition*, *129* (4), pp.1079-1083.
8. Kwon, H., Kim, M., Seo, Y., Moon, Y.S., Lee, H.J., Lee, K. and Lee, H., 2018. Emergence of synthetic mRNA: In vitro synthesis of mRNA and its applications in regenerative medicine. *Biomaterials*, *156*, pp.172-193.
9. Furuichi, Y., 2015. Discovery of m7G-cap in eukaryotic mRNAs. *Proceedings of the Japan Academy, Series B*, *91* (8), pp.394-409.
10. Roers, A., Hiller, B. and Hornung, V., 2016. Recognition of endogenous nucleic acids by the innate immune system. *Immunity*, *44* (4), pp.739-754.
11. Goss, D.J. and Kleiman, F.E., 2013. Poly (A) binding proteins: are they all created equal?. *Wiley Interdisciplinary Reviews: RNA*, *4* (2), pp.167-179.
12. Wadhwa, A., Aljabbari, A., Lokras, A., Foged, C. and Thakur, A., 2020. Opportunities and challenges in the delivery of mRNA-based vaccines. *Pharmaceutics*, *12* (2), p.102.
13. Kawaguchi, D., Kodama, A., Abe, N., Takebuchi, K., Hashiya, F., Tomoike, F., Nakamoto, K., Kimura, Y., Shimizu, Y. and Abe, H., 2020. Phosphorothioate modification of mRNA accelerates the rate of translation initiation to provide more efficient protein synthesis. *Angewandte Chemie International Edition*, *59* (40), pp.17403-17407.
14. Sahin, U., Karikó, K. and Türeci, Ö., 2014. mRNA-based therapeutics-developing a new class of drugs. *Nature Reviews Drug Discovery*, *13* (10), pp.759-780.
15. Devoldere, J., Dewitte, H., De Smedt, S.C. and Remaut, K., 2016. Evading innate immunity in nonviral mRNA delivery: don't shoot the messenger. *Drug Discovery Today*, *21* (1), pp.11-25.
16. Karikó, K., Muramatsu, H., Welsh, F.A., Ludwig, J., Kato, H., Akira, S. and Weissman, D., 2008. Incorporation of pseudouridine into mRNA yields superior nonimmunogenic vector with increased translational capacity and biological stability. *Molecular Therapy*, *16* (11), pp.1833-1840.

17. Vaidyanathan, S., Salahudeen, A.A., Sellers, Z.M., Bravo, D.T., Choi, S.S., Batish, A., Le, W., Baik, R., Kaushik, M.P., Galper, N. and Lee, C.M., 2020. High-efficiency, selection-free gene repair in airway stem cells from cystic fibrosis patients rescues CFTR function in differentiated epithelia. *Cell Stem Cell*, *26* (2), pp.161-171.
18. Warren, L., Manos, P.D., Ahfeldt, T., Loh, Y.H., Li, H., Lau, F., Ebina, W., Mandal, P.K., Smith, Z.D., Meissner, A. and Daley, G.Q., 2010. Highly efficient reprogramming to pluripotency and directed differentiation of human cells with synthetic modified mRNA. *Cell Stem Cell*, *7* (5), pp.618-630.
19. Thess, A., Grund, S., Mui, B.L., Hope, M.J., Baumhof, P., Fotin-Mleczek, M. and Schlake, T., 2015. Sequence-engineered mRNA without chemical nucleoside modifications enables an effective protein therapy in large animals. *Molecular Therapy*, *23* (9), pp.1456-1464.
20. Giuliani, E., Piovan, C., Bossi, S., Corna, S., Scavullo, C., Pema, M., Di Tomaso, T., Genovese, P., Lombardo, A., Naldini, L. and Bordignon, C., 2016. 130. Purification of large scale mRNA encoding ZFN nucleases by dHPLC technology. *Molecular Therapy*, *24*, pp.S53-S54.
21. Scaringe, S.A., 2001. RNA oligonucleotide synthesis via 5′-silyl-2′-orthoester chemistry. *Methods*, *23* (3), pp.206-217.
22. Dellinger, D.J., Timár, Z., Myerson, J., Sierzchala, A.B., Turner, J., Ferreira, F., Kupihár, Z., Dellinger, G., Hill, K.W., Powell, J.A. and Sampson, J.R., 2011. Streamlined process for the chemical synthesis of RNA using 2′-O-thionocarbamate-protected nucleoside phosphoramidites in the solid phase. *Journal of the American Chemical Society*, *133* (30), pp.11540-11556.
23. Pardi, N., Hogan, M.J., Porter, F.W. and Weissman, D., 2018. mRNA vaccines-a new era in vaccinology. *Nature Reviews Drug Discovery*, *17* (4), pp.261-279.
24. Chen, Q., Zhang, Y. and Yin, H., 2021. Recent advances in chemical modifications of guide RNA, mRNA and donor template for CRISPR-mediated genome editing. *Advanced Drug Delivery Reviews*, *168*, pp.246-258.
25. Liu, Y., Holmstrom, E., Zhang, J., Yu, P., Wang, J., Dyba, M.A., Chen, D., Ying, J., Lockett, S., Nesbitt, D.J. and Ferré-D'Amaré, A.R., 2015. Synthesis and applications of RNAs with position-selective labelling and mosaic composition. *Nature*, *522* (7556), pp.368-372.
26. Kim, S., Koo, T., Jee, H.G., Cho, H.Y., Lee, G., Lim, D.G., Shin, H.S. and Kim, J.S., 2018. CRISPR RNAs trigger innate immune responses in human cells. *Genome Research*, *28* (3), pp.367-373.
27. Mu, W., Tang, N., Cheng, C., Sun, W., Wei, X. and Wang, H., 2019. In vitro transcribed sgRNA causes cell death by inducing interferon release. *Protein & Cell*, *10* (6), pp.461-465.
28. Wienert, B., Shin, J., Zelin, E., Pestal, K. and Corn, J.E., 2018. In vitro-transcribed guide RNAs trigger an innate immune response via the RIG-I pathway. *PLoS Biology*, *16* (7), p.e2005840.
29. Allen, D., Rosenberg, M. and Hendel, A., 2021. Using synthetically engineered guide RNAs to enhance CRISPR genome editing systems in mammalian cells. *Frontiers in Genome Editing*, *2*, p.617910.
30. Abdur Rahman, S.M., Seki, S., Obika, S., Yoshikawa, H., Miyashita, K. and Imanishi, T., 2008. Design, synthesis, and properties of 2', 4'-BNANC: a bridged nucleic acid analogue. *Journal of the American Chemical Society*, *130* (14), pp.4886-4896.
31. Basila, M., Kelley, M.L. and Smith, A.V.B., 2017. Minimal 2'-O-methyl phosphorothioate linkage modification pattern of synthetic guide RNAs for increased

stability and efficient CRISPR-Cas9 gene editing avoiding cellular toxicity. *PLoS One*, *12* (11), p.e0188593.
32. Finn, J.D., Smith, A.R., Patel, M.C., Shaw, L., Youniss, M.R., van Heteren, J., Dirstine, T., Ciullo, C., Lescarbeau, R., Seitzer, J. and Shah, R.R., 2018. A single administration of CRISPR/Cas9 lipid nanoparticles achieves robust and persistent in vivo genome editing. *Cell Reports*, *22* (9), pp.2227-2235.
33. Manning, K.S., Rao, A.N., Castro, M. and Cooper, T.A., 2017. BNANC Gapmers Revert Splicing and Reduce RNA Foci with Low Toxicity in Myotonic Dystrophy Cells. *ACS Chemical Biology*, *12* (10), pp.2503-2509.
34. Mir, A., Alterman, J.F., Hassler, M.R., Debacker, A.J., Hudgens, E., Echeverria, D., Brodsky, M.H., Khvorova, A., Watts, J.K. and Sontheimer, E.J., 2018. Heavily and fully modified RNAs guide efficient SpyCas9-mediated genome editing. *Nature Communications*, *9* (1), pp.1-9.
35. Rahdar, M., McMahon, M.A., Prakash, T.P., Swayze, E.E., Bennett, C.F. and Cleveland, D.W., 2015. Synthetic CRISPR RNA-Cas9–guided genome editing in human cells. *Proceedings of the National Academy of Sciences*, *112* (51), pp.E7110-E7117.
36. Ryan, D.E., Taussig, D., Steinfeld, I., Phadnis, S.M., Lunstad, B.D., Singh, M., Vuong, X., Okochi, K.D., McCaffrey, R., Olesiak, M. and Roy, S., 2018. Improving CRISPR–Cas specificity with chemical modifications in single-guide RNAs. *Nucleic Acids Research*, *46* (2), pp.792-803.
37. Yin, H., Song, C.Q., Suresh, S., Wu, Q., Walsh, S., Rhym, L.H., Mintzer, E., Bolukbasi, M.F., Zhu, L.J., Kauffman, K. and Mou, H., 2017. Structure-guided chemical modification of guide RNA enables potent non-viral in vivo genome editing. *Nature Biotechnology*, *35* (12), pp.1179-1187.
38. Ribeiro, L.F., Ribeiro, L.F., Barreto, M.Q. and Ward, R.J., 2018. Protein engineering strategies to expand CRISPR-Cas9 applications. *International Journal of Genomics*, *2018*.
39. Jiang, F. and Doudna, J.A., 2017. CRISPR-Cas9 structures and mechanisms. *Annu Rev Biophys*, *46* (1), pp.505-529.
40. Sun, B., Chen, H. and Gao, X., 2021. Versatile modification of the CRISPR/Cas9 ribonucleoprotein system to facilitate in vivo application. *Journal of Controlled Release*, *337*, pp.698-717.
41. Doudna, J.A. and Charpentier, E., 2014. The new frontier of genome engineering with CRISPR-Cas9. *Science*, *346* (6213), p.1258096.
42. Jinek, M., Jiang, F., Taylor, D.W., Sternberg, S.H., Kaya, E., Ma, E., Anders, C., Hauer, M., Zhou, K., Lin, S. and Kaplan, M., 2014. Structures of Cas9 endonucleases reveal RNA-mediated conformational activation. *Science*, *343* (6176), p.1247997.
43. Zuris, J.A., Thompson, D.B., Shu, Y., Guilinger, J.P., Bessen, J.L., Hu, J.H., Maeder, M.L., Joung, J.K., Chen, Z.Y. and Liu, D.R., 2015. Cationic lipid-mediated delivery of proteins enables efficient protein-based genome editing in vitro and in vivo. *Nature Biotechnology*, *33* (1), pp.73-80.
44. Troiber, C., Edinger, D., Kos, P., Schreiner, L., Kläger, R., Herrmann, A. and Wagner, E., 2013. Stabilizing effect of tyrosine trimers on pDNA and siRNA polyplexes. *Biomaterials*, *34* (5), pp.1624-1633.
45. Kuhn, J., Lin, Y., Krhac Levacic, A., Al Danaf, N., Peng, L., Höhn, M., Lamb, D.C., Wagner, E. and Lächelt, U., 2020. Delivery of Cas9/sgRNA ribonucleoprotein complexes via hydroxystearyl oligoamino amides. *Bioconjugate Chemistry*, *31* (3), pp.729-742.

46. Lodish, H., Berk, A., Zipursky, S.L., Matsudaira, P., Baltimore, D. and Darnell, J., 2000. Structure of nucleic acids. In *Molecular Cell Biology. 4th edition*. WH Freeman.
47. Groll, A.V., Levin, Y., Barbosa, M.C. and Ravazzolo, A.P., 2006. Linear DNA low efficiency transfection by liposome can be improved by the use of cationic lipid as charge neutralizer. *Biotechnology Progress*, *22* (4), pp.1220-1224.
48. McLenachan, S., Sarsero, J.P. and Ioannou, P.A., 2007. Flow-cytometric analysis of mouse embryonic stem cell lipofection using small and large DNA constructs. *Genomics*, *89* (6), pp.708-720.
49. Boo, S.H. and Kim, Y.K., 2020. The emerging role of RNA modifications in the regulation of mRNA stability. *Experimental & Molecular Medicine*, *52* (3), pp.400-408.
50. Wei, T., Cheng, Q., Min, Y.L., Olson, E.N. and Siegwart, D.J., 2020. Systemic nanoparticle delivery of CRISPR-Cas9 ribonucleoproteins for effective tissue specific genome editing. *Nature Communications*, *11* (1), pp.1-12.
51. Kouranova, E., Forbes, K., Zhao, G., Warren, J., Bartels, A., Wu, Y. and Cui, X., 2016. CRISPRs for optimal targeting: delivery of CRISPR components as DNA, RNA, and protein into cultured cells and single-cell embryos. *Human Gene Therapy*, *27* (6), pp.464-475.
52. Josipović, G., Zoldoš, V. and Vojta, A., 2019. Active fusions of Cas9 orthologs. *Journal of Biotechnology*, *301*, pp.18-23.
53. Kim, S., Kim, D., Cho, S.W., Kim, J. and Kim, J.S., 2014. Highly efficient RNA-guided genome editing in human cells via delivery of purified Cas9 ribonucleoproteins. *Genome Research*, *24* (6), pp.1012-1019.
54. Xu, C.F., Chen, G.J., Luo, Y.L., Zhang, Y., Zhao, G., Lu, Z.D., Czarna, A., Gu, Z. and Wang, J., 2021. Rational designs of in vivo CRISPR-Cas delivery systems. *Advanced Drug Delivery Reviews*, *168*, pp.3-29.
55. Liang, X., Potter, J., Kumar, S., Zou, Y., Quintanilla, R., Sridharan, M., Carte, J., Chen, W., Roark, N., Ranganathan, S. and Ravinder, N., 2015. Rapid and highly efficient mammalian cell engineering via Cas9 protein transfection. *Journal of Biotechnology*, *208*, pp.44-53.
56. Tu, Z., Yang, W., Yan, S., Yin, A., Gao, J., Liu, X., Zheng, Y., Zheng, J., Li, Z., Yang, S. and Li, S., 2017. Promoting Cas9 degradation reduces mosaic mutations in non-human primate embryos. *Scientific Reports*, *7* (1), pp.1-11.
57. Yang, S., Li, S. and Li, X.J., 2018. Shortening the half-life of Cas9 maintains its gene editing ability and reduces neuronal toxicity. *Cell Reports*, *25* (10), pp.2653-2659.
58. Aschenbrenner, S., Kallenberger, S.M., Hoffmann, M.D., Huck, A., Eils, R. and Niopek, D., 2020. Coupling Cas9 to artificial inhibitory domains enhances CRISPR-Cas9 target specificity. *Science Advances*, *6* (6), p.eaay0187.
59. Zetsche, B., Volz, S.E. and Zhang, F., 2015. A split-Cas9 architecture for inducible genome editing and transcription modulation. *Nature Biotechnology*, *33* (2), pp.139-142.
60. Davis, K.M., Pattanayak, V., Thompson, D.B., Zuris, J.A. and Liu, D.R., 2015. Small molecule–triggered Cas9 protein with improved genome-editing specificity. *Nature Chemical Biology*, *11* (5), pp.316-318.
61. Nihongaki, Y., Kawano, F., Nakajima, T. and Sato, M., 2015. Photoactivatable CRISPR-Cas9 for optogenetic genome editing. *Nature Biotechnology*, *33* (7), pp.755-760.
62. Guilinger, J.P., Thompson, D.B. and Liu, D.R., 2014. Fusion of catalytically inactive Cas9 to FokI nuclease improves the specificity of genome modification. *Nature Biotechnology*, *32* (6), pp.577-582.

63. Kleinstiver, B.P., Pattanayak, V., Prew, M.S., Tsai, S.Q., Nguyen, N.T., Zheng, Z. and Joung, J.K., 2016. High-fidelity CRISPR-Cas9 nucleases with no detectable genome-wide off-target effects. *Nature*, *529* (7587), pp.490-495.
64. Slaymaker, I.M., Gao, L., Zetsche, B., Scott, D.A., Yan, W.X. and Zhang, F., 2016. Rationally engineered Cas9 nucleases with improved specificity. *Science*, *351* (6268), pp.84-88.
65. Chen, J.S., Dagdas, Y.S., Kleinstiver, B.P., Welch, M.M., Sousa, A.A., Harrington, L.B., Sternberg, S.H., Joung, J.K., Yildiz, A. and Doudna, J.A., 2017. Enhanced proofreading governs CRISPR-Cas9 targeting accuracy. *Nature*, *550* (7676), pp.407-410.
66. Casini, A., Olivieri, M., Petris, G., Montagna, C., Reginato, G., Maule, G., Lorenzin, F., Prandi, D., Romanel, A., Demichelis, F. and Inga, A., 2018. A highly specific SpCas9 variant is identified by in vivo screening in yeast. *Nature Biotechnology*, *36* (3), pp.265-271.
67. Lee, J.K., Jeong, E., Lee, J., Jung, M., Shin, E., Kim, Y.H., Lee, K., Jung, I., Kim, D., Kim, S. and Kim, J.S., 2018. Directed evolution of CRISPR-Cas9 to increase its specificity. *Nature Communications*, *9* (1), pp.1-10.
68. Hu, J.H., Miller, S.M., Geurts, M.H., Tang, W., Chen, L., Sun, N., Zeina, C.M., Gao, X., Rees, H.A., Lin, Z. and Liu, D.R., 2018. Evolved Cas9 variants with broad PAM compatibility and high DNA specificity. *Nature*, *556* (7699), pp.57-63.
69. Ran, F.A., Hsu, P.D., Lin, C.Y., Gootenberg, J.S., Konermann, S., Trevino, A.E., Scott, D.A., Inoue, A., Matoba, S., Zhang, Y. and Zhang, F., 2013. Double nicking by RNA-guided CRISPR Cas9 for enhanced genome editing specificity. *Cell*, *154* (6), pp.1380-1389.
70. Charlesworth, C.T., Deshpande, P.S., Dever, D.P., Camarena, J., Lemgart, V.T., Cromer, M.K., Vakulskas, C.A., Collingwood, M.A., Zhang, L., Bode, N.M. and Behlke, M.A., 2019. Identification of preexisting adaptive immunity to Cas9 proteins in humans. *Nature Medicine*, *25* (2), pp.249-254.
71. Hemmi, H., Takeuchi, O., Kawai, T., Kaisho, T., Sato, S., Sanjo, H., Matsumoto, M., Hoshino, K., Wagner, H., Takeda, K. and Akira, S., 2000. A Toll-like receptor recognizes bacterial DNA. *Nature*, *408* (6813), pp.740-745.
72. Vaidyanathan, S., Azizian, K.T., Haque, A.A., Henderson, J.M., Hendel, A., Shore, S., Antony, J.S., Hogrefe, R.I., Kormann, M.S., Porteus, M.H. and McCaffrey, A.P., 2018. Uridine depletion and chemical modification increase Cas9 mRNA activity and reduce immunogenicity without HPLC purification. *Molecular Therapy-Nucleic Acids*, *12*, pp.530-542.
73. Crudele, J.M. and Chamberlain, J.S., 2018. Cas9 immunity creates challenges for CRISPR gene editing therapies. *Nature Communications*, *9* (1), pp.1-3.
74. Simhadri, V.L., McGill, J., McMahon, S., Wang, J., Jiang, H. and Sauna, Z.E., 2018. Prevalence of pre-existing antibodies to CRISPR-associated nuclease Cas9 in the USA population. *Molecular Therapy-Methods & Clinical Development*, *10*, pp.105-112.
75. Behr, M., Zhou, J., Xu, B. and Zhang, H., 2021. In vivo delivery of CRISPR-Cas9 therapeutics: Progress and challenges. *Acta Pharmaceutica Sinica B*, *11* (8), pp.2150-2171.
76. Coelho, T., Adams, D., Silva, A., Lozeron, P., Hawkins, P.N., Mant, T., Perez, J., Chiesa, J., Warrington, S., Tranter, E. and Munisamy, M., 2013. Safety and efficacy of RNAi therapy for transthyretin amyloidosis. *New England Journal of Medicine*, *369* (9), pp.819-829.

77. Igyártó, B.Z., Jacobsen, S. and Ndeupen, S., 2021. Future considerations for the mRNA-lipid nanoparticle vaccine platform. *Current Opinion in Virology*, *48*, pp.65-72.
78. Chen, Z., Liu, F., Chen, Y., Liu, J., Wang, X., Chen, A.T., Deng, G., Zhang, H., Liu, J., Hong, Z. and Zhou, J., 2017. Targeted delivery of CRISPR/Cas9-mediated cancer gene therapy via liposome-templated hydrogel nanoparticles. *Advanced Functional Materials*, *27* (46), p.1703036.
79. Wan, T., Chen, Y., Pan, Q., Xu, X., Kang, Y., Gao, X., Huang, F., Wu, C. and Ping, Y., 2020. Genome editing of mutant KRAS through supramolecular polymer-mediated delivery of Cas9 ribonucleoprotein for colorectal cancer therapy. *Journal of Controlled Release*, *322*, pp.236-247.
80. Wan, T., Pan, Q. and Ping, Y., 2021. Microneedle-assisted genome editing: A transdermal strategy of targeting NLRP3 by CRISPR-Cas9 for synergistic therapy of inflammatory skin disorders. *Science Advances*, *7* (11), p.eabe2888.
81. Ban, Q., Yang, P., Chou, S.J., Qiao, L., Xia, H., Xue, J., Wang, F., Xu, X., Sun, N., Zhang, R.Y. and Zhang, C., 2021. Supramolecular Nanosubstrate-Mediated Delivery for CRISPR/Cas9 Gene Disruption and Deletion. *Small*, *17* (28), p.2100546.
82. Liu, Q., Cai, J., Zheng, Y., Tan, Y., Wang, Y., Zhang, Z., Zheng, C., Zhao, Y., Liu, C., An, Y. and Jiang, C., 2019. NanoRNP overcomes tumor heterogeneity in cancer treatment. *Nano Letters*, *19* (11), pp.7662-7672.
83. Deng, S., Li, X., Liu, S., Chen, J., Li, M., Chew, S.Y., Leong, K.W. and Cheng, D., 2020. Codelivery of CRISPR-Cas9 and chlorin e6 for spatially controlled tumor-specific gene editing with synergistic drug effects. *Science Advances*, *6* (29), p.eabb4005.
84. Rui, Y., Wilson, D.R., Choi, J., Varanasi, M., Sanders, K., Karlsson, J., Lim, M. and Green, J.J., 2019. Carboxylated branched poly (β-amino ester) nanoparticles enable robust cytosolic protein delivery and CRISPR-Cas9 gene editing. *Science Advances*, *5*(12), p.eaay3255.
85. Chen, G., Abdeen, A.A., Wang, Y., Shahi, P.K., Robertson, S., Xie, R., Suzuki, M., Pattnaik, B.R., Saha, K. and Gong, S., 2019. A biodegradable nanocapsule delivers a Cas9 ribonucleoprotein complex for in vivo genome editing. *Nature Nanotechnology*, *14* (10), pp.974-980.
86. Liu, C., Wan, T., Wang, H., Zhang, S., Ping, Y. and Cheng, Y., 2019. A boronic acid–rich dendrimer with robust and unprecedented efficiency for cytosolic protein delivery and CRISPR-Cas9 gene editing. *Science Advances*, *5* (6), p.eaaw8922.
87. Kumar, R., Le, N., Tan, Z., Brown, M.E., Jiang, S. and Reineke, T.M., 2020. Efficient polymer-mediated delivery of gene-editing ribonucleoprotein payloads through combinatorial design, parallelized experimentation, and machine learning. *ACS Nano*, *14* (12), pp.17626-17639.
88. Ho, T.C., Kim, H.S., Chen, Y., Li, Y., LaMere, M.W., Chen, C., Wang, H., Gong, J., Palumbo, C.D., Ashton, J.M. and Kim, H.W., 2021. Scaffold-mediated CRISPR-Cas9 delivery system for acute myeloid leukemia therapy. *Science Advances*, *7* (21), p.eabg3217.
89. Aksoy, Y.A., Yang, B., Chen, W., Hung, T., Kuchel, R.P., Zammit, N.W., Grey, S.T., Goldys, E.M. and Deng, W., 2020. Spatial and Temporal control of CRISPR-Cas9-mediated gene editing delivered via a light-triggered liposome system. *ACS Applied Naterials & Interfaces*, *12* (47), pp.52433-52444.
90. Ryu, J.Y., Won, E.J., Lee, H.A.R., Kim, J.H., Hui, E., Kim, H.P. and Yoon, T.J., 2020. Ultrasound-activated particles as CRISPR/Cas9 delivery system for androgenic alopecia therapy. *Biomaterials*, *232*, p.119736.

91. Lee, K., Conboy, M., Park, H.M., Jiang, F., Kim, H.J., Dewitt, M.A., Mackley, V.A., Chang, K., Rao, A., Skinner, C. and Shobha, T., Nanoparticle delivery of Cas9 ribonucleoprotein and donor DNA in vivo induces homology-directed DNA repair. Nature Biomedical Engineering. 2017; 1: 889–901.
92. Shahbazi, R., Sghia-Hughes, G., Reid, J.L., Kubek, S., Haworth, K.G., Humbert, O., Kiem, H.P. and Adair, J.E., 2019. Targeted homology-directed repair in blood stem and progenitor cells with CRISPR nanoformulations. *Nature Materials*, *18* (10), pp.1124-1132.
93. Zhang, L., Wang, L., Xie, Y., Wang, P., Deng, S., Qin, A., Zhang, J., Yu, X., Zheng, W. and Jiang, X., 2019. Triple-targeting delivery of CRISPR/Cas9 to reduce the risk of cardiovascular diseases. *Angewandte Chemie International Edition*, *58* (36), pp.12404-12408.
94. Wu, J., Peng, H., Lu, X., Lai, M., Zhang, H. and Le, X.C., 2021. Binding-mediated formation of ribonucleoprotein corona for efficient delivery and control of CRISPR/Cas9. *Angewandte Chemie International Edition*, *60* (20), pp.11104-11109.
95. Mout, R., Ray, M., Tay, T., Sasaki, K., Yesilbag Tonga, G. and Rotello, V.M., 2017. General strategy for direct cytosolic protein delivery via protein–nanoparticle co-engineering. *ACS Nano*, *11* (6), pp.6416-6421.
96. Lee, Y.W., Mout, R., Luther, D.C., Liu, Y., Castellanos-García, L., Burnside, A.S., Ray, M., Tonga, G.Y., Hardie, J., Nagaraj, H. and Das, R., 2019. In Vivo Editing of Macrophages through Systemic Delivery of CRISPR-Cas9-Ribonucleoprotein-Nanoparticle Nanoassemblies. *Advanced Therapeutics*, *2* (10), p.1900041.
97. Li, X., Pan, Y., Chen, C., Gao, Y., Liu, X., Yang, K., Luan, X., Zhou, D., Zeng, F., Han, X. and Song, Y., 2021. Hypoxia‐responsive gene editing to reduce tumor thermal tolerance for mild-photothermal therapy. *Angewandte Chemie International Edition*, *133* (39), pp.21370-21374.
98. Hansen-Bruhn, M., de Ávila, B.E.F., Beltrán-Gastélum, M., Zhao, J., Ramírez-Herrera, D.E., Angsantikul, P., Vesterager Gothelf, K., Zhang, L. and Wang, J., 2018. Active intracellular delivery of a Cas9/sgRNA complex using ultrasound-propelled nanomotors. *Angewandte Chemie International Edition*, *57* (10), pp.2657-2661.
99. Alsaiari, S.K., Patil, S., Alyami, M., Alamoudi, K.O., Aleisa, F.A., Merzaban, J.S., Li, M. and Khashab, N.M., 2018. Endosomal escape and delivery of CRISPR/Cas9 genome editing machinery enabled by nanoscale zeolitic imidazolate framework. *Journal of the American Chemical Society*, *140* (1), pp.143-146.
100. Alyami, M.Z., Alsaiari, S.K., Li, Y., Qutub, S.S., Aleisa, F.A., Sougrat, R., Merzaban, J.S. and Khashab, N.M., 2020. Cell-type-specific CRISPR/Cas9 delivery by biomimetic metal organic frameworks. *Journal of the American Chemical Society*, *142* (4), pp.1715-1720.
101. Yang, X., Tang, Q., Jiang, Y., Zhang, M., Wang, M. and Mao, L., 2019. Nanoscale ATP-responsive zeolitic imidazole framework-90 as a general platform for cytosolic protein delivery and genome editing. *Journal of the American Chemical Society*, *141* (9), pp.3782-3786.
102. Liu, J., Luo, T., Xue, Y., Mao, L., Stang, P.J. and Wang, M., 2021. Hierarchical Self-assembly of Discrete Metal–Organic Cages into Supramolecular Nanoparticles for Intracellular Protein Delivery. *Angewandte Chemie International Edition*, *133* (10), pp.5489-5495.
103. Liu, B., Ejaz, W., Gong, S., Kurbanov, M., Canakci, M., Anson, F. and Thayumanavan, S., 2020. Engineered interactions with mesoporous silica facilitate intracellular delivery of proteins and gene editing. *Nano Letters*, *20* (5), pp.4014-4021.
104. Pan, Y., Yang, J., Luan, X., Liu, X., Li, X., Yang, J., Huang, T., Sun, L., Wang, Y., Lin, Y. and Song, Y., 2019. Near-infrared upconversion–activated CRISPR-Cas9

system: A remote-controlled gene editing platform. *Science Advances*, *5* (4), p.eaav7199.
105. Chen, C., Ma, Y., Du, S., Wu, Y., Shen, P., Yan, T., Li, X., Song, Y., Zha, Z. and Han, X., 2021. Controlled CRISPR-Cas9 Ribonucleoprotein Delivery for Sensitized Photothermal Therapy. *Small*, *17* (33), p.2101155.
106. Yue, H., Zhou, X., Cheng, M. and Xing, D., 2018. Graphene oxide-mediated Cas9/sgRNA delivery for efficient genome editing. *Nanoscale*, *10* (3), pp.1063-1071.
107. Zhou, W., Cui, H., Ying, L. and Yu, X.F., 2018. Enhanced cytosolic delivery and release of CRISPR/Cas9 by black phosphorus nanosheets for genome editing. *Angewandte Chemie International Edition*, *130* (32), pp.10425-10429.
108. Ramakrishna, S., Dad, A.B.K., Beloor, J., Gopalappa, R., Lee, S.K. and Kim, H., 2014. Gene disruption by cell-penetrating peptide-mediated delivery of Cas9 protein and guide RNA. *Genome Research*, *24* (6), pp.1020-1027.
109. Yin, J., Wang, Q., Hou, S., Bao, L., Yao, W. and Gao, X., 2018. Potent protein delivery into mammalian cells via a supercharged polypeptide. *Journal of the American Chemical Society*, *140* (49), pp.17234-17240.
110. Yin, J., Hou, S., Wang, Q., Bao, L., Liu, D., Yue, Y., Yao, W. and Gao, X., 2019. Microenvironment-responsive delivery of the Cas9 RNA-guided endonuclease for efficient genome editing. *Bioconjugate Chemistry*, *30* (3), pp.898-906.
111. Kim, S.M., Shin, S.C., Kim, E.E., Kim, S.H., Park, K., Oh, S.J. and Jang, M., 2018. Simple in vivo gene editing via direct self-assembly of Cas9 ribonucleoprotein complexes for cancer treatment. *ACS Nano*, *12* (8), pp.7750-7760.
112. Park, H., Oh, J., Shim, G., Cho, B., Chang, Y., Kim, S., Baek, S., Kim, H., Shin, J., Choi, H. and Yoo, J., 2019. In vivo neuronal gene editing via CRISPR–Cas9 amphiphilic nanocomplexes alleviates deficits in mouse models of Alzheimer's disease. *Nature Neuroscience*, *22* (4), pp.524-528.
113. Krishnamurthy, S., Wohlford-Lenane, C., Kandimalla, S., Sartre, G., Meyerholz, D.K., Théberge, V., Hallée, S., Duperré, A.M., Del'Guidice, T., Lepetit-Stoffaes, J.P. and Barbeau, X., 2019. Engineered amphiphilic peptides enable delivery of proteins and CRISPR-associated nucleases to airway epithelia. *Nature Communications*, *10* (1), pp.1-12.
114. Thach, T.T., Bae, D.H., Kim, N.H., Kang, E.S., Lee, B.S., Han, K., Kwak, M., Choi, H., Nam, J., Bae, T. and Suh, M., 2019. Lipopeptide-Based Nanosome-Mediated Delivery of Hyperaccurate CRISPR/Cas9 Ribonucleoprotein for Gene Editing. *Small*, *15* (46), p.1903172.
115. Jain, P.K., Lo, J.H., Rananaware, S., Downing, M., Panda, A., Tai, M., Raghavan, S., Fleming, H.E. and Bhatia, S.N., 2019. Non-viral delivery of CRISPR/Cas9 complex using CRISPR-GPS nanocomplexes. *Nanoscale*, *11* (44), pp.21317-21323.
116. Lostalé-Seijo, I., Louzao, I., Juanes, M. and Montenegro, J., 2017. Peptide/Cas9 nanostructures for ribonucleoprotein cell membrane transport and gene edition. *Chemical Science*, *8* (12), pp.7923-7931.
117. Montagna, C., Petris, G., Casini, A., Maule, G., Franceschini, G.M., Zanella, I., Conti, L., Arnoldi, F., Burrone, O.R., Zentilin, L. and Zacchigna, S., 2018. VSV-G-enveloped vesicles for traceless delivery of CRISPR-Cas9. *Molecular Therapy-Nucleic Acids*, *12*, pp.453-462.
118. Campbell, L.A., Coke, L.M., Richie, C.T., Fortuno, L.V., Park, A.Y. and Harvey, B.K., 2019. Gesicle-mediated delivery of CRISPR/Cas9 ribonucleoprotein complex for inactivating the HIV provirus. *Molecular Therapy*, *27* (1), pp.151-163.
119. Gee, P., Lung, M.S., Okuzaki, Y., Sasakawa, N., Iguchi, T., Makita, Y., Hozumi, H., Miura, Y., Yang, L.F., Iwasaki, M. and Wang, X.H., 2020. Extracellular

nanovesicles for packaging of CRISPR-Cas9 protein and sgRNA to induce therapeutic exon skipping. *Nature Communications*, *11* (1), pp.1-18.
120. Yao, X., Lyu, P., Yoo, K., Yadav, M.K., Singh, R., Atala, A. and Lu, B., 2021. Engineered extracellular vesicles as versatile ribonucleoprotein delivery vehicles for efficient and safe CRISPR genome editing. *Journal of Extracellular Vesicles*, *10* (5), p.e12076.
121. Ye, Y., Zhang, X., Xie, F., Xu, B., Xie, P., Yang, T., Shi, Q., Zhang, C.Y., Zhang, Y., Chen, J. and Jiang, X., 2020. An engineered exosome for delivering sgRNA: Cas9 ribonucleoprotein complex and genome editing in recipient cells. *Biomaterials Science*, *8* (10), pp.2966-2976.
122. Zhuang, J., Tan, J., Wu, C., Zhang, J., Liu, T., Fan, C., Li, J. and Zhang, Y., 2020. Extracellular vesicles engineered with valency-controlled DNA nanostructures deliver CRISPR/Cas9 system for gene therapy. *Nucleic Acids Research*, *48* (16), pp.8870-8882.
123. Mangeot, P.E., Risson, V., Fusil, F., Marnef, A., Laurent, E., Blin, J., Mournetas, V., Massouridès, E., Sohier, T.J., Corbin, A. and Aubé, F., 2019. Genome editing in primary cells and in vivo using viral-derived Nanoblades loaded with Cas9-sgRNA ribonucleoproteins. *Nature Communications*, *10* (1), pp.1-15.
124. Hamilton, J.R., Tsuchida, C.A., Nguyen, D.N., Shy, B.R., McGarrigle, E.R., Espinoza, C.R.S., Carr, D., Blaeschke, F., Marson, A. and Doudna, J.A., 2021. Targeted delivery of CRISPR-Cas9 and transgenes enables complex immune cell engineering. *Cell Reports*, *35* (9), p.109207.
125. Sun, W., Ji, W., Hall, J.M., Hu, Q., Wang, C., Beisel, C.L. and Gu, Z., 2015. Self-assembled DNA nanoclews for the efficient delivery of CRISPR-Cas9 for genome editing. *Angewandte Chemie International Edition*, *127* (41), pp.12197-12201.
126. Ding, F., Huang, X., Gao, X., Xie, M., Pan, G., Li, Q., Song, J., Zhu, X. and Zhang, C., 2019. A non-cationic nucleic acid nanogel for the delivery of the CRISPR/Cas9 gene editing tool. *Nanoscale*, *11* (37), pp.17211-17215.
127. Liu, J., Wu, T., Lu, X., Wu, X., Liu, S., Zhao, S., Xu, X. and Ding, B., 2019. A self-assembled platform based on branched DNA for sgRNA/Cas9/antisense delivery. *Journal of the American Chemical Society*, *141* (48), pp.19032-19037.
128. Shi, J., Yang, X., Li, Y., Wang, D., Liu, W., Zhang, Z., Liu, J. and Zhang, K., 2020. MicroRNA-responsive release of Cas9/sgRNA from DNA nanoflower for cytosolic protein delivery and enhanced genome editing. *Biomaterials*, *256*, p.120221.
129. Rouet, R., Thuma, B.A., Roy, M.D., Lintner, N.G., Rubitski, D.M., Finley, J.E., Wisniewska, H.M., Mendonsa, R., Hirsh, A., de Oñate, L. and Compte Barrón, J., 2018. Receptor-mediated delivery of CRISPR-Cas9 endonuclease for cell-type-specific gene editing. *Journal of the American Chemical Society*, *140* (21), pp.6596-6603.
130. He, X., Long, Q., Zeng, Z., Yang, L., Tang, Y. and Feng, X., 2019. Simple and Efficient Targeted Intracellular Protein Delivery with Self-Assembled Nanovehicles for Effective Cancer Therapy. *Advanced Functional Materials*, *29* (50), p.1906187.
131. Qiao, J., Sun, W., Lin, S., Jin, R., Ma, L. and Liu, Y., 2019. Cytosolic delivery of CRISPR/Cas9 ribonucleoproteins for genome editing using chitosan-coated red fluorescent protein. *Chemical Communications*, *55* (32), pp.4707-4710.
132. Zhu, X., Lv, M.M., Liu, J.W., Yu, R.Q. and Jiang, J.H., 2019. DNAzyme activated protein-scaffolded CRISPR-Cas9 nanoassembly for genome editing. *Chemical Communications*, *55* (46), pp.6511-6514.

133. Pan, X., Pei, X., Huang, H., Su, N., Wu, Z., Wu, Z. and Qi, X., 2021. One-in-one individual package and delivery of CRISPR/Cas9 ribonucleoprotein using apoferritin. *Journal of Controlled Release*, *337*, pp.686-697.
134. Li, Y., Glass, Z., Huang, M., Chen, Z.Y. and Xu, Q., 2020. Ex vivo cell-based CRISPR/Cas9 genome editing for therapeutic applications. *Biomaterials*, *234*, p.119711.
135. Lu, Y., Xue, J., Deng, T., Zhou, X., Yu, K., Deng, L., Huang, M., Yi, X., Liang, M., Wang, Y. and Shen, H., 2020. Safety and feasibility of CRISPR-edited T cells in patients with refractory non-small-cell lung cancer. *Nature Medicine*, *26* (5), pp.732-740.
136. González-Romero, E., Martínez-Valiente, C., García-Ruiz, C., Vázquez-Manrique, R.P., Cervera, J. and Sanjuan-Pla, A., 2019. CRISPR to fix bad blood: a new tool in basic and clinical hematology. *haematologica*, *104* (5), p.881.
137. Mullard, A., 2019. First in vivo CRISPR candidate enters the clinic. *Nature Reviews Drug Discovery*, *18* (9), pp.656-657.
138. Gillmore, J.D., Gane, E., Taubel, J., Kao, J., Fontana, M., Maitland, M.L., Seitzer, J., O'Connell, D., Walsh, K.R., Wood, K. and Phillips, J., 2021. CRISPR-Cas9 in vivo gene editing for transthyretin amyloidosis. *New England Journal of Medicine*, *385* (6), pp.493-502.
139. Wei, S.C., Duffy, C.R. and Allison, J.P., 2018. Fundamental Mechanisms of Immune Checkpoint Blockade TherapyFundamental Mechanisms of Immune Checkpoint Blockade Therapy. *Cancer Discovery*, *8* (9), pp.1069-1086.
140. Darvin, P., Toor, S.M., Sasidharan Nair, V. and Elkord, E., 2018. Immune checkpoint inhibitors: recent progress and potential biomarkers. *Experimental & Molecular Medicine*, *50* (12), pp.1-11.
141. Hodi, F.S., O'day, S.J., McDermott, D.F., Weber, R.W., Sosman, J.A., Haanen, J.B., Gonzalez, R., Robert, C., Schadendorf, D., Hassel, J.C. and Akerley, W., 2010. Improved survival with ipilimumab in patients with metastatic melanoma. *New England Journal of Medicine*, *363* (8), pp.711-723.
142. El-Khoueiry, A.B., Sangro, B., Yau, T., Crocenzi, T.S., Kudo, M., Hsu, C., Kim, T.Y., Choo, S.P., Trojan, J., Welling 3rd, T.H. and Meyer, T., 2017. Nivolumab in patients with advanced hepatocellular carcinoma (CheckMate 040): an open-label, non-comparative, phase 1/2 dose escalation and expansion trial. *The Lancet*, *389* (10088), pp.2492-2502.
143. Socinski, M.A., Jotte, R.M., Cappuzzo, F., Orlandi, F., Stroyakovskiy, D., Nogami, N., Rodríguez-Abreu, D., Moro-Sibilot, D., Thomas, C.A., Barlesi, F. and Finley, G., 2018. Atezolizumab for first-line treatment of metastatic nonsquamous NSCLC. *New England Journal of Medicine*, *378* (24), pp.2288-2301.
144. Postow, M.A., Sidlow, R. and Hellmann, M.D., 2018. Immune-related adverse events associated with immune checkpoint blockade. *New England Journal of Medicine*, *378* (2), pp.158-168.
145. Han, X., Li, H., Zhou, D., Chen, Z. and Gu, Z., 2020. Local and targeted delivery of immune checkpoint blockade therapeutics. *Accounts of Chemical Research*, *53* (11), pp.2521-2533.
146. Ou, X., Ma, Q., Yin, W., Ma, X. and He, Z., 2021. CRISPR/Cas9 gene-editing in cancer immunotherapy: Promoting the present revolution in cancer therapy and exploring more. *Frontiers in Cell and Developmental Biology*, p.1179.
147. Yahata, T., Mizoguchi, M., Kimura, A., Orimo, T., Toujima, S., Kuninaka, Y., Nosaka, M., Ishida, Y., Sasaki, I., Fukuda‐Ohta, Y. and Hemmi, H., 2019. Programmed cell death ligand 1 d isruption by clustered regularly interspaced short

palindromic repeats/Cas9-genome editing promotes antitumor immunity and suppresses ovarian cancer progression. *Cancer Science*, *110* (4), pp.1279-1292.
148. Herbst, R.S., Baas, P., Kim, D.W., Felip, E., Pérez-Gracia, J.L., Han, J.Y., Molina, J., Kim, J.H., Arvis, C.D., Ahn, M.J. and Majem, M., 2016. Pembrolizumab versus docetaxel for previously treated, PD-L1-positive, advanced non-small-cell lung cancer (KEYNOTE-010): a randomised controlled trial. *The Lancet*, *387* (10027), pp.1540-1550.
149. Sharma, P. and Allison, J.P., 2015. The future of immune checkpoint therapy. *Science*, *348* (6230), pp.56-61.
150. Liu, L., You, X., Han, S., Sun, Y., Zhang, J. and Zhang, Y., 2021. CD155/TIGIT, a novel immune checkpoint in human cancers. *Oncology Reports*, *45* (3), pp.835-845.
151. Stamm, H., Oliveira-Ferrer, L., Grossjohann, E.M., Muschhammer, J., Thaden, V., Brauneck, F., Kischel, R., Müller, V., Bokemeyer, C., Fiedler, W. and Wellbrock, J., 2019. Targeting the TIGIT-PVR immune checkpoint axis as novel therapeutic option in breast cancer. *Oncoimmunology*, *8* (12), p.e1674605.
152. Zhang, C., Wang, Y., Xun, X., Wang, S., Xiang, X., Hu, S., Cheng, Q., Guo, J., Li, Z. and Zhu, J., 2020. TIGIT can exert immunosuppressive effects on CD8+ T cells by the CD155/TIGIT signaling pathway for hepatocellular carcinoma in vitro. *Journal of Immunotherapy (Hagerstown, Md.: 1997)*, *43* (8), p.236.
153. Wu, L., Mao, L., Liu, J.F., Chen, L., Yu, G.T., Yang, L.L., Wu, H., Bu, L.L., Kulkarni, A.B., Zhang, W.F. and Sun, Z.J., 2019. Blockade of TIGIT/CD155 Signaling Reverses T-cell Exhaustion and Enhances Antitumor Capability in Head and Neck Squamous Cell CarcinomaBlockade of TIGIT/CD155 Signaling in HNSCC. *Cancer Immunology Research*, *7* (10), pp.1700-1713.
154. Li, S., Ding, J., Wang, Y., Wang, X. and Lv, L., 2022. CD155/TIGIT signaling regulates the effector function of tumor-infiltrating CD8+ T cell by NF-κB pathway in colorectal cancer. *Journal of Gastroenterology and Hepatology*, *37* (1), pp.154-163.
155. Inozume, T., Yaguchi, T., Furuta, J., Harada, K., Kawakami, Y. and Shimada, S., 2016. Melanoma cells control antimelanoma CTL responses via interaction between TIGIT and CD155 in the effector phase. *Journal of Investigative Dermatology*, *136* (1), pp.255-263.
156. Kučan Brlić, P., Lenac Roviš, T., Cinamon, G., Tsukerman, P., Mandelboim, O. and Jonjić, S., 2019. Targeting PVR (CD155) and its receptors in anti-tumor therapy. *Cellular & Molecular Immunology*, *16* (1), pp.40-52.
157. Sloan, K.E., Stewart, J.K., Treloar, A.F., Matthews, R.T. and Jay, D.G., 2005. CD155/PVR enhances glioma cell dispersal by regulating adhesion signaling and focal adhesion dynamics. *Cancer Research*, *65* (23), pp.10930-10937.
158. Tane, S., Maniwa, Y., Hokka, D., Tauchi, S., Nishio, W., Okita, Y. and Yoshimura, M., 2013. The role of Necl-5 in the invasive activity of lung adenocarcinoma. *Experimental and Molecular Pathology*, *94* (2), pp.330-335.
159. Manieri, N.A., Chiang, E.Y. and Grogan, J.L., 2017. TIGIT: a key inhibitor of the cancer immunity cycle. *Trends in Immunology*, *38* (1), pp.20-28.
160. Rodriguez-Abreu, D., Johnson, M.L., Hussein, M.A., Cobo, M., Patel, A.J., Secen, N.M., Lee, K.H., Massuti, B., Hiret, S., Yang, J.C.H. and Barlesi, F., 2020. Primary analysis of a randomized, double-blind, phase II study of the anti-TIGIT antibody tiragolumab (tira) plus atezolizumab (atezo) versus placebo plus atezo as first-line (1L) treatment in patients with PD-L1-selected NSCLC (CITYSCAPE).
161. Lin, Y., Wagner, E. and Lächelt, U., 2022. Non-viral delivery of the CRISPR/Cas system: DNA versus RNA versus RNP. *Biomaterials Science*, *10* (5), pp.1166-1192.

162. Berger, S., Krhač Levačić, A., Hörterer, E., Wilk, U., Benli-Hoppe, T., Wang, Y., Öztürk, O., Luo, J. and Wagner, E., 2021. Optimizing pDNA lipo-polyplexes: a balancing act between stability and cargo release. *Biomacromolecules*, *22* (3), pp.1282-1296.
163. Luo, J., Höhn, M., Reinhard, S., Loy, D.M., Klein, P.M. and Wagner, E., 2019. IL4-Receptor-Targeted Dual Antitumoral Apoptotic Peptide—siRNA Conjugate Lipoplexes. *Advanced Functional Materials*, *29* (25), p.1900697.
164. Levačić, A.K., Berger, S., Müller, J., Wegner, A., Lächelt, U., Dohmen, C., Rudolph, C. and Wagner, E., 2021. Dynamic mRNA polyplexes benefit from bioreducible cleavage sites for in vitro and in vivo transfer. *Journal of Controlled Release*, *339*, pp.27-40.
165. Zhang, P., He, D., Klein, P.M., Liu, X., Röder, R., Döblinger, M. and Wagner, E., 2015. Enhanced Intracellular Protein Transduction by Sequence Defined Tetra-Oleoyl Oligoaminoamides Targeted for Cancer Therapy. *Advanced Functional Materials*, *25* (42), pp.6627-6636.
166. Kuhn, J., Klein, P.M., Al Danaf, N., Nordin, J.Z., Reinhard, S., Loy, D.M., Höhn, M., El Andaloussi, S., Lamb, D.C., Wagner, E. and Aoki, Y., 2019. Supramolecular assembly of aminoethylene-lipopeptide PMO conjugates into RNA splice-switching nanomicelles. *Advanced Functional Materials*, *29* (48), p.1906432.
167. Benli-Hoppe, T., Göl Öztürk, Ş., Öztürk, Ö., Berger, S., Wagner, E. and Yazdi, M., 2021. Transferrin Receptor Targeted Polyplexes Completely Comprised of Sequence-Defined Components. *Macromolecular Rapid Communications*, p.2100602.
168. Schaffert, D., Troiber, C., Salcher, E.E., Fröhlich, T., Martin, I., Badgujar, N., Dohmen, C., Edinger, D., Kläger, R., Maiwald, G. and Farkasova, K., 2011. Solid-phase synthesis of sequence-defined T-, i-, and U-shape polymers for pDNA and siRNA delivery. *Angewandte Chemie International Edition*, *50* (38), pp.8986-8989.
169. Klein, P.M., Kern, S., Lee, D.J., Schmaus, J., Höhn, M., Gorges, J., Kazmaier, U. and Wagner, E., 2018. Folate receptor-directed orthogonal click-functionalization of siRNA lipopolyplexes for tumor cell killing in vivo. *Biomaterials*, *178*, pp.630-642.
170. Reinhard, S., Zhang, W. and Wagner, E., 2017. Optimized solid-phase-assisted synthesis of oleic acid containing siRNA nanocarriers. *ChemMedChem*, *12* (17), pp.1464-1470.
171. Nie, Y., Günther, M., Gu, Z. and Wagner, E., 2011. Pyridylhydrazone-based PEGylation for pH-reversible lipopolyplex shielding. *Biomaterials*, *32* (3), pp.858-869.
172. Souza, T.G., Ciminelli, V.S. and Mohallem, N.D.S., 2016, July. A comparison of TEM and DLS methods to characterize size distribution of ceramic nanoparticles. In *Journal of Physics: Conference Series* (Vol. 733, No. 1, p. 012039). IOP Publishing.
173. Zhang, W., Cheng, Q., Guo, S., Lin, D., Huang, P., Liu, J., Wei, T., Deng, L., Liang, Z., Liang, X.J. and Dong, A., 2013. Gene transfection efficacy and biocompatibility of polycation/DNA complexes coated with enzyme degradable PEGylated hyaluronic acid. *Biomaterials*, *34* (27), pp.6495-6503.
174. Wittrup, A., Ai, A., Liu, X., Hamar, P., Trifonova, R., Charisse, K., Manoharan, M., Kirchhausen, T. and Lieberman, J., 2015. Visualizing lipid-formulated siRNA release from endosomes and target gene knockdown. *Nature Biotechnology*, *33* (8), pp.870-876.
175. Masson, D., Jarry, A., Baury, B., Blanchardie, P., Laboisse, C., Lustenberger, P. and Denis, M.G., 2001. Overexpression of the CD155 gene in human colorectal carcinoma. *Gut*, *49* (2), pp.236-240.
176. Zhang, H.X., Zhang, Y. and Yin, H., 2019. Genome editing with mRNA encoding ZFN, TALEN, and Cas9. *Molecular Therapy*, *27* (4), pp.735-746.

177. Dagan, N., Barda, N., Kepten, E., Miron, O., Perchik, S., Katz, M.A., Hernán, M.A., Lipsitch, M., Reis, B. and Balicer, R.D., 2021. BNT162b2 mRNA Covid-19 vaccine in a nationwide mass vaccination setting. *New England Journal of Medicine*.
178. Lv, J., Fan, Q., Wang, H. and Cheng, Y., 2019. Polymers for cytosolic protein delivery. *Biomaterials*, *218*, p.119358.
179. Cheng, Y., 2021. Design of polymers for intracellular protein and peptide delivery. *Chinese Journal of Chemistry*, *39*(6), pp.1443-1449.
180. Cookson, J., Vickers, M.S., Paul, R.L., Cowley, A.R. and Beer, P.D., 2008. Amide functionalised dithiocarbamate ruthenium (II) bis-bipyridyl receptors: A new class of redox-responsive anion sensor. *Inorganica Chimica Acta*, *361* (6), pp.1689-1698.
181. Berchet, G.J., 1938. Methyliminodiacetic acid. *Organic Synth*, *18*, p.56.
182. Kim, H.J., Ogura, S., Otabe, T., Kamegawa, R., Sato, M., Kataoka, K. and Miyata, K., 2019. Fine-tuning of hydrophobicity in amphiphilic polyaspartamide derivatives for rapid and transient expression of messenger RNA directed toward genome engineering in brain. *ACS Central Science*, *5* (11), pp.1866-1875.
183. Troiber, C., Edinger, D., Kos, P., Schreiner, L., Kläger, R., Herrmann, A. and Wagner, E., 2013. Stabilizing effect of tyrosine trimers on pDNA and siRNA polyplexes. *Biomaterials*, *34* (5), pp.1624-1633.
184. Wadia, J.S., Stan, R.V. and Dowdy, S.F., 2004. Transducible TAT-HA fusogenic peptide enhances escape of TAT-fusion proteins after lipid raft macropinocytosis. *Nature Medicine*, *10* (3), pp.310-315.
185. Farbiak, L., Cheng, Q., Wei, T., Álvarez-Benedicto, E., Johnson, L.T., Lee, S. and Siegwart, D.J., 2021. All-In-One Dendrimer-Based Lipid Nanoparticles Enable Precise HDR-Mediated Gene Editing In Vivo. *Advanced Materials*, *33* (30), p.2006619.

7 Publications

Original article

Kuhn, J., **Lin, Y.**, Krhac Levacic, A., Danaf, N. A., Peng, L., Höhn, M., Lamb, D. C., Wagner, E., Lächelt, U. (2019) *Delivery of Cas9/sgRNA Ribonucleoprotein Complexes via Hydroxystearyl Oligoamino Amides.* Bioconjugate Chemistry, 31(3), 729-742.

Lyu, M., Yazdi, M., **Lin, Y.**, Höhn, M., Lächelt, U, Wagner, E. *Receptor-targeted dual pH-triggered intracellular protein transfer.* (online, find attached; https://doi.org/10.1021/acsbiomaterials.2c00476)

Review

Lin, Y., Wagner, E., Lächelt, U. (2022) *Non-viral delivery of the CRISPR/Cas system: DNA versus RNA versus RNP.* Biomaterials Science, 10(5), 1166-1192.

Submitted/Prepared Manuscripts

Lin, Y., Wilk, U., Pöhmerer, J., Hörterer, E., Höhn, M., Mai, H., Wagner, E., Lächelt, U. *Dual PD-L1/PVR immune checkpoint disruption by receptor-specific Cas9 RNP nanocarriers.* (submitted 2022)

Lin, Y., Luo, X., Burghardt, T., Dörrer, D., Höhn, M., Wagner, E., Lächelt, U. *Sequence-based fine tuning the hydrophobicity of artificial amino acids in lipopeptides enables potent Cas9 ribonucleoprotein delivery and gene editing.* (ready for submission, patent filing in progress)

Mirzazadeh Dizaji, N., **Lin, Y.**, Bein, T., Wagner, E., Wuttke, S., Lächelt, U., Engelke, H. *Biomimetic mineralization of iron-fumarate nanoparticles for protective encapsulation and intracellular delivery of proteins*. (submitted 2022)

Meeting abstracts and poster presentations

Lin Y, Wagner E, Lächelt U. *Folate-targeted Cas9/sgRNA ribonucleoprotein delivery for dual immune checkpoints disruption*. 2021. Poster presentation at the 28th Annual Congress of the European Society of Gene & Cell Therapy, Virtual.

Lin Y, Kuhn J, Krhac Levacic A, et al. *Cas9/sgRNA ribonucleoprotein delivery by hydroxystearyl oligoamino amides*. 2020. Poster flash session at the 24th Annual Meeting of the CRS Local Chapter Germany, “Delivery and Formulation of Biologics”, Munich, Germany.

Patent

Wagner, E., Lächelt, U., **Lin, Y.** *Artificial oligoamino acids for the synthesis of sequence-defined nucleic acid and CRISPR/Cas9 carriers.* (Patent filing in progress)

8 Acknowledgements

People say time flies when you are having fun, the fun for me is the research in our lab. At the end of my PhD study, I would like to express my gratitude to all people supporting me during the past four years.

First of all, I would like to thank Prof. Dr. Ernst Wagner for giving me the opportunity to do my PhD in his research group. I greatly appreciate his support and professional guidance. I have learned a lot from him and his passion for the chemistry and the science motivated me a lot during the past four years.

Next, I would like to thank Prof. Dr. Ulrich Lächelt for supervising me and supporting me. I greatly appreciate his patience on teaching me everything in the lab and always answering me questions. It is a lot of fun for me to discuss the research and share my “little” progress from time to time with him, and I have learnt a lot from him.

I would like to thank Dr. Jasmin Kuhn for teaching me everything about Cas9 in our lab. I would like to thank Dr. Ana Krhač Levačić for teaching me all the cell culture and transfection techniques. I would also like to thank all my collaborators: thank Ulrich Wilk, Jana Pöhmerer, and Elisa Hörterer for their generous help on the animal experiment; thank Miriam Höhn for her help on the CLSM experiments and the production of high-quality Cas9 proteins; thank Hongcheng Mai for his help on the CLSM experiments; thank Xianjin Luo, Sarah Dörrer and Tobias Burghardt for the help on the synthesis of building blocks and peptides; thank Teoman Benli-Hoppe and Simone Berger for the MALDI-TOF MS measurements; thank Özgür Öztürk for TEM measurements; thank Prof. Hanna Engelke and Negar Mirzazadeh Dizaji for the corporation of the MOF/Cas9 project.

I would like to thank Wolfgang for his support in the lab, as well as Ursula, Melinda, Marus and Olga for keeping the lab running. I would also like to thank Dr. Andreas Roidl for safety instructions.

I would like to thank several groups: thank “Monday Meeting Group”-Anni, Özgür, and Faqian for weekly discussion, I really enjoy meeting you on every week’s Monday morning and listening to your presentations; thank “UPGRADE Meeting Group”-Janin, Franzi, Şurhan, Xianjin, and Eric for monthly discussion on the Cas9

projects, it is so exciting to see the progress on the Cas9 projects in our lab from you; thank “Lunch Group”-Lun, Meng, Faqian, Xianjin, Fengrong as well as Jie and Yanfang, it is the most relaxing time of the day for me to talk with you.

Many thanks to all the AK Wagner members for the nice atmosphere and unforgettable time we spent together. Special thanks to China Scholarship Council for supporting my PhD study and life in Munich. Many thanks to all my friends for helping and caring me all the time during the past four years.

Last, I want to thank my parents for their supports all the time. Due to the pandemic, we haven’t seen each other for 3 years, now my PhD journey in Germany is coming to an end, and we will meet in China soon!